

Evaluating Shear Links for Use in Seismic Structural Fuses

Alireza Farzampour

Dissertation submitted to the faculty of the Virginia Polytechnic Institute and State University in partial fulfillment of the requirements for the degree of

Doctor of Philosophy  
In  
Civil Engineering

Matthew R. Eatherton  
Roberto T. Leon  
Ioannis Koutromanos  
Matthew H. Hebdon

Nov. 30, 2018  
Blacksburg, VA

Keywords: Structural Fuses, Energy dissipation, Flexural and shear behavior, Buckling limit state, Butterfly-shaped links, Straight links

Copyright

# Evaluating Shear Links for Use in Seismic Structural Fuses

Alireza Farzampour

## ABSTRACT

Advances in structural systems that resist extreme loading such as earthquake forces are important in their ability to reduce damages, improve performance, increase resilience, and improve the reliability of structures. Buckling resistant shear panels can be used to form new structural systems, which have been shown in preliminary analysis to have improved hysteretic behavior including increased stiffness and energy dissipating ability. Both of these characteristics lead to reduced drifts during earthquakes, which in turn leads to a reduction of drift related structural and nonstructural damage. Shear links are being used for seismic energy dissipation in some structures. A promising type of fuse implemented in structures for seismic energy dissipation, and seismic load resistance consists of a steel plate with cutouts leaving various shaped shear links. During a severe earthquake, inelastic deformation and damage would be concentrated in the shear links that are part of replaceable structural fuses, while the other elements of the building remain in the elastic state.

In this study, by identifying the issues associated with general fuses previously used in structures, the behavior of the links is investigated and procedures to improve the behavior of the links are explained. In this study, a promising type of hysteretic damper used for seismic energy dissipation of a steel plate with cutouts leaving butterfly-shaped links subjected to shear deformations. These links have been proposed more recently to better align bending capacity with the shape of the moment diagram by using a linearly varying width between larger ends and a smaller middle section. Butterfly-shaped links have been shown in previous tests to be capable of substantial ductility and energy dissipation, but can also be prone to lateral torsional buckling. The mathematical investigations are conducted to predict, explain and analyze the butterfly-shaped shear links behavior for use in seismic structural fuses. The ductile and brittle limit states identified based on the previous studies, are mathematically explained and prediction equations are proposed accordingly. Design methodologies are subsequently conceptualized for structural shear links to address shear yielding, flexural yielding and buckling limit states for a typical link subjected to shear loading to promote ductile deformation modes. The buckling resistant design of the links is described with the aid of differential equations governing the links' buckling behavior. The

differential equations solution procedures are developed for a useful range of link geometries and the statistical analysis is conducted to propose an equation for critical buckling moment.

Computational studies on the fuses are conducted with finite element analysis software. The computational modeling methodology is initially verified with laboratory tests. Two parametric computational studies were completed on butterfly-shaped links to study the effect of varying geometries on the shear yielding and flexural yielding limit states as well as the buckling behavior of the different butterfly-shaped link geometries. It is shown that the proposed critical moment for brittle limit state has 98% accuracy, while the prediction equations for ductile limit states have more than 97% accuracy as well. Strategies for controlling lateral torsional buckling in butterfly links are recommended and are validated through comparison with finite element models. The backbone behavior of the seismic butterfly-shaped link is formulized and compared with computational models. In the second parametric study, the geometrical properties effects on a set of output parameters are investigated for a 112 computational models considering initial imperfection, and it is indicated that the narrower mid-width would reach to their limit states in lower displacement as compared to wider mid-width ones.

The work culminates in a system-level validation of the proposed structural fuses with the design and analysis of shear link structural fuses for application in three buildings with different seismic force resisting systems. Six options for shear link geometry are designed for each building application using the design methodologies and predictive equations developed in this work and as guided by the results of the parametric studies. Subsequently, the results obtained for each group is compared to the conventional systems. The effect of implementation of the seismic links in multi-story structures is investigated by analyzing two prototype structures, with butterfly-shaped links and simple conventional beam. The results of the nonlinear response history analysis are summarized for 44 ground motions under Maximum Considered Event (MCE) and Design Basic Earthquake (DBE) ground motion hazard levels. It is shown that implementation of the butterfly-shaped links will lead to higher dissipated energy compared to conventional Eccentrically Braced Frame (EBF) systems. It is concluded that implementation of the seismic shear links significantly improves the energy dissipation capability of the systems compared to conventional systems, while the stiffness and strength are close in these two systems.

# Evaluating Shear Links for Use in Seismic Structural Fuses

Alireza Farzampour

## General Audience Abstract

Structural fuses are replaceable elements of a structure that are designed to yield and protect the surrounding members from damages, and then be accessible and replaceable after a major event. Several studies have indicated that steel plates with cutouts would have advantages for use in structural fuses. Having cutouts in a steel plate would make different shapes inside of the plate, which are called structural links. To have the same yielding condition all over the links, it is tried to better align the capacity of the links with the shape of the demand diagram caused by loading, which would be leading to the efficient implementation of the steel. In general, links are implemented to substantially increase the energy dissipation capacity of a structure and significantly reduce the energy dissipation demand on the framing members of a structure. For these purposes, various shapes have been proposed in this research study.

The main feature of a replaceable link system is that the inelasticity is concentrated at the steel link while the beams and columns remain almost elastic. This study investigated the general behavior of the fuses, the applicability of them for space-constrained applications, the flexure, shear and buckling limit states affecting the behavior of the links. The computational analysis methodologies to model the links are explained and confirmed with the behavior of the different experiment tests as well as the proposed brittle limit state prediction equations. Subsequently, the two parametric studies are done to investigate the effect of geometrical properties on the links output results and establish prediction equations. The results from the analytical and computational studies for the seismic links are incorporated for seismic investigation of multi-story buildings. The results of seismic analysis of the two buildings are summarized for 44 ground motions.

## Acknowledgements

This material is based upon the work supported by the National Science Foundation under Grant No. CMMI-1453960. Any opinions, findings, and conclusions or recommendations expressed in this material are those of the authors and do not necessarily reflect the views of the National Science Foundation or other sponsors. The Advanced Research Computing (ARC) facilities at Virginia Tech provided computational resources and technical support for this project.

## Contents

1. INTRODUCTION .....	1
1.1. The motivation for structural shear links.....	1
1.2. A brief description of links behavior.....	4
1.3. Overview of the research and research objectives .....	4
1.4. Organization of this dissertation.....	7
2. LITERATURE REVIEW .....	9
2.1. Introduction .....	9
2.2. Investigation of Butterfly-shaped Fuses .....	9
2.3. Investigation of Straight Fuses .....	37
2.4. Investigation of Hourglass-shaped dampers.....	43
2.5. Investigation of Perforated Steel Plates and Ring Shaped Fuses .....	49
2.6. Investigation of Triangularly shaped fuses.....	53
2.7. Investigation of solid plate .....	55
2.8. Investigation of miscellaneous shapes and further investigations.....	59
2.8.1. Metal band.....	59
2.8.2. E- Shape .....	61
2.8.3. Effect of cut-outs in steel plate and corrugated plates .....	62
2.9. Topology optimization on links.....	64
2.10. Potential Applications for Shear Acting Structural Fuses .....	71
2.10.1. Metal buildings.....	71
2.10.2. Solid Steel Plates.....	72
2.10.3. Eccentrically braced steel frames .....	73
2.10.4. Bay Bridge.....	77

2.10.5.	Linked column.....	86
2.10.6.	Steel shear walls and coupled steel shear walls .....	87
3.	LINK SHAPE INVESTIGATION, CONCEPTS, AND PROPOSALS.....	92
3.1.	Introduction .....	92
3.2.	Link shape based on uniform yielding along the link length .....	92
3.3.	Link shape based on the uniform curvature .....	95
3.4.	The proposition of different shapes for fuses based on literature and mathematical concepts.....	98
3.5.	Optimization criteria investigation .....	104
4.	INVESTIGATION OF LIMIT STATES FOR BUTTERFLY AND STRAIGHT LINKS. 107	
4.1.	Introduction .....	107
4.2.	Butterfly-shaped links .....	107
4.2.1.	Butterfly links strength investigation .....	107
4.2.2.	Derivation of the limit state criteria and critical butterfly angle .....	113
4.2.3.	Butterfly-shaped link stiffness formulation.....	117
4.2.4.	Consideration the effect of shear and flexure simultaneously .....	120
4.3.	Straight seismic shear link’s yielding investigations.....	125
4.3.1.	Straight link strength formulation .....	125
4.3.2.	Shear yielding or flexural fielding controlling the behavior .....	126
4.3.3.	Straight link stiffness formulation.....	127
5.	LATERAL TORSIONAL BUCKLING INVESTIGATION .....	129
5.1.	Introduction .....	129
5.2.	The governing differential equation for butterfly-shaped links .....	129
5.3.	Solution assessment using parameter non – dimensionalization for governing differential equations .....	133

5.3.1.	Solving the differential equation using MATHEMATICA implementing the shooting method.....	134
5.3.2.	Establishing lateral torsional buckling equation based on the parametric study on geometrical properties of the butterfly-shaped links .....	135
6.	COMPUTATIONAL STUDY ON LINKS, STRATEGY, AND VERIFICATION OF THE METHODOLOGY .....	140
6.1.	Introduction .....	140
6.2.	Computational study.....	140
6.3.	Validation of numerical results .....	142
6.3.1.	Stanford test by Ma et al. (2011) on butterfly-shaped links (B10-36) .....	142
6.3.2.	Four-story steel plate shear wall by Driver et al. (1998).....	146
6.3.3.	Links inside of the beam web from Ascheim and Halterman (2002) .....	148
6.3.4.	Straight shear links done by Lee et al. (2015).....	150
7.	COMPUTATIONAL STUDY TO COMPARE TO BUCKLING, SHEAR AND FLEXURE LIMIT STATE EQUATIONS .....	153
7.1.	Introduction .....	153
7.2.	Comparison of the elastic results in finite element analysis software with the proposed lateral torsional buckling method results .....	153
7.3.	Non-dimensionalization of the shear and flexural limit state and comparison with LTB equation.....	156
7.4.	Comparison of the inelastic and LTB results in FE analysis software.....	158
7.5.	Investigation of the combined effect of shear and flexural stresses simultaneously on the behavior of the BF links.....	163
7.6.	Verification of the yielding limit states equations with FE software .....	164
7.7.	Geometrical hardening investigation, formulation, and concepts .....	167
7.8.	Guideline to design butterfly-shaped links.....	175
8.	PARAMETRIC STUDY ON BUTTERFLY AND STRAIGHT LINKS .....	181

8.1. Introduction .....	181
8.2. The parameters study variable investigation and general backbone behavior of butterfly-shaped links.....	181
8.3. The results of the parametric study: .....	187
8.3.1. The group of butterfly-shaped links with $L=0.5$ , and $a/b=0.1$ .....	187
8.3.2. The group of butterfly-shaped links with $L=0.5$ , and $a/b=0.33$ .....	189
8.3.3. The group of butterfly-shaped links with $L=0.5$ , and $a/b=0.75$ .....	192
8.3.4. The group of butterfly-shaped links with $L=0.5$ , and $a/b=1$ .....	194
8.4. Investigation of the output parameters .....	198
8.5. Overstrength Evaluation:.....	203
8.6. Energy dissipation and Damping ratio: .....	204
9. EXPLORATION OF SHAPES FOR THREE STRUCTURAL APPLICATIONS .....	209
9.1. Single Row of Links (SRLs) .....	209
9.1.1. Model description.....	211
9.1.2. Design and results of analysis for single row of links.....	211
9.2. Multiple Rows of Links (MRLs).....	215
9.2.1. Model description.....	217
9.2.2. Design and results of analysis for multiple rows of links .....	217
9.3. Perforated Rows of Links (PRLs) .....	224
9.3.1. Model description.....	224
9.3.2. Design and results of analysis for perforated rows of links .....	225
10. SEISMIC RESPONSE ANALYSIS OF MULTI-STORY BUILDINGS .....	233
10.1. The validation of numerical modeling .....	233
10.2. Nonlinear Response History Analysis for multi-story building .....	238
10.2.1. The comparison of the monotonically loaded frames with conventional EBF system and BF fuses.....	242

10.2.2.	The scale factor analysis .....	246
10.2.3.	The analysis of the frame for a specific ground motion.....	247
10.2.4.	NRHA results for 44 ground motions .....	251
11.	Conclusions .....	258
11.1.	Summary of the steps of this research and applications.....	258
11.2.	Summary the analytical investigations, prediction equation, and limit states investigations .....	260
11.3.	Summary of the finite element investigations .....	262
11.4.	Summary of a computational parametric study on seismic links .....	263
11.5.	Summary the applications of seismic fuse system and nonlinear-response history analysis .....	264
11.6.	Concluding remarks and recommendation for further studies: .....	265
REFERENCES	.....	267
APPENDIX	.....	275
APPENDIX A: FINITE ELEMENT MODELING PROCEDURES, PROCEDURES, AND RECOMMENDATIONS:	.....	275
A.1. Modeling techniques for structural fuses:	.....	275
A.2. Meshing strategy:	.....	279
APPENDIX B: IMPERFECTION STUDY:	.....	283
B.1. Method I:	.....	283
B.2. Method II:	.....	286
APPENDIX C: APPLYING THE IMPERFECTION REGARDING THE METHOD II IN ABAQUS:	.....	289
APPENDIX D: THE DETAILED RESULTS OF PARAMETRIC STUDY:	.....	291
D.1. The group of butterfly-shaped link fuses with $L=0.5$ , $a/b=0.1$ .....		291
D.2. The group of butterfly-shaped link fuses with $L=0.5$ , $a/b=0.33$ .....		296

D.3. The group of butterfly-shaped link fuses with $L=0.5$ , $a/b=0.75$ .....	301
D.4. The group of butterfly-shaped link fuses with $L=0.5$ , $a/b=1$ .....	305
APPENDIX E: THE REGRESSION STUDY FOR CRITICAL MOMENT:.....	310
APPENDIX F: THE PARAMETRIC RESULTS:.....	312

# 1. INTRODUCTION

## 1.1. The motivation for structural shear links

Many structures are in need of proper design and construction to resist seismic loads without experiencing a significant amount of damage. Having sufficient strength, and stiffness would prevent vulnerability to serious damages under seismic loading. Therefore, structural fuses can be used to protect the surrounding structure from damage and to be accessible and replaceable after a major event. There are many forms of structural elements with adequate ductility and energy dissipating capability, which could be implemented as structural fuses. These elements are replaceable and are designed to yield and protect the surrounding members from damages, and then be accessible and easily replaceable after a major event.

A promising type of fuse implemented in structures for seismic energy dissipation, and seismic load resistance consists of a steel plate with cutouts leaving butterfly-shaped shear links subjected to shear deformations (Figure 1). Prior research has been conducted on shear panels with straight links, also referred to as steel straight panels or straight steel plate shear walls (Figure 2). Butterfly-shaped links have been proposed to better align bending capacity with the shape of the moment diagrams.



a) Tested specimen by Lee et al. (2016)



b) The implementation of the links in structures in California (Luth et al., 2008)

Figure 1. Butterfly-shaped links used in previous applications



a) Tested specimen by Lee et al. (2016)



b) Links in structures in California (Luth et al., 2008)

Figure 2. Straight shaped links used in previous applications

The concept of designing fuses is to have sacrificial elements to dissipate the seismic energy under significant loads while the structural stability is preserved. By appropriately arranging the fuses in a way that facilitates the replacement, they could be replaced or repaired more efficiently than replacing integral structural components. Therefore, interruptions to human occupancy is reduced.

The structural shear links could be implemented in structural fuse systems by having engineered cutouts leaving shear links that exhibit controlled yielding as it is shown Figure 3a, b, and f. The structural shear links could be designed for conventional systems based on the applied demand forces. Figure 3a, c, d, and e show schematic examples of structural shear links implementation for eccentrically braced frame, coupled shear wall, steel plate shear wall and linked column, respectively. The structural shear links are designed in various shapes and sizes to address different structural issues, among which three typical link shapes of butterfly-shaped, straight-shaped and hourglass-shaped are represented in Figure 3g.

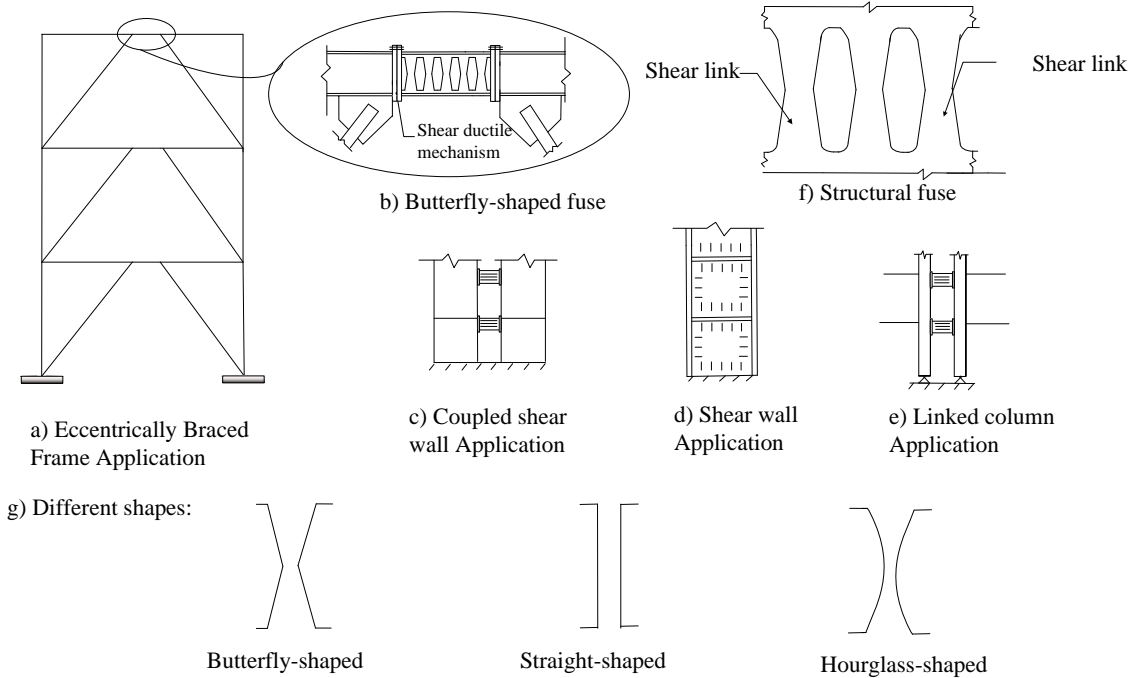


Figure 3. The fuse and shear links concepts, applications and general shapes

The devices used for seismic resistance systems are generally classified into several groups. These groups include flexural type fuses such as hourglass-shaped added damping and stiffness, ADAS (e.g. Whittaker et al., 1991), or triangular added damping and stiffness, TADAS (e.g., Tsai et al., 1992); shear type fuses such as yielding shear panel device, YSPD (e.g. Chan et al. 2009); and axial type fuses such as buckling restrained braces (e.g. Lopez and Sabelli 2004). The design concept of fuses necessitates satisfying several engineering requirements. First, the fuses should improve the strength and stiffness of the whole structure in such a way that it would not be excited to inelastic regions under service loads. Second, the fuses should have stable energy dissipation capacity. Third, the fuses should have sufficient ductility to prevent early fractures in initial stages of loading.

A number of studies have been conducted on the behavior and issues associated with the structural shear links as well. It was found that not only these elements exhibit appropriate, stable and ductile cyclic behavior; but also they would be economical to be produced and maintained. It is mentioned that the inelastic shear strains would be fairly distributed over the entire link permitting the development of significant inelastic deformation without having high strain concentration.

## 1.2. A brief description of links behavior

The butterfly-shaped links show four different categories of behavior based on the geometry of the link (e.g. Lee et al., 2015; Ma et al, 2011), which are concisely mentioned below:

- 1- The pure flexural behavior, which develops flexural hinges,  $M_p$ . This mode of behavior happens along the link length, and the energy dissipation occurs by developing flexural hinges.
- 2- The pure shear behavior, which develops shear forces,  $V_p$ , along the length of the links. The energy dissipation occurs by shear plastic deformations.
- 3- The combination of flexural and shear stresses together. For this type of link, the shear and flexure mechanisms both contribute to the energy dissipation.
- 4- In addition to the flexural and shear limit states, lateral torsional buckling behavior represents a critical limit state, which has been observed in a number of studies (Ma et al., 2010). Lateral torsional buckling is considered brittle, and could limit the lateral resistance capacity and stiffness of the links significantly (Lee et al., 2016).

In general, any sacrificial structural elements with appropriate ductility and capability of energy dissipation used in the structure could be implemented as a fuse. The fuses with structural shear links studied in this research are shown to have advantages over the conventional systems (e.g., buckling resistance). In addition, these structural fuses could be employed with self-centering mechanisms for having approximately zero residual drifts, which allows replacing the links.

## 1.3. Overview of the research and research objectives

The purpose of this research is to investigate the behavior of structural links in seismic structural fuses. The research objectives are categorized into three major parts and several subparts, which are listed as below:

- 1- This research studies the behavior of butterfly-shaped and straight-shaped shear links and proposes some new shapes. The detailed objectives of this task are listed below:
  - a. The shortcomings of the links as well as the implementation of the links in various applications are studied based on experimental and computational works in the

literature. Subsequently, the issues associated with each link are identified and discussed.

- b. Innovative structural seismic links with different geometrical shapes are proposed and studied for improving behavioral aspects (e.g. strength, and stiffness).
- c. The different limit states governing the behavior of structural seismic links are investigated for butterfly-shaped and straight-shaped links. In addition, this study investigates different modes of behavior (e.g. flexure, shear, and buckling) related to shear links and develops prediction equations for ductile and brittle limit states.
- d. A design methodology based on encouraging ductile modes of behavior instead of brittle modes is established.
- e. The backbone behavior of the butterfly-shaped structural seismic links is predicted with analytical equations.

2- Finite element (FE) modeling is used to investigate structural fuse behavior. The detailed objectives of this task are listed below:

- a. The finite element modeling approach is validated against hysteretic behavior of previously conducted laboratory tests. A mesh sensitivity study is conducted to reach to the appropriate fine mesh size for different structural shear links. From the computational studies, fundamental understanding about the mechanics of the behavior of the ductile shear link under loading is achieved.
- b. Two parametric computational studies were completed on the butterfly-shaped links to study the effect of varying geometries on the shear yielding and flexural yielding limit states as well as the buckling behavior of the different butterfly-shaped link geometries.
- c. Butterfly-shaped and straight-shaped links are computationally studied for comparison with the derived limit state prediction equations and stiffness equations. Subsequently, the effects of shear and flexural stress interaction, and links' second-order behavior are computationally evaluated.

3- Structural fuses with shear links are designed and implemented in three prototype structures. Pushover analysis, modal analysis, and nonlinear response history analyses are conducted for different buildings with and without shear links. The fuse behavior, inter-story drifts,

stiffness, strength, and natural modes are studied and compared. The detailed objectives of this task are listed below:

- a. Structural fuses are designed for use in three prototype buildings with different seismic force resisting systems. The design guidelines developed earlier in this research are implemented for designing these three prototype structures.
- b. The designed prototype structures are computationally studied. The advantages and disadvantages of using shear links in different configurations are evaluated using a set of output parameters.
- c. Reduced order models are used in this research to build computational models of two prototype buildings, with seismic structural shear links and conventional fuse systems.
- d. The behavior of the multi-story building designed with seismic shear links is compared with conventional system under different seismic hazard levels. Two systems under two hazard levels of MCE and DBE are evaluated and studied in details for 44 ground motions.
- e. The results of nonlinear response history analysis are summarized to show advantages and disadvantages of using links within the structures.

The result from this task will be practical guidelines, procedures, and recommendations leading to excellent performance and practices.

### **1.3.1. The original contributions conducted in this research**

By synthesizing the results of this study, design rules will be developed with an emphasis on the ability to separately design for the system properties such as strength, and stiffness. The original contributions of this research are organized as follows:

- Deriving differential equations to characterize lateral torsional buckling behavior and developing lateral torsional buckling prediction equation.
- Deriving equations to describe strength, stiffness, and second-order behavior of the butterfly-shaped and straight-shaped links based on shear and flexural modes of behavior.

- Conducting parametric studies on the butterfly-shaped and straight links with different geometrical properties, which leads to a better understanding of the shear links' behavior in details.
- Establishing guidelines for designing butterfly-shaped and straight-shaped shear links.
- Designing and computationally studying the behavior of three prototype structures using structural fuses as compared to a conventional seismic force resisting system.
- Designing and studying two multistory buildings with and without seismic shear links, using nonlinear response history analysis to compare the structural behavior.

#### **1.4. Organization of this dissertation**

This dissertation elaborates on the behavior, governing limit states, and computational analysis of the links (e.g. butterfly-shaped links, and straight links). It is organized as follows:

- Chapter 1 briefly explains the overview of the implementation of the links in structures and typical challenges associated with the performance of the currently available link. This chapter also highlights the motivations behind the implementation of the shear links and describes the limit states governing the behavior of the seismic shear links.
- Chapter 2 investigates the fuse behavior investigated previously in literature. The possible implementation of shear links in real-world applications is presented. The previous topology optimization investigations on the links are considered, and new topology functions are explained.
- Chapter 3 presents the general mathematical concepts for the butterfly-shaped shear links based on the uniform yielding distribution and constant curvature concepts. The various objectives of topology optimization proposed previously in literature are investigated and new topology optimization criteria are discussed.
- Chapter 4 establishes the mathematical concepts for shear and flexural modes. The butterfly-shaped or straight-shaped shear links are studied and the governing modes are compared. The stiffness of the links is formulated based on the links' shear stiffness, flexural stiffness and banding zone stiffness. The initial yielding and capacity of the links are investigated and strength equations are proposed.

- Chapter 5 conceptualizes the lateral torsion limit state behavior of the butterfly-shaped links. The differential equations governing lateral torsional buckling limit state are derived and non-dimensionalization of the parameters are described. The shooting method is implemented to solve the differential equations. Subsequently, the regression analysis study based on the lateral torsional buckling analysis is done and the simplified equation for critical lateral torsional buckling moment is proposed.
- Chapter 6 describes the computational study of the links. The meshing strategy is proposed to have a precise behavior predication assessment of the links. Some experimental tests investigated previously are validated against the computational models.
- Chapter 7 investigates the buckling, shear and flexural limit states associated with links. The proposed equations in previous chapters are verified with FE analysis. The limit states' prediction equation results are compared with FE models. Subsequently, the interaction of shear and flexural stresses is explained and studied.
- Chapter 8 describes a complete parametric study on the butterfly-shaped links with different geometries. The effect of imperfection on the behavior of the links is investigated, and 112 models are developed and analyzed in FE program considering the initial imperfection. The pushover results are represented and explained in details.
- Chapter 9 describes the implementation of the links in the different structural application. The concept of structural fuses are categorized for three applications and the models representing these concepts are proposed. The implementation of the structural shear links in prototype buildings is investigated accordingly.
- Chapter 10 describes the implementation of the seismic links in multistory buildings. Two different systems, with proposed seismic shear links, and with the conventional linking beam for EBF systems are evaluated. The behavior of the two systems is investigated for 44 ground motions under two hazard levels.
- Chapter 11 highlights the motivations behind the implementation of the butterfly-shaped links. The results based on the studies done in this research are summarized, and briefly explained.

## **2. LITERATURE REVIEW**

### **2.1. Introduction**

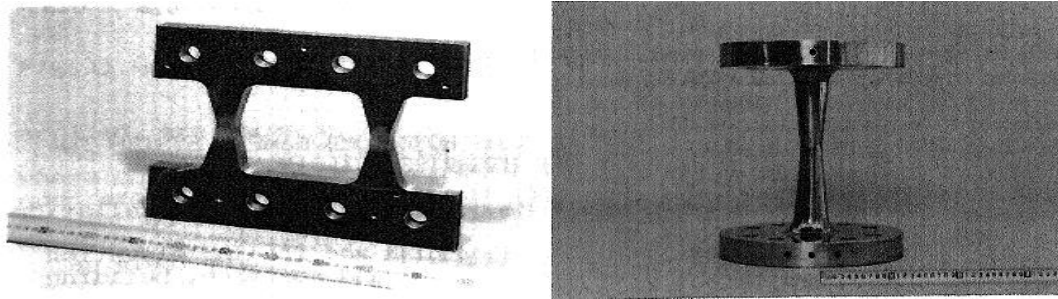
In this chapter, the various shapes of links performance are investigated. The quantitative results related to the behavior of the links with various shapes are obtained from the experimental tests as well as computational analysis are considered. Topology optimization works through literature to effectively improve specific parameter of interests are included. The problems and issues associated with the links are mentioned. The utilization of the fuses in real-world applications are investigated and related common issues are discussed.

### **2.2. Investigation of Butterfly-shaped Fuses**

The butterfly-shaped (BF) links have a linearly varying width between larger ends and a smaller middle section. These links have been shown in previous tests to be capable of substantial ductility and energy dissipation, but can also be prone to lateral torsional buckling. The butterfly-shaped dampers have been utilized in a number of studies to improve the structural performance. Traditionally these fuses are introduced for a passive control system in out-of-plane condition (Tsai et al., 1992), the plane with the direction of perpendicular to the loading, which was called as added damper and stiffness (ADAS), or with a different shapes as triangular-plate added damping and stiffness (TADAS). However, some researchers recommended using these dampers in in-plane condition.

The two innovative damper configurations of butterfly and joint damper system have been investigated by Kobori et al. (1992) as shown in Figure 4.a and Figure 4.b. These two dampers were introduced to decrease the response of high-rise structures (e.g. the story drifts). The butterfly-shaped dampers could be utilized in structural framing system leading to high stiffness and less story displacements. The joint damper could work with any loading with any direction by connecting two or more adjacent structural elements with different movement between them. The joint dampers is fastened rigidly to each story at the upper and lower extended plates, which allows middle portion to horizontally move with the plastic range of the damper. The shape of the middle portion is such that it will yield uniformly over the length due to the relative displacement between the upper and the lower flanges.

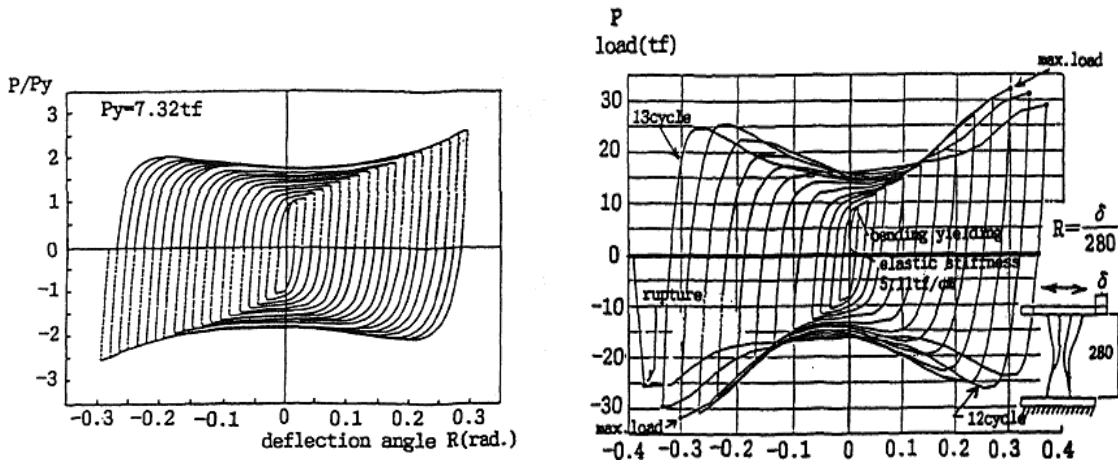
The butterfly-shaped damper is meant to be used when loads act in their own plane. However, the joint damper could work with any loading in any directions with less efficiency in dissipating energy due to limitation of movement. However, the hysteric behavior of butterfly-shaped and joint dampers indicates a low amount of pinching which makes the use of these dampers desirable in areas with high seismicity (Figure 5).



a) The Butterfly-shaped damper

b) The joint damper

Figure 4. Hysteric dampers [from (Kobori et al, 1992)]



a) The Butterfly-shaped damper

b) The joint damper

Figure 5. The hysteric behavior of butterfly-shaped link [from (Kobori et al, 1992)]

There are some examples of buildings around the world utilizing the concept of butterfly-shaped fuses. Figure 6 shows an example of a building in which the walls extending from the upper and lower beams of the story are detached and the butterfly-shaped damper is attached between them with the aid of the high strength bolts, thus, the story drift is concentrated in the damper plates.

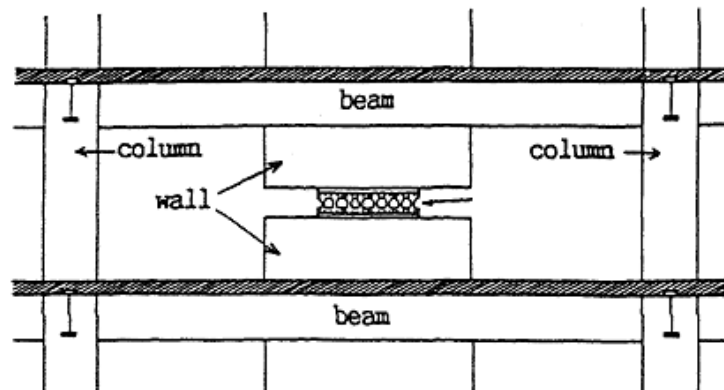


Figure 6. The butterfly links used in the wall system [from (Kobori et al, 1992)]

The damper part with the height of the 135 mm is designed to yield with the bending stress caused by the lateral drifts. The stable energy dissipation has been observed from the pushover curves. Compared to the condition where no detachment in the walls is conducted, the maximum story shear and maximum story angles of the system with butterfly-shaped fuses between the walls are reduced about 65%-90 % and 55%-122%, respectively. The butterfly-shaped dampers show a significant and consistent amount of the energy dissipation. In general, butterfly-shaped and joint dampers, due to special geometry, can be fit well in structural frames to improve the seismic characteristic of the building by providing superior hysteric energy-absorbing capability.

Another example of butterfly-shaped fuses usages in structural systems is introduced by Hanson et al. (1992) with a set of damping devices named added damper and stiffness used in structural passive control systems (ADAS shown in Figure 7). The reason that the out-of-plane implementation of these dampers is common is that the stress distribution caused by the flexure would be uniform along the length of the fuse. ADAS could dissipate energy by moving horizontally relative to the bottom.

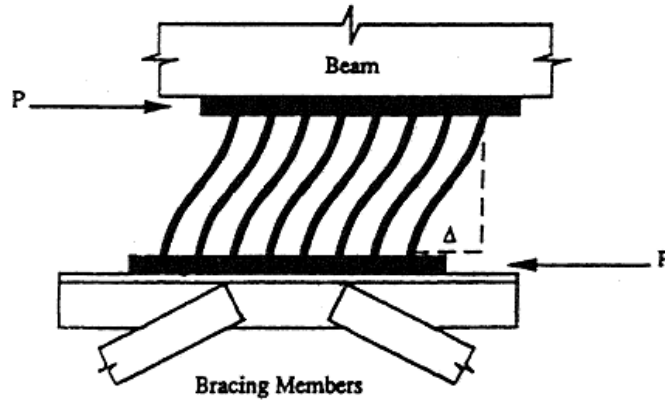


Figure 7. ADAS concept [from (Hanson et al., 1992)]

To understand the value of how effective the yielding elements are, two frames were experimented with and without the ADAS system. The results show that the implementation of ADAS would induce more stiffness and strength as well as more stable hysteric energy dissipation as shown in Figure 8. By conducting the parametric study, Hanson et al. (1992) have indicated that lower material yield displacement could have better behavior; however, the yield displacement should be large enough to control the device ductility.

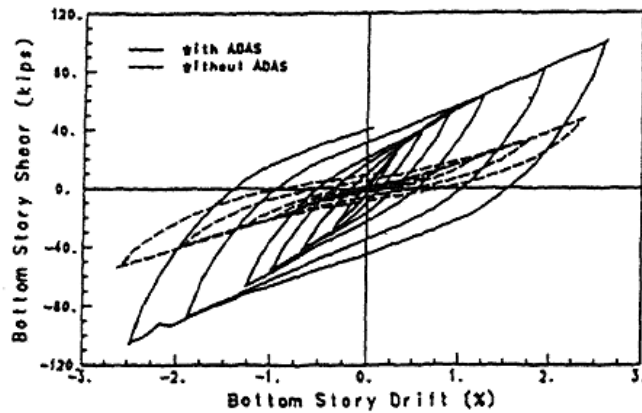


Figure 8. The ADAS effect on the hysteric behavior of the frame [from (Hanson et al., 1992)]

Substantial energy dissipation per drift is observed utilizing the ADAS systems in frame structural applications. The plastic deformation is uniformly distributed along the height of the device, this leads to maximum curvatures and strains in the plates that will be significantly smaller than those in the rectangular plate for smaller lateral displacements, and it would decrease the amount of steel used for production due to the specific geometrical properties. The mathematical

concepts associated with the best geometry chosen briefly stated in their work. The design displacement of the ADAS is based on the yielding displacement in general, which is indicated with the demands of the earthquake and capacity of the steel plate. The elastic stiffness, yield strength, and yield displacement are the most effective factors. The susceptibility of the ADAS to low cycle fatigue is negligible according to previous literature which shows one of the essential advantages of this system (Tsai et al., 1992)

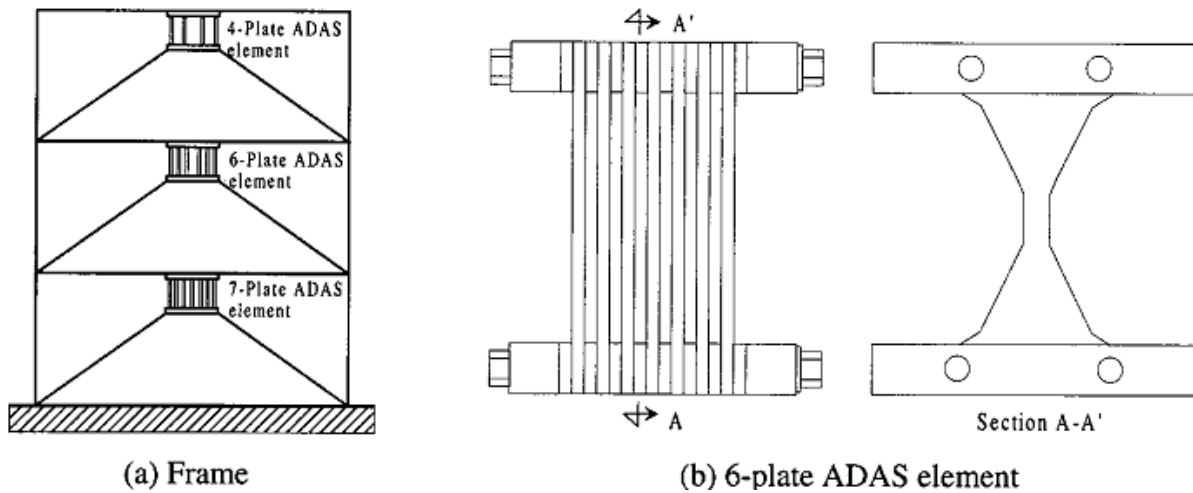


Figure 9. The ADAS a) in frame configuration b) section [from (Tsai et al., 1992)]

For investigating the behavior of the ADAS links, Hanson et al. (1992) experimentally established hysteric dampers to be used as ADAS. They claimed that implementing of hysteric dampers even with having them bent over the weak axis increases the stiffness, strength, and energy dissipation capabilities of the whole structure. They observed that these devices could sustain a large cycles of load reversals which would be about 100 or more. In addition, the ductility of ADAS is significantly dependent on yield displacement which is confirmed with other studies as well (Whittekhar et al., 1991). Therefore, to have the ductility values set to a specific number, the yielding displacement is a matter of importance, which should be 0.0014 times to 0.002 times of story height.

One of the Examples of the usage of this system is the ADAS applied for typical buildings alienations. The hospital with a buttress structure was modeled by Tsai et al. (1992). Implementation of such fuses has led to significant reduction base shears and inter-story displacements, which is the result of the external stiffening by the buttres and additional damping

by ADAS. With this system, the reduction in base shear was about 50%. If the buttres is connected to the actual structure with high rigidity, the base shear values would have been much larger resulting in significant forces. This concept of utilizing buttres with ADAS appears to have some limitations for the low-rise buildings with adequate space area. In addition, there are also more innovative structures having ADAS in which the implementation of these devices lead to a significant increase in energy dissipation capability (e.g. Tsai et al. 1992; Hanson 1992).

Whittekarak et al. (1991) worked on the implementation of the butterfly-shaped links in ADAS systems. They mentioned that for MRF systems, it is needed to have at least 2% of drift to initiate dissipation of energy, however, with this amount large amount of damage would occur to the building. Therefore, the need for energy dissipator fuses is justified since these devices would increase the stiffness, strength, and ability of energy dissipation.

Following the implementation of the butterfly-shaped fuses, Li and Li (2007) worked on the butterfly-shaped dampers to address the inelastic issues associated with the conventional implementation of the passive control ADAS systems. In passive control systems, the inelastic deformation of the damper would happen after a small disturbance leading to the fact that even under a small amount of lateral loads the system would experience inelastic mode due to the insignificant out-of-plane stiffness of metallic plates. Therefore, the conventional usage of ADAS needs to be improved. This issue is a common issue for normal metallic dampers used in out-of-plane format to provide damping for structure and reduce the dynamic response. However, ADAS dampers could be easily replaced without compromising the whole structure since they are not used for gravity-resisting purposes.

In contrast to ADAS, which normally bolted to top and bottom plates, the TADAS introduced by Tsai et al. (1992), is welded to the bottom plate while it is bolted to the top plate. From the experimental results, it was shown that the behavior of the TADAS is quite similar to the ADAS. Despite having the issue of welding to the plate in a small area, it is shown that using such devices separates the effects of the gravity load in the frame by using the slotted holes in connection. Therefore, the lateral forces only generate the plasticity of the plate; however, the construction procedures for these devices are far more elaborated compared to the ADAS. In addition, having the bolt connection for ADAS makes it easier to be removed in the case of large damages to the dissipation devices.

Tsai et al. (1992) have proposed a dissipation device, which could endure a number of yielding reversal without any stiffness and strength degradation. They used half of the butterfly-shaped link as fuses for investigating the energy dissipation capability. They mentioned that by the implementation of TADAS (shown in Figure 10) with the frame, the first mode of vibration was reduced from 0.8s to 0.5s showing that the system was getting stiffer. They have also stated that the seismic response of these devices could be adequately controlled and tuned. The constant curvature method for out-of-plane fuses are used in Tsai et al. (1992) studies, which resulted in less plastic strains over the length of the fuses.

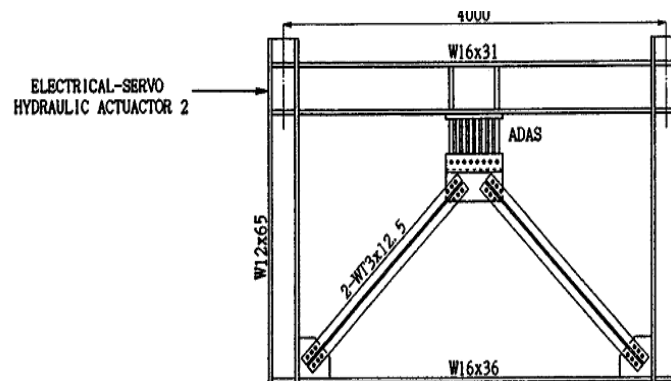


Figure 10. The TADAS effect on the hysteric behavior of the frame [from (Tsai et al., 1992)]

The curvature and strain demand on a steel plate in the end regions are high, A triangular plate bent in single curvature, or a butterfly-shaped link bent in double curvature would have the uniformly yielding over its height and plastic deformation will be distributed uniformly over its height. The maximum curvature and strains in these steel plate will be significantly less than a typical rectangular plate for the same lateral displacement. To avoid the stress concentration and reduce the low-cycle fatigue life of plate, the butterfly-shape links are recommended. They also reported the overstrength factor of 1.82 based on the analysis.

By doing quasi-static and ground motions loading types on a specific butterfly-shaped links shown in Figure 11, Figure 12, and Figure 13, Li and Li (2007) concluded that these dampers are able to have sufficient stability and energy dissipation capabilities up to stop point, which is shown in Figure 13. The criteria to stop the test is taken as 25% drop in strength carrying capacity or observation of any fracture on the damper.

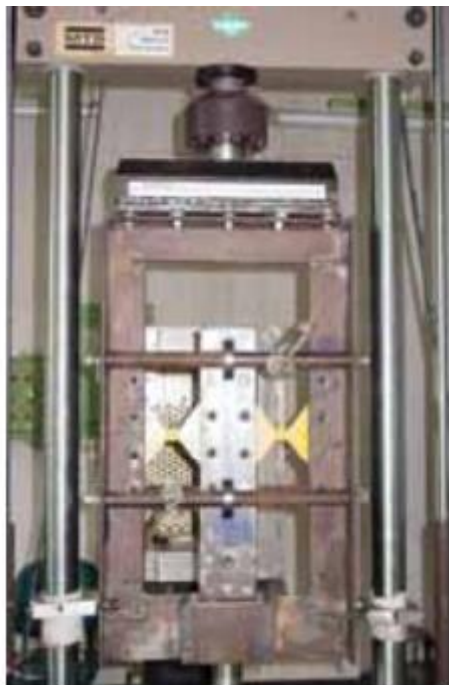
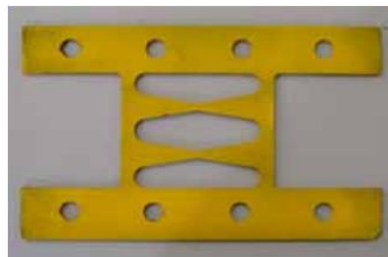


Figure 11. Set-up used by Li and Li (2007)

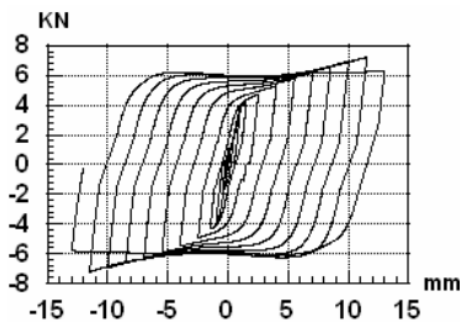


a) BF damper with a round-hole damper

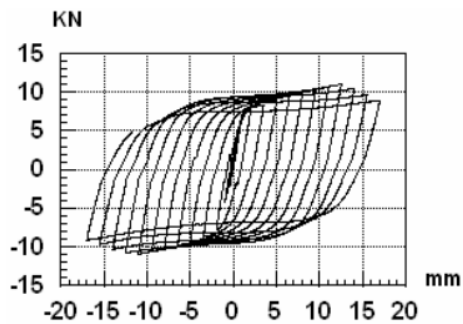


b) Butterfly-shaped damper

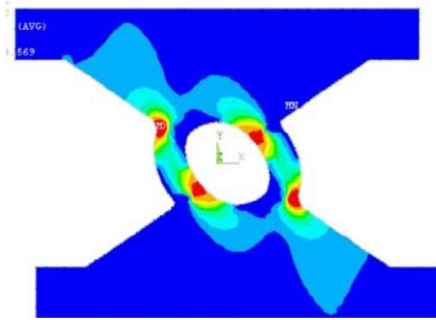
Figure 12. Dampers investigated in the study by Li and Li (2007)



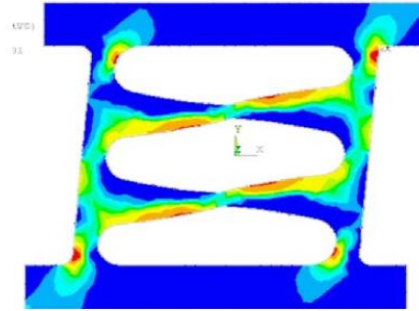
a) BF damper Round-hole damper



b) Butterfly-shaped damper



c) The plastic strain accumulation for the BF-shaped link with a ring hole



c) The plastic strain accumulation for simple BF-shaped link

Figure 13. Dampers hysteric behavior by Li and Li (2007)

It is concluded that butterfly-shaped links provide suitable stiffness in normal applications and appropriate energy dissipation capabilities (about 50%-90% of the total energy). It is noted that the real world applications of such dampers shown in Figure 14 show significant stiffness and a significant ability of seismic energy dissipation (Li and Li, 2010).



a) Single Round-hole damper



b) Double X shape damper

Figure 14. Dampers hysteric behavior by Li and Li (2007)

Li and Li (2013) mentioned that ordinary metallic damper is dependent on the out-of-plane bending deformation to provide additional damping for structures, even to reduce the structural response subjected to environmental loadings. The advantages of this deformation are the uniform distribution along the full length; however, inelastic deformation happens even if the links are subjected to small loading since the out-of-plane stiffness is relatively low; it has to be replaced after any insignificant disturbance. The authors thoroughly investigated the specimens of single

round-hole and X shape dampers (the same terminology used by authors instead of butterfly-shaped damper). They claimed that the out-of-plane buckling happened in the strip region imposed a significant abrupt reduction in strength. Implementation of such dampers in applications indicated that the peak displacements reduced by four times in different stories compared to conventional structures. However, the acceleration and base shear increased. The authors' suggestion to avoid the buckling in out-of-plane was to use the links with width to length ratio of one or more.

The sacrificial members known as fuses are designed to dissipate the seismic energy while preserving the integrity of other main components. Teruna et al. (2015) initially studied different shapes of dampers fabricated from mild steel having different shapes on the side namely straight, concave, convex lines (Figure 15). Based on this study, they chose to work on four different butterfly-shaped dampers with various geometry properties (Figure 16). The overall test results indicated that the proposed dampers have similar hysteric behavior and the specimen with convex-shaped shows more stable and excellent hysteric behavior as well as ductility factor.

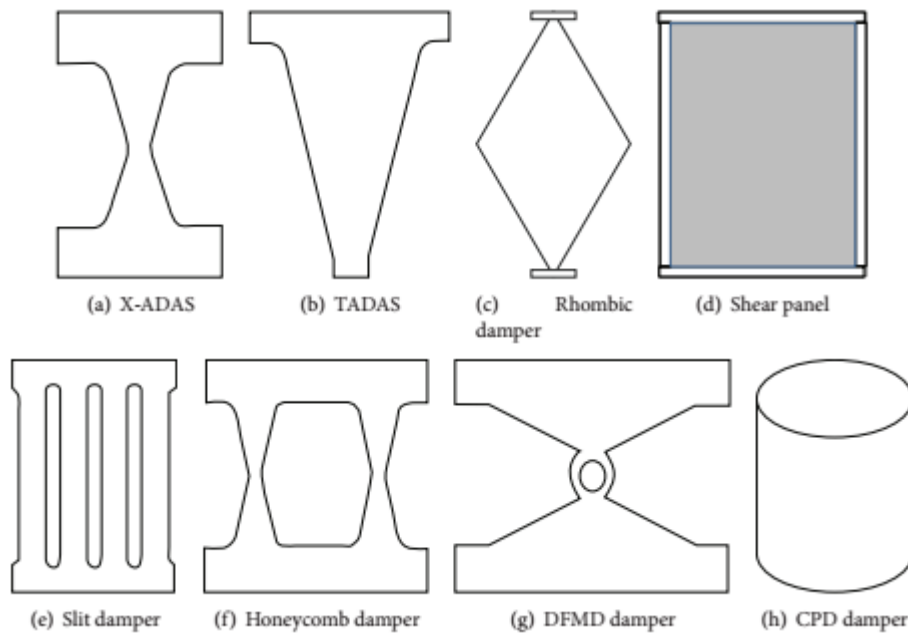


Figure 15. Proposed dampers [from (Teruna et al., 2015)]

From the comparison between butterfly-shaped dampers and other types of dampers, it is concluded that yielding occurs simultaneously and uniformly through the full height of dampers

to have the structure sustained large deformations without premature fracture or buckling. Traditionally, Straight dampers have been used for dissipations energy purposes; however, these dampers would concentrate the yielding inelasticity at both ends under the combination of shear and flexural stresses which is elaborated in section 2.3 in details. In addition, compared to other types of dampers such as rhombic dampers (shown in Figure 15) which are commonly installed having the weak direction as the bending direction, the butterfly-shaped damper is installed in an in-plane format having the strong axis as the bending axis. This would lead to the fact that higher initial stiffness at the beginning would be obtained sufficiently compared to other corresponding above-mentioned dampers. The low initial stiffness of the other dampers would impose the problem of yielding under insignificant loads, which would be considered as a cost issue.

The authors concluded that the maximum peak strength  $P_{max}$ , (during loading) or  $P_{min}$  (during unloading) obtained from the pushover study is about 1.33 times and 1.92 times of yield strength due to strain hardening. The Bauschinger effect, indicating that the steel specimens would not reach to the same amount of strength under cyclic load reversals is observed; however, this effect would not make changes to the strength more than 5%. In addition, the effect of various sizes of the fillet at the edges where the cutout are made due to having a reduction of the stress concentration would not make a significant difference based on the comparisons of the specimens. Figure 16 indicates one of the four specimens tested by the authors.

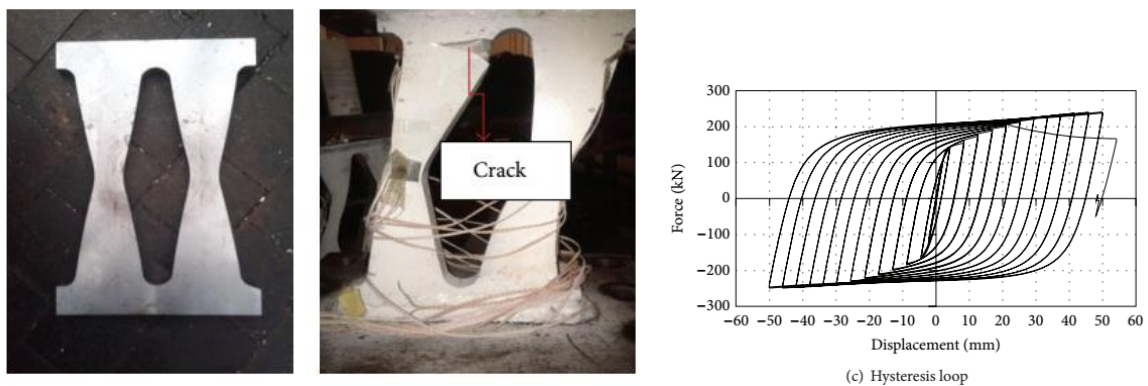


Figure 16. The butterfly-shaped link number 4 [from (Teruna et al, 2015) ]

The authors without investigating the reasons for better performance of the fuses recommended a specific shape for further use as shown in Figure 17. Further study on the specimen number 4 (Figure 17) indicates that this dampers have more flexurally dominated mode and different mid-

width to end-width ratio compared to other specimens. Therefore, the flexural hinge locations are important to be studied in details.

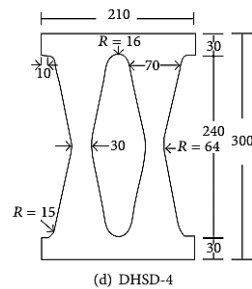


Figure 17. Specimen Number 4 [from (Teruna yet al, 2015) ]

The location of the cracks observed in the test coincides with the maximum bending moment happened. The equations of effective stiffness and effective damping ratio coefficient are used in this study to compare all the specimens with each other. The damping ratio at the displacement of 20mm was about 0.4 for this specimen.

The implementation of the links in bridges is recently getting more attention. El-Bahey and Bruneau (2009, 2010) worked on the butterfly-shaped links effect on the general performance for bridges. They concluded that adding fuses would increase both stiffness and strength of a bare system about 40% as well as the amount of energy dissipated by the frame. They mentioned that various shear links exhibit the most stable and ductile cyclic behavior. They concluded that the shear links with short length have uniformly distributed inelastic shear strains, which permits the development of large inelastic deformation without the presence of high local strains. Based on the previous studies by the authors, the behavior of the flexural dominated links with long length indicates that the high bending stresses at the ends leading to large inelastic deformations.

The buckling problem was an issue through the history of these links. According to El-Bahey and Bruneau (2010), the buckling resistance design associated with butterfly-shaped links would be significantly important, since the appropriate and stable hysteric behavior without large pinching would be achieved only if the buckling is prevented through the design of these dampers. Concerning butterfly links in bridge applications, El-Bahey and Bruneau et al. (2012) have studied columns equipped with the butterfly links used in bridge system. In this study, the accelerated bridge construction with new design methods has been investigated. Three specimens had

experimented; two bare columns, BRB columns, and steel-plate shear links (SPSL) column, which the butterfly link is implemented inside of the columns, as shown in Figure 18.

As it is mentioned in this study, the concept of designing sacrificial member to dissipate the seismic energy, while preserving the integrity of other components is known as structural fuses concept. One of the major issues with fuse implementation is the replace-ability of these elements. The authors observed that the BRB and SPSL increase the overall strength and stiffness of the structure compared to a structure without such systems, while dissipating energy through inelastic hysteric behavior and keep the two columns in elastic mode.

It is mentioned that the structural fuse has been designed to yield in  $0.6\sigma_y$ . The design of the structural fuses with significantly low yield could be beneficent in terms of having the fuses yielded and reached to limit state while other elements of the structure remain elastic and undamaged. However, the procedure of best design method and appropriate understanding of which limit state would be governing is not clarified in this research.

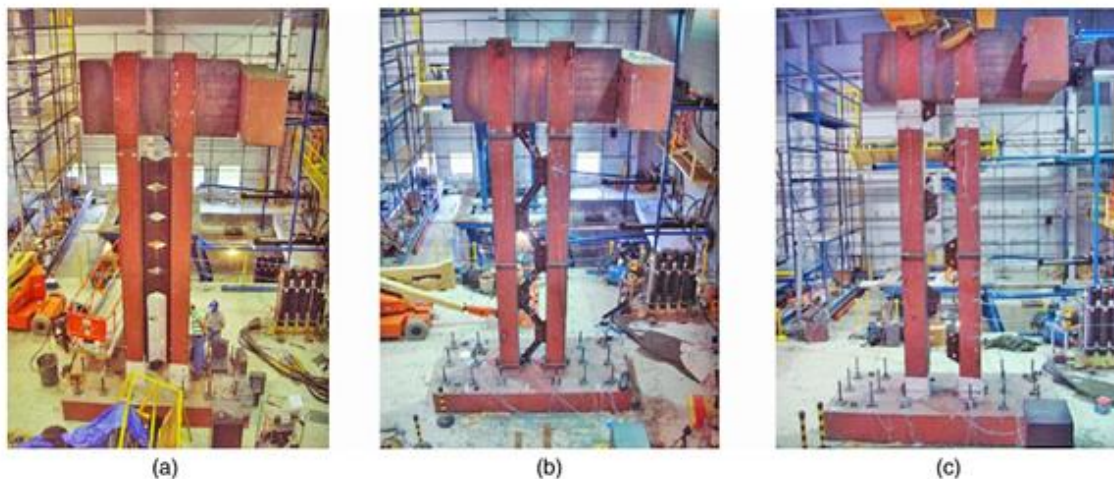


Figure 18. Illustration of a) the SPSL b) BRB c) No links used inside [from (El-Bahey and Bruneau, 2012)]

The SPSL and BRB increased the column strength by 80%. In addition, the SPSL column increased the stiffness by 31%, while the BRB column increased the stiffness by 20%. The authors did not mention how much more steel is used in each of these specimens, since the higher amount of steel used in this structure, the higher strength and stiffness; therefore, the amount of steel used should be measured to estimate the efficiency of added steel.

The general design concept is not elaborated for SPSL, but it is mentioned that the design is based on the curvature of the links (Figure 19). The cracking modes mostly occur from the middle part of the links, which indicate the links are not efficiently designed, and not all the limit states are considered. The software and analytical modeling were not compatible with the actual test due to a couple of reasons. First, due to unanticipated strong wall effect, which shows a higher amount of stiffness and lower amount of yield displacements. Second, the actual material used was 40% stronger than what was designed. There is a couple of unclear experimental changes while running the test. First, the splices have been oversized generously due to the limitation of brittle mode. Second, the out of plane restraints was removed because the intent was having yielding of fuses before column fracture.

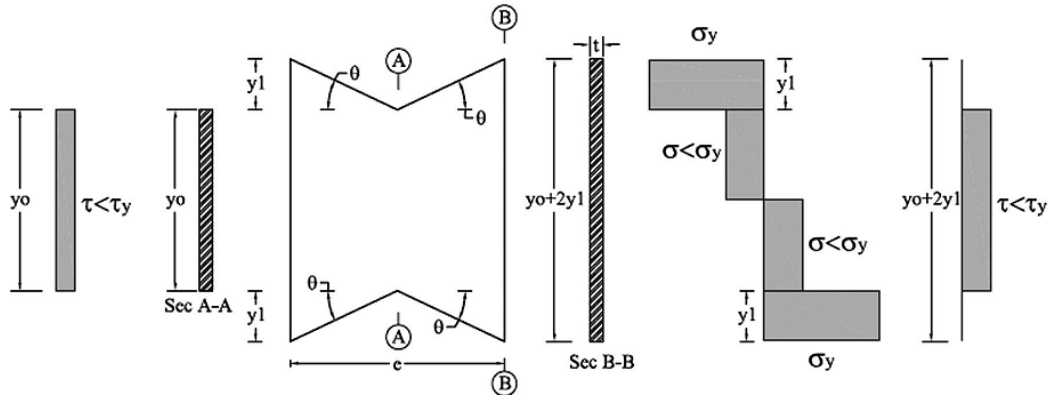


Figure 19. The links used between the columns [from (El-Bahey and Bruneau, 2012)]

The signs of yielding have occurred in the middle of the links, the idling point in the hysteric response is recommended as the onset of the softening in hysteric responses of the structure. There are three fracture points, first the east column has weld fracture in the connection segment in lower parts; second, in the splices in west column although it was mentioned that the splices were oversized generously; third, in the mid-height of the column in the splice location.

A significant amount of degradation in stiffness and especially in strength has been observed from the hysteric curves (Figure 20). The pinching in response is obvious and it is even more obvious when the BRB is used in the system compared to the actual bare columns, which normally does not happen. There was a couple of times that the experiment was stopped and the welding

condition has been retrofitted, which makes the results to be uncertain. The authors did a couple of experimental tests on fuses itself with out-of-plane restrained and unrestrained conditions.

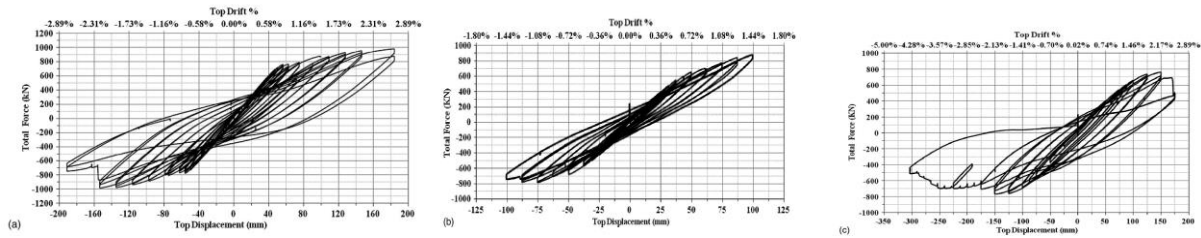


Figure 20. Specimen hysteresis a) S1b) S2-1c) S2-2 [from (El-Bahey and Bruneau, 2012)]

The comparison made between the two out-of-plane restrained fuses with unrestrained ones. The restraint condition is made by the fiberglass building material. The loading protocol is chosen based on the AISC seismic provision for EBF. Yielding of the restrained specimen stated to occur at 0.015 rad. The wedge part has not experienced any buckling as it was designed. Initial cracks from the strength degradation are guessed to occur at 0.08 rad (Figure 21).

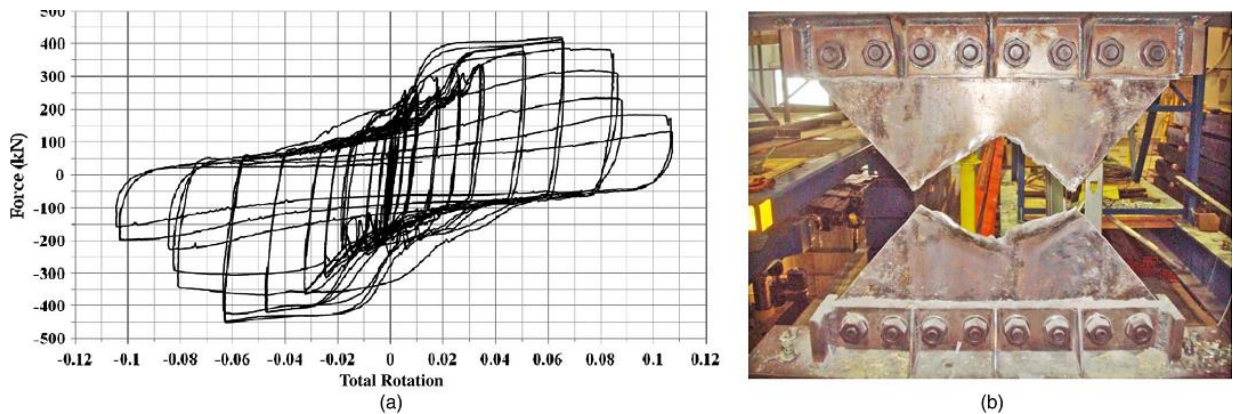


Figure 21. The wedge in restrained condition [from (El-Bahey and Bruneau, 2012)]

The specimens not restrained against out-of-plane buckling are observed to have a similar trend. The only noticeable difference is the high amount of pinching in the hysteric curves compared to the restrained one. The mode of fracture is different as well; as it is shown in Figure 22, the corner fracture has happened for unrestrained one while the middle part is cracked in a restrained condition, which could be due to torsional buckling and shear conditions.

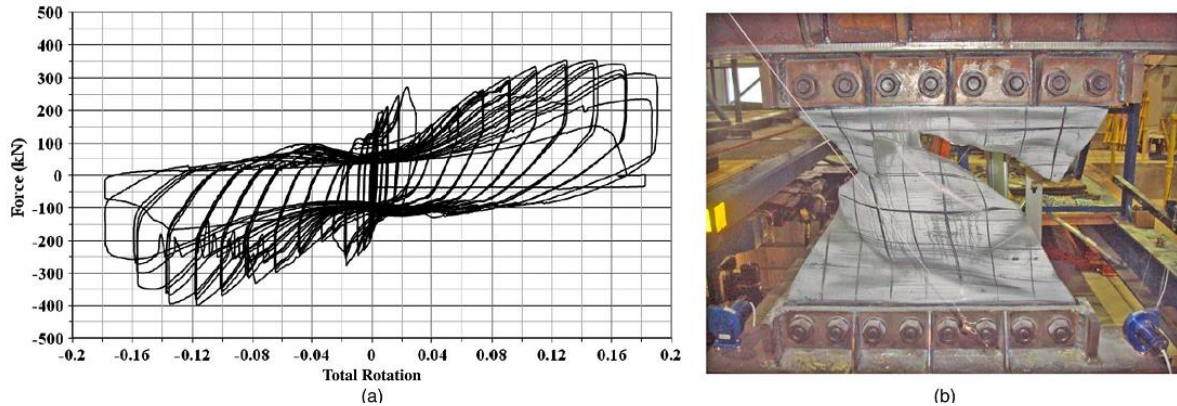


Figure 22. The wedge in unrestrained condition [from (El-Bahey and Bruneau, 2012)]

To have a better understanding of the behavior of the butterfly-shaped links, Lee et al. (2015) experimentally investigate three different shapes of non-uniform strip dampers. Beside the butterfly-shaped with uniform and non-uniform thicknesses (also called strip damper), the straight dampers are studied in this research. The straight damper and straight link are made out of rectangular cutout inside of steel plate (Figure 23). The results indicated that compared to conventional prismatic dampers (which is called straight dampers) the behavior of strip dampers under cyclic loading condition would lead to more full hysteric behavior.

The problem associated with straight dampers is that these dampers made in steel plate so that they begin to work in low strength. However, the damage usually is concentrated at the ends due to the geometry of the links, which eventually would decrease the energy dissipation capability compared to BF dampers (Figure 23). They recommended that the high ductility dampers should be used in structure since it would have better performance in controlling the vibration. High ductility correlates with a low yielding point; therefore, the low yielding steel is recommended for use. The range of thicknesses implemented in the tests was between 10mm up to 17mm to have enough resistance against buckling in initial cycles without detailed investigation. The thick thickness of the plate chosen in this study is considered in a way that the buckling would be prevented, for which the authors recommended further studies.

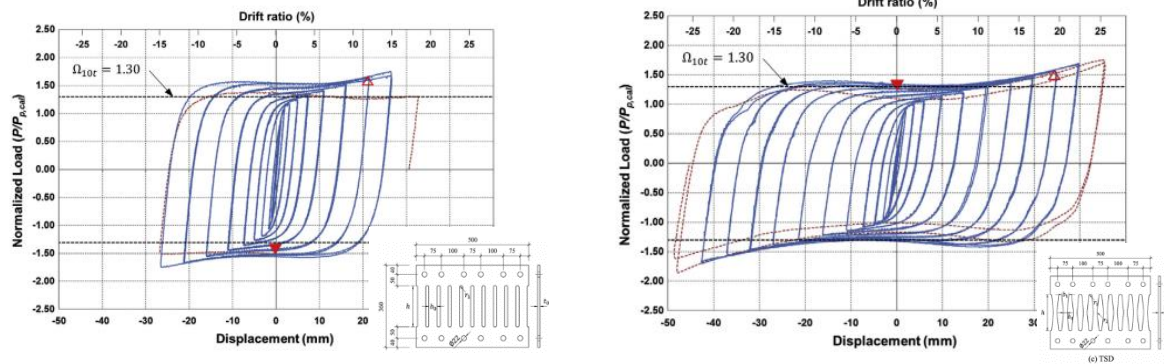


Figure 23. The comparison of Straight dampers and Butterfly-shaped dampers [from (Lee et al., 2015)]

The initial stiffness equations provided by the authors needed to be revised with a factor of  $C$  to account for the rigidity of the dampers. The stiffness for pure flexurally dominated dampers could be adjusted with the  $C$  factor between 0.55 up to 0.706, which is to account for the softening behavior according to the author which shows the need for accurate estimation of the stiffness of these links. More studies on stiffness is necessary for finding the stiffness prediction equation considering the butterfly-shaped links. Lee et al. (2015) observed that the overstrength factor for these links would be between 1.70 to 2.030 times  $\Phi$ , which  $\Phi$  is the tensile strength over yielding strength. The second-order behavior is observed in the specimens, an appreciable membrane effect happens in large displacements; thus, the external load would be resisted by the combination of flexure and tension mechanisms in larger displacements.

The crack distribution for the specimens designed to have a linearly decreasing thickness was more uniform than the rest. This could be compared to straight specimens in which the specimens cracked at the ends and grew considerably. The necking was also observed due to the unbalanced distribution of stresses. In addition, those specimens having the better out-of-plane capacity for torsional deformation would have better energy dissipation capability. In the study done by Lee et al. (2015), the damping coefficient is assessed. The damping provided for the dampers was between 0.48-0.51. Implementation of butterfly-shaped dampers with uniform or non-uniform thickness improved the cumulative ductility (1.13-1.75 time better) and energy dissipation (2-2.36) compared to straight dampers.

Along the same lines, Lee et al. (2016) investigated the behavior of the butterfly-shaped dampers with non-uniform thickness also called as strip dampers used with shear-type friction dampers as

indicated in Figure 24. The concept of the work is that under cyclic loading the friction damper would resist the lateral loading, while under more significant loading condition the strip dampers would begin to work and dissipate the energy through the inelastic deformation.

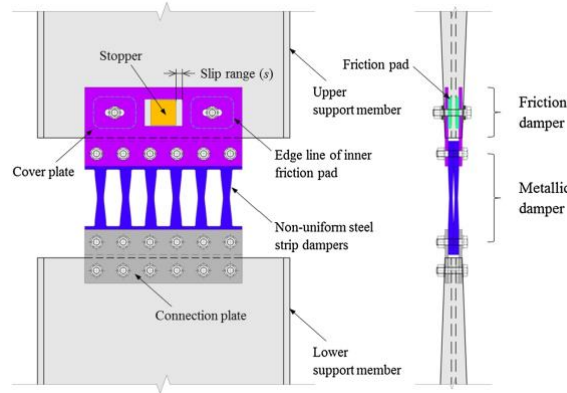


Figure 24. Friction and strip dampers [from (Lee et al., 2016)]

Lee et al. (2016) used butterfly-shaped dampers to improve the common butterfly-shaped dampers. The results indicated that these dampers have substantial load-resistance capacity under monotonic loading condition, and excellent ductility and energy dissipation capability under cyclic loading condition with an even distribution of the damage along the length of the link. For the seismic application of the metallic damper, two criteria are required. First, the damper should provide adequate stiffness to the structure under service load. Second, seismic dissipation should be done by the damper, not the surrounding structure; therefore, the damper should be designed to yield in a low displacement. In the study done by Lee et al. (2016), the dampers are designed in such a way that the transition between the different parts of the geometry would be happening in a smooth way. The concentration of the stresses is tried to be avoided in the middle and at the ends. The strip dampers proposed by Lee et al. (2016) would have the height to the width at the end ratio of five while the thickness of the plate would be varying from 17mm at the top edge to 10mm at the middle. The links are designed thick enough to avoid buckling limit state. This necessitate the need for buckling prediction evaluation for seismic structural links.

In addition the methods used in Lee et al. (2016) studies to design the shear links would not make the yielding to happen simultaneously all over the section since we have a stronger section at the end and a weak section at the middle, which impose flexural yielding not to occur at the

same time. In addition, the shear mode would be a matter of concern for this type of strip links due to having insignificant cross-sectional properties, which was not investigated by the authors.

It is observed that the specimens would experience axial tension force, double curvature bending moment and constant shear force. The monotonically loaded dampers would be able to withstand the loading twice as much as cyclically loaded dampers. All the specimens tested by the authors represented higher values for ultimate strength because of the strain hardening. For the monotonically tested specimens, the values are higher as much as three times of the first yielding, while for the cyclically tested specimens it was higher by 1.8 times. It is mentioned that the poison ratio would not affect the maximum strength, and the number of dampers. The expected yield value over the yield stress ( $R_y$ ) could be taken into account for estimation of the strength values, which is prescribed to be 1.3. The authors verified the behavior of the link by using two hardening criteria. To verify the experiment, it is regarded that first, the kinematic hardening and isotropic hardening rules are better to be combined, and the degradation in post-yield stiffness should be adequately considered.

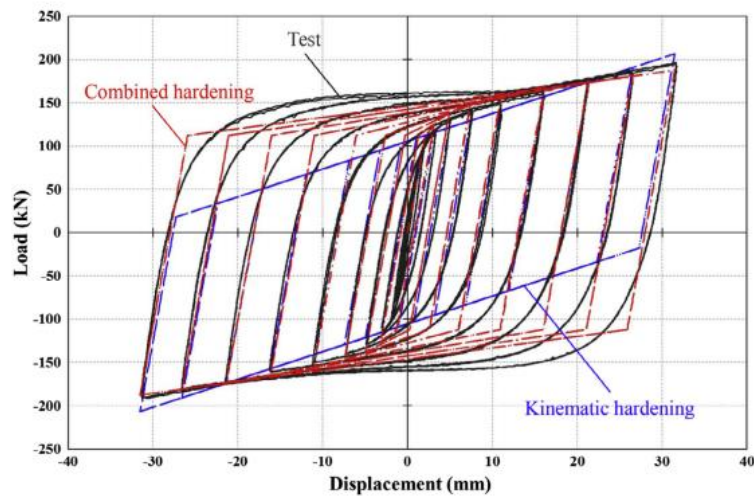


Figure 25. Combined hardening consecutive model use in verification of the BF behavior [from (Lee et al., 2015)]

To have the yielding mechanisms govern the behavior instead of the buckling, Koppal and Eatherton (2013) considered the implementation of butterfly-shaped links in steel plates (BF-SSW). In BF-SSW indicated in Figure 26, the increase of the thickness of the plate would lead to higher ultimate strength. The thickness is more effective in developing stiffness rather than

strength. It is also suggested that to have the appropriate energy dissipation capability, plate thickness should be more than 0.5 inches, which is considered a high value for thickness comparing the values used in other studies. Having thicker plate suggested, they did not mention the effect of thickness on the fracture potential. The issue of capturing and predicting buckling of the links is mentioned by to be a major issue associated with the links.

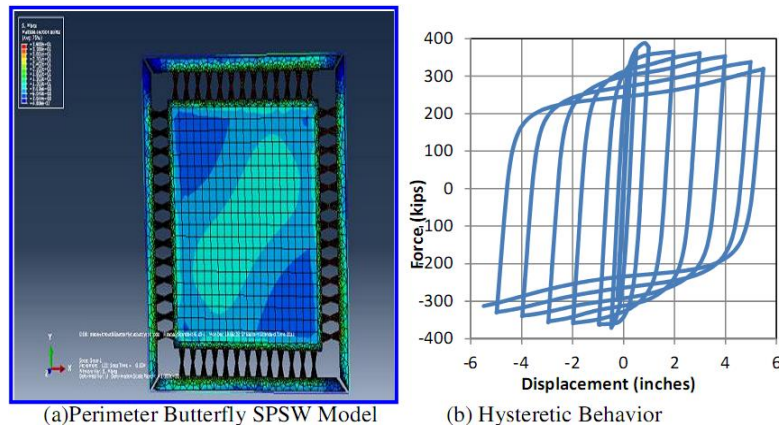


Figure 26. The Butterfly-shaped BF-SSW model [ from ( Koppal and Eatherton, 2013)]

The stress concentration in corners of butterfly perforation possibly causes a fracture. It is noted that larger cutouts or lower number of links could cause the plate to buckle at an early age as the solid plate buckling. In another point of view, the larger the cutouts and the lower number of cutouts, the higher cost of fabrication as well. Generally, the implementation of cutouts inside of the plate would change the failure mode and resistance mechanism from the elastic, inelastic buckling to yielding of the plates elements; hence, the full capacity of the plates has been implemented which is more economical.

Katayama et al. (2000) worked on the energy dissipation capability of steel plates. They mentioned that the implementation of low yield point plate would have significant appropriate performance due a couple of reasons: the low yield steel would act as fuse since the yielding point is less than the other elements in structure, and the elongation of this type of steel is more than another type of steel which induces significant ductility in the system. They mentioned that the static loading results would be different with the dynamic loading ones. The 20% increase in the results of actual time-history loading than static loading is expected. The reason according to the authors is the

strain hardening which consists of kinematic and isotropic hardening. The cumulative ductility factor under static loading would be less than that of the dynamic loading due to the fact that the shear resistance is higher in the later one. This phenomenon is observed in energy absorption capability for the same reason as well.

Chaofeng et al. (2012) studied improvement of deformation capacity of the low yield strength steel shear panel damper. It is indicated that the arc transition of the plate could be effective only in the elastic region, and this type of transition would not be significantly effective under large plastic strains. It is needed to be careful about designing the holes inside of the links since these areas are subjected to low cycle issues. In general the sharp discontinuity is better to be prevented as much as possible. In addition, 70% shear strain is largest deformation capacity that the panels could experience. Along the same lines, Chan et al. (2009) investigated the yielding of shear devices. They mentioned that common stiffness equations would be significantly off compared to equations proposed. They guessed that the issue of stiffness difference would be related to bolt slippage in addition to geometric imperfection. The equivalent damping ratio is proposed to compare the ability of energy dissipation of the links.

Köken and Koroğlu (2012) investigated the implementation of the butterfly-shaped panel in controlling the inelasticity concentration at the end of the beam. The main of their work is to prevent damage that was placed in the beam-column connection when earthquake occurs. It means that after an earthquake, by replacing dampers in the beam-column connection of the structure, the structure could be still serviceable and no damages would occur to beam and columns. The usage of dampers would not only prevent serious damages to the structure and loss of lives but also it will ensure that it can be repaired and serviceable as soon as possible with minimum cost. The main difference of this work with work done by Oh et al (2009) is that, for Oh et al. (2009) work, it is needed to replace not only the dampers but some of the end frame parts, while for Köken and Koroğlu (2012), it is needed to change the dampers only. One damper is also used in the work done by Köken and Koroğlu (2012) as compared to more than dampers used by Oh et al. (2009). With the aid of the solid elements, the authors computationally analyzed the specimen. The monotonic loading is considered for FE, which was compatible with experimental values with 95% accuracy. The energy dissipation of the specimens with butterfly-shaped links, butterfly-shaped links with stiffener were lower than that of the simple end moment connection which was due to

the less amount of rotation that the actual beam and column had. However, the stiffness and strength of the system generally increased by adding butterfly-shaped links at the end. The authors made conclusion that the behaviour of the proposed specimen with butterfly-shaped would be much simpler than the specimen done by Oh et al. (2009). In general, even though the traditional end plate connection has appropriate hysteric behavior, the repair and strengthening of the beam after a possible earthquake would be significant due to occurrence of local buckling in the beam.

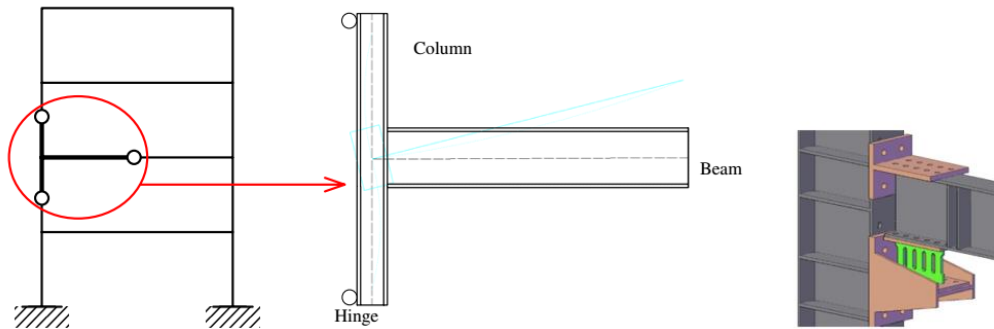


Figure 27. The implementation of the butterfly-shaped links for connection



Figure 28. The implementation of the fuses in structural applications [from (Luth et al., 2008)]

By using the butterfly-shaped links instead of straight links, Luth et al. (2008) mentioned that the new fuses due to special geometrical properties would show better flexibility. One way to design these devices according to Luth et al. (2008) is to reach to limit states at the end and in the middle. If this design concept is used the yielding initiates in the middle and propagates to the ends, resulting 100% yielding all over the length of the link and appropriate energy dissipation.

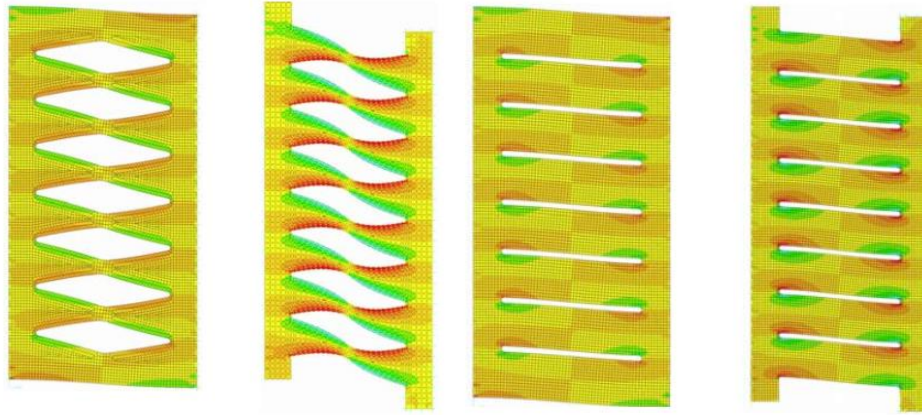


Figure 29. The butterfly-shaped and straight links [from (Luth et al., 2008)]

The recommended length for use was  $8 \frac{1}{4}$  " and  $10 \frac{1}{4}$  " for straight links and butterfly-shaped links. By strategically managing the number, stiffness and strength and location of the plates, it is possible to reach 110% of the code recommended strength values. It is reported that at the corners, stress concentration has been occurred, which was avoided by using the "ears" at the corners. The typical weld was  $\frac{5}{16}$ " which was done with one pass; however, at the corners the fillet weld was increased to  $\frac{7}{16}$  to avoid any crack initiation.

The other observation was the edges of the links were more uniformly stressed than edges of the straight links. It is mentioned that the stress at the supports behind the length of the link plays a significant role in controlling the flexibility of the assembly. Without further investigations, the author mentioned that the  $\frac{1}{2}$ " thickness could be appropriate in controlling the buckling. The behavior of the links is described as two stages. First, the links exhibit a flexural beam behavior, and then the tension action would take place by 90 rotation of the links. The distortion is reported to be occurred at 41% drift, with more than twice of the yield load. In general, it is concluded that the butterfly-shaped links are robust and well suited as fuses.

For the straight links, it is mentioned that if the b/L ratio is high (i.e. shear governed), the energy dissipation happens faster and higher stiffness is expected; however, this type of geometry suffers from earlier fracture and high overstrength (Hitaka and Matsui, 2008). For high b/L ratios, the flexible behavior is expected as compared shear governed links.

Koborie et al. (2017) mentioned that implementation of the BF dampers in the structures would reduce the shakes of the building caused by earthquakes. These dampers are used in specifically

high-rise and to some extent low rise structures as well as the existing ones which make a spacious room for residence without affecting the inside and outside of the building as shown in Figure 30. In addition, due to a reduction in seismic forces, the cost of the structure at the end would be reduced and the structure would be more light-weighted. The sufficient durability of BF dampers makes them appropriate in terms of maintenance costs.

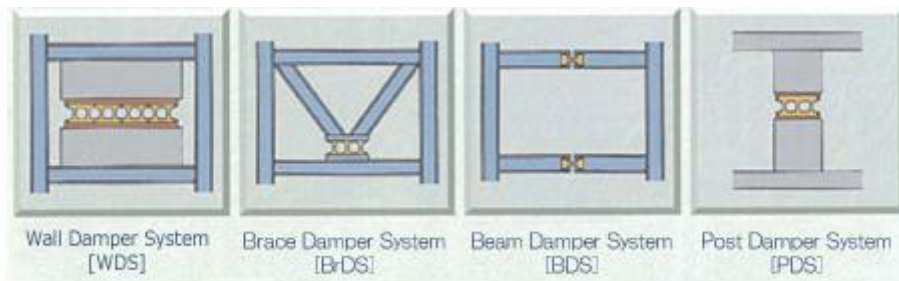


Figure 30. The possible applications of the BFs in buildings [Koborie et al., 2017]

The suitable energy dissipation capability due to full hysteric pushover curves and reduction of the seismic responses are verified previously as it is shown in Figure 31. It is mentioned that the reduction in response could go up to 20-30%, and the damper would not be destroyed by one great event due to the margin of rotation capability of  $\frac{1}{2}$ - $\frac{1}{4}$  degrees.

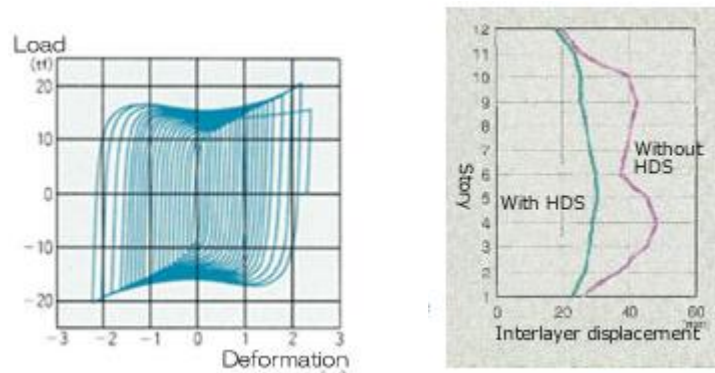


Figure 31. The energy dissipation capability and reduction of the seismic response [Koborie et al., 2017]

Along the same lines, Ma et al. (2011) have investigated the two sets of opening energy dissipation fuses (Figure 32). They have mentioned that walls with links indicated ductile behavior around 5% shear deformation. However, the major problem associated with these fuses is low cycle fatigue for more than 20% to 30 % shear deformation. However, there are butterfly-shaped

specimens which could reasonably resist the displacement loading up to 25% drift ratio (Ma et al, 2011; Eatherton 2010)



Figure 32. The butterfly-shaped link [from (Ma et al., 2011)]

Earlier fracture and buckling resistance are two new observations associated with the plates compared to solid plate shear wall. Ma et al. (2011) have extended the previous works on straight plate shear walls and butterfly links from previous literature (Kobori et al., 1992; Hanson et al, 1992). The implementation of the butterfly-shaped concept as a dissipating link is to align the bending capacity with the shape of the moment diagram as indicated in Eq. (1). It is important to design such butterfly cutouts in a way that all the points along the edges of the link yield simultaneously. This idea as well other ideas would be implemented to mathematically explain the possible new shapes in Chapter 3.

$$\frac{M(x)w(x)}{2I(x)} = \sigma_y \quad (1)$$

Satisfaction of the above formula needs butterfly-shaped links to be curved in edges, which would be mathematically investigated in later chapters. It is observed that, if the straighter butterfly-shaped link is chosen, the overall performance would be reduced meaning that not all the points on the edge would be yielded at the same time. This phenomenon is thoroughly investigated in Chapter 4. The  $a/b$  factor could be a suitable dimensionless parameter to indicate the behavior of the link. This ratio could be related to fracture of the shear wall having butterfly link fuses (Figure 33).

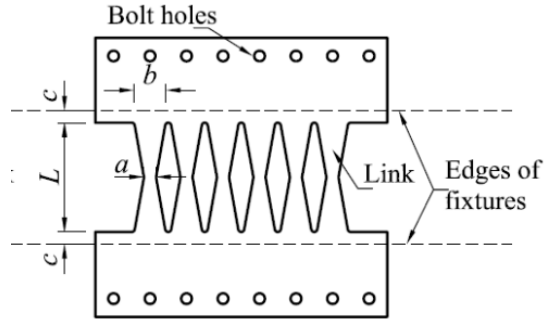


Figure 33. The butterfly-shaped links and the  $a/b$  ratio [from (Ma et al., 2011)]

It is noted that the change of curvature and plastic hinge could be the potential locations for fracture (Ma et al., 2011). The author recommends the quarter point hinges to be considered as the areas in which the yielding occurs. The issue associated with this is that the quarter points are assumed based on the simplification of the behavior of the link, which resulted in  $a/b=1/3$  (Figure 34). However, the behavior of the link would be affected by shear stresses, which needs to be further investigated. In addition, the central part of the link could be highly vulnerable to yielding, buckling and fracture as it is observed in the (Figure 34).



Figure 34. Hinges in butterfly links [from (Ma et al., 2011)]

According to Lee et al. (2015) and Ma et al. (2011), the amount of the  $P_{max}/P_{cal}$  indicates the expected increase in strength due to strain hardening and membrane effect. This range is about 1.7-2.3 for the specimens done by Lee et al. (2015) and it is about 1.4-2.3 for the specimens done by Ma et al (2011). The results indicate that the load-bearing factor is affected by some other factors besides the flexural resistance (Lee et al., 2015). Since the top and bottom of the damper

are restrained to prevent the vertical displacement, longitudinal elongation of the strips happen when the specimens are subjected to horizontal movement. According to the Lee et al. (2015) and Ma et al. (2010), a significant membrane effect occurs in large displacement; thus, the external load would be resisted by the combination of the flexural and tensional mechanisms. Thick butterfly fuses could be desirable for the purpose of energy dissipation without the occurrence of buckling; however, significant over-strength could be considered as a challenge to the capacity-designed members. Therefore, when designing the connection details, as the tests indicated, the overstrength should be accounted for the connection.

According to Ma et al. (2011), the phenomena of over-strength occurrence are specifically important for straight and butterfly-shaped fuses since the developed strength is averagely twice as much as the nominal strength due to the combined effect of strain hardening and tension mode behavior under cyclic loading condition. The latter effect subjects the connection to double shear in vertical and horizontal directions. The butterfly-shaped fuses indicate the post-yield stiffness and enough redundant strength causing by strain hardening and membrane effect (Figure 35). In studies done by Ma et al. (2010), it is shown that if the yielding point is low, the higher over-strength could be expected.

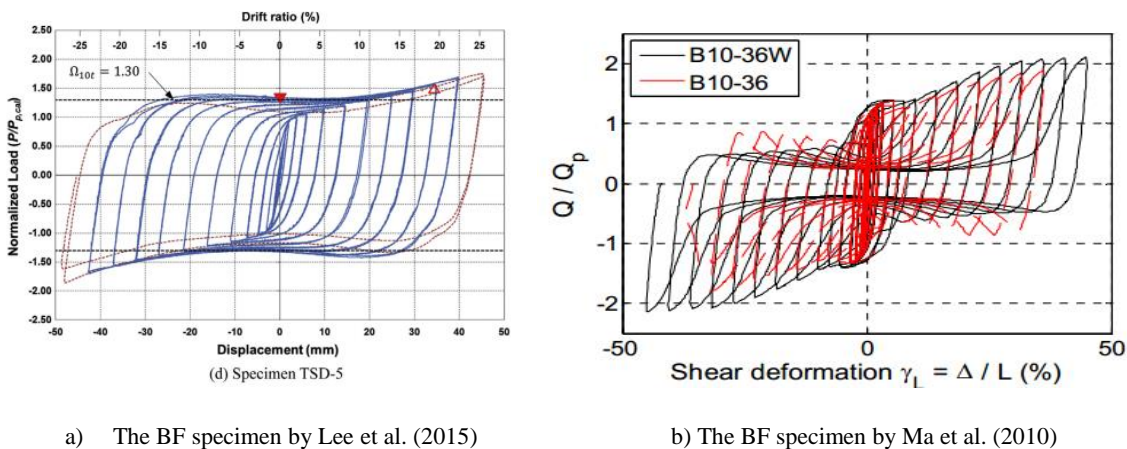
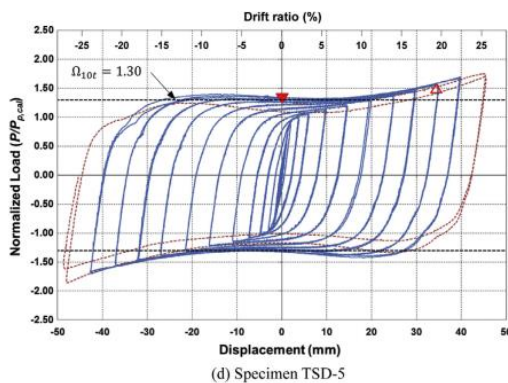


Figure 35. The pushover curves on BF

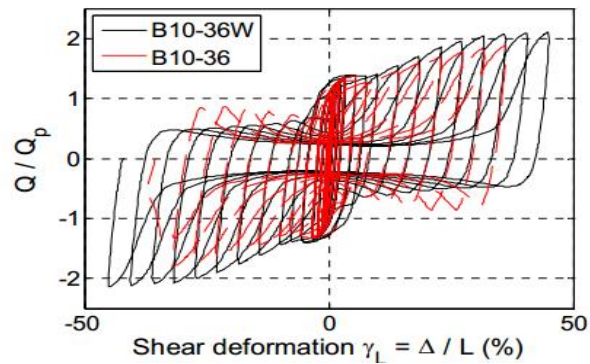
According to Lee et al. (2015) and Ma et al. (2010), the amount of the  $P_{max}/P_{cal}$  indicates the expected increase in strength due to strain hardening and membrane effect. This range is about 1.7-2.3 for the specimens done by Lee at al. and it is about 1.4-2.3 for the specimens done by Ma

et al (2010). The results indicate that the load-bearing factor is affected by some other factors besides the flexural resistance (Lee et al., 2010). Since the top and bottom of the damper are restrained to prevent the vertical displacement, longitudinal elongation of the strips happen when the specimens are subjected to horizontal movement. According to the Lee et al. (2010) and Ma et al. (2010), a significant membrane effect occurs in large displacement; thus, the external load would be resisted by the combination of the flexural and tensional mechanisms. Thick butterfly fuses could be desirable for the purpose of energy dissipation without the occurrence of buckling; however, significant overstrength could be considered a challenge to the capacity-designed members. Therefore, when designing the connection details, as the tests indicated, the overstrength should be accounted for the connection.

According to Ma et al. (2010), the phenomena of over-strength occurrence are specifically important for straight and butterfly-shaped fuses since the developed strength is averagely twice as much as the nominal strength due to the combined effect of strain hardening and tension mode behavior. The latter effect subjects the connection to double shear in vertical and horizontal directions. The butterfly-shaped fuses indicate post-yield stiffness and enough redundant strength causing by strain hardening and membrane effect.



a) The BF specimen by Lee et al. (2015)



b) The BF specimen by Ma et al. (2010)

Figure 36. The pushover curves on BF

From the parametric study, the amount of over strength proposed by the Lee et al. (2015) and Ma et al. (2011) could be observed in the models, which averagely have overstrength of 2-3 ( Figure 36). Along the same lines, the parametric study on the modeled BF link indicates that if the links

with narrow mid-width ( $a/b$  equal to 0.1) the membrane effect would take off faster at initial stages of the pushover analysis. The second-order behavior would be happening at initial displacement.

### 2.3. Investigation of Straight Fuses

The Steel Straight Panel Frames (SSP) are among the lateral resisting systems with high energy capabilities, the potential for architectural flexibility, the simplicity of installation and seismic retrofitting possibilities. When the panel is subjected to a horizontal displacement, the links behave as beams in double curvature, dissipating energy in flexure. These “slitted walls” are believed to be the first passive energy dissipation system for buildings as indicated in Figure 37 (Hitaka and Matssui. 2006).

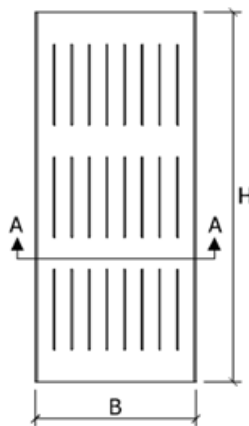


Figure 37. An example of slitted panel [from (Hitaka and Matssui. 2006)]

It is noted that the link, which is made by cutting the plate, would result in the higher amount of ductility compared to the corresponding solid plate (Hitaka and Matssui. 2006, Hitaka and Matssui, 2003). Slit wall shows more flexibility and primarily exhibits flexural flexibility mode behavior rather than predominated shear mode behavior of the original solid plate, which would be mathematically investigated and proved in the later chapters. Moreover, the width over thickness ratio significantly decrease for each one of the links; therefore, the local buckling resistance would be improved. The common issues associated with straight linked plate is the low cycle fatigue and large over strength factor [Chan and Albermani, 2008]. From the previous studies, it was found that if the width over thickness ratio is commonly about 10, the steel shear wall system could

sustain at least 2.5 % drift ratio without buckling. In addition, the gravity load is investigated and it is mentioned that the load demand could be higher than the critical load, which the panel could resist. It is mentioned that the gravity load would not make any problem although important to be considered. The Slitted Steel Plate Frame (SSPF) should have enough resistance for the lateral loads and sufficient stiffness to avoid excessive sway of the building.

The stiffness requirements control the design most often in these systems as well as this requirement control the number of panels needed in the frame. It is important to notice that the rotation of the beams could have a negative effect on the overall stiffness of the SSPF. The optimum stiffness in which the beams are able to have sufficient moment of inertia is proposed by Cortes and Liu (2008). However, the proposed stiffness is about 20% less than the actual real stiffness of the system in general. Therefore, precise equations to estimate the stiffness of such systems are needed. It is also observed that the higher stories would experience a higher amount of stiffness reduction due to higher aggregation of rotation. Therefore, the important factors, which affect the stiffness of the system, are the number of the panels, thickness and the location of the panels.

It is mentioned that for increasing the strength and stiffness of the slitted panel, the width of each link could be changed. The equations stated for the strength and stiffness of the panel could verify this phenomenon. According to McCloskey (2006), the  $b/t$  ratio should be between 10-14 for the sake of the drifts in higher story level.

It is stated that the implementation of stiffener as shown in Figure 38 indicates twice more stiffness and a 33% increase in strength compared to the corresponding without stiffener panels. The global buckling mode and the stress concentration are associated with issues with this type of structures (Figure 38).

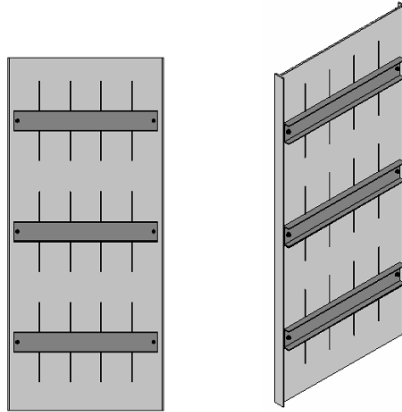


Figure 38. The stiffened straight link panel [from (Cortes and Liu, 2008)]

In another study by Hitaka and Matsui (2006), it was delineated that even the walls designed with details, the flexural links would experience some inelasticity at the top and bottom parts, which is the common areas for flexural limit states. It is delineated that the aspect ratio of the flexural links is an important parameter governing the whole stiffness and strength of the straight wall. It is noted that the procedure of the out of plane stiffening is important for energy dissipation mechanisms. To design such systems in general, it is mentioned that the first yielding of the damping system has to be set low to trigger the energy dissipation as early as possible, while the yielding level of the parent structure has to be set high for the purpose of delaying in serious damages.

The implementation of the straight panel as fuses are getting to be common. Two main features of such damping structures are 1) to have a stable and large energy dissipative capability 2) to have a representative model of cyclic behavior. By arranging the devices in a way that facilitates replacement, damaged devices can be replaced with minimum time and cost, hence interruption to human occupancy is minimized. More often, the straight links are designed such way that the ends would be curved that the stress concentration is reduced by the large amount, this observation would once more be considered in mesh sensitivity study in Chapter six.

Under small relative displacements between the two supported flanges, the strips behave as a series of partially fixed-ended beams and deform in double curvature. One important application of the butterfly-shaped link could be found here as well which is to use the straight panel outside of the floor beam area, as indicated in Figure 39.

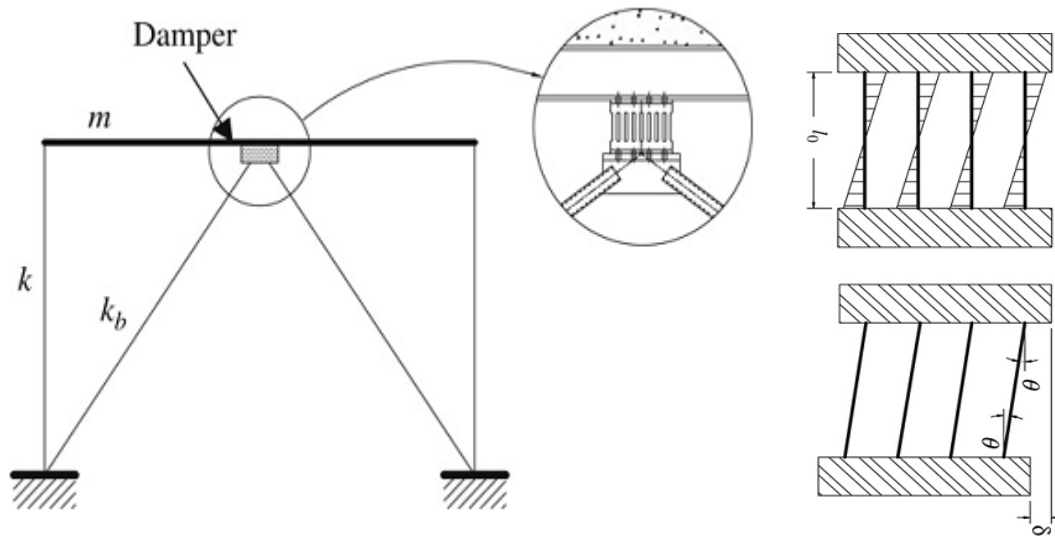


Figure 39. inverted V bracing damping straight panels [from (Hitaka and Matsui, 2006)]

It is observed that the straight links inside of the panel made double curvatures. Specimen with the highest  $b/L$  has the most desirable response in terms of taking more load. The stress concentration is reported at the end of the links, which lead to cracks and ultimately strength degradation. Variable straight link length was not effective in overall behavior of the straight panel; however, more cracks initiated in shorter link length. Lowest  $b/L$  straight panels travel the longest and all the specimens experienced the ductility ratio of 29-40.

The lowest slenderness plate has dissipated energy significantly but cracked early in small displacements. The equivalent damping ratio and effective stiffness are mentioned in Eq. (2) and Eq. (3) as two common parameters for comparing the behavior of the straight panel, which could be calculated for each cycle.

$$K_{eff} = \frac{P_{max} - P_{min}}{\delta_{max} - \delta_{min}} \quad (2)$$

$$\xi_{eq} = \frac{1}{4\pi} E_D / E_{SO} \quad (3)$$

In addition, the strain hardening effect would result in twice strength larger than the first yield strength (Hitaka and Matssui. 2006). It is mentioned that devices with longer and wider straight links behave more flexible while devices with shorter or narrower straight links dissipate more

energy. The shorter straight links suffer from the early crack propagation. Additionally, the crack at the ends of the links propagated after 27 cycles of loading or 500 mm of displacement in usual (Hitaka and Matssui. 2006).

Along the same lines a new structural system, a mechanical joint that is equipped with a metallic damper as the beam-to-column connection is proposed by Oh et al. (2009). They indicated that the proposed connection showed sufficient hysteretic behavior. While the advantages of this connection are the simple construction and superior stiffness of the connection, the compression force can cause local buckling on the beam flange. During an earthquake, it is preferable that the damage is limited to those energy absorption elements that have good hysteretic characteristics and could prevent transmitting forces to the mainframe such as the beam and column.

In addition, the energy dissipation and plastic deformation in this system were concentrated only at the straight dampers, while the inelastic behavior of the beams and columns is prevented through appropriate capacity design according to authors (Figure 40).

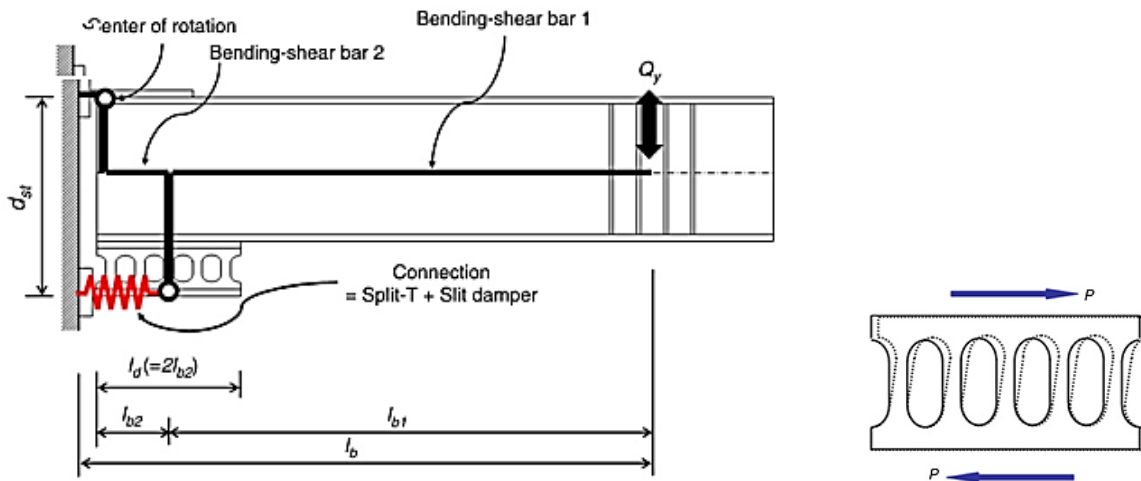


Figure 40. Straight links used at the connection by oh et al. (2009)

It is also mentioned that for the proposed system, initial stiffness is governed by the design of the damper. As the strength of the straight damper increases, the initial stiffness also increases. They stated that the main feature of the damper usage is the fact that after large damage, it could be replaced easily. It is found that the concentration of plastic deformation is mainly at the end of the dampers while the beams and columns remain almost elastic.

Similarly, It is mentioend that implementation of straight could have desirable energy dissipation if the width to thickness ratio would be around 10 (Ma et al., 2010). In the straight shear walls, the hinge location is at the end. However, in the butterfly link the location of plastic hinge depends on a/b ratio and the formation of hinges could be between the end and middle sections.

Köken and Alpaslan Köroğlu (2013) worked on an implementation of straight dampers at the connection zone of a beam similar to Oh et al. (2009). They looked for finding ways to have the beams and columns remain elastic as much as possible under heavy lateral forces, while all the inelasticity and damage would be concentrated at the dampers, which could be changed or repaired easily. Figure 41 indicates a typically extended end plate, a connection with straight damper at the bottom, a connection with straight damper and stiffener at the end.

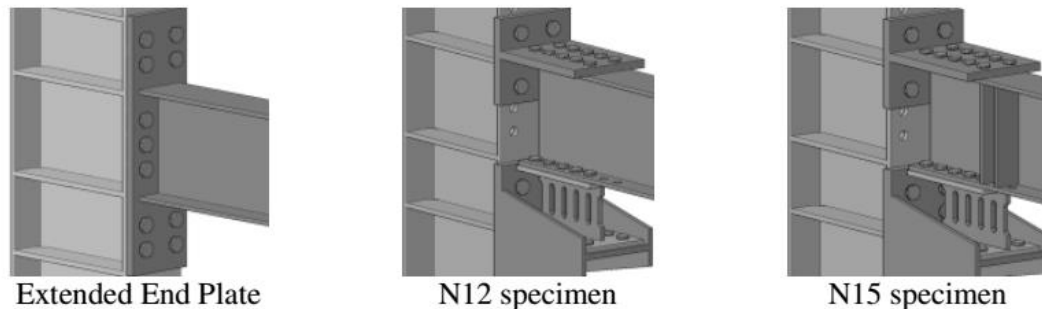


Figure 41. The connection equipped with straight dampers [from (Köken and Alpaslan Köroğlu, 2013)]

The advantage of using a straight damper at the connection zone is the increasing rigidity of the connection while the energy dissipation capability would be significantly reduced. The stiffener would increase the carrying moment strength by 11%. It is mentioned that the traditionally extended end plate connection seems to exhibit stable hysteric behavior and appropriate plastic deformation capacity, the repair for the beams and columns after any applied loading seems to be impossible and ineffective due to local buckling limit states.

Köken and Köroğlu (2012) investigated the implementation of the straight panel for controlling the inelasticity concentration at the end of the beam (Figure 42). The goal of their work is to prevent damages that were placed in the beam-column connection when earthquake occurs. It means that after an earthquake, by replacing dampers in the beam-column connection of the structure, the structure could be still serviceable and no damages would occur to beams, columns,

and the connections. The usage of dampers would not only prevent serious damages to the structure and loss of lives but also it will ensure that it can be repaired and serviceable as soon as possible with minimum cost. The main difference of this work with work done by Oh et al (2009) is that, for Oh et al. (2009) work, it is needed to replace not only the dampers but some of the end frame parts, while for Köken and Köroğlu (2012), it is needed to change the dampers only. One damper is also used in the work done by Köken and Köroğlu (2012) as compared to more than one damper used by Oh et al. (2009). With the aid of the solid elements, the authors computationally analyzed the specimens. The monotonic loading is considered for FE, which was compatible with experimental values with 95% accuracy. The energy dissipation of the specimens with straight links and straight links with stiffener was lower than that of the simple-end moment connection, which was due to the less amount of rotation that the actual beam and column had. However, the stiffness and strength of the system generally were increased by adding straight links at the end. The authors made conclusion that the behavior of the proposed specimens with straight links would be much simpler than the specimen done by Oh et al. (2009). In general, even though the traditional end plate connection has appropriate hysteric behavior, the repair and strengthening of the beam after a possible earthquake would be significant due to occurrence of local buckling in the beam.

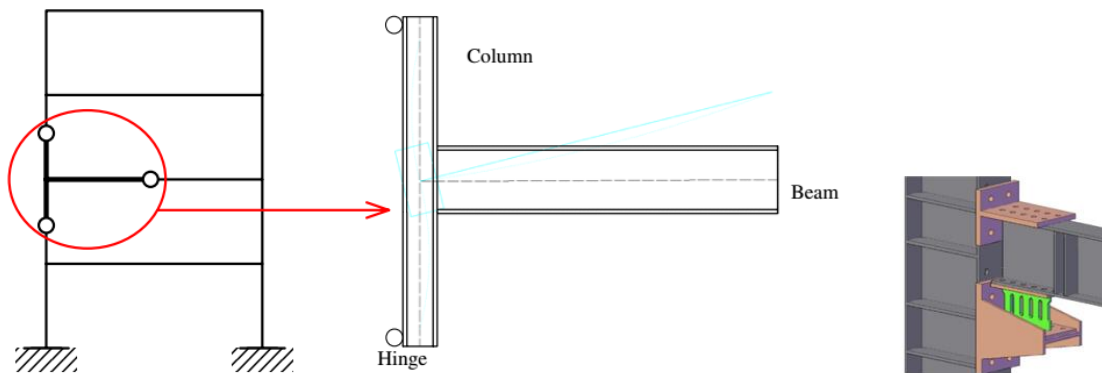


Figure 42. The implementation of the straight links for connection[from (Köken and Alpaslan Köroğlu, 2013)]

## 2.4. Investigation of Hourglass-shaped dampers

Hourglass shaped dampers represents strategically made circular cutout inside of a steel plate, to have the yielding mechanisms occurred before buckling limit states. Aschheim and Halterman (2002) have worked on the beam with cutout inside of the web. Reduced web section is a different

way of web design to shift the yielding from the connection to that of the beam and limit the damage (Figure 43). Large openings are installed inside of the web, and the mechanism and arrangement of these openings are in such a way that the inelastic deformation would happen off the connection area. After the Northridge earthquake, approaches have been devised to improve the connections behavior. All the steel was assumed to have yielding of 345 MPa except the links, which were 250 MPa. Shin et al. (2017) worked on the finite element modeling of the specimens done by Aschheim and Halterman (2002), to capture and validate the behavior.

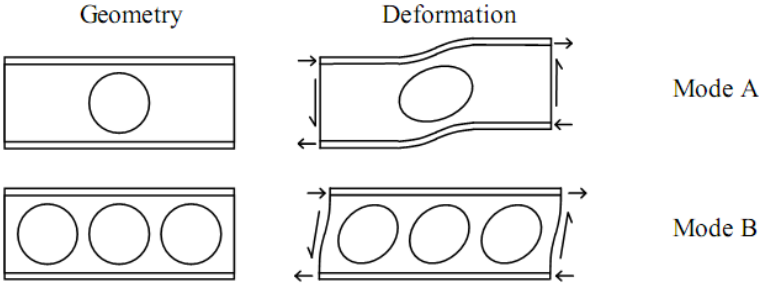
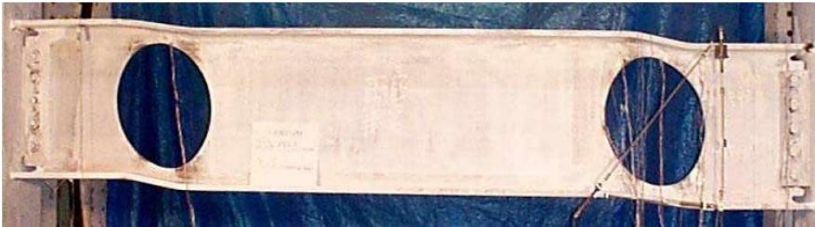
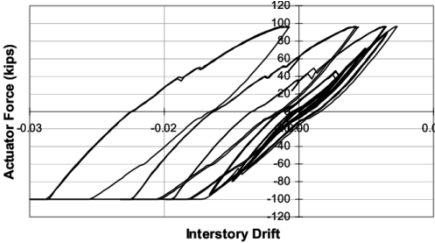


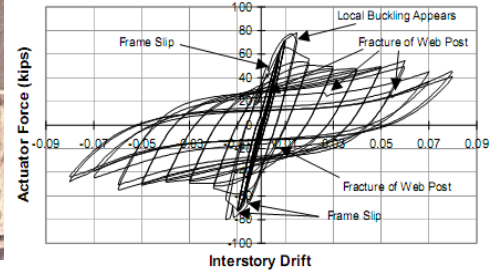
Figure 43. Different configurations of the hole inside of the beam web [from (Aschheim and Halterman, 2002)]

The issue with this test was about gravity loads. In this test as it is mentioned the loading is in lateral format. Therefore, when distributed gravity load is applied to the beam, the shear at the end supports would be higher than the middle part in the same area where the openings are. Therefore, the beam would be vulnerable enough against loading because neither of flanges nor reduced web could be there to resist against loading. The behavior of different configurations of openings is indicated in Figure 44.

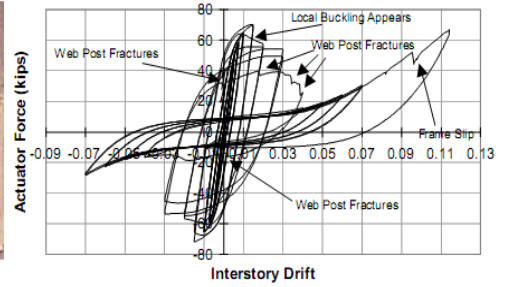
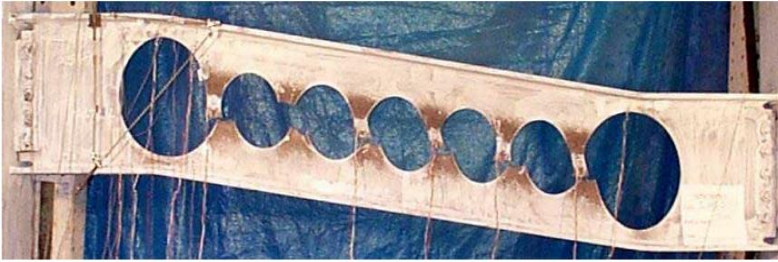


a)

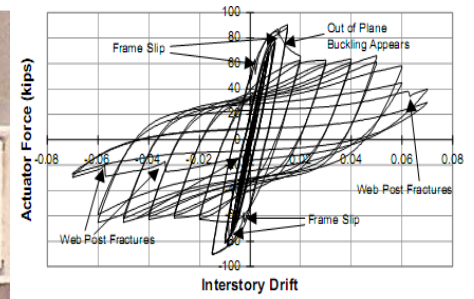




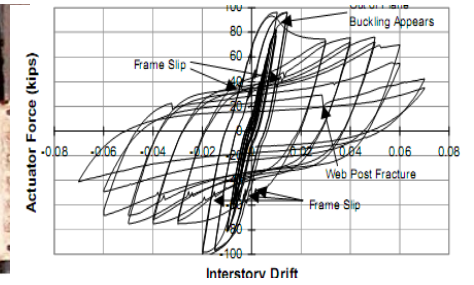
b)



c)



d)



e)

Figure 44. The different configurations and cyclic behavior at 0.06 drift angle [from (Aschheim and Halterman, 2002)]

The two-sided opening could be an option as far as the energy dissipation capacity is not a matter of concern. It is shown that the varying the opening size in Figure 44, could not have the desirable condition as if the flow rate would change and the degradation of stiffness and strength would occur. It is concluded that procedure to postpone the limit states, specifically the buckling limit states is significantly needed. Considering the stiffness, strength and energy dissipation, the specimen number 5 indicated in Figure 44 is better than the rest. Under service loads, the stiffness of the beam should be similar to that of an un-perforated beam. The thicker plate is recommended for having the plate buckles with more delay but generally no well-established procedure to capture, predict, or avoid the buckling condition. Less reduction in strength and stiffness is due to the thicker plates. However, if the thicker plate is used, in lower drifts fracture initiates compared to the slender ones. The connections do not experience any inelastic behavior up to 11% drifts, and the web of the beam initiates the yielding around 1% drifts, and buckling would occur around 1.5% drifts. The important matter is that with having the web buckled, the strengths would be tangibly decreased by 21-33%. Buckling would have higher strength degradation impact, especially in lower thicknesses.

Koppal and Eatherton (2013) have designed a new perforated steel plate shear wall (SSW) with the thicker plate. Steel plate shear walls often experience early buckling and pinched hysteric behavior due to very thin web plates. These systems are in need of large-sized beams especially in the first and last floor to tolerate diagonal tension field imposed by plate buckling. In addition, SSWs with solid plates needs to be supported by moment connections to create resistance against reversed loading condition because the buckled plate has no stiffness unless the post-buckling diagonal tension field would be created in opposite direction. Therefore, the design of SSW with a thin plate, moment connection, and higher sized boundary elements are inefficient.

The proposed shape by the authors (Figure 45), had less strength compared to the solid plate steel shear wall; however, the less demand for boundaries and early buckling prevention have been achieved. Additionally, by varying the size and spacing of the cutouts, the strength, stress, ductility and energy dissipation could be tuned as they have claimed. The fuse plate mostly used in butterfly links are effective in dissipating seismic energy because of initiation of yielding and plastic hinging at the quarter points of the butterfly link which could be designed in a way that yielding spreads

along the length as the loading increases. The reason that the quarter points are observed and how to control the hinging location is not mentioned.

The authors further mentioned that due to the large strength developed by SSW tension field, the designers' implements thinner web plates. As indicated in Figure 45, the pinching behavior of the plate is eliminated and initial stiffness is in the desirable range. In addition, by cutting some straight links on the corner of the shear wall the stress concentration tangibly decreases resulting in fewer demands on the connections resulting in a reduction in fewer boundary elements inward acting forces.

They have suggested that implementation of butterfly-shaped perforation could result in higher strength compared to corresponding circular perforation. In addition, in Perimeter Perforated (PP-SSW), the strength and stiffness are decreased by any reduction in spacing between the perforations (increasing  $D/S$ ) in which  $D$  is the diameter of the hole and  $S$  is the distance between a couple of holes. The distance  $D/S$  that could be a suitable parameter for tuning the strength of the SSW, has a tangible effect on results and increase in thickness. In spite of the PP-SSW, the increase in thickness would result in higher energy dissipation capability.

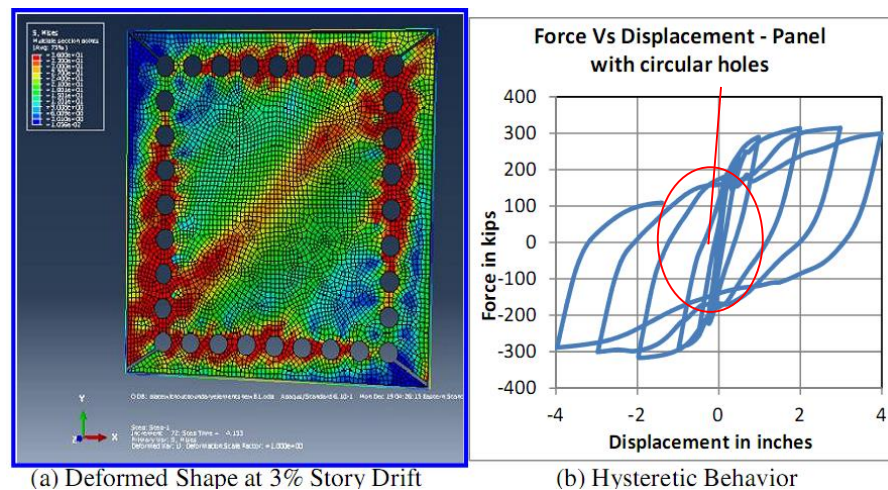


Figure 45. The Perimeter Perforated (PP-SSW) model [ from (Koppal and Eatherton, 2013)]

Some pros and cons of implementation of such strategic perforation existed. In PP-SSW, the ductility is improved, stiffness and strength increased, and it is suggested that the appropriate formulation based on  $D/S$  would result in tunability. The Energy dissipation could be also stated

based on D/S. For BF-SSW with corner edged cut out, less demand on the connection is observed and the energy dissipation is improved compared to PP-SSW.

Along the same lines, Kawai et al. (2016) worked on plates having circular holes inside. Having ring-shaped ribs of burring holes effectively prevented the chance of large out-of-plane waveforms to happen. Large initial stiffness, stable strength, and constant energy dissipation could be observed from the behavior of the plates with circular holes as it is shown in Figure 46.



Figure 46. Steel sheet shear walls with holes [from (Kawai et al., 2016)]

They observed that under medium to large seismic loads the walls had stress concentration at the intervals between the aligned burring holes, and showed elastic behavior without damage. The concentrated stress finally reaches to the ultimate level due to shear buckling or yielding. They mentioned that having ribs around the holes significantly improved the performance of the plate which is shown in Figure 47 due to the prevention of the out-of-plane waveform. It is worthy to notice that the plates had the thickness of 1.2 mm, which is the cause of the early buckling limit state. It is concluded that the walls with bearing holes allowed shear stresses to be concentrated between the aligned holes which ultimately ended up in shear buckling and shear yielding.

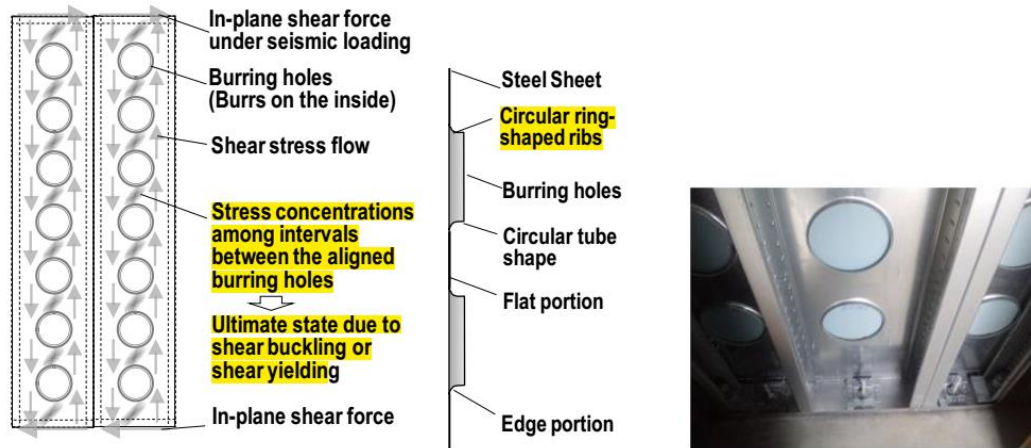


Figure 47. The ribs and stress concentration [from (Kawai et al., 2016)]

## 2.5. Investigation of Perforated Steel Plates and Ring Shaped Fuses

It is not common to produce specific types of Low Yield Steel (LYP) steel plate with various yielding properties in the market; hence, based on the design procedures, the need for uncommon types of plates might still be existent (Berman, and Bruneau, 2003). Three different configurations of steel shear walls were studied by Vian et al. (2003) as shown in Figure 48 for addressing the mentioned issues. The Solid Plate, Cutout Reinforced Corner and Perforated Steel Plate were investigated. The problem addressed in this study was to produce low strength and stiffness for cases when the Low Yield Point (LYP) steel plate is not available. The large thickness means larger stiffness, which ultimately results in lower displacement during a seismic event. Subsequently, this lower displacement would lead to large forces on the boundary and surrounding elements, which must be detailed to ensure adequate performance.

Vian et al. (2003) studied the steel plates with perforated holes. The test was concluded at the 3% drift when the continuing plate weld began to experience some fractures leading to subsequent distortions. The ATC 24 loading has twisted the top beams a little bit, not severely, but the columns twisted and led to a severe distortion of the top beam at the end of the test, which was at 3% drift. In addition to that, the web buckling in the lower beam has occurred around the 1.5 % drift of the shear wall near the RBS location. The testing has ceased following the strength drop at 3 % of drift due to rupture of the bottom flange in each beam RBS connection.

The Perforated Plate (PP) specimen behaved well especially in the elastic small displacement and exhibited a stable hysteric behavior in the inelastic range. The stiffness and strength have been reduced, as it was desired compared to the solid plate. Yielding spread through the entire wall between the holes in the narrow regions of the links. One of the interesting issues was the reduction of the audible sound of the buckling of the panel, as the specimen cyclically loaded which could be beneficial in a building application, towards the negative perception of the building occupants.

The corner cutout steel plate exhibited a stable hysteric behavior until 2.5% drift, during which, ruptures occurred in the lower flange of each RBS beam. This event significantly changed the load path resulting in a 20% reduction of strength and termination of the loading after two cycles at 7 % drift.

The perforated panel showed a promising behavior toward the alleviation of the stiffness and over-strength concerns using conventional hot-rolled plates useful for the markets in which LYS is not available. In addition, this option could opt for the provision of the access for utilities to penetrate into the system; in addition, the perforation could be highly important for retrofitting the building purposes.



Figure 48. The test by Vian et al. (2003)

Along the same lines, Egorova et al. (2014) and Phillips et al. (2014) indicated that, although implementation of SSWs could lead to fast and economical construction, more space and thinner wall systems, there are quite a few problems. The hysteric behavior of the SSW is very pinched, during load reversals, the infill plate does not interact to add stiffness to the resistance system, and

there is a need for moment connection leads to noticeable expense. New Ring Shaped Steel Shear Wall is proposed to control buckling (Figure 49). By implementation of this shear wall system, the need for moment connection would be eliminated, and the full capacity of infill plate would be incorporated. They have indicated that due to large inward pull on the boundary elements from diagonal tension field, especially in the first and last story, thinner infill plates are chosen. Hence, the welding could be problematic for these conventional SSWs. Furthermore, utilizing ringed shaped shear walls would lead to fuller hysteric behavior without the necessity of moment connection, the capability of strength, stiffness and ductility tunability.

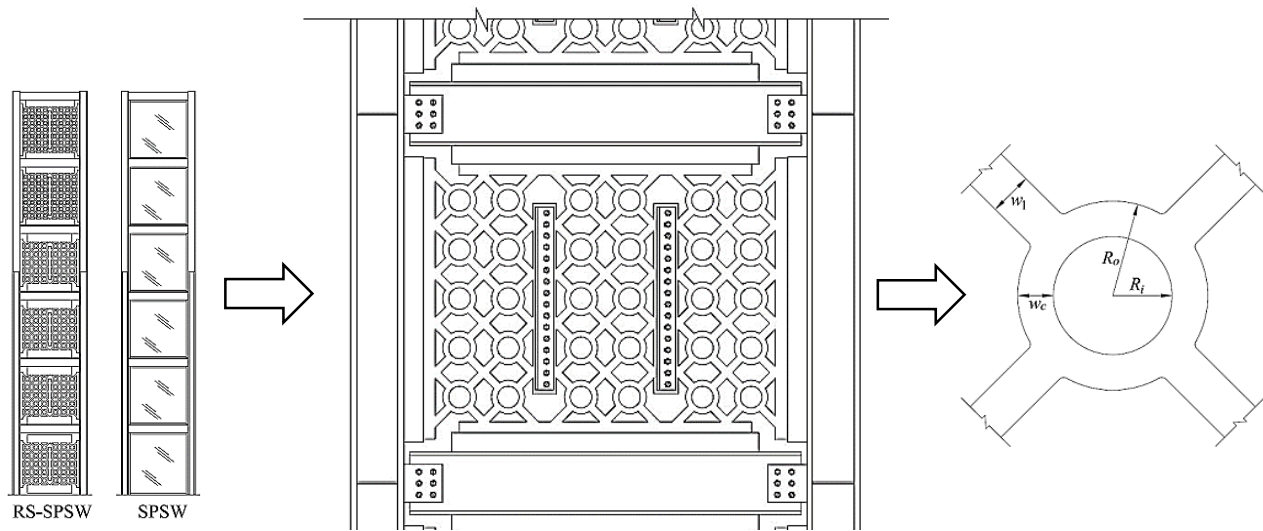


Figure 49. The ringed shaped steel plate shear wall [from (Phillips et al., 2014)]

The concept of utilizing ring-shaped cutouts is based on the elongation of the ring in direction of tension field ( $\delta_1$ ), and the shortening in direction perpendicular to the tension field would occur ( $\delta_2$ ). The relation between these two displacements could be achieved by Uler Formula. Figure 50 indicates the relation between elongation and shortening of the ring shape as well as the comparison between ringed shaped steel plate shear walls with simple solid plates. As it is indicated in previous literature, the  $\delta_2$  over  $\delta_1$  indicate the position ratio. The different displacement values indicated in Eq.(4) for solid plates is the reason why the excessive material initiates the buckling.

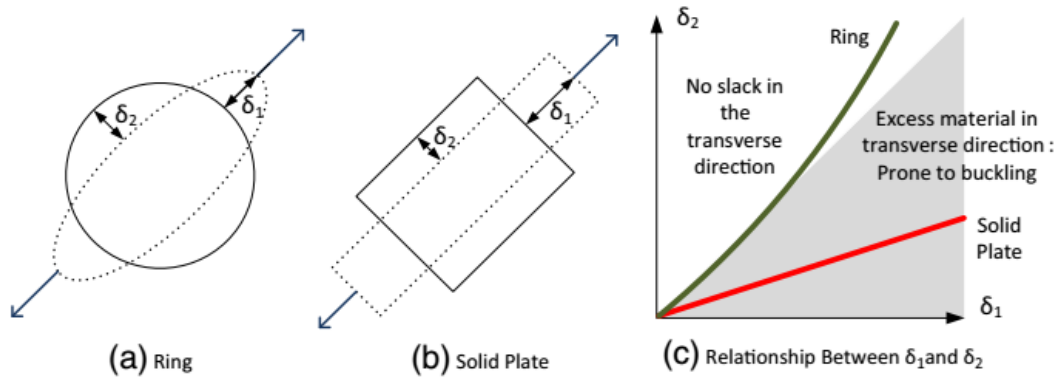


Figure 50. The concept of ringed shape steel shear wall [from (Phillips et al., 2014)]

$$\delta_2 = r - \frac{1}{2} \sqrt{4r^2 - 4\delta_1^2 - 8r\delta_1} \quad (4)$$

From software and experimental tests, Egorova et al. (2014) have concluded that implementation of ringed shaped steel plate shear wall could be highly beneficent regarding the pinching behavior, although the basic analytical work is done a long time ago. The important factors are plate thickness, ring radius, ring width and a number of cutout circle in a row. The infill plate strength could be estimated by the following formulas:

$$\phi V_n = \phi \cdot \frac{\frac{4}{\sqrt{2}} N_r M_p}{[R_i - \frac{W_1}{2}]} \quad (5)$$

$$M_p = \frac{F_y W_c^2 t}{4} \quad (6)$$

In which,  $N_r$  is the number of cutouts per row,  $F_y$  is the yielding strength,  $R_i$  is the inner radius,  $t$  is the plate thickness,  $R_0$  is the outer radius,  $W_1$  is the link width,  $W_c$  is the ring width. There are some issues still with the proposed system. Two important issues are mentioned in this work: First, the initiation of fractures inside of the plate near the fishplate in the test could change the flow of the stress and out-perform the plate. Second, the economic and precision aspect of cutting should be considered. There are some slenderness recommendations on  $R_0$ ,  $t$ ,  $W_c$  to have enough buckling and load reversal resistance as follows.

$$\frac{R_0}{t} \leq 18 \quad (7)$$

$$\frac{W_c}{t} \leq 8 \quad (8)$$

$$2.5 \leq \frac{R_0}{W_c} \leq 3.33 \quad (9)$$

In this study, the effect of ringed shaped steel plate shear wall has been investigated on the multi-story shear wall. As the story level goes higher, the number of circular rings inside of the plate would increase. This would lead to first higher construction cost due to having more cutouts length, second, by putting more circular openings, the probability of fracture would be increased. It is concluded that, by utilizing the ringed shaped steel plate shear wall, the shear wall would maintain the stiffness during load reversals, indicating that there would be no need to implement a moment connection. In addition, the hysteric behavior of the ringed shaped steel plate shear wall indicates more stable hysteric behavior, the higher capability of energy dissipation, the capability of being tuned as well as more economical boundary elements.

## **2.6. Investigation of Triangularly shaped fuses**

Asselin et al. (2012) investigated the effect of implementation of triangular fuses in hybrid systems. The system is constructed with masonry wall with steel frame (Figure 51 and Figure 52). The particular fuse was manufactured from a 6" (153 mm) wide by 1/2" (12.7 mm) thick A36 flat bar using a plasma cutter (Figure 52). In general, there are two designing procedures for these plates, first, the fuses are designed to be strong enough to remain elastic during loading in which the masonry wall is the element with energy dissipating capability, and the second way is to design the fuses as the energy-dissipating element so that the masonry walls remain elastic. The second method has been used and investigated in this study (Figure 53).



Figure 51. Implementation of specific links to dissipate energy in masonry structures [from (Asseelin et al., 2012)]

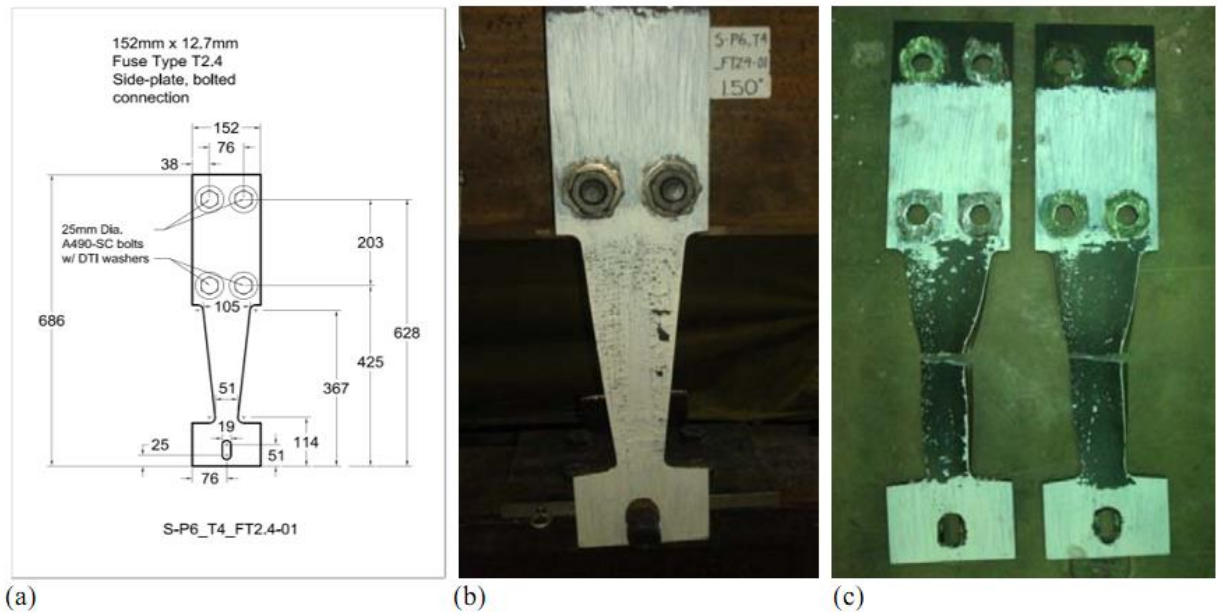


Figure 52. The geometry of the triangular fuse [from (Asseelin et al., 2012)]

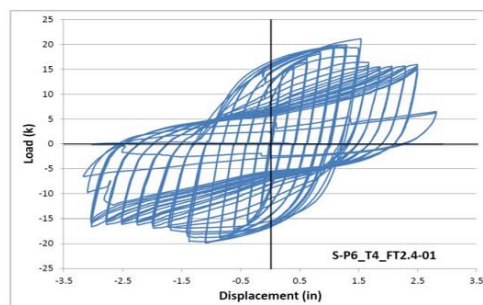


Figure 53. Geometry and properties of fuses and hysteric behavior of fuse [from (Asseelin et al., 2012)]

The peak lateral load of 20 kips and maximum displacement of 2.75 in has been observed. The torsional buckling immediately after ultimate load caused the fuse to lose a significant amount of strength and stiffness. It is shown that the torsional buckling limit state should be studied thoroughly to avoid these modes reducing the load-bearing capacity. Different story level buildings have been modeled, and it is concluded that this kind of structures could be constructed with lower heights in places with high seismicity.

## 2.7. Investigation of solid plate

This type of links is commonly used in a various application for the seismic resistance purposes. Ji et al (2015) proposed a new set of the short shear link (Figure 54) for coupling beams, which can be replaced after significant damages. The shear links are mainly designed for EBF systems with lower values of yielding strength to ensure the ability of energy dissipation under high seismic loading condition. However, the main issue associated with short shear links, according to authors, is the large over strength factor leading to significant boundary element sizes.

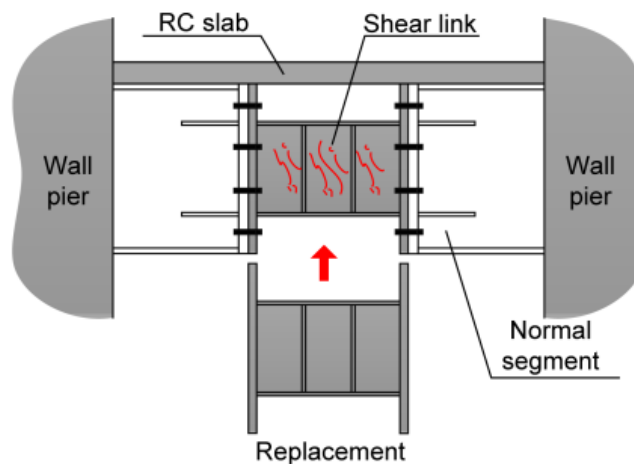


Figure 54. The experimental test done by Ji et al. (2015)

The values suggested in AISC 341 for over strength is less than 1.5, while the short links studied by Ji et al. (2015) reached 1.9. However, the inelastic rotation capacity, which is the ability to

maintain at least 80 percent of the maximum strength in their test, was about 0.15 rad, while this value is implied in AISC 341 to be 0.08. In addition, the effect of the stiffener is studied, and it was observed that if the stiffener spacing requirements proposed by the codes were met then the stable hysteric response, as well as inelastic deformation capacity, would be achieved. However, it does not mean that the overall response would be significantly different if the spacing is 50 % more than what is suggested in the codes for spacing requirements. It is worthy of mentioning that the overstrength factor could be estimated by dividing the maximum shear value ( $V_{max}$ ) over the designed shear which is the smaller of the equations in AISC 360 for shear and flexure ( $V_p$  or  $2M_p/L$ ).

Along the same lines, Castiglioni et al. (2012) have studied the fuse implementation in composite steel frames. Their study has investigated the behavior of two different types of seismic resistant structures, in which the damage would only concentrate on fuses. The fuses could be replaced and changed easily after being damaged. Like bumpers in cars that absorb the crash energy and are replaced afterward, innovative devices will be developed to dissipate energy, protect the overall structure and may be disassembled and replaced after a strong earthquake. The links connecting the beam to connection joints are indicated in (Figure 55).

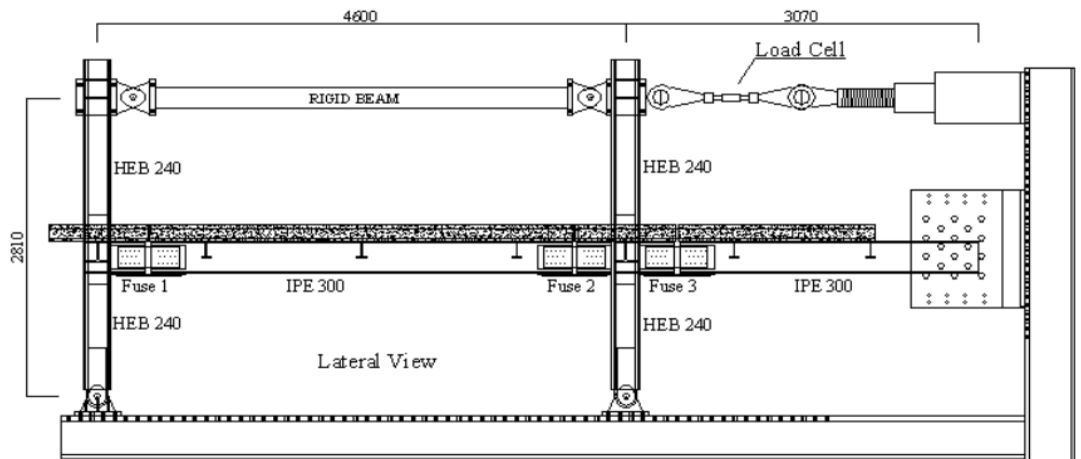
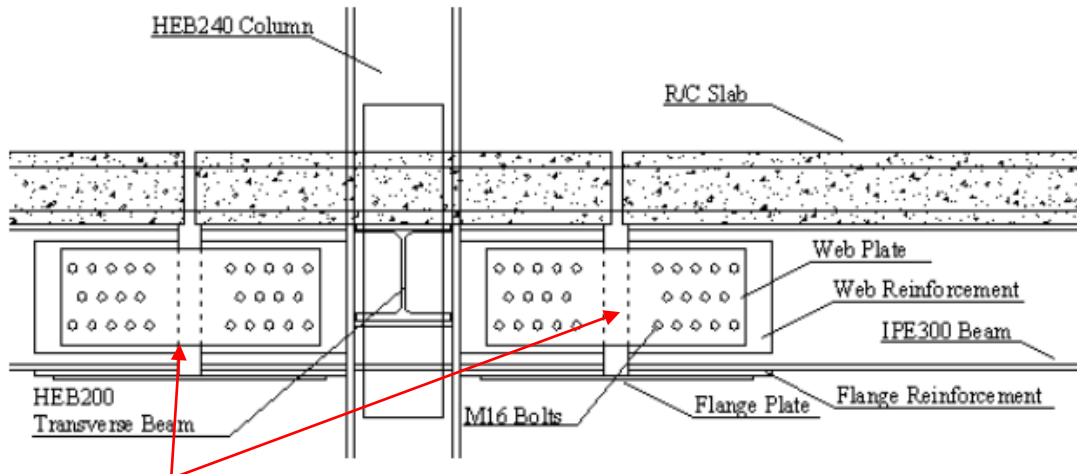


Figure 55. Links used in-between of the beam section [from (Castiglioni et al., 2012)]



Rectangular links Figure 56. The link details [from (Castiglioni et al., 2012)]

Thanks to this connection arrangement, the center of rotation at the fuse device is shifted above, and it stays in between the two reinforcement layers. As a result, the steel plates in the fuse devices can be easily deformed and buckled, causing energy dissipation without damaging the whole structure. At the same time, the reinforced concrete slab does not get a significant damage due to large story drifts, which cause large rotations in the fuse devices. There are four different configurations used as the flange plates (Table 1) which could indicate the normal thicknesses considered for these links.

Table 1. The link properties [from (Castiglioni et al., 2012)]

Specimen	B (mm)	t (mm)	Area of cross section (mm <sup>2</sup> )
Flange Plate A	120	10	1200
Flange Plate B	170	10	1700
Flange Plate C	150	12	1800
Flange Plate D	140	8	1120

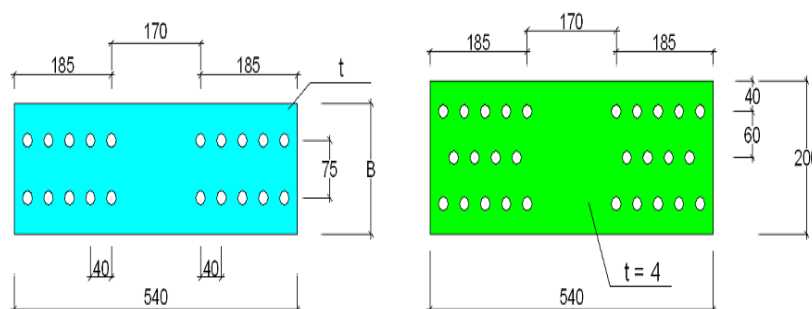


Figure 57. Links configurations [from (Castiglioni et al., 2012)]

The maximum rotation of 42mrad is recorded for the fuses. Therefore, it can be pointed out that the thickness of the plates in the fuse device D was too small to achieve the desired ductility, while the other devices gave satisfactory results. It has been suggested that the alpha ratio (the ratio of fuse moment capacity to that of the beam) should be in the specific range as follows indicated in Eq. (10):

$$0.4 < \alpha < 0.75 \quad (10)$$

One of the main advantages of the “FUSES” design approach is the reparability. After the seismic event, the damage is concentrated in the fuses, and the rest of the structure would remain elastic, without having any plastic deformation. During the experimental activities, it is observed that the damaged fuse plates can be replaced. After each test, two workers accomplish the replacement of three fuse devices in about 1.5 hours, which means that the process of changing such fuses seems to be fast.

It is mentioned that the implementation of low yield point plate would have significant appropriate performance due a couple of reasons (Katayama et al., 2000 ): the low yield steel would act as fuse since the yielding point is less than the other elements in structure, and the elongation of this type of steel is highly more than other types of steel which induce significant ductility in the system. It is indicated that the static loading results would be different with the dynamic loading ones. The 20% increase in the results of actual time-history loading compared to static loading is expected. The reason according to the authors is the strain hardening which consists of kinematic and isotropic hardening. The cumulative ductility factor under static loading would be less than that of the dynamic loading due to the fact that the shear resistant is higher in the later one. This phenomenon is observed in energy absorption capability for the same reason as well.

Chaofeng et al. (2012) studied improvement of deformation capacity of the low yield strength steel shear panel damper. It is indicated that the arc transition of-of the plate could be effective only in the elastic region, and this type of transition would not be significantly effective under large plastic strains. It is needed to be careful about designing the holes inside of the links since these areas are subjected to low cycle issues. In general the sharp discontinuities, it is better to be

prevented as much as possible. In addition, 70% shear strain is largest deformation capacity that the panels could experience. Chan et al. (2009) investigated the yielding of shear devices. They mentioned that common stiffness equation would be significantly off compared to equations proposed.

## 2.8. Investigation of miscellaneous shapes and further investigations

### 2.8.1. Metal band

Previously shear walls with banding system were proposed as a shear wall with metal band energy dissipater as shown in Figure 58 (Juan Enrique and Martinez-Rueda, 2002). It is mentioned that if the shearing and normal stresses making the band yielding are chosen properly, this panel is able of significant energy dissipation. The problems associated with the proposed shear wall were the significant details between the actual panel and the banding metal, which makes significantly expensive to be installed.

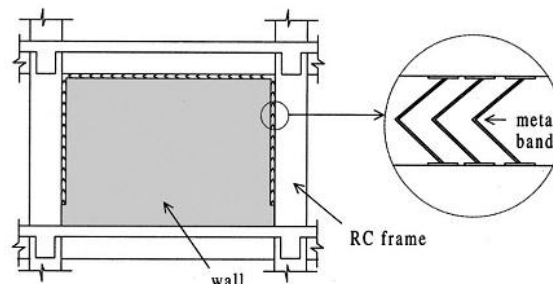


Figure 58. The dissipation links between the panel and the boundary frame [from (Juan Enrique and Martinez-Rueda, 2002)]

The U shape dissipation devices (Figure 59) are proposed as another type of dissipation device, the semicircular shape moves along the strip and this change in radius curvature from semicircular to straight conditions would make the energy dissipation mechanism.

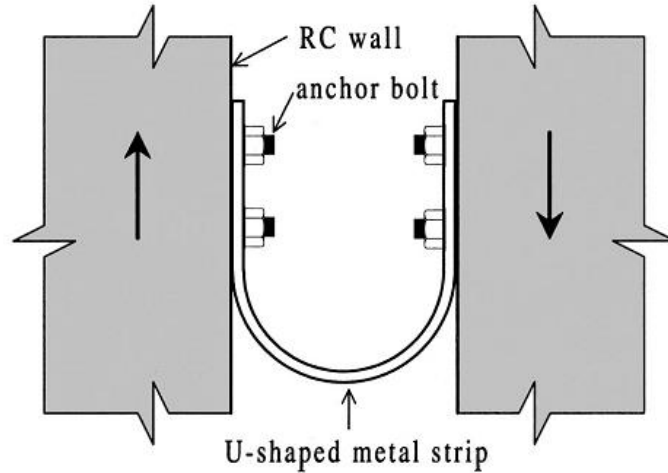


Figure 59. U shape dissipation device [from (Juan Enrique and Martinez-Rueda, 2002)]

Following this innovative U shape dissipation device, the oval element has been introduced which has the complex analysis as the rolling and yielding mechanisms experienced by steel strips work at the same time. Low stiffness is expected for such devices shown in Figure 60.

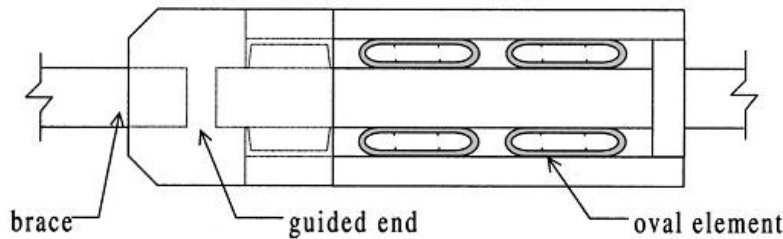


Figure 60. The oval dissipation device [from (Juan Enrique and Martinez-Rueda, 2002)]

Along the same lines, the behavior of the pipes filled with and without concrete is investigated in another article by Maleki and Bakeri (2010). Four bare and two filled steel pipes are investigated. As of previous studies, one of the well-known devices devised to avoid inelastic behavior through the flexural-yielding mechanism of deformation is ADAS. The U shape strip has introduced to operate with very large displacement in the inelastic range and dissipate energy through plastic deformation of the steel. It has been observed that the pipe with concrete despite the large amount of initial stiffness, did not have the stable hysteric behavior as compared to the pipe without any concrete infill. This is because of the fact that the pipe with concrete lost a sudden large amount of stiffness and strength at a specified step.



Figure 61. The pipe filled with concrete [from (Maleki and Bakeri, 2010)]

It was concluded that the bare steel could have promising potential of energy dissipation capacity only if the details are correctly done.

### 2.8.2. E- Shape

Xiang et al. (2017) worked on the two common types of hysteric dampers. E- Shape, which shows appropriate energy dissipation capacities through each cycle of loading. It indicated an efficient seismic control of the system and economical provision of stable solutions for seismic retrofitting. The E- Shape damper is proposed having three elastic legs and transverse beams as indicated in Figure 62. This damper is cut from a thick mild steel plate and then optimized so that the plasticization is almost uniformly distributed without having localization of deformation in any parts of the damper. The links are to be remained elastic while the transverse beam is subjected to nearly flexural moments. The Energy Dissipating Bearings (EDB) and E-Shape steel damper group are among the common implementation of such systems.

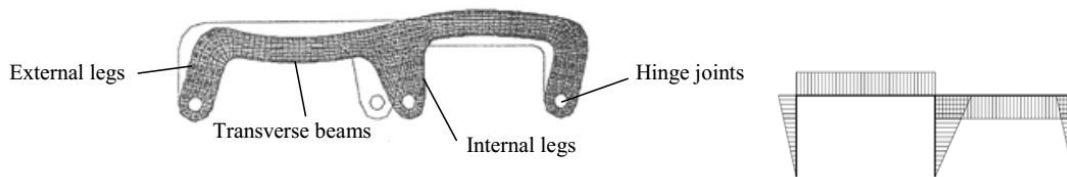


Figure 62. E- shape link [from (Xiang et al., 2017)]

In addition, the authors worked on the X- Shape dampers (which is another name for the butterfly-shaped dampers). They concluded that these dampers show a great damping, hysteric curves, appropriate insensitive behavior under environmental effects, and low maintenance. The installation of the X- Shape dampers improves the stiffness, the yielding of the dampers would limit the build-up of inertial forces significantly, and protecting the substructures from severe damages compare to other dampers. Besides the common advantages of these dampers, which is substantial energy dissipation capabilities, preventing the seismic unexpected vibrations under service loads, and reduction of seismic demands could be considered.

### 2.8.3. Effect of cut-outs in steel plate and corrugated plates

In regard to the installation of perforation, a different work done by the Shubhrata and Sanyal (2011) have been proposed to indicate cutout concept for reducing the stress concentration. The presence of holes and notches in structural elements would result in stress concentration. This stress concentration will eventually lead to lower mechanical strength. Efforts are made to reduce this stress concentration. Stress relief holes or notches are proposed to be implemented around the main hole. Stress concentration can be reduced by introducing smaller auxiliary holes near the original hole. This would help to smooth the flow of the tensile principal stress. According to previous literature utilization of stress relief holes could lead to a reduction in stress concentration factor (SCF) up to 30%. It is shown that the presence of auxiliary holes/notches will reduce the SCF value around main discontinuity (Figure 63).

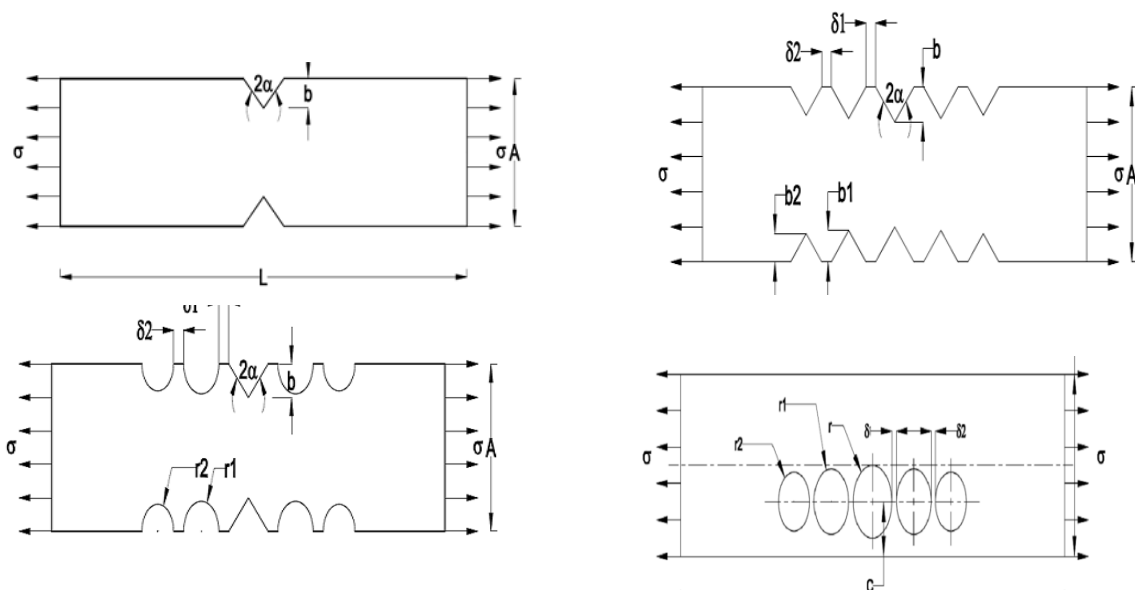


Figure 63. The different stress relief holes configurations [from (Shubhrata and Sanyal, 2011)]

In Figure 63, the auxiliary V notches and auxiliary semicircular holes around the main notch are shown. It is stated that both auxiliary holes and notches had a significant effect on the SCF reduction; however, the reduction percentage would be higher for the V notches ones. It has been reported that maximum mitigation is by providing two sets of relief notches.

Along the same lines, Farzampour et al. (2015) have investigated the effect of the opening in corrugated steel shear walls with. The corrugated plate could have out of plane resistance against buckling; therefore, the out-of-plane buckling would be postponed if this type of wall would be implemented. The corrugation geometry would make out of plane resistance against buckling (Farzampour et al., 2018c; Farzampour et al., 2018d; Farzampour et al., 2017) , this happens for any adjacent pane as it is indicated in Figure 64, the plastic strain for simple steel shear wall is significantly higher than that of the corrugated steel shear wall. The plastic strain could be considered as the initiation of crack inside of the plate. It is worthy of notice that implementation of corrugated steel panel could be a suitable solution for perimeter perforated steel plate shear wall or ringed shaped steel plate shear wall because one of the main concerns about these shear walls is the early cracks which are tremendously correlated with high plastic strain values (Ghabrai et al., 2010)

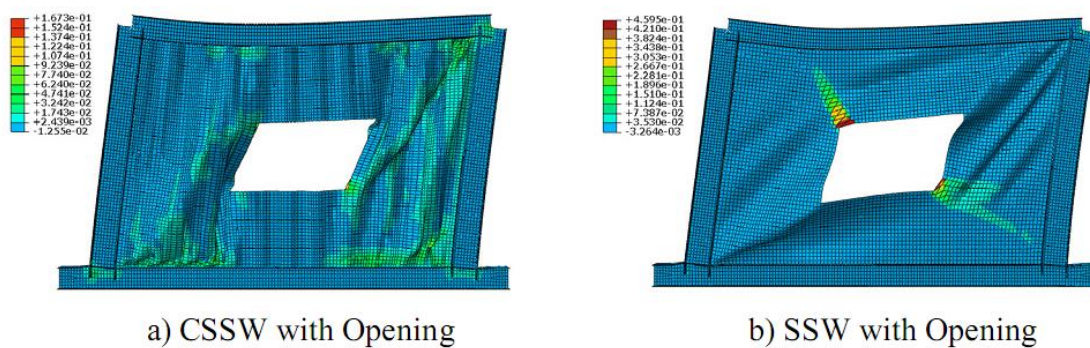


Figure 64. The effect of opening on the reduction of damage concentration [from (Farazampour et al., 2015)]

The concept of creating openings in the corrugated steel sheathing was to force the material yielding and rupture to occur in the sheathing at the opening locations, and to make the out of

plane deformation and material yielding to be the energy dissipation mechanism of the shear wall. Another advantage of installation of the openings in the sheathing was that the damage locations could be controlled to be away from the boundary elements and fasteners on the edges so that the building could be intentionally protected from collapse. Different whole configurations were tested in this project. The concept of creating openings in the corrugated steel sheathing was to force out of plane deformation and material yielding to be the efficient energy dissipation mechanism of the shear wall. It was expected that the wall would lose its strength gradually as the ruptures grow gradually during the cyclic loading. Another advantage of introducing the openings in the sheathing was that the damage locations could be controlled to be away from the boundary elements and fasteners on the edges so that the building could be intentionally protected from collapse.

## 2.9. Topology optimization on links

A number of studies are conducted to improve the general behavior of the links subjected to loading reversals using topology optimizations. He et al. (2106) worked on the topology optimization of the steel plate fuses having a low yield. They investigated the best interior and boundary hollows to have maximum stiffness, and to have a full stress state as the objectives for a specified volume reduction rate. According to the authors, full stress design is widely accepted and used in structural optimization analysis. The authors recommended the low yield steel to be implemented due to the fact that not only the low yield point steel would be able to absorb the shock appropriately but also has high stability and safety. The authors started to work on the already proposed dampers by Deng et al. (2014) as indicated in Figure 65.

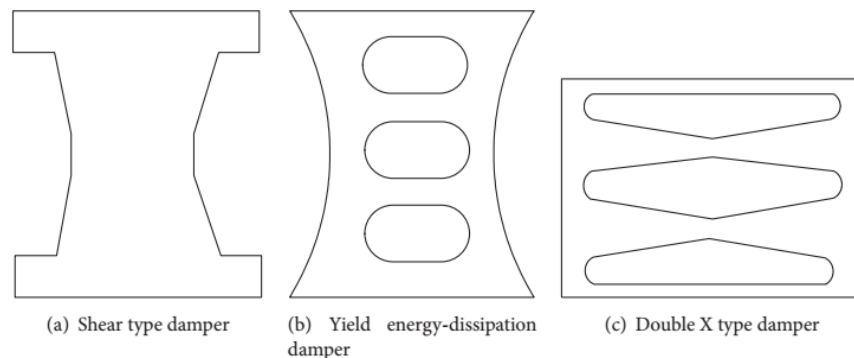


Figure 65. The proposed shapes by Deng et al. (2010)

The general concept of optimization started with one of the commonly used dampers, and the minimum volume reduction rate is set. After the shape optimization, the stress contours are checked to have uniformly distributed stress all over the link. If the result of the stress is uniform, then the shape is optimized for stress distribution. If the stress is not uniformly distributed, those areas that the stress is low would be removed or weakened. Once again, the volume reduction rate would be assigned to the models, and the next step would be similar to the previous ones. Figure 66 indicates the optimization flow chart used in He et al. (2106). Figure 67 indicates the final results of the optimization study.

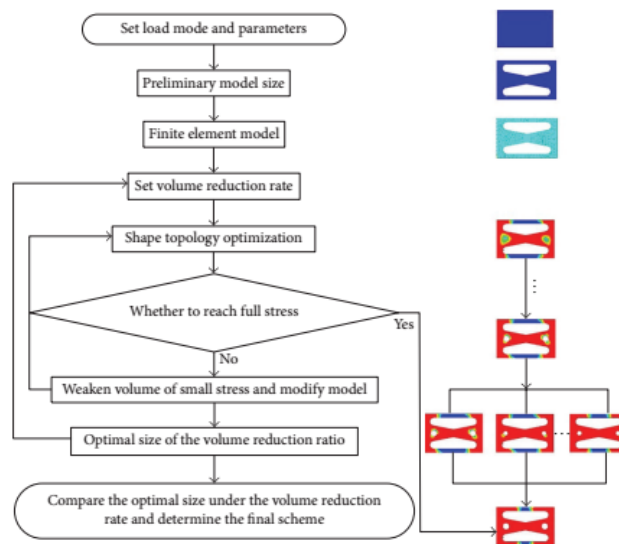


Figure 66. The optimization flow chart [from (He et al., 2106)]

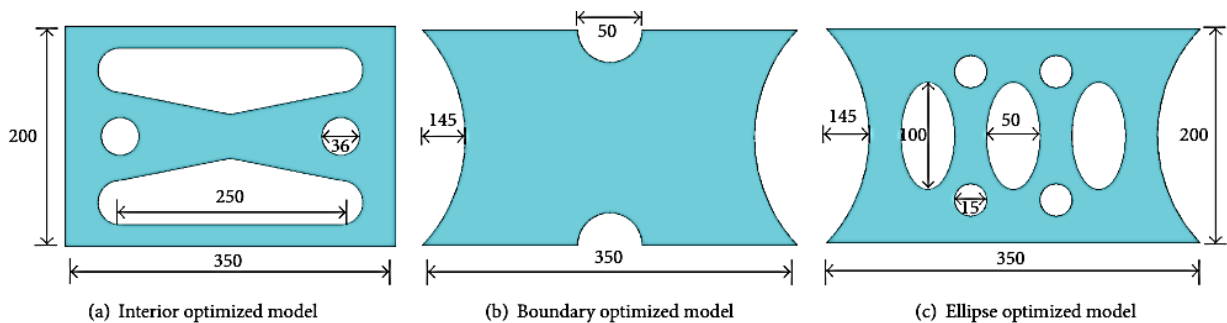


Figure 67. The optimized shapes based on the stress distribution [from (He et al., 2106)]

The damping ratio and damage index for the proposed shapes are calculated by the authors. It is concluded that the damping performance of a low yield point metal damper is excellent, stable and it would improve the structural load-carrying capacity. The results also indicate that the damage index and damping ratio are almost equal for the proposed shapes. However, the pushover load for boundary-optimized dampers is highest while the interior optimized damper is the lowest. The boundary-optimized dampers have better performance in dissipating the energy than interior optimized damper, which is the recommendation of the author for practical use.

Deng et al. (2010) presented a shape optimization method to improve the low cycle fatigue performance steel shear panels. This method is based on the fact that the low cycle fatigue performance of steel plate is negatively affected by the maximum plastic strain (PEEQ). The simulated annealing algorithm is used for the optimization purposes. In this study, the maximum plastic strain under a prescribed cyclic loading is considered as the objective of optimization. The low cycle fatigue is reported in the literature as one the main concerns associated with butterfly-shaped and straight links. The finite element analysis is done with the aid of the FE software on the models with shell elements. The kinematic hardening is chosen as the consecutive model (Figure 68).

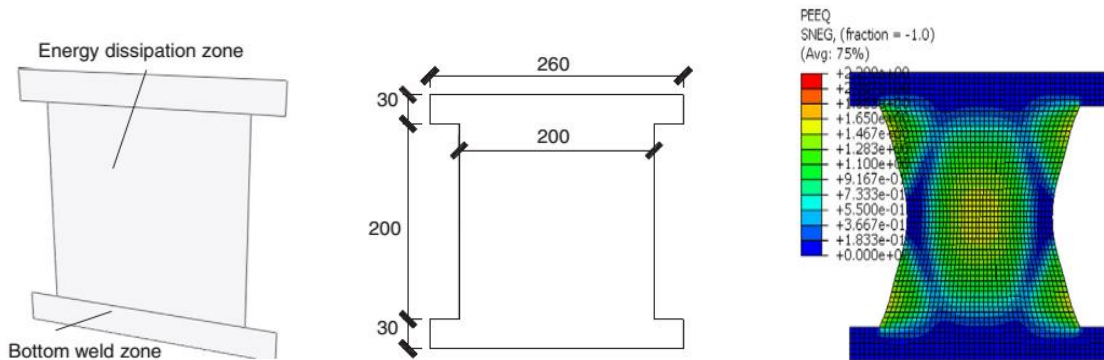


Figure 68. The plate optimized for min equivalent plastic strain [from (Deng et al., 2010)]

The main purpose of this study was to have more energy dissipation at the central parts of the link and to have uniformly distributed plastic strain all over the plate.

Xu et al. (2010) worked on the straight steel plates to improve them by using new sets of shapes with shape optimization methodologies. They claimed that the only stresses working in butterfly-shaped dampers are associated with bending stresses if the height to weight ratio is 5 or more.

They recommended using the width of the damper in a way that it varies with root mean square of  $z$  to have the dampers experience yielding at the same time over the link. It was concluded that the stress concentration could be avoided by changing the width to height ratios.

Along the same lines, Ghabrai et al. (2010) implemented the Bi-directional Evolutionary Structural Optimization as a well-established optimization methodology to propose the better-performance dampers from the straight dampers. They mentioned that the properties of an appropriate damper are to possess sufficient elastic strength and stiffness such that the device does not excited to the inelastic region under service loads. The damper should have stable energy dissipation capabilities and it should have reasonable resistance against low-cycle fatigue. In the Bi-directional Evolutionary Structural Optimization optimization method, besides removal of the inefficient elements, the rest of the efficient elements would be improved. The algorithm maximizes the plastic dissipation, which would lead to less concentration of stresses compared to initial design. Figure 69 indicates the basic model for optimization study. The optimization objective function in this study is plastic energy dissipation for a 10 mm thick straight link with a fixed volume constraint. Figure 70 indicates the basic and optimized dampers. The energy dissipation and stress concentration have been improved. The butterfly-shaped damper has dissipated 37% more energy compared to the straight ones. The experimental test on the dampers also indicated that the low-cycle-fatigue have been improved significantly.

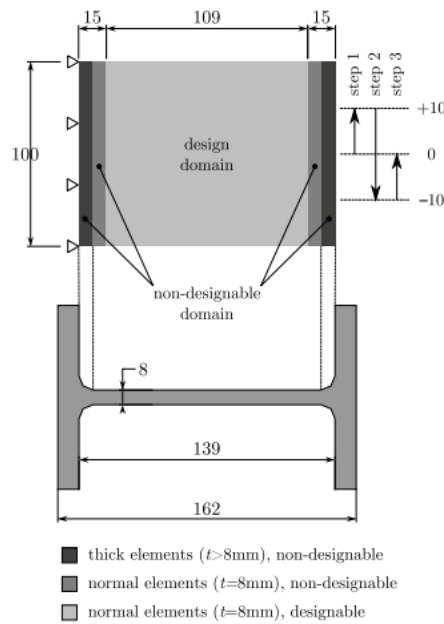


Figure 69. The initial model before optimization procedures by Ghabra et al (2010).

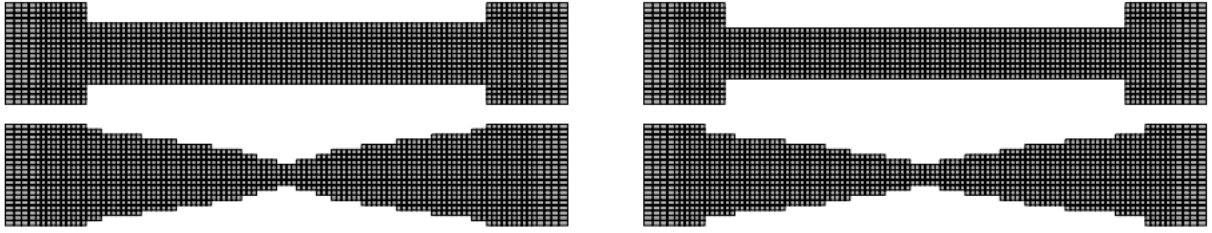


Figure 70. The optimization procedures on damper [from (Ghabra et al., 2010)]

Liu and Shimoda (2013), worked on the optimization of butterfly-shaped links based on the minimization of the maximum cumulative plastic strain, with regard to having a minimum specified energy dissipation capability.

In general, if the steel plate dampers are not properly designed, the cracks could initiate at the edges and corners in the early stages of cyclic loading due to stress concentration and grow along with each cycle that eventually would decrease the energy absorption capability drastically. They did shape optimization based on numerical analysis. To avoid buckling in the plate, the equation for critical buckling stress is met also as indicated in Eq. (11) and Eq. (12).

$$\left(\frac{W}{t_w}\right) = \frac{W}{t_w} \sqrt{\frac{\sigma_y}{E}} \quad (11)$$

$$\frac{\tau_{cr}}{\tau_y} = 1.02 \left[ \left(\frac{W}{t_w}\right) - 0.26 \right] + 0.6 \quad (12)$$

In which the  $W$  and  $t_w$  are the width and thickness of the plate at the initial stage as shown in Figure 71.  $\tau_{cr}$  and  $\tau_y$  are critical shear stress and yielding shear stress. Figure 72 indicates the final optimized link. The authors used the combined kinematic and isotropic material model to consider the translation of the yield surface in stress space and the evolution of the of the yield surface together.

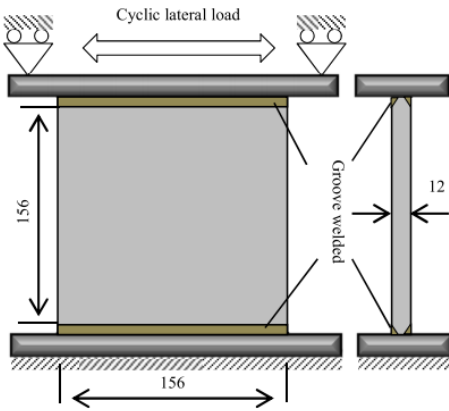


Figure 71. The basic plate on which the optimization is done [from (Liu and Shimoda, 2013)]

The optimization criteria is based on the following requirements: 1- Design  $L, H$ , 2- Find Optimum  $(L, H)$  3-Minimize CEP  $S_{\max}(L, H)$  4- Subject to  $E(L, H) > k \cdot I_{\text{initial}}$  Where  $k$  is 0.9. The flow chart of optimization procedure is indicated in Figure 73.

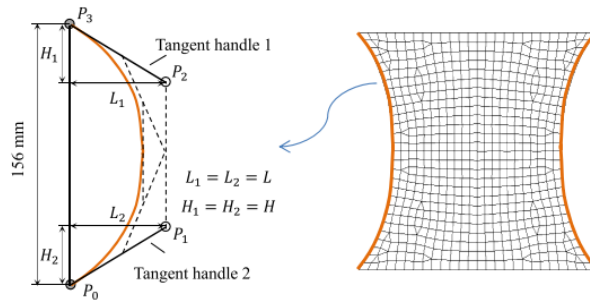


Figure 72. The optimum design [from (Liu and Shimoda, 2013)]

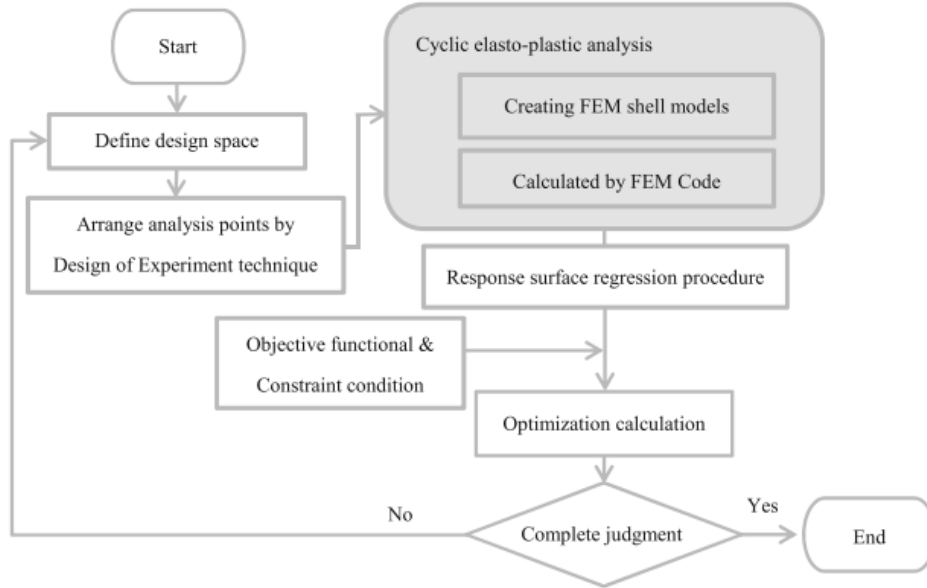


Figure 73. The flowchart [from (Liu and Shimoda, 2013)]

The best result according to this study was obtained with  $L$  is equal to 35.5mm,  $H$  is equal to 119.3mm, and  $a/b$  approximately equal to 0.75, which significantly reduces the plastic strain accumulating at the end of the plate which is a common problem with any straight link (Figure 74). It is noted although the total energy dissipation for the straight link is higher than the optimized link; however, for the optimization about 70 percent of the steel used for the rectangular basic link is used which indicates more efficiency in the implementation of the steel. This is important to notice that the initiation of the cracks would be significantly delayed by reducing the equivalent plastic strain values. The authors mentioned that the equivalent plastic strain have been reduced by about 80 percent and comparing to arc-shape links investigated in previous experimental studies, the optimal shape had a better plastic strain distribution.

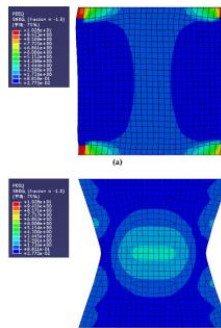


Figure 74. Reduction of equivalent plastic strain ability [from (Liu and Shimoda, 2013)]

## 2.10. Potential Applications for Shear Acting Structural Fuses

In this section, the potential applications for the proposed fuses in this study are discussed. The literature is studied for each of the applications. Figure 75 shows four of the many possible ways a butterfly-shaped structural fuse can be implemented in a building including use as the link beam in an eccentrically braced frame, coupling beam in a coupled shear wall, butterfly-shaped links can be used around the perimeter of the web plate in a steel plate shear wall, or as the replaceable links in the relatively new linked column frame system. Butterfly-shaped structural fuses have also been used as hysteretic dampers in a number of buildings, proposed for use in self-centering rocking frame structures, and proposed as structural fuses in moment connections.

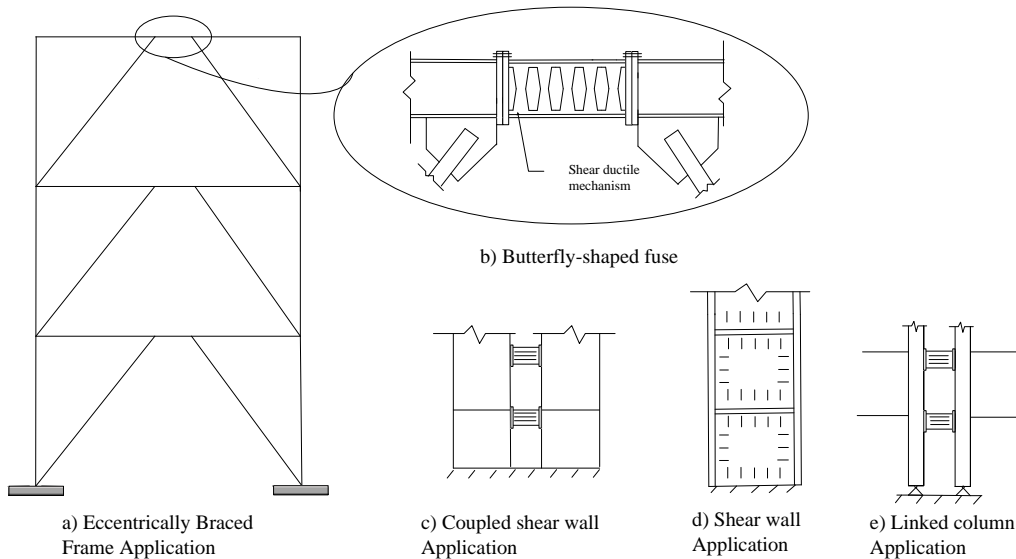


Figure 75. Examples of the implementation of the butterfly-shaped fuse

### 2.10.1. Metal buildings

In metal buildings (Figure 76) there is an area at the intersection of the column to beam connection, called panel zone. Panel zones are subjected to reversal loading are subject to buckling in early drifts. The stiffeners are used in panel zones to prevent the buckling issues. However, the welding of the stiffener to the plates is not easy to be done; therefore, there is the possibility of defects, which prevent the stiffeners to work during significant seismic loading. Instead, the buckling resistant systems could be used to eliminate the existence of stiffeners and detailed installation imposing time and cost issues (Figure 77).



Figure 76. Metal buildings [RHINO, Prefabricated steel building]

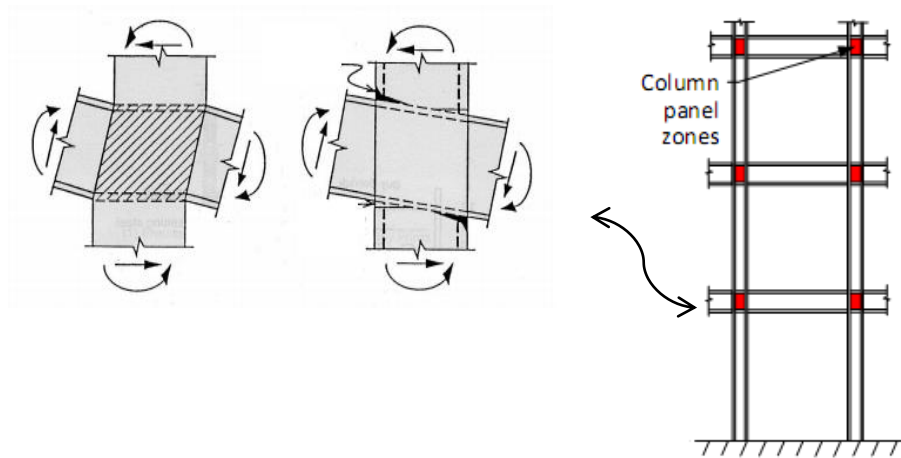


Figure 77. Panel zone in columns [from (Cheng and Cheng, 2004)]

### 2.10.2. Solid Steel Plates

To significantly reduce the large structural drifts and to facilitate repairs, structural fuses are designed. These structural fuses are designed to develop the resilient building to provide safe, cost-effective earthquake resistance. The plate indicated in Figure 78 and Figure 79 would dissipate energy through shear deformation. Implementation of buckling resistant systems could lead to

better use of steel with no pinching in the dissipation of energy. With the aid of these fuses, the system will minimize building downtime and the associated disruption following severe earthquakes.

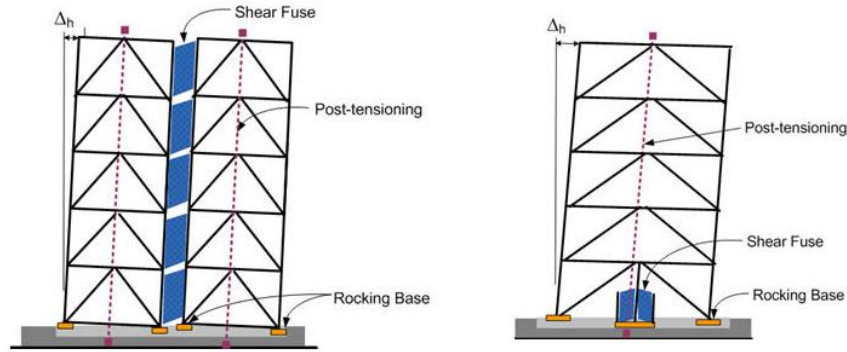


Figure 78. Example of structural fuses [from (Ma et al., 2011)]

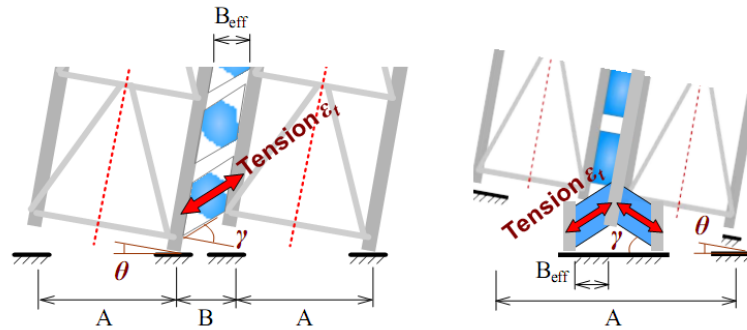


Figure 79. Structural fuses used for energy dissipation [from (Ma et al., 2011)]

It is worthy of notice that equations or procedures to control the buckling limit states while having a true prediction of shear and flexural limit state are significantly necessary. Since in these type of applications, the buckling limit states could prevent the system to perform as it is expected. Better control of crack mitigation due to stiffener attachment to the web area and plastic strain accumulation is also typical issues.

### 2.10.3. Eccentrically braced steel frames

Another application of buckling resistant concept is within the eccentrically braced systems (Figure 80). The braces are eccentric to beam-column connections and they do not directly frame into the connection. The metallic shear fuse indicated in Figure 80 is designed to yield during load

reversals. Due to desired shear yielding, the link is designed to have an upper limit to yield in shear for maximizing the energy dissipation.

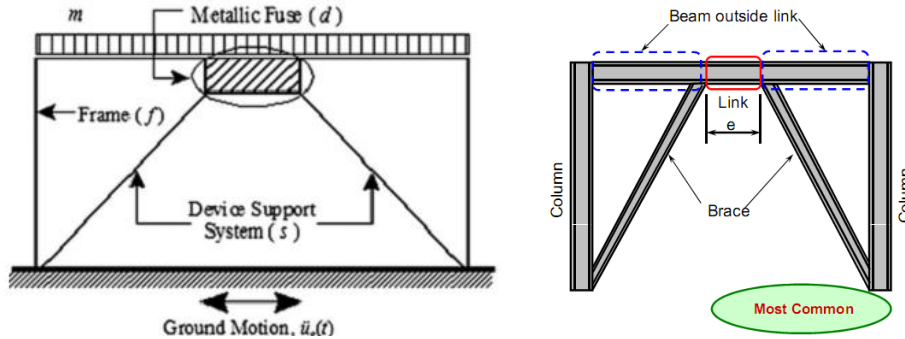


Figure 80. Eccentrically braced system (EBF) [from (Dutta, 2008)]

According to the Figure 81, if the link length is less than  $1.6M_p/v_p$  and the rotation of link is limited to the 0.08 rad, and the spacing of stiffeners should be less than  $30t_w - d/5$  (Figure 81). These requirements are essential for appropriate performance of the EBF links under seismic loading conditions.

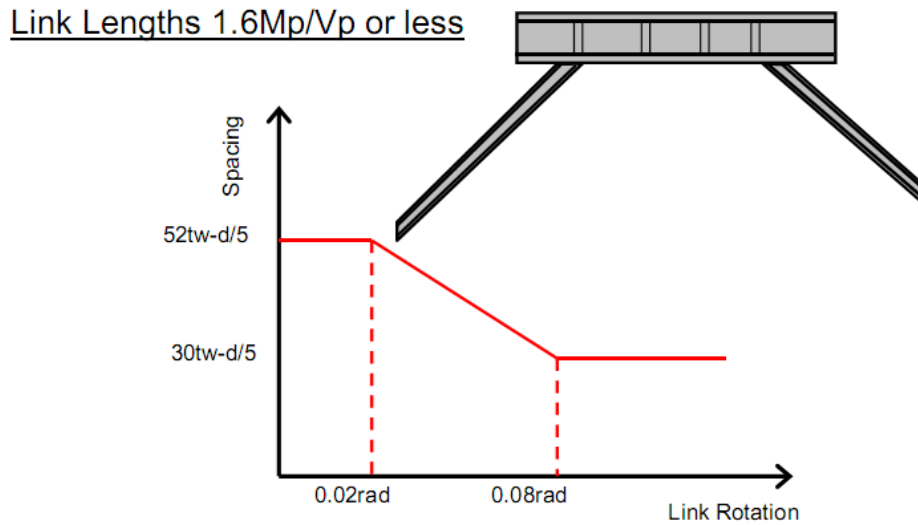


Figure 81. The stiffener spacing [from (Dutta, 2008)]

Nabil Mansour and Constantin Christopoulos (2008) designed the EBFs to sustain damages through repeated inelastic deformation and localized buckling. As it is mentioned the connection of the links to the frame has large importance. Two back-to-back channels were investigated

(Figure 82 and Figure 83). The links act as ductile fuses, dissipating energy through stable hysteric behavior while limiting the force transmitted to other components.

One drawback of such systems is inside braces of the floors. After damage occurs, it is almost impossible to get them repaired or assess the amount of damage. The shear link, which has a lower height compared to the floor beam section, is not connected to the floor system because, during the earthquakes, it should move forth and back to dissipate energy. There were two different experimental tests. First, the traditional format, which was the implementation of the end plate, welded to the floor beam, and the second was the implementation of two back-to-back channels, which made the installation procedure easy enough.

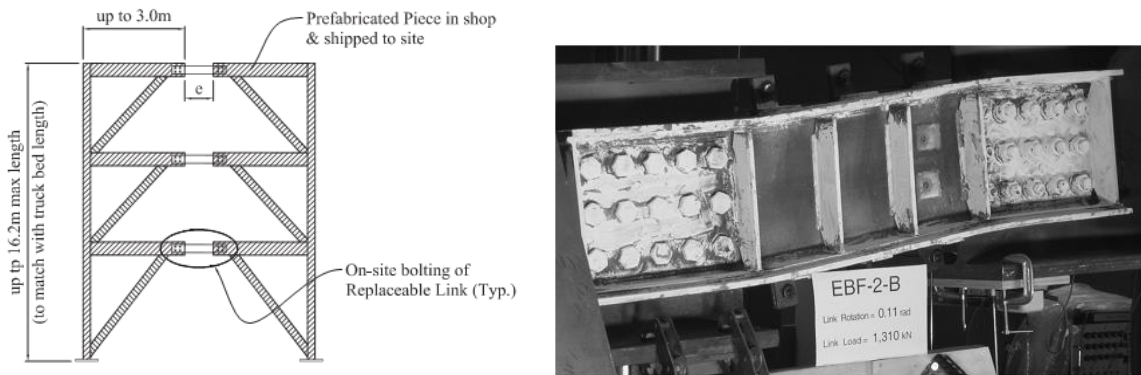


Figure 82. Innovative EBF systems [from (Nabil and Christopoulos, 2008)]

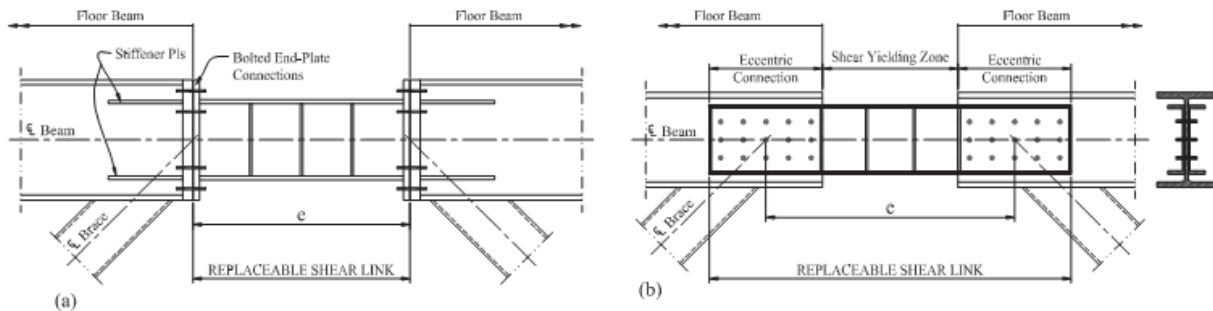


Figure 83. Detailed link properties [from (Nabil and Christopoulos, 2008)]

The behavior of the connection depends on the thickness of the link and the floor beam webs preventing from localized bolt fractures. As the connection gets stronger the portion of the total link deformation associated with shear, yielding of the link panels would be increased. Due to

localized deformation, the EBFs are capable of achieving large deformations without loss of strength.

M. Itani (2003) has investigated the behavior of the built-up shear links and compared them with the conventionally rolled shape sections. The potential of using built-up sections with thick flange and the thin web is investigated. During earthquakes, the eccentric brace applies a shear loading to the shear links and the energy dissipation occurs through yielding of the web link. To achieve the lower amount of plastic rotation, local instabilities such as a flange or web buckling should be delayed. The flange local buckling is controlled by choosing a certain amount of width to thickness ratio, while the web buckling is controlled by adding a number of transverse stiffeners along the web link.

The built sections more often than not are preferred to the rolled section, because it is possible to set the ultimate capacity of the section to any desired value. Compared to rolled sections, the built-up sections have thinner, but the deeper web. It is recommended to delay the local buckling in the web of the link as far as possible so that the plastic rotation would fully be developed. Figure 84 indicates the moment and shear diagram of the loading applied to the shear link.

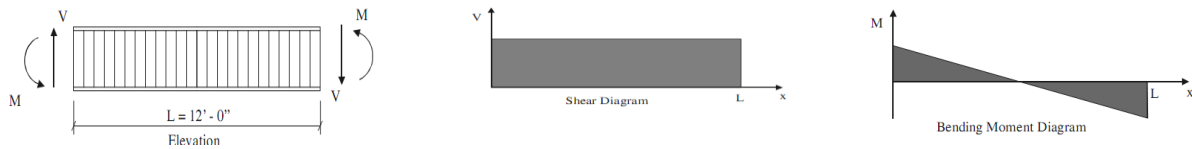


Figure 84. The moment and shear diagram of the link [from (M.Itani, 2003)]

In general, the shear capacity of the link could be calculated by Eq.(13):

$$V_u = \frac{R_y \alpha V_n}{\phi_b} \quad (13)$$

In which the  $R_y$  is the steel variability factor,  $\alpha$  is the over strength factor equates to 1.25,  $V_n$  is the shear capacity of the web and  $\phi_b$  is the resisting factor equates to 0.9. The pushover curve for these types of links is indicated in Figure 85.

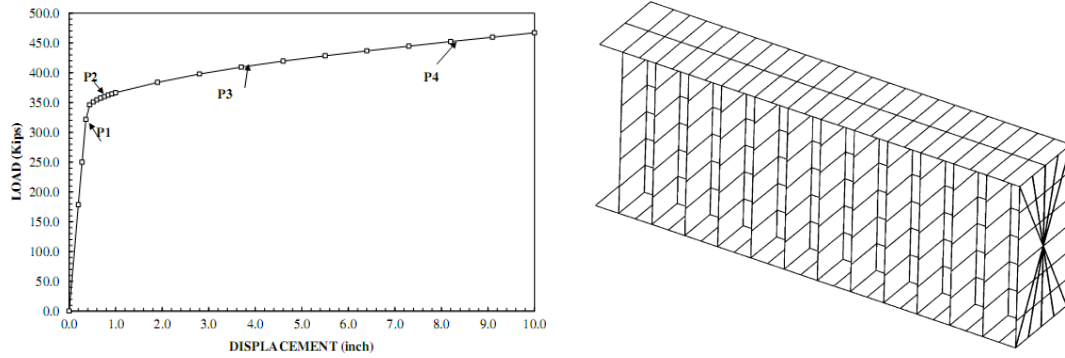


Figure 85. The EBF link pushover curve [from (M.Itani, 2003)]

Having an upper limit for rotation in out of plane direction would impose the need to have stiffeners; therefore, the fracture possibility would be enhanced. Implementation of fuses with shear links could possibly improve these criteria. The noticeable disadvantage of EBF systems is the inability to be replaced. Because EBF links are attached to the floor system, it would be difficult to be replaced. The improvement of such system could be significantly beneficial. Even in studies aiming to address the replace-ability issues, there would be some amount of damage occurred in the system. Therefore, buckling restrained design methods considering limit states could be the best solution for such problems.

#### 2.10.4. Bay Bridge

Another application for buckling resistant plates is in bay bridges. Between towers of the bridges, the plates are used to form a coherent movement. Bridge towers could sway especially during wind and earthquake extreme loading. These panels could dissipate energy by lateral movement.

Nader et al. (2000) have investigated the replaceable sacrificial steel links. The seismic design strategy of the new San Francisco-Oakland Bay bridge self-anchored suspension span was studied (Figure 86 and Figure 87)



Figure 86. San Francisco bay bridge [from (Nader et al., 2000)]

The Bay Bridge lies between the Hayward and the San Andreas faults which are capable of producing magnitude 7.5M and 8M earthquakes, respectively. The plastic mechanism is achieved through four stages. (1) Limitation of plastic hinging to the east and west piers, (2) provision of shear links between the tower shafts which would yield in the event of a major earthquake (these links will be replaced right afterward), (3) providing a tie down counter weight at the west pier to ensure stability after the west pier forms plastic hinge and (4) improving the seismic response of this bridge by using seismic devices between the tower and the deck and at the expansion joints. The rotation on the shear links is limited to 0.03, as compared to the ultimate rotation, which is 0.09. It is required that the bridge sway especially during the earthquakes. By swaying laterally, the loading would be absorbed by shear links and most of the energy imposed on the structure would be dissipated.

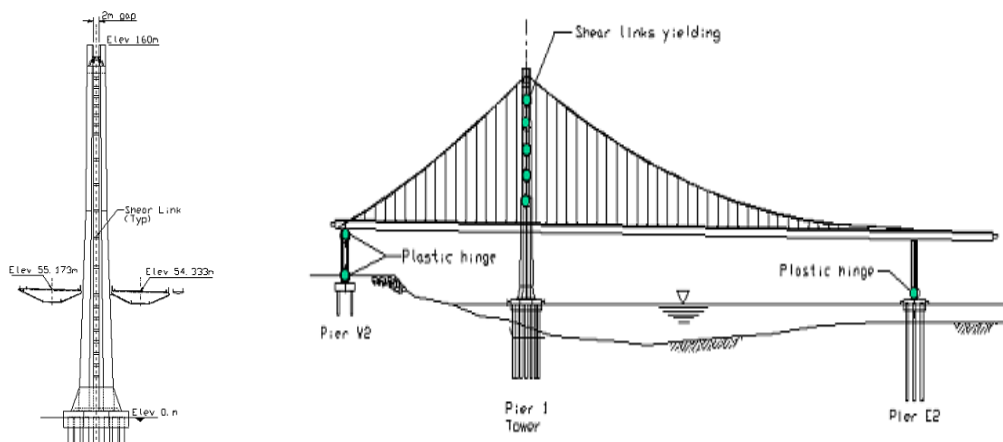


Figure 87. San Francisco bay bridge [from (Nader et al., 2000)]

The shear links between two towers shafts are designed to yield in shear and not in flexure. These links under normal condition of loadings such as wind and mild earthquakes are designed to stiffen the system so that the deflections would be limited; however, under heavy earthquakes, these links are designed to yield and participate in energy dissipation.

At the two-thirds height of the tower are those links that are going to be most vulnerable. These links provide additional damping to the bridge by dissipating energy while going through the inelastic cycles, thereby reducing the seismic forces and displacements. It is also mentioned that the shear links could be the major reason why we have one tower by reduction loads carried into the actual bridge. The shear link beams (Figure 88) also allow the tower's four legs to move independently, which releases even more energy. This idea of maximizing flexibility is crucial to minimize an earthquake's impact on the new bridge.

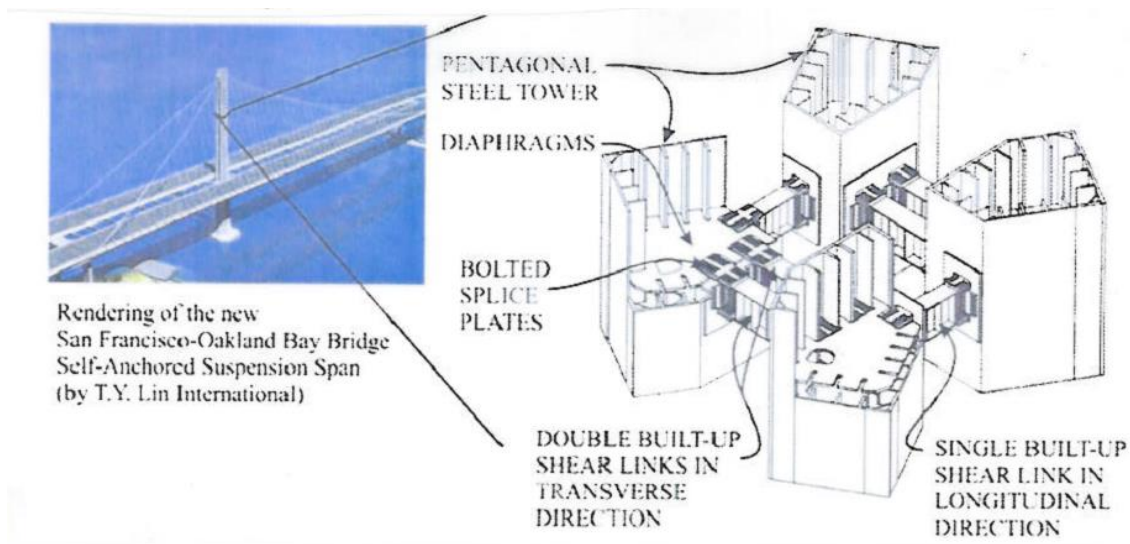


Figure 88. The shear link geometry [from (Carpio, 2005)]

Each shear link has three components, the deformable portion in the middle and two connection zones at the end. It is mentioned that to compensate for the amount of bolts' net area, the shear links are designed with more strength or with higher thickness than what it is designed for. Figure 89 indicates the details of shear links used for dissipation energy.

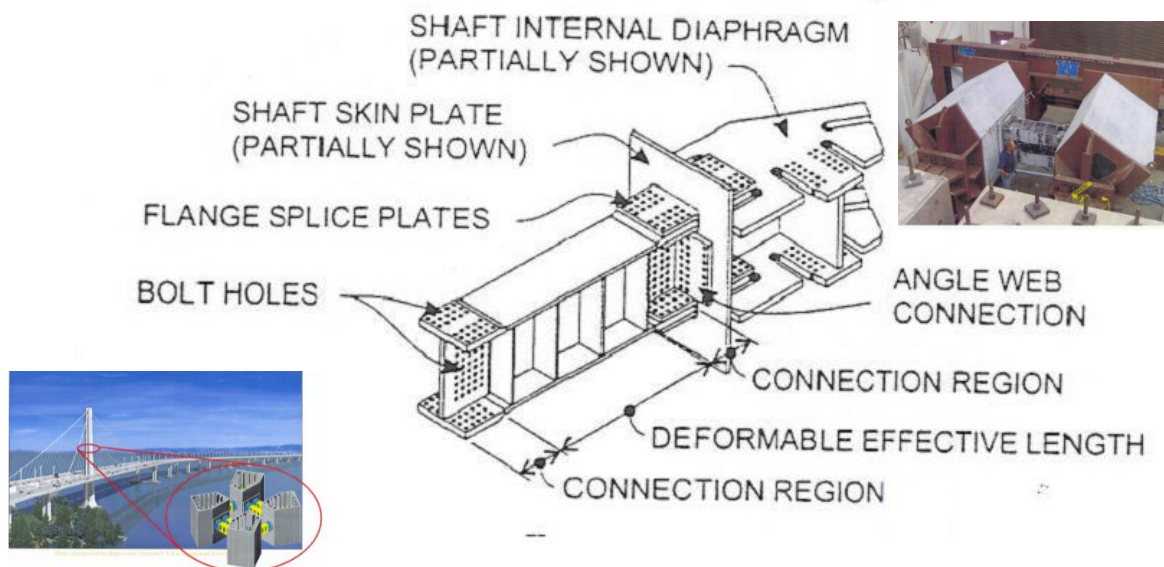


Figure 89. Shear link in detail [from (Buckle et al., 2005)]

The shaft diaphragms, splice plates, connection angles are made from 485 MPa high weathering steel, the remainder of the test setup was made from 345 MPa steel.

Duski et al (2004) have investigated the shear links in details. Plastic strain demands on the different components of the links were indicated. It is concluded that the finite element models combined with appropriate stress-strain relationship may be used to adequately check the design of links. The shear links were commonly used in EBF systems, and it gradually finds its way into other structural applications. Retrofit and bay bridges could be examples of new applications of shear links. Four different structural grade steel have been investigated (Table 2). In addition, the stiffeners are used to delay the onset of buckling during inelastic link deformation. However, by utilizing low yield point steel, the web thickness could be increased and stiffeners excluded.

Table 2. The properties of specimens [from (Dusika, 2004)]

Link type	C345	H485	L225	L100
Steel grade within	A709 Grade	A709 HPS	LYP	LYP
effective length (MPa)	345	485	225	100
Stiffener spacing (mm)	280	168	N.A.	N.A.
Web compactness ratio, $h_w/t_w$	31	43	20	10
Flange compactness ratio, $b_f/2t_f$	6.8	6.7	6.6	6.8
Nominal shear $V_p$ (kN)	1245	1250	1270	1160
Nominal moment $M_p$ (kNm)	1252	1273	1290	1223

As it is shown in Table 2, the  $F_y t$  is remained same the for all of the cases. The isotropic strain hardening was used for the steel along with two post-yield material relationships: elasto-plastic and cyclic strain behavior. As the elasto-plastic stress-strain relationship is considered, there would be no strain hardening and the steel plate effect on the post-yield stiffness of the shear link would be ignored. The properties of different types of steel are indicated in Figure 90.

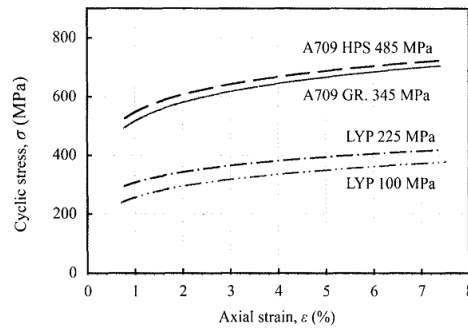


Figure 90. Properties of steel [from (Dusika, 2004)]

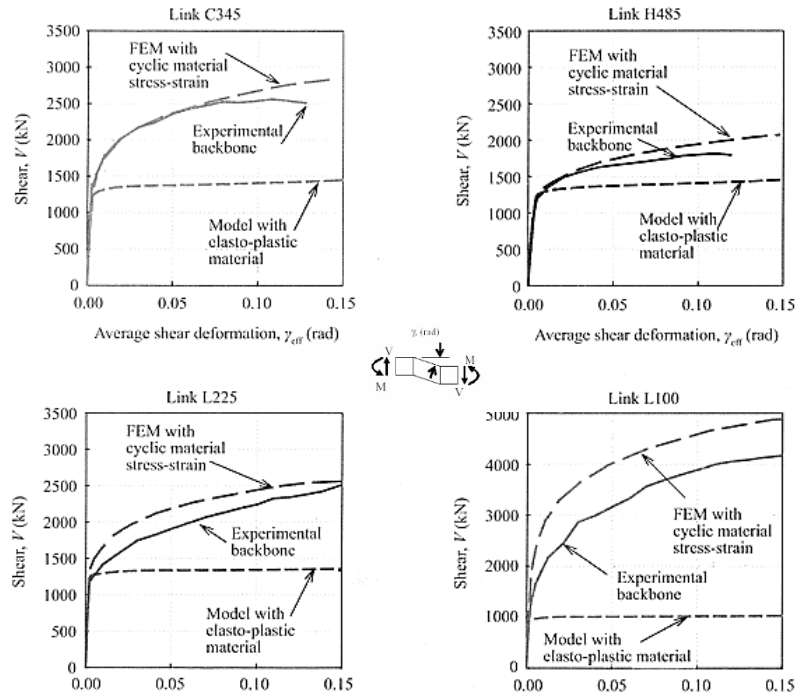


Figure 91. The verification of shear link behavior [from (Dusika, 2004)]

The results show that the stress-strain characteristics have a significant influence on built-up shear link behavior. Therefore, implementation of the cyclic stress-strain with a relationship with monotonic finite element analysis was shown to approximate closely the experimental backbone curves that were obtained through a cyclic experiment. It is well noted that the finite element analysis provided the opportunity for close investigation of plastic strain accumulation, which can lead to fatigue and cracking (Figure 91). The cracking patterns are observed in the web, stiffeners, and flanges of the links during experiments. A consistent correlation was found between the location of initial crack and the location of localized plastic strain in the finite element model. Most of the strain accumulation is occurred at the ends of the stiffener to a web connection, next to the stiffener chamfer. The plastic strain is about 20% higher in the stiffener to the beam welding area compared to other places showing the crack was likely caused by the combination of heat-affected zone from welding and the plastic strain concentration. Any work to reduce the number of the stiffener, increase the buckling resistance and reduce the plastic strain values, would be important.

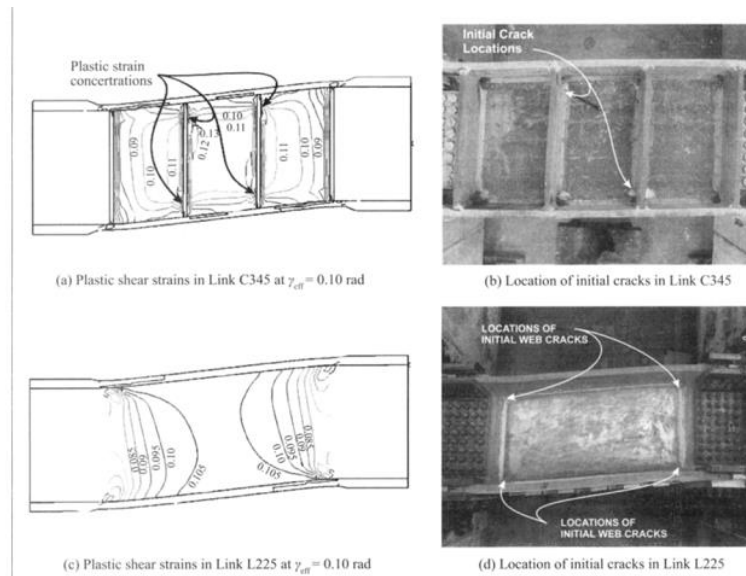


Figure 92. The actual experiment done by Dusika (2004)

By removing the ties constraint between the stiffener and flange, it was found that the reason of stress concentration in the web is due to stiffener attachment to the web (Figure 92). It is noted that the cracks in shear links have occurred earlier in those links having stiffeners compared to those without any stiffeners.

Buckle et al. (2005) investigated the development of built-up shear links. The proposed new east bay crossing of the San Francisco –Oakland Bay bridge has used steel shear links as energy dissipating devices for added protection during the earthquakes. Although throughout the bridge steel of Grade 70 has been implemented, the shear links are made of steel grade 50 due to lack of data on the inelastic behavior of steel Grade 70. It is concluded that shear links are very efficient energy absorbers, and can be designed to have a high tolerance for the inelastic strain. Applications of such shear links could be attractive because of the low cost of maintenance.

It is well mentioned that failure has begun in the location of stiffener weld to the web. It is also suggested that stiffeners could be eliminated if the low yield steel and the thicker plate is used. The LYP demonstrated a high capacity for inelastic strains because there would be no stiffeners leading to less yielding areas with high plastic yield strain.

The concept of shear links implementation goes back to eccentric brace frame in structural lateral systems, where the force capacity is limited due to section sizes and build-up sections must be used if a large device is implemented.

The design conducted in such a way that the structure would remain elastic during the maximum earthquake. To consider this design criterion, the links are provided to dissipate energy in shear; thus, reducing the demands on tower and foundations (Figure 93).

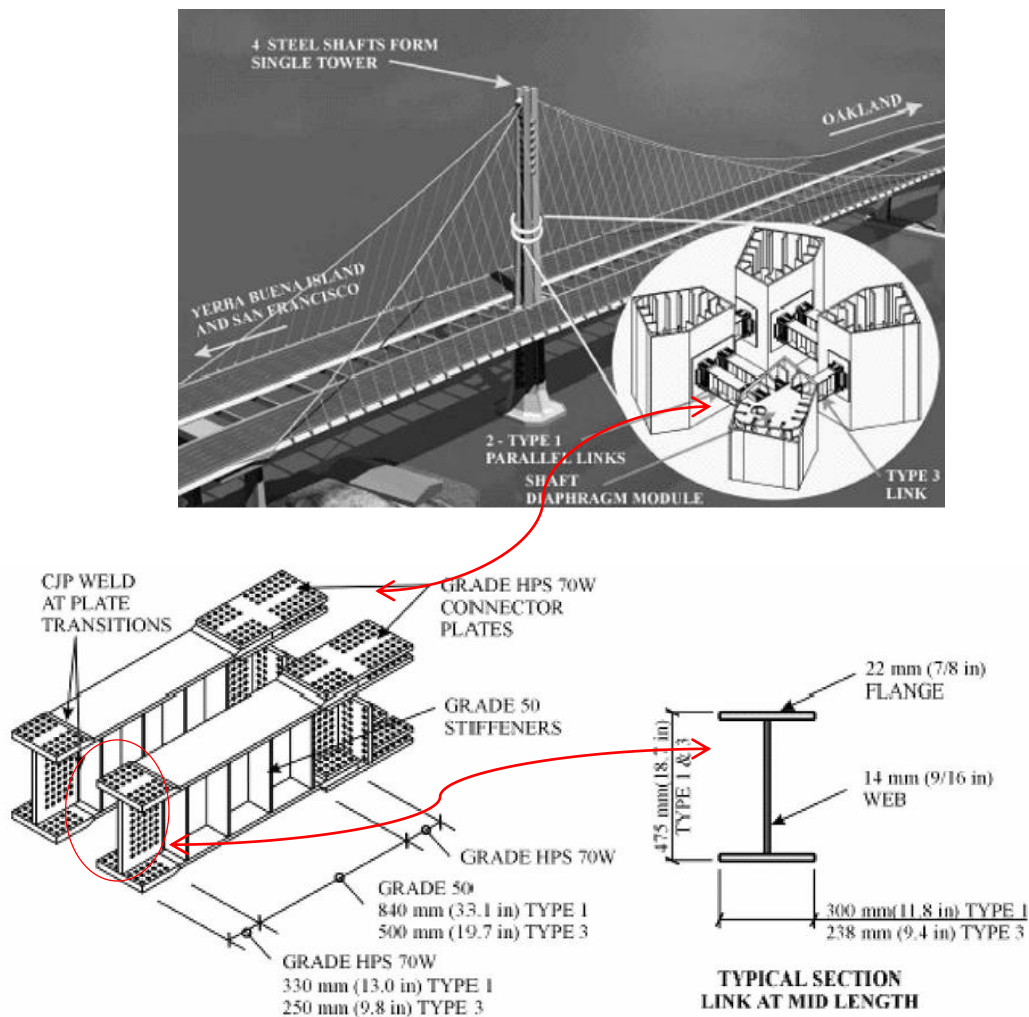


Figure 93. The shaft and link [from (Buckle et al., 2005)]

As it is indicated in Figure 93, the links are bolt connected to the shaft, the less the ultimate strength of the links, the more the section sizes. With the aid of the diaphragm inside of the shaft the load path is completed, the shear links would carry the load using the bolted plates between the shear links and the diaphragms, and diaphragms subsequently will carry the loads to the shafts.

The stiffeners are designed based on the grade 50 steel. It is mentioned that the rupture occurs in 13% shear strain. The modes of failure in all of the samples are the rupture between the stiffener and the web.

As far as the ductility is concerned, low yield plate shows greater ductility and the failure strain; compared to the high yielding point. The lowest strength (100 MPa) has considerable over strength factor near 3.1 compared to 225 MPa plate with over strength ratio of 2.1, 230 MPa with 2.2 over strength and 490 MPa with over strength of 1.5. However, high over strength observed in the LYP 100 caused failure in the connection plates for this link leading to premature termination of the experiment before full capacity of the link itself reached.

In sum, failure in both cases of grade 50 and grade 70 is initiated from the stiffener to web plate welding. It was also shown that the stiffeners could be eliminated altogether if thicker webs and low-yield-point steels are used (for the same nominal shear capacity). These low yield point links demonstrated a very high capacity for inelastic strains, due to a reduction in welding areas and imposing high plastic strains. The failure occurred at about the 20 % and 15 % for low yield steel plates (225 and 100 MPa ) as compared to 13% for higher ones (345 and 490 MPa).

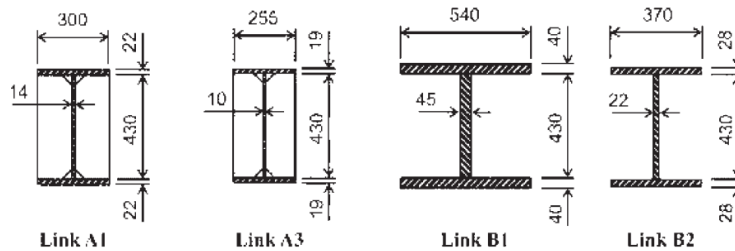


Figure 94. The different studied sections [from( Buckle et al., 2005)]

Table 3. Properties of the Section investigated by Buckle et al. (2005)

Set	ID	Material	Nominal yield (MPa) (ksi)	Link type	Single/dual beam	Web stiffeners	Number tested
A (stiffeners)	A1	A709 G50	340 (50)	3	Single	Yes	1
	A2	A709 G50	340 (50)	1	Dual	Yes	1
	A3	A709 HPS70W	480 (70)	3	Single	Yes	1
B (no stiffeners)	B1	LYP 100	100 (15)	3	Single	No	2
	B2	LYP 225	225 (33)	3	Single	No	2
	B3	LYP100/400	100 web/400 flanges (15/60)	Hybrid	Single	No	2

Amelioration of the effect of lowering the strength yielding point and increasing the thickness ratio in bay bridge plates is observed to be positive; however, reduction in this factor would lead

to higher overstrength factors causing a fracture in connection plates leading not to gaining full capacity of the link.

### 2.10.5. Linked column

Malakoutian et al. (2012) have proposed a new lateral resistance system to limit the seismic damage to relatively easily replaceable elements. Linked column frame (LCF), is made of the dual column with the secondary frame, in which the elements inside of the dual column with yielding link mode, would make the significant energy dissipation capability (Figure 95). A design procedure is proposed to ensure that plastic hinges develop in the links of the linked columns at a significantly lower story drift compared to when plastic hinges develop in the moment frame beams. The significance of the implementation of such system is due to the fact that conventional lateral resistance systems, especially during inelastic deformation would be damaged heavily and the downtime is significant. The links are the sacrificial elements that yield to provide the ductility, energy dissipation and softening behavior while the inelastic deformation and related damage to the structural frame are prohibited.

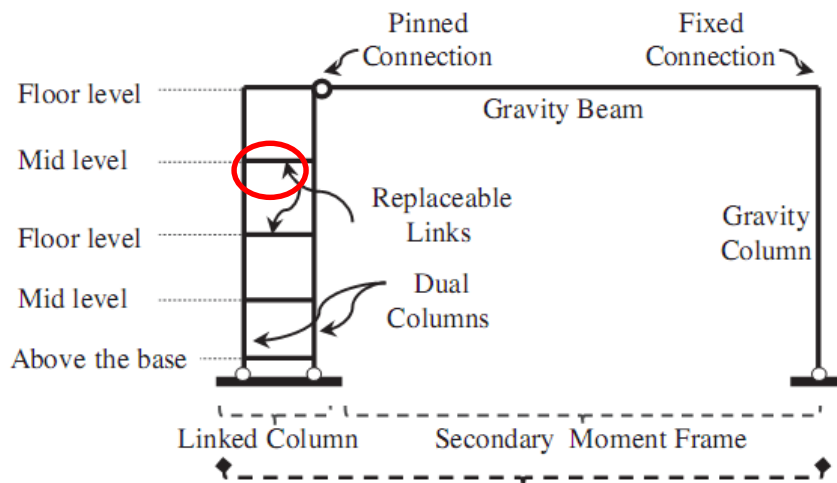


Figure 95. The new lateral system [from(Malakoutian et al., 2012)]

It is mentioned that in taller LCFs, the effect of the overturning moment is significant. The larger span of the linked column and correspondingly longer links would have smaller drifts and better overturning moment resistance.

Along the same line, Loes and Dusicka (2102) designed the linked column structural system. The linked column frame is designed for a rapid return to occupancy. Andres Lepage et al. (2004) compared the efficiency of core outrigger frame. Free cantilever cores are used for 20 stories buildings and 30-40 stories building in San Francisco. After the Northridge earthquake. The implementation of the moment frame is prohibited due to unexpected fracture initiation in column-beam connections, and extensive innovative studies were initiated among those the RBS in which the flange section of the beam is reduced, or some sort of the opening inside of the beam web is used has been proposed.

Tests showed that in general, the succession of the yield mechanisms that provides ductility and toughness to large drifts of 6% could be possible. To limit the stress and strain demands placed on the beam-column welds in moment-resisting frames, the forces and moments that develop the beam-column connection can be limited by removing web material To create a structural fuse.

### 2.10.6. Steel shear walls and coupled steel shear walls

The main role of a steel shear wall is to collect the lateral forces of earthquakes and winds and transfer those in shear, to the foundation and ground. To mitigate the non-ductile buckling and early fracture behavior of the system, these buckling resistant shear walls could be implemented. The coupled shear wall is one of the common means of lateral resistance systems (Figure 96). As it is discussed, the implementation of coupling beams with moment resistance capability would not be desired due to the difficulty of installation (Figure 97). It is mentioned that the coupling beam connection to adjacent steel shear walls is not assumed to be fixed; some flexibility should be accounted for the modeling of such beams. Therefore, for having an accurate estimation of the length of the beam, 1/3 of embedment length should not be considered.

$$L = L_{clear} + 0.6 L_{emb} \tag{14}$$

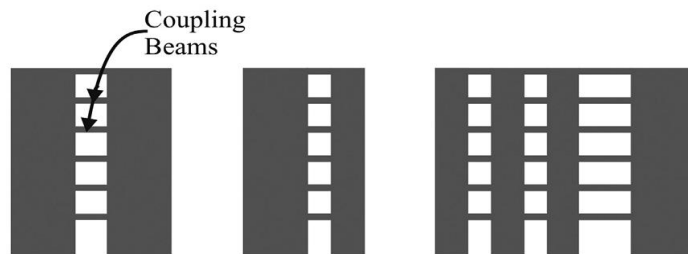


Figure 96. The coupled steel shear wall [from (Harries et al., 2000)]

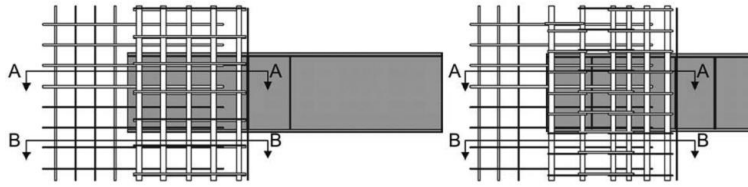


Figure 97. The highly detailed installation [from (SherifEl-Tawil, 2010)]

It is mentioned that coupling beams have the same response as the shear links in EBFs. It is noted that to have moment resistance, the embedment length should be enough. The reason why the coupling steel beam is preferred over other types of coupling beams is that this kind of beams has the significantly lower amount of detailing issues associated with ductility provision, and it has an easier way to be modeled and investigated.

Sherif El-Tawil (2010) has indicated the preferred yielding mechanism is the coupling beam yield at first followed by the yielding at the base. Energy dissipation from the beams could reduce the amount of damage in moderate earthquakes. Having appropriate strength, stiff and ductility are among the most important features of these links (Figure 98 and Figure 99).



Figure 98. Installation of coupling beam [from (SherifEl-Tawil, 2010)]

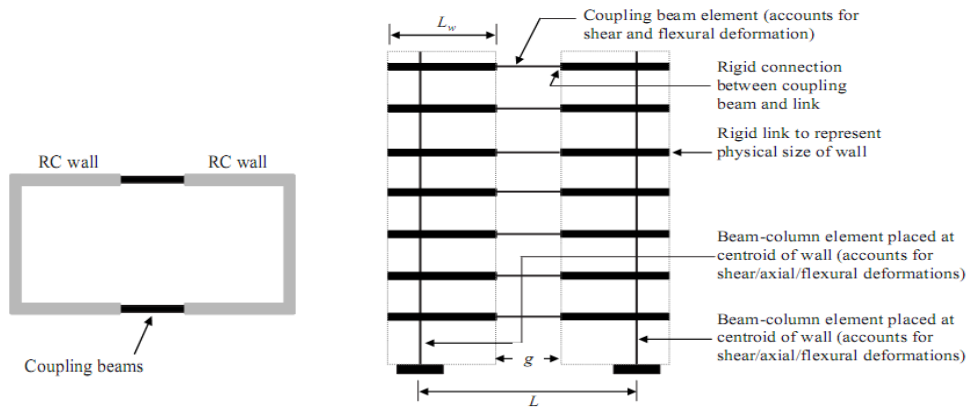


Figure 99. Coupling beams in the structure [from (SherifEl-Tawil, 2010)]

In addition, to prevent the adverse effect of coupling beam design for taller buildings on the piers, it is recommended that the design for coupling beams should be in grouping format (Figure 100).

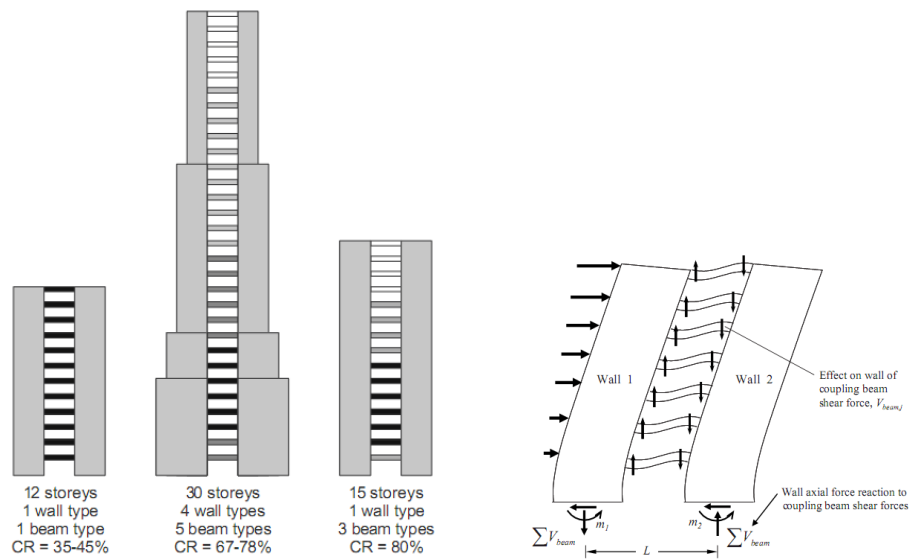


Figure 100. Grouping of coupling beam links [from (SherifEl-Tawil, 2010)]

In general, the coupling behavior of the shear wall is important because of three reasons. First, the moment experienced by each of the walls would decrease; second, it provides a means of dissipating energy over the entire height of the wall as the coupling beams undergo inelastic deformations, and third, it has significant lateral resistance stance.

Generally, it is more interesting to have the shorter length for coupling beam rather than the longer ones because the longer the beams are, the more energy is dissipated through the flexural mechanism. Mechanisms that involve well-controlled inelastic shear deformation in steel coupling beams are generally more ductile than those involving flexure-related plastic hinge deformations. Therefore, proposing limit states that the designers could design any fuses in such a way that the shear or flexural limit state would be governed without being worry about buckling limit state is highly valuable.

Along the same lines, the coupling ratio (CR) equals to zero means that the beam is like pinned connected and the coupling beams have no moment and there is no coupling action. CR=50% means that the half of the imposed overturning moment (OTM) is resisted by the coupling effect. The CR equals to 100% means that theoretically two-wall piers behave as a single pier, which may be envisioned as the case where the beam length approaches to zero. Harries (200) proposed an upper limit for the CR ratio as of 66%; however, El-Tawil recommend the 30-45 % range for CR ratios. It is concluded for the coupling ratios of 30%-70%, the design of the coupling beams is in need of buckling preventions consideration.

The coupling beam should be detailed to undergo inelastic deformation reversals. The strength and ductility should be carefully tuned along with the strength and ductility of RC wall piers to achieve appropriate system economy and acceptable behavior. Same as the EBF systems, the expected coupling beam rotation angle plays an important role in required beam details.

The usual method of design more often than not assumes the plastic hinges to occur at the base of the shear wall and simulates yielding at the beams over the height of the structure. This method of design is assumed to be acceptable for those buildings with 12 to 18 stories height, because as the building goes higher, the more beams would remain in elastic and hinges would not occur.

Shahrooz (2004) studied the behavior of coupling beams embedded in reinforced concrete shear walls with the boundary and connection region under the compressive stress. The primary objective of the coupled walls is to dissipate energy through the major energy in the coupling beams, where plastic hinges should form. Generally, about the 70% of the energy dissipation mechanism is occurred within the beam by plastic hinges. The contribution of flexural and shear deformation in coupling beams is significant. In addition, if the boundary element is subjected to

compression, the plastic moment capacity could be fully developed; however, if the boundary element is subject tension, the stiffness would be reduced and the full capacity is not attainable.

El-Tawil and Kuenzli (2002) indicated that openings are frequently required for structural walls to accommodate windows and doors. In this case, sometimes there would be a need to have the structural resistance system walls connected by coupling beams. Under severe loading condition, cantilever action of the individual walls imposes sufficient deformation demands on the coupling beams and make them yield. Steel coupling beams are designed to yield in flexure (hinge) or shear. Of both of the idling mechanism, the shear yielding is more preferred because it indicates more ductile behavior and stability. It is well suggested that the shear beam should be designed in a way that no local buckling would occur. To prevent web buckling, implementation of the stiffeners and encased web are introduced.

The coupling action could lead to high limitation of base wall rotation (Figure 101). Meaning that uncoupled shear wall could show a large amount of rotation at the base. Important notice here is that increasing the coupling behavior of the wall would not lead to meet the requirements due to reduction factors in rotational requirements. In other words, the 30 and 45% of coupling have better performance compared to others. It is worthy of notice that implementation of the links with the coupling beams could lead to more flexibility in designing coupled shear walls with specified coupling ratio values.

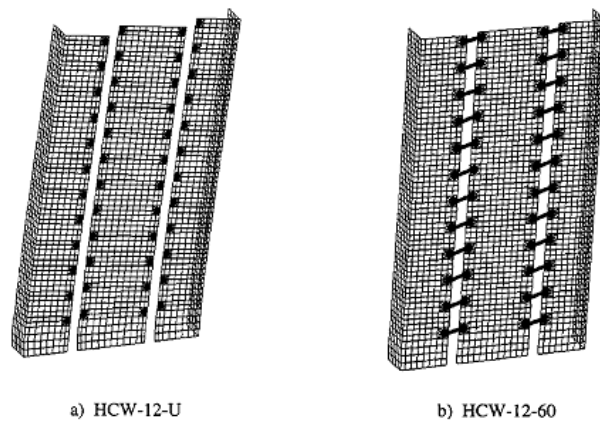


Figure 101. Coupled and uncoupled shear walls [from (El-Tawil and Kuenzli, 2002)]

# **3. LINK SHAPE INVESTIGATION, CONCEPTS, AND PROPOSALS**

## **3.1. Introduction**

A promising type of fuse implemented in structures consists of a steel plate with cutouts leaving various shaped shear links subjected to shear deformations by applying a load at top of the shear link. As described in the previous chapter, a common class of structural fuses consists of structural steel elements deformed in shear. Links are defined here as relatively short lengths of steel that undergo shear or flexural yielding and are utilized in the larger structural fuse panel. Links are chosen for use in these structural fuses to improve the overall behavior of the structure (e.g. strength, stiffness, ductility, and energy dissipation). Use of strategic cutouts would lead to the efficient implementation of the material and postpone or prevent the brittle limit state such as lateral torsional buckling.

In this chapter, the concepts mentioned in the literature have been evaluated to propose innovative shapes for shear links. In addition, mathematical concepts are proposed based on the developed structural shear links with different shapes. For the typical three general applications elaborated previously, eccentrically braced system, coupled shear wall, and steel plate shear wall, links are designed and the systems with and without different link shapes are analyzed. Subsequently, based on the issues identified from literature review, the optimization criterion based on which the links' shape could be improved is proposed and explained.

## **3.2. Link shape based on uniform yielding along the link length**

One of the important criterion studied previously literature to design link and fuses is to utilize the steel as efficiently as possible (Ma et al., 2011; Deng et al. 2014), which in this case means designing the link in such a way that ductile yielding limit states would be happening simultaneously along the length.

Figure 102 shows the hourglass shape links. Based on Figure 101, the link would have an end moment due to the loading at the ends. The capacity curve, as well as the demand curve along the length of the link, are indicated in Figure 103.

As it is indicated the two intersection points of the moment capacity and moment demand are the possible plastic hinges. This shape is one of the common shapes of the fuses used before in literature. In general, in shear links, the hinges are designed to be developed in any specific point of the link, preferably far from sharp areas. The simplicity of the production and replaceability should be considered. In addition, the potential to resist buckling and transform the inelastic behavior of ductile metal plates subjected to shear loadings through strategic removal of material are recommended to be studied. Along the same lines, the conversion of global shear buckling into local yielding, which is more ductile and stable with better aligning the bending capacity with the shape of the moment diagram is suggested for further investigation. Based on the Figure 103, the demand moment shown in Eq. (15) and the capacity moment shown in Eq. (16) was derived.

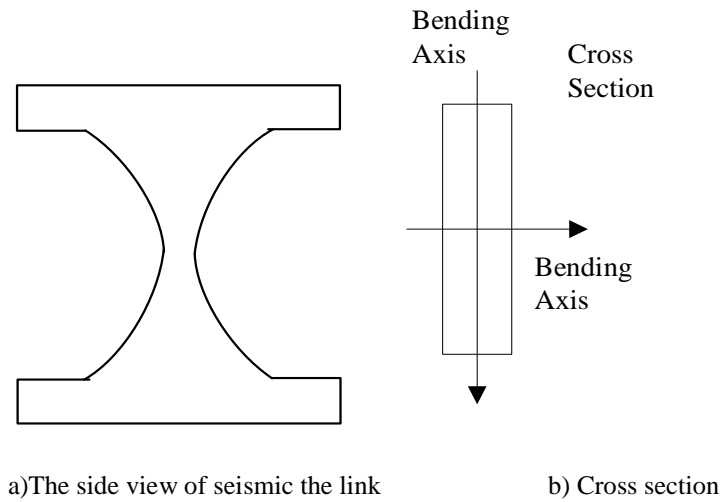


Figure 102. The concept of uniform yielding for the shear link used

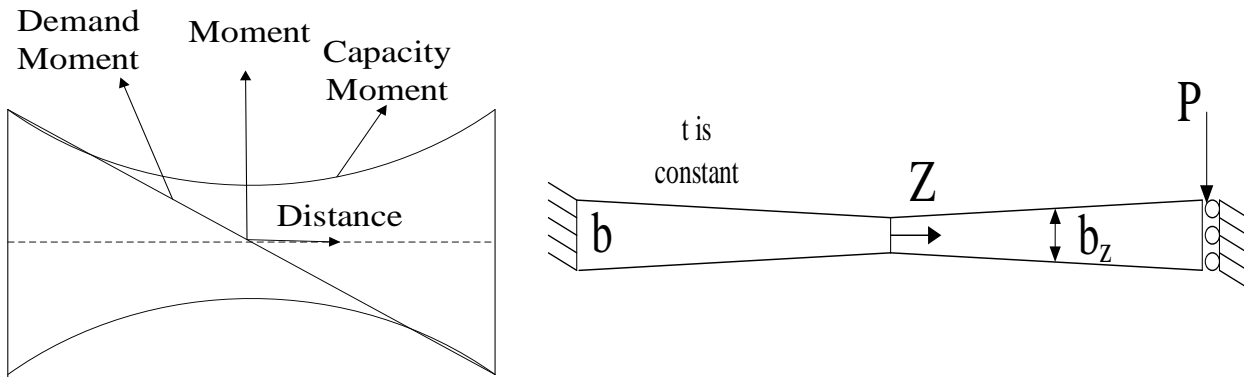


Figure 103. The loading and capacity curve for butterfly links

$$M_p = \frac{w(z)^2 t}{4} \sigma_y \quad (15)$$

$$M_{\text{loading}} = Pz \quad (16)$$

in which,  $t$  and  $w(z)$  are the thickness and width along the length, respectively;  $M_{\text{loading}}$  is the loading moment demand;  $M_p$  is the capacity of the link.  $z$  is the distance from the center, and  $P$  is the shear force applied to the end of the link. By equating the demand and capacity curves, the width along the length could be derived:

$$w(z) = \sqrt{\frac{4Pz}{t\sigma_y}} \quad (17)$$

This equation indicates that the  $w(z)$  should be varying non-linearly (as it looks like a hourglass-shaped link with curved lines). Therefore,  $b$ , the end width of the shear link, could be obtained as shown in Eq. (18):

$$b = \sqrt{\frac{2PL}{t\sigma_y}} \quad (18)$$

The width of the link in each section is found based on Eq.(19).

$$(w(z)/b) = \sqrt{\left(\frac{z}{L}\right)} \quad (19)$$

This indicates that if width along the length,  $w(z)$ , has a variation with the square root of the  $z$ , the demand and capacity would have close values in majority of the points along the length of the shear link. The shape of the link could be described as the following Figure 104. It is noted that if only Eq.(19) is considered, the width at the middle should be equal to zero. This obviously is not realistic and at the middle section the hourglass shaped link could have higher shear stresses. Therefore, link should have a specified width at the middle to resist the shear stresses.

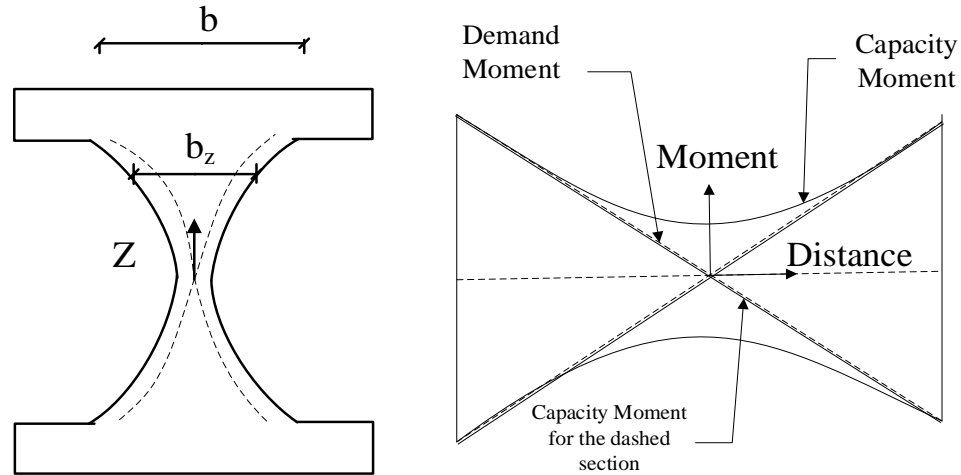


Figure 104. The geometry of the butterfly-shaped link

This shape is an appropriate option for higher thickness steel plates if designed appropriately for the lateral torsional buckling limit state. It is noted that the effect of torsion and axial force are separately evaluated in Chapter 5 and Chapter 10, respectively.

### 3.3. Link shape based on the uniform curvature

This section incorporates a commonly used uniform curvature concept for developing link shapes related to in-plane structural link. The goal is deriving a link shape to produce constant curvature, which leads to initial yielding to be occurred uniformly along the length of link. Based on the studies by Tsai et al. (1992), Whittaker et al. (1991), Hanson et al. (1991), Enrique and Martinez-Rueda (2002), and Kobori et al. (1991), it is suggested that to have uniform curvature for spreading the plasticity along the length of the link.

The curvature could be uniformly distributed if specific geometrical properties are used for the one-edge fixed triangular plate bending out of plane subjected to a finite end displacement is imposed perpendicular to the plane. Therefore, the flexural yielding can occur uniformly over the length of the triangular plate without having any plasticity concentration. This concept is implemented in this section for developing new in-plane shear link shapes.

It is worthy of notice that this concept was initially developed for TADAS system (Tsai et al., 1992). The loading direction is perpendicular to the weak bending axis for TADAS; however, in the case of the in-plane fuses, the loading direction is perpendicular to the strong axis. This idea

could be extended to hourglass shaped links also. Therefore to enjoy the benefits of the same curvature for subsequently having the yielding simultaneously, it is needed to set  $b_z$  in such a way that the curvature would be the constant along the length of the link as it is shown in Eq. (20). The shape of the hourglass-shaped link would split into two halves as a result, and the constant curvature is imposed which is shown in Figure 105. Tsai et al. (1992) proposed similar concepts previously for designing out-of-plane shear links in passive control system.

$$\phi = \frac{M}{EI} = \frac{Pz}{EI} = \frac{Pz}{E \left( \frac{b_z^3 t}{12} \right)} \quad (20)$$

By simplifying the above-mentioned curvature equations, it is concluded that:

$$b_z = \sqrt[3]{\left( \frac{12Pz}{E\phi t} \right)} \quad (21)$$

The  $b$  at the end could be calculated based on substituting  $z$  with  $L/2$  which is shown in Eq. (22).

$$b = \sqrt[3]{\left( \frac{6PL}{E\phi t} \right)} \quad (22)$$

Therefore, Eq. is obtained.

$$\frac{w(z)}{b} = \sqrt[3]{\frac{2z}{L}} \quad (23)$$

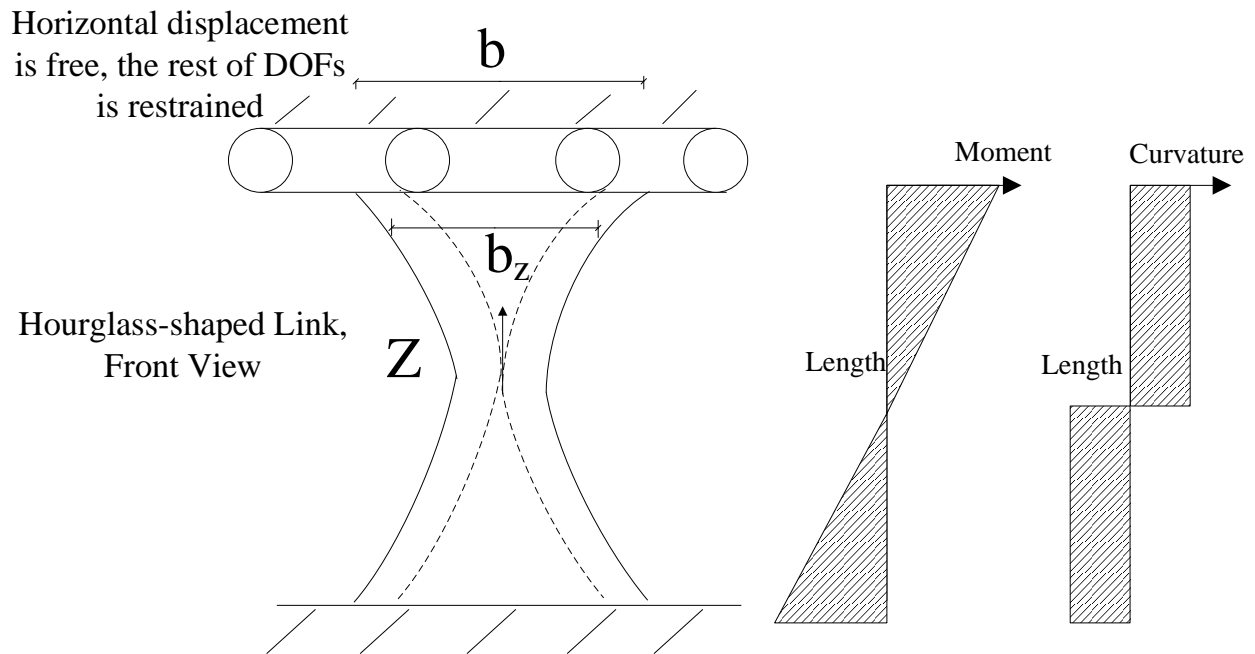


Figure 105. The constant curvature concept

The “uniform yielding along the link length method” indicates that the width of the hourglass-shaped link,  $w(z)$ , should be corresponding to the square root of  $z$ , while the “same curvature” method indicates that  $b$  is better to align with the cube root of  $z$ . In general, the variations of width along the length with respect to  $z$ , the square root of  $z$  and cube root of  $z$  are the variations for use in seismic structural fuses. Figure 106 shows the a general link with added two rectangular plates, commonly referred to as banding plate based on the uniform curvature concept.

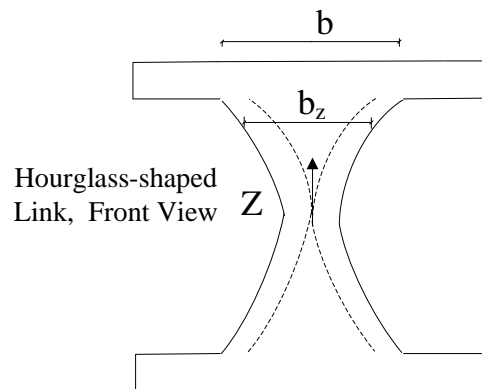


Figure 106. The shape resulted from the constant curvature concept

### **3.4. The proposition of different shapes for fuses based on literature and mathematical concepts**

The strategically shifting the ductile mechanism from buckling and yielding in tension toward local flexure and shear yielding would enhance the hysteretic behavior and energy dissipation which indicates the ability of the system to resist the lateral loads without significant stiffness and strength degradation. The proposed description of the links include the experimental information, the computation analysis, the mathematical concepts and the topology optimization mentioned in details earlier. The fuses are generally divided into three groups according to the applications studied in the second chapter. The difference between the three groups is how the links are configured. The three groups are named as follows:

- First, Single Row of Links (SRLs), which indicates a set of links in a row, which is based on the EBF, coupling beam and linked column, etc. applications.
- Second, Multiple Rows of Links (MRLs), which are based on the panel behavior (e.g. bay bridge application).
- Third, Perimeter Links (PLs) which essentially based on the implementation of the links in the plate (e.g. steel shear walls).

The mathematical concepts mentioned in previous chapters are used. Based on what is mentioned in previous chapters, the cutouts from the steel link, panel and plate would be done. The cutout shapes would be linear, square root, cube root variation with respect to  $z$ . Other possibilities also would be considered which are mainly based on the literature (i.e. straight or rectangular, circular, dumbbell shape). Table 4 indicates the groups based on this and previous studies.

The butterfly-shaped link with the flexural and shear dominated mode of the behavior (FBF and SBF) are designed. The perforated circular cutouts are designed based on the uniform curvature concept. The Oval shape link is proposed to consider the uniform yielding concept. The dumbbell-shape links are proposed in the literature (Lee et al., 2015; Teruna et al., 2014) to consider and investigate the effect of a smooth transition in discontinuities. The straight links are proposed as

an alternative to butterfly-shaped links; these links are proposed to be compared to butterfly-shaped links.

For the multiple rows of links and perimeter, links are designed with the aid of the same concepts; however, since the applications are different, the configuration of the links would be different. It is worthy of notice that with the aid of the explanations in previous sections, the links would be designed to have the ductile mechanism worked instated of the buckling.

Table 4. The abbreviations used in determining the links

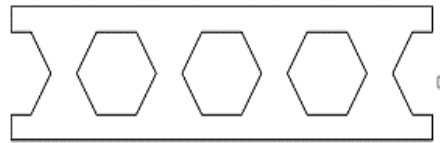
<b>Prototype</b>	<b>NO.</b>	<b>Abbreviation Table</b>	<b>Full Name</b>
<b>SRL</b>	1	Simple Link	Simple ( No cut-out)
	2	FBF-SRL	Flexural dominated Butterfly-shaped Single Row of Links
	3	Straight-SRL	Straight Single Row of Links
	4	P-SRL	Perforated Single Row of Links
	5	SBF-SRL	Shear Dominated butterfly-shaped Single Row of Links
	6	Oval-SRL	Oval Single Row of Links
	7	Dumbbell-SRL	Dumbbell shape Single Row of Links
	8	OP-SRL	Oval perforated Single Row of Links
<b>MRL</b>	9	Simple MRL	Simple panel (No cut-out)
	10	FBF-MRL	Flexural dominated Butterfly-shaped Multiple Row of Links
	11	Straight-MRL	Straight Multiple Row of Links
	12	P-MRL	Perforated Multiple Row of Links
	13	SBF- MRL	Shear Dominated BF-shaped Multiple Row of Links
	14	Oval-MRL	Oval Multiple Row of Links
	15	Dumbbell- MRL	Dumbbell Multiple Row of Links
	16	OP-MRL	Oval perforated Multiple Row of Links
<b>PL</b>	17	Simple PL	Simple plate (No cut-out)
	18	FBF PL	Flexural dominated Butterfly-shaped Perimeter Links

	19	Straight PL	Straight Perimeter Links
	20	PP PL	Perimeter perforated Perimeter Links
	21	SBF PL	Shear Dominated Butterfly-shaped Perimeter Links
	22	OV-PL	Perimeter perforated oval Perimeter Links
	23	DSP-PL	Dumbbell Perimeter Links
	24	OVP-PL	Oval perforated Perimeter Links

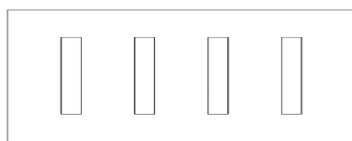
The first group is a single row of the links, which is shown in Figure 107, constructed by a set of proposed links in a row for being used in eccentrically braced systems link beam, linked column and coupled shear wall link beams. At the plate interior, because the shear force across the plate is limited by the links and because the plates are typically thicker than a conventional use, the plate buckling is reduced and initial stiffness is improved.



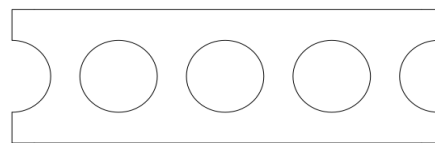
a) The Simple



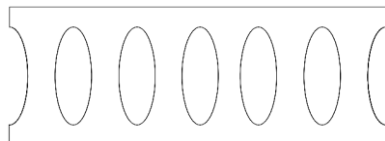
b) The FBF SRL



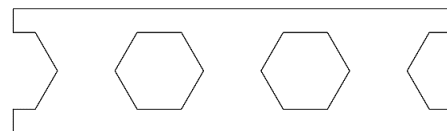
c) The Straight SRL



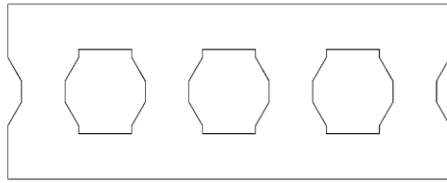
d) P SRL



e) The Oval SRL



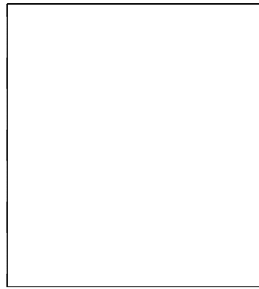
f) The SBF SRL



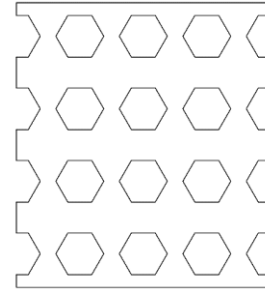
**g) The Dumbbell SRL**

Figure 107. The different configuration of the hysteretic damper

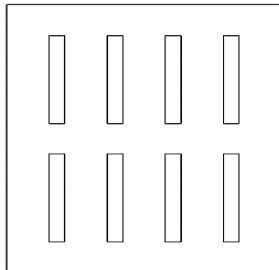
The second group is multiple rows of the links used as panel (e.g. bay bridges) which is shown in Figure 108.



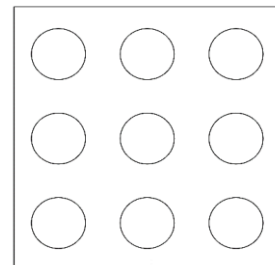
**a) The Simple Panel**



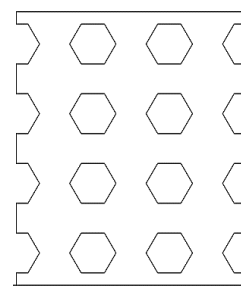
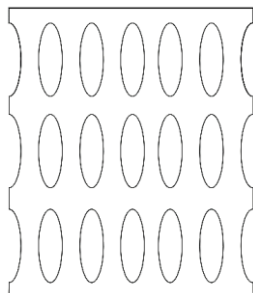
**b) The FBF Panel**



**c) The Straight Panel**



**d) P Panel**



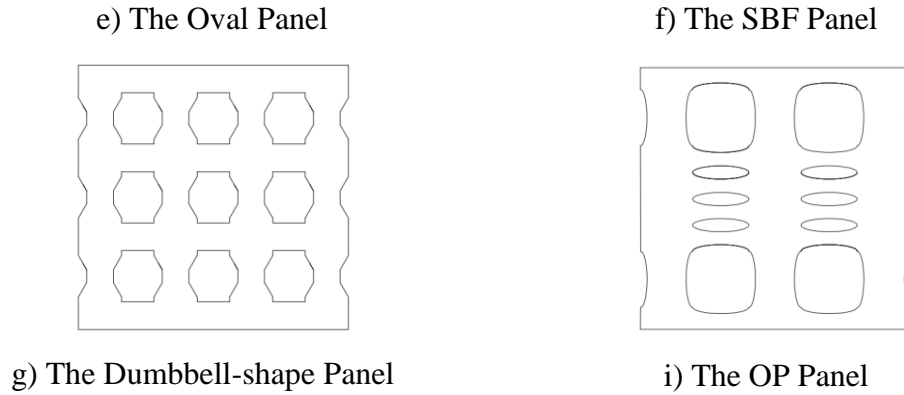
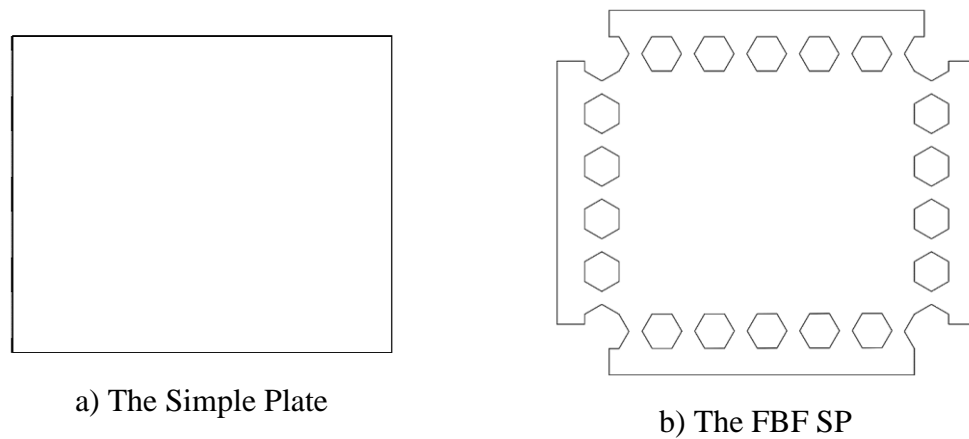
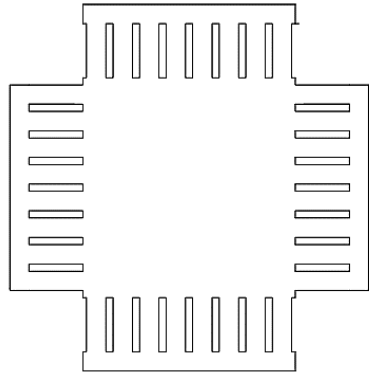


Figure 108. The different configuration of Panels

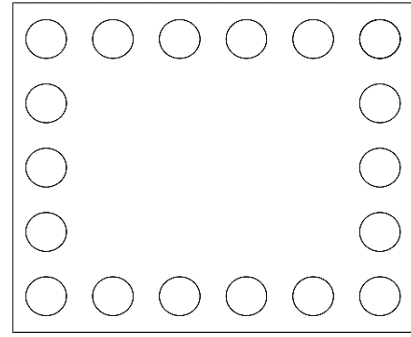
The third group of links, perimeter links, is shown in Figure 109. These type of links would be useful for structural applications such as bay bridges and steel plate shear walls. In addition, the corner cutout indicated in some of the models shown in Figure 109 would be investigated, since these corner cutouts would reduce the demand forces at the connections areas which are reported by researchers before as one of the main issues associated with steel plate shear walls (Berman and Bruneau, 2006).

The flow of the stresses is altered by having cutouts inside of the steel plates. The force is encouraged to be shear parallel with the axis of boundary elements, instead of axis parallel to tension field action. This would prevent from developing large force components perpendicular to the boundary elements, which eventually reduce the moment demand on the connections. This result in considerable reduction of costs due to the efficient design of connections.

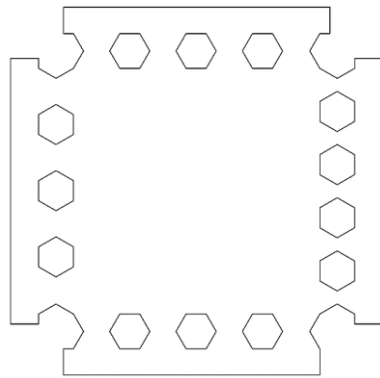




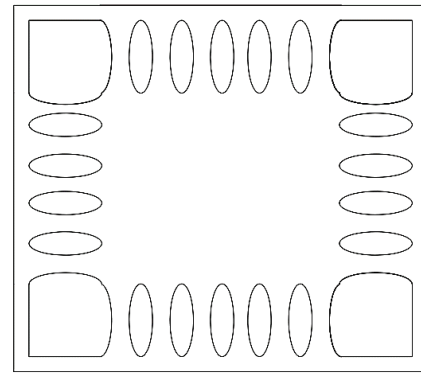
c) The S SP



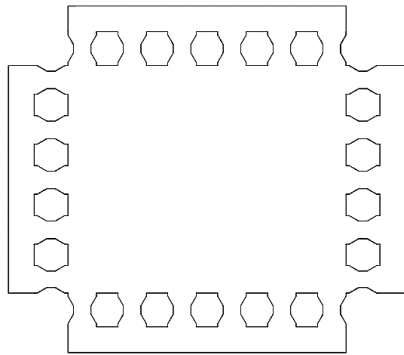
d) The PP SP



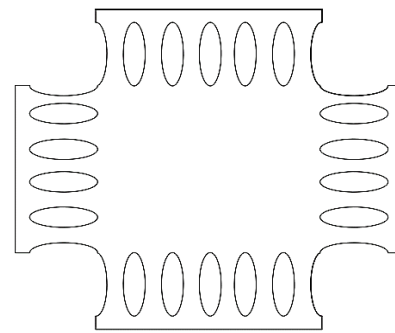
e) The SBF SP



f) PP OV SP



g) The D SP



h) OVP SP

Figure 109. The different configuration of Panels

The effect of axial load is not considered in this study. Considering the application section (Chapter 2), the effect of axial force would be significant in EBF, since the bracing configuration would apply some axial forces on the links. However, for the rest of the applications, the axial forces would not have significant contributions. It is noted even for EBF systems, the flanges of the linking beam could resist the axial force, while the shear mechanism could be resisted by butterfly-shaped links inside the web.

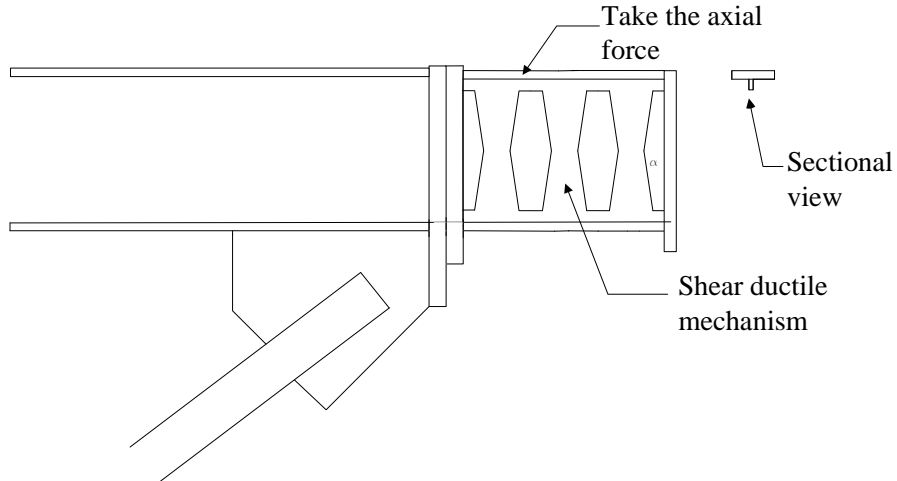


Figure 110. The resisting mechanism for axial force and shear ductile mechanism

In addition, this work would be more concentrated in geometry rather than material. For material, the experimental test would be the appropriate solution rather than just FE modeling methodologies. However, it is mentioned that implementation of low yield steel would make the element prone to low cycle fatigue; therefore, the yielding is recommended to be more than 100 MPA (Lee et al., 2015; Dusika et al., 2004).

### 3.5. Optimization criteria investigation

This section describes the study on the possibility of implementing topology optimizations to come up with better-performance links. The objective of this part is to indicate optimization criteria which would be used for further investigation by others. There is a few number of works done in the past, conducted on basic optimization modeling of the plate, which were mainly focused on stiffness, plastic strain , energy dissipation and amount of used mass (e.g. Deng et al., 2014; Liu et al., 2013; Ghabrai et al., 2010) . In general, the parameters of interest summarized through literature are listed below.

1- Having sufficient ductility. Sufficient ductility would address the problems related to low cycle fatigue for thicker plates (Ma et al., 2011, Lee et al., 2015; Teruna et al., 2015), and prevent early fracture (El-Bahey and Bruneau, 2014). It would also improve inelastic deformation angle and deformation capacity. Spreading the plasticity and having the plasticity focused away from the discontinues could be accomplished by considering this factor (Deng et al., 2014). Ductility is correlated with plastic strains accumulated in the links, which would tremendously affect the low-cycle fatigue. Spreading plastic strains over the link is the subject of many optimization studies (Ghabrai et al. 2010).

2- Having resistance against buckling. The buckling delay would make the links reach to the yielding limit states, whether it is shear or flexure, which is the economical implantation of the material and efficient path to reach to the full strength of the fuse based on ductile mode of behavior (Lee et al., 2016, Farzampour and Eatherton, 2017).

3- Having energy dissipation capability. The energy dissipation is related to how much the specimens are able to move without degradation in strength and stiffness; although, the in-plane stiffness of butterfly-shaped links are reasonable (Whitaker et al., 1991; Koberi et al., 1991). The pinching effect, highly dependent on degradation of strength and stiffness, would significantly reduce the energy dissipation capability; therefore, to reduce the negative aspects of pinching from the hysteric behavior of the link (Lee et al., 2016), one important parameter should be the energy dissipation capability (Deng et al., 2014).

4- Having the ability to reduce boundary forces. The inward boundary forces, especially in steel plate shear walls would impose the high components of the forces for which the connections are supposed to be designed (Berman and Bruneau, 2003; Driver et al 1998, Sabouri et al. 2012, Farzampour et al. 2015). The boundary forces may not be an issue for panels and dampers in general, but it has been reported to be one of the major issues in the steel plate shear walls. Implementation of the links inside of a plate and the effect of adding links on boundary force reduction would be useful in reducing moment demands for steel plates. Another issue in regard to links, is the amount of over strength which is considerably related to the material properties used; therefore, the really low yield steel material should not be implemented due to significant over strength values (This is observed in the specimens done by Ma et al., 2011; Lee et al., 2015),

especially for narrower links ( in Chapter 8, by doing parametric study it is shown that second-order effect for narrower link would take off faster).

5- Having a reasonable amount of mass used for the links. In a number of studies done in the past, the mass limit was set to have an upper bound or lower bound (He et al, 2016).

To summarize the above-mentioned parameters in a practical way, which could be measurable, four concepts are introduced which the optimization criteria will be based on. Therefore, to cover all the issues associated with the links observed in computational, experimental and analytical studies, Figure 111 is represented as an initial step for topology optimization assessments.

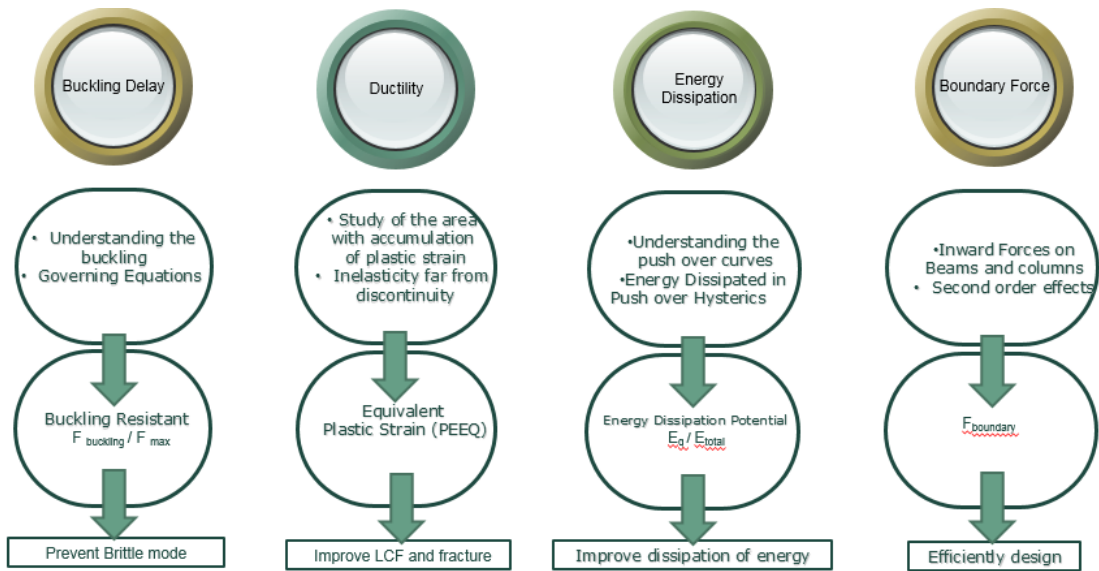


Figure 111. The parameters for topology optimization

The possible procedure to come up with new shapes is summarized. It is represented that for a simple plate with the defined boundary condition, two sets of analysis would be done. The buckling analysis which determines buckling force, and nonlinear analysis for one large cycle with no buckling which determines the maximum force, equivalent plastic strain, boundary forces, and energy index. By having all the outputs, the topology optimizations would iterate to refine the model. The end result of the topology optimization is a plate with elements strategically removed. These cut-outs need to be once smoothed and interpreted as new possible shapes

# 4. INVESTIGATION OF LIMIT STATES FOR BUTTERFLY AND STRAIGHT LINKS.

## 4.1. Introduction

In this chapter, the behavior of butterfly-shaped and straight link are investigated. The equations for strength associated with two limit states of shear yielding and flexure yielding are proposed. The full capacity and initial yielding strength for a general type butterfly-shaped and straight link are explained. Based on the stresses generated in the section of the links, the transition of one limit state (e.g. flexure yielding) to another limit state is discussed. By considering the link's flexural stiffness, link's shear stiffness and shear and flexural stiffness of the banding zone effect, the total stiffness of the butterfly-shaped and straight links are formulated. The behavior of the link after experiencing one limits state is considered and post-yielding behavior for a typical butterfly-shaped link is investigated. Ultimately, to assess the accuracy of the proposed equations, finite element results are implemented for a set of computational models.

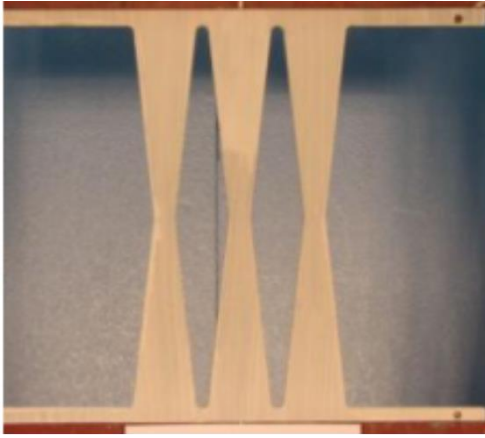
## 4.2. Butterfly-shaped links

### 4.2.1. Butterfly links strength investigation

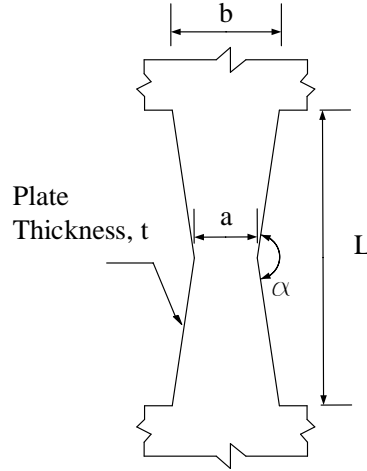
#### 4.2.1.1. *First yield shear strength corresponding to flexural limit state:*

The butterfly-shaped links have shear and flexural ductile yielding limits states. Among which, the lateral torsional buckling, the shear yielding, and flexure yielding are general limit states associated with these links. In this section, the butterfly link capacity for flexure is detailed and formulated. To calculate the strength of the butterfly links, it is needed to derive the maximum values for the stress inside of the link based on the general link loading and geometrical condition (Figure 112).

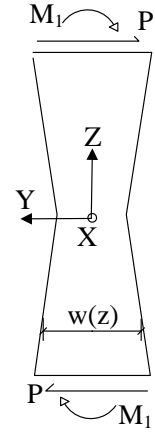
Eq.(24) indicates the moment along a length which is formulated based on the distance from the center. Eq. (25) indicates the width of any rectangular section based on the distance from the center and Eq.(26) is associated moment of inertia.



a) Butterfly fuse plate (Ma et al. 2011)



b) Butterfly link geometry



c) Loading and coordinate axes

Figure 112. The butterfly fuse, link geometry, and loading

$$M(z) = \frac{2M_1z}{L} \quad (24)$$

$$w(z) = \frac{2(b-a)z}{L} + a \quad (25)$$

$$I(z) = \frac{1}{12} w(z)^3 t = \frac{1}{12} \left[ \frac{2(b-a)}{L} z + a \right]^3 t \quad (26)$$

By plugging back the above equations into the general flexural stress indicated the stress along the length at any point with a distance of  $z$  from the middle sections is derived, which is shown in Eq. (27):.

$$\begin{aligned} \sigma &= \frac{MC}{I} = \frac{M(z) w(z)}{I(z) \cdot 2} = \left( \frac{\frac{2M_1z}{Lt}}{\frac{1}{12} \left[ \frac{2(b-a)}{L} z + a \right]^3} \right) \left( \frac{\left[ \frac{2(b-a)}{L} z + a \right]}{2} \right) \\ &= \frac{\frac{121}{Lt}}{\left[ 2(b-a) \frac{\sqrt{(z)}}{l} + \frac{a}{\sqrt{z}} \right]^2} \end{aligned} \quad (27)$$

In which the  $M_1$  and  $P$  is the end moment,  $a$ ,  $b$ ,  $L$ , and  $t$  are geometrical properties associated with butterfly link. To find the maximum values for the above-mentioned equation it is needed to take the derivative of the above equation and equalize it to zero. This would yield to the flexural hinge location ( $z_m$ ) as it is represented in Eq. (28).

$$\sigma_{max} = \frac{3M_1}{2(b-a)at} \text{ at } z_m = \frac{a}{b-a} \frac{L}{2} \quad (28)$$

$z_m$  indicates the point at which the flexural first yielding would occur. Common types of butterfly-shaped links behavior are governed by flexural limit states in general (Xu et al. 2010). The possible areas which are susceptible to strain accumulation, and subsequently a fracture are those areas that hinges are developed, which deformation concentrates, and areas in which a joint of two edges with different curvatures are located.

The butterfly-shaped link has a geometrical change at the end of the links as well as the at the middle section, which are the areas with strain accumulation potential. Therefore, the best area to develop the hinges are those areas, which are far from the sharp angles, meaning that the quarter points which are between the middle section and the end section of the BF links. This concept would be utilized in further investigation of the link considering shear and flexural stress simultaneously. The appropriate  $a/b$  ratio causing the hinges to occur in the quarter points ( $z_m=L/4$ ), is  $1/3$  (Ma et al., 2011). Eq. (29) also indicates if the hinges are located at quarter points, then the  $a/b$  ratio should be equal to  $1/3$  based on the flexural stress estimation.

$$z_m = \frac{a}{b-a} \frac{L}{2} = \frac{L}{4} \rightarrow \frac{a}{b} = \frac{1}{3} \quad \text{and} \quad M_1 = \frac{2}{3}(2a)a \sigma_{max} \quad (29)$$

The hinge location is calculated from the middle of the link; therefore, the values of the  $z_m$  should be less than  $L/2$ . If the  $a/b$  ratio is more than 0.5, then it means that the inelasticity would be at the ends, a transition of behavior is expected.

$$z_m = \frac{a}{b-a} \frac{L}{2} < \frac{l}{2} \rightarrow \text{for } \frac{a}{b} < 0.5 \quad (30)$$

For the cases with  $a/b > 0.5$ , it is shown that the hinge would be formed at the end of the link. This phenomenon mathematically proved by using Eq. (28). In addition, in Chapter 7, it will be shown

that the equations mentioned here are accurate, and the flexural hinges for these cases are developed at the end of the butterfly-shaped link.

Considering Figure 112, the hinges in the flexural limit state would be formed when the maximum stresses reach to yielding limit state. By equating the maximum stress with flexural yielding stresses as indicated in Eq. (31), the amount force needed to initiate the first flexural yielding are obtained which is represented in Eq. (32). The moment at the end associated with the applied force could be calculated by  $P_y L/2$ . It is worthy of notice that the equation at the end could be extended to n butterfly-shaped links.

$$\frac{3M_1}{2(b-a)at} = \sigma_y \rightarrow M_1 = \frac{2(b-a)at\sigma_y}{3} \quad (31)$$

$$P_y^{flexure} = \frac{4(b-a)at\sigma_y}{3L} \quad (32)$$

#### 4.2.1.2. Full capacity investigation of flexural limits state:

Capacity investigation under flexure means that the whole section would be completely plastic. Under the flexural limit state, the force causing the whole section to be plastic is derived by re-establishing force associated with flexural plastic stress equations as it is represented in Eq. (33), and Eq. (34) and Eq. (35). The general stresses are specific section along the length of the butterfly-shaped link is shown in Figure 113.

$$M_p = Pz \quad (33)$$

$$\sigma_y \frac{tw(z)^2}{4} = Pz \quad (34)$$

$$P = \frac{\sigma_y tw(z)^2}{4z} = \frac{\sigma_y t \left( \frac{2(b-a)z}{L} + a \right)^2}{4z} \quad (35)$$

Taking the derivative of the Eq.(33), and equate to zero to find the minimum amount of force would yield to the point in which the full flexural capacity is reached.

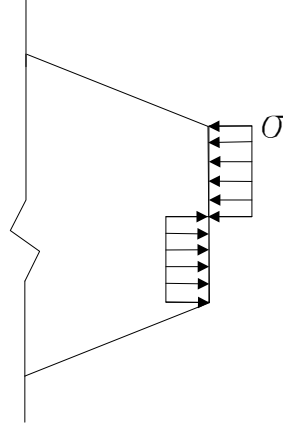


Figure 113. The flexural and shear stresses

$$z_m = \frac{a}{b-a} \frac{L}{2} \left[ \text{for } \frac{a}{b} < 0.5 \right] \quad (36)$$

It is noted that Eq. (36) indicates that the section in which the first elements experience the flexural yielding would eventually be plastic first. The force associated with the formation of full plastic hinging is shown in Eq. (37). The moment associated with  $P_p$  could be formulated with  $-P_p L/2$ .

$$P_p = \frac{\sigma_y t \left( \frac{2(b-a) \left( \frac{a}{b-a} \frac{L}{2} \right) + a}{L} \right)^2}{4 \left( \frac{a}{b-a} \frac{L}{2} \right)} \quad (37)$$

$$P_p = \frac{2(b-a)at\sigma_y}{L} \quad (38)$$

The shear strength of multiple links can be calculated as the shear strength of a single link, given by Eq. (38), multiplied by the number of links.. It should be noted that the moment associated with full plastic flexural hinging of the butterfly-shaped link is 3/2 times greater than the corresponding moment associated with first flexural yielding of the section due to the ratio of plastic section modulus to flexural section modulus.

#### 4.2.1.3. First-yield moment strength corresponding to Shear limit state:

The shear limit state is formulated in this section. The geometry of the butterfly link is according to Figure 114. The maximum shear stress could be for the critical section which is the middle of

the butterfly-shaped link as shown in Figure 114. The maximum shear stress for a rectangular section (Boresi et al., 1992) is calculated based on the Eq.(39). It is indicated that for any rectangular section, maximum shear stress is 3/2 times of the average shear stresses applied to a section.

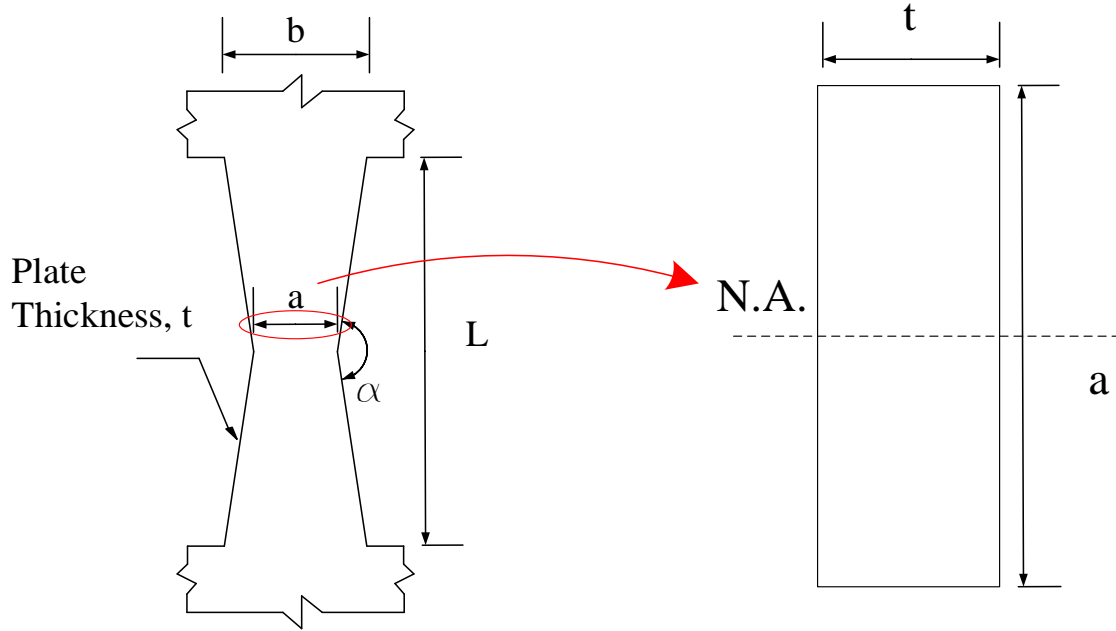


Figure 114. The cross-section of the middle section of a butterfly-shaped link

$$\max [\sigma_{shear}] = \max \left[ \frac{\frac{3}{2} Pt}{w(z)t^2} \right] = \frac{3 P}{2 at} \quad (39)$$

To find the shear values associated with the first yielding limit state, the Von- Mises criterion is implemented. The moment associated with the yielding shear at the end of the link could be calculated with  $P_y L/2$ . For the yielding moment, the shear is not assumed to be uniform.

$$\frac{3 P_y}{2 at} = \frac{1}{\sqrt{3}} \sigma_y \quad (40)$$

$$P_y = \frac{2\sigma_y at}{3\sqrt{3}} \quad (41)$$

#### 4.2.1.4. Full capacity investigation of shear limits state:

Along the same lines, the capacity of the butterfly-shaped associated with the shear yielding limit state is obtained from the Eq.(42). The moment at the end associated with the force could be calculated from  $P_p L/2$ . For the capacity moment, the shear is assumed to be uniform.

$$P_p^{shear} = \frac{\sigma_y a t}{\sqrt{3}} \quad (42)$$

#### 4.2.2. Derivation of the limit state criteria and critical butterfly angle

The governing limit state between flexure and shear is investigated in this section. In this section, the critical geometry in which the shear yielding or flexure yielding would be the governing limit state is investigated. It is assumed that the loading condition is based on Figure 115 and Figure 116. For this section, the residual stress effect and over strength were not taken into account in the mathematical equations. The points along the length of the link that yielding initiates based on the corresponding limit state are investigated for general geometrical link properties.

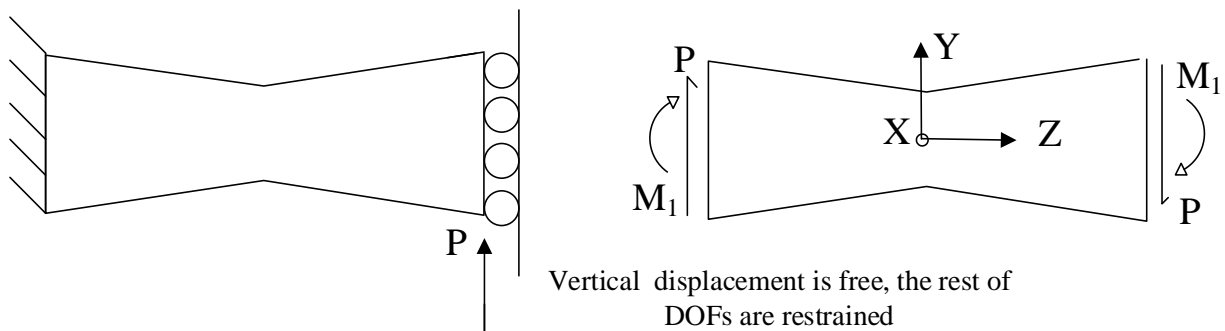


Figure 115. The general geometry and moment-shear distribution

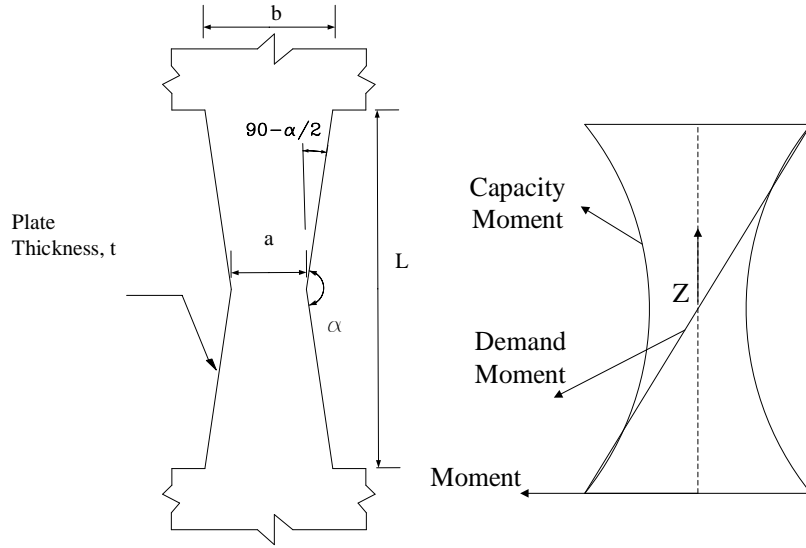


Figure 116. The hexagonal openings and butterfly link

To come up with an equation from which we are able to solve, whether the shear yielding or flexure yielding would be governing, it is needed to consider flexural stress and shear stress equations, and compare them together as it is shown in Eq.(43), Eq. (44) and Eq. (45) . This means that the first yielding limit state would be flexure and definitely the shear limit state would occur after flexural limit state.

$$\sigma_y^{flexure} < \sigma_y^{shear} \quad (43)$$

$$\frac{\frac{3PL}{2}}{2(b-a)at} < \left(\frac{\frac{3}{2}Pt}{at^2}\right) \left(\frac{1}{\left(\frac{1}{\sqrt{3}}\right)}\right) \quad (44)$$

Therefore,

$$\frac{b-a}{L} > 0.28 \text{ Flexure Controls} \quad (45)$$

The right-hand side of the Eq. (45) could be restated with regard to the butterfly angle. By using Figure 116, and Eq. (46) could be re-established as follows:

$$\frac{\frac{b-a}{2}}{\frac{L}{2}} = \tan\left(90 - \frac{\alpha}{2}\right) \quad (46)$$

The Eq. (46) could be solved for  $\alpha$ :

$$\alpha > 148^\circ \quad \text{Flexure Controls} \quad (47)$$

Analytically, if  $\alpha$  is more than  $148^\circ$ , then the flexural limit state would be governing first. In addition, if  $\alpha$  is less than  $148^\circ$  the links are supposed to be yielded in shear compared to flexure. This criterion also would be investigated in Chapter 6 and Chapter 7 by studying FE computational models. It is worthy of notice that, through literature, it has been observed that when the butterfly angle is more than  $148^\circ$ , the flexural limit state is governed (Ma et al., 2011; Lee et al., 2015).

#### 4.2.2.1. *The effect of butterfly-shaped angle on governing limit state:*

It is shown that the geometrical properties indicating that the dominated mode change from shear yielding to flexure, is related to butterfly-shaped angle,  $\alpha$ . Figure 117 indicates how to have the flexure mode to be governing limit state instead of shear mode.

As is this shown for butterfly-shaped links, the angle  $\alpha$  is significantly important parameter for determining whether shear yielding or flexure yielding will control. To understand the behavior of the butterfly links,  $a$ ,  $\alpha$  and  $L$  should be considered. It is noted that the flexural yielding is expected to produce more deformation capacity. To produce the largest deformation capacity, limit  $\alpha$  to be below the limit to ensure flexural hinging ( $\alpha < 148$ ) and set  $a/b=1/3$  to put the flexural hinges as far from points of stress concentration. This would imposes the hinges to be developed at quarter points along the length, which is desirable due to being far from the discontinuities.

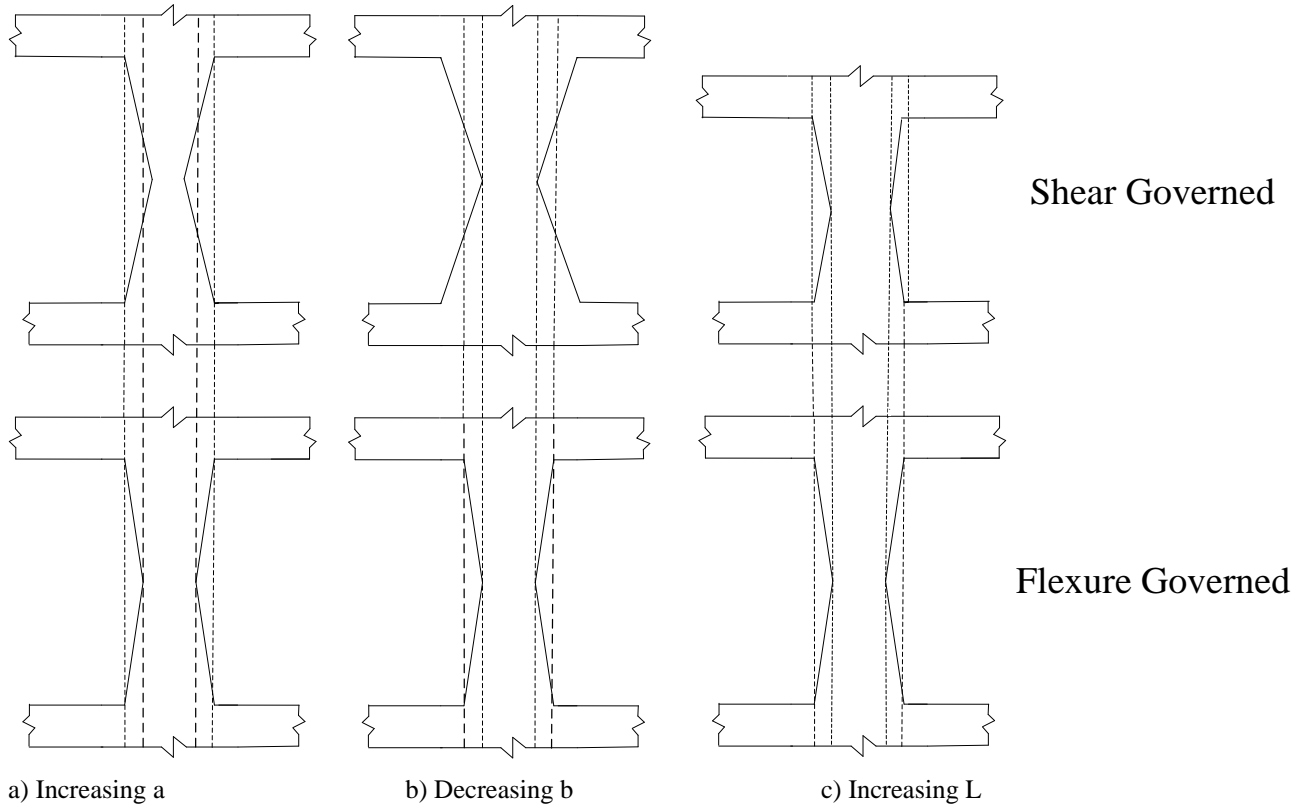


Figure 117. To be going from flexure governed to shear governed

#### 4.2.2.2. The effect of butterfly-shaped link angle on the links capacity:

In this section, based on the capacity concepts for shear yielding and flexure yielding, the forces associated with each limit state is formulated. If the section gets to be yielded fully in shear before flexure, then it means that the total force needed to have the link in shear yielding should be less than the total force for the flexural hinge, this idea is shown in Eq. (48). Eq.(49) and Eq.(50) are based on the comparison of the shear capacity and flexural capacity.

$$P_p^{shear} < P_p^{flexure} \quad (48)$$

$$\frac{\sigma_y}{\sqrt{3}} < \frac{(\sigma_y)at(2b - 2a)}{L} \quad (49)$$

$$0.28 < \frac{b - a}{L} \quad (50)$$

Simplifying Eq. (48), and re-establishing the equation based on the geometrical properties would result in:

Therefore:

$$\alpha < 148 \quad (51)$$

The general governing equations are developed to have a clear view of shear yielding and flexural yielding limit states for butterfly-shaped links. The yielding initiations equations are developed on butterfly link geometry. The butterfly-shaped link angle is introduced as the key parameter indicating which yielding mode will govern. Furthermore, the capacity equation associated with shear yielding and flexural yielding are introduced. Based on which, the parameter of the butterfly angle is calculated. The important result of this analytical study was that the same result would be achieved if also the capacity method is considered. It is concluded that:

-First, to have the plastic yielding initiation of a section along the whole length in flexure mode rather than shear mode we have to have the  $\alpha$  more than 148.

-Second, capacity investigation shows exactly the same results as of the first hinge formation. It is concluded that the initial yielding in shear requirement is the same as having the link to be completely plastic in shear before flexure. Therefore, if the butterfly angle is less than 148, analytically, not only it is expected that the yielding initiates due to shear yielding, but also the whole section would be plasticized in shear before flexure.

### **4.2.3. Butterfly-shaped link stiffness formulation**

Stiffness could be achieved through the virtual work method applied. The force is applied to the top edge of the butterfly-shaped link. It is noted that the total displacement is a combination of the displacement associated with flexural displacement of the butterfly-shaped link ( $\delta_b$ ), shear displacement of butterfly-shaped link ( $\delta_v$ ), and the displacement associated with banding zone rotation ( $\delta_c$ ). The banding zone is the plate with depth of  $c$  attached to the butterfly-shaped link. The stiffness of the butterfly-shaped link includes the banding zone and the link itself

$$\delta_b = \int_{-L/2}^{L/2} \left[ \frac{M(z)^2}{EI(z)} = \frac{Pz^2}{E \left( \frac{1}{12} t \left( a + \frac{2(b-a)}{L} z \right)^3 \right)} \right] \quad (52)$$

$$= \frac{3P \left[ 2L_n \left( \frac{a}{b} \right) + \left( \frac{a}{b} - 1 \right) \left( \frac{a}{b} - 3 \right) \right] L^3}{2 \left( \frac{a}{b} - 1 \right)^3 E b^3 t}$$

$L_n$  is the logarithm based on the natural logarithm. For the shear, the following equation should be regarded:

$$\delta_v = \int_{-L/2}^{L/2} \left[ \frac{\frac{6}{5} V(z)^2}{GA(z)} = \frac{\frac{6}{5} (P)}{Gt \left( \left( a + \left( \frac{2(b-a)}{L} z \right) \right) \right)} \right] = \frac{6PL}{5Gt} \left[ \frac{l_n \left( \frac{b}{a} \right)}{b-a} \right] \quad (53)$$

In which, E is the modulus of elasticity.

Therefore, the stiffness associated with butterfly-shaped link flexural behavior is calculated in Eq. (54). Along the same lines, the stiffness associated with butterfly-shaped link shear behavior is indicated in Eq. (55).

$$K_b = n \left( \frac{P}{\delta_b} \right) = n E b^3 t \left( \frac{2 \left( \frac{a}{b} - 1 \right)^3}{3 \left[ 2L_n \left( \frac{a}{b} \right) + \left( \frac{a}{b} - 1 \right) \left( \frac{a}{b} - 3 \right) \right] L^3} \right) \quad (54)$$

$$K_v = n \left( \frac{P}{\delta_v} \right) = \frac{5Gt}{6L} (b-a) \ln \left( \frac{b}{a} \right) \quad (55)$$

Where n is the number of butterfly-shaped links. The effect of banding zone would be delineated with the help of defining the rotation at the bottom of the butterfly-shaped link as it is shown in Eq. (56).

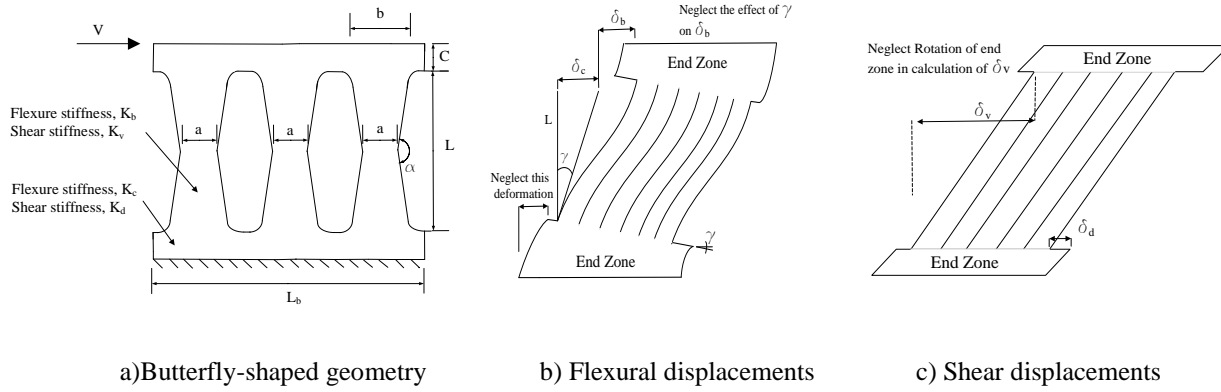


Figure 118. The butterfly-shaped links in a row

$$\gamma = \frac{\delta_c}{L} \quad (56)$$

In which the  $\delta_c$  is the displacement associated with rotational behavior of the banding zone. It is assumed that the curvature is constant along the length of banding zone, which is  $C$ .

$$\int_0^C \phi_y dy = \phi C \quad (57)$$

Eq. (57) indicates that the integration of the curvature from zero up to  $C$ , which could be described as the difference of the rotation between the zero, which is horizontal line and rotation associated with the point vertically located in distance  $C$  from the bottom of the butterfly-shaped link.

$$\int_0^C \phi_y dy = \phi C = \gamma \quad (58)$$

Along the same lines, the rotational displacement of the band zone ( $\delta_c$ ) could be evaluated with Eq. (59)

$$\gamma = \frac{\delta_c}{L} = \phi C = \frac{M}{EI} C = \frac{P * (\frac{L}{2})}{E(\frac{1}{12}(L_b)^3 t)} C \quad (59)$$

$$(60)$$

$$\delta_c^{flexure} = \frac{6PL^2C}{Et(L_b)^3} \rightarrow K_c = n \frac{P}{\delta_c} = \frac{nEtL_b^3}{6C(L)^2}$$

$$L_b = n(b + s) \quad (61)$$

The shear stiffness of the banding zone is calculated based on the following criteria:

$$\delta_d = \frac{6}{5} \frac{PL}{GtL_b} \rightarrow K_d = \frac{5}{6} \frac{GtL_b}{L} \quad (62)$$

In which n is the total number of fuses,  $L_b$  is the total length of n number of links. The total stiffness is equal to the summation of the flexural, shear and banding zone stiffness. It is noted that the total stiffness is calculated based on Eq. (63)

$$K_T = \frac{K_b K_v K_c K_d}{K_b K_v K_c + K_b K_v K_d + K_b K_c K_d + K_v K_c K_d} \quad (63)$$

The effect of the banding zone on the stiffness is suggested to be further studied precisely due to its effect on the overall stiffness. It is recommended that the band zone would be considered in stiffness equations (Ma et al., 2011).

#### 4.2.4. Consideration the effect of shear and flexure simultaneously

In this section, both shear and flexure limit states would be investigated simultaneously. Figure 114 and Figure 115 are considered for derivation of the equations. In addition, the Von- Mises criterion is used to develop the upper limit for the total stress of a butterfly-shaped link. The flexural stresses could be formulated based on the same concepts discussed in previous sections. The moment along the length (formulated from the middle point), and the end moment are indicated in Eq. (64). The varying width and inertia of the butterfly-shaped link are indicated in Eq. (65), and Eq. (66)

$$M(z) = \frac{2M_0 z}{L} \text{ and } M_0 = PL/2 \quad (64)$$

$$w(z) = \frac{2(b-a)x}{L} + a \quad (65)$$

$$I(x) = \frac{1}{12} w(x)^3 t = \frac{1}{12} \left[ \frac{2(b-a)}{L} z + a \right]^3 t \quad (66)$$

In which all the geometrical parameters are defined in Figure 115 and Figure 116. Therefore, the flexural stress is as follows (Eq. (67)):

$$\sigma = \frac{M(z)}{I(z)} \frac{w(z)}{2} = \frac{Pz(w(z)/2 - y)}{\frac{1}{12} \left[ \frac{2(b-a)}{L} z + a \right]^3 t} \quad (67)$$

Along the same lines, we are able to develop the shear stress equations for the butterfly-shaped links Eq (68).

$$\eta = \frac{VQ}{It} = \frac{Pyt(w(z)/2 - y/2)}{I(z)t} = \frac{Pyt \left( \left[ \frac{2(b-a)}{L} z + a \right] - y \right) / 2}{\frac{1}{12} \left[ \frac{2(b-a)}{L} z + a \right]^3 t^2} \quad (68)$$

In addition, yielding criterion Von- Mises stress:

$$\sigma_y^2 = \frac{1}{2} [(\sigma_{11} - \sigma_{22})^2 + (\sigma_{22} - \sigma_{33})^2 + (\sigma_{33} - \sigma_{11})^2 + 6(\sigma_{23}^2 + \sigma_{31}^2 + \sigma_{12}^2)] \quad (69)$$

Therefore, re-establishing the equation would yield to Eq. (70):

$$\sigma_y^2 = \frac{1}{2} \left[ \left( \frac{Pz}{\frac{1}{12} \left[ \frac{2(b-a)}{L} z + a \right]^3 t} \left( \frac{\left[ \frac{2(b-a)}{L} z + a \right]}{2} - y \right) \right)^2 + 6 \left( \frac{Py \left( \left[ \frac{2(b-a)}{L} z + a \right] - y \right) / 2}{\frac{1}{12} \left[ \frac{2(b-a)}{L} z + a \right]^3 t} \right)^2 \right] \quad (70)$$

If inelasticity is needed to be concentrated far from the edges, and to reduce the possibility of crack propagation and brittle modes,  $z$  should be equalized to  $L/4$  which is the farthest point from the sharp edges ( Ma et al.; 2011), substituting the  $L/4$  for  $z$  would lead to Eq. (71). Therefore,

$$\sigma_y = \sqrt{\frac{1}{2} \left[ \left( \frac{\frac{PL}{4}}{\frac{1}{12} \left[ \frac{b+a}{2} \right]^3 t} \left( \left[ \frac{b+a}{4} \right] - y \right) \right)^2 + 6 \left( \frac{Py \left( \left[ \frac{b+a}{2} \right] - y \right)}{\frac{1}{12} \left[ \frac{b+a}{2} \right]^3 t} \right)^2 \right]} \quad (71)$$

The right-hand side of the Eq. (71) indicates the function called stress state function which combines the effect of shear with flexure at the specific section located at L/4 from the midpoint of a BF link. The general stress state function is a continuous function over any specified section along the length of the link (Figure 119), and to have equal state of stresses all over the any specified section of the link, the difference between minimum and maximum critical point should be approaching to zero; therefore, the stress would reach to limit state simultaneously along the length of the link (Farzampour et al., 2018f).

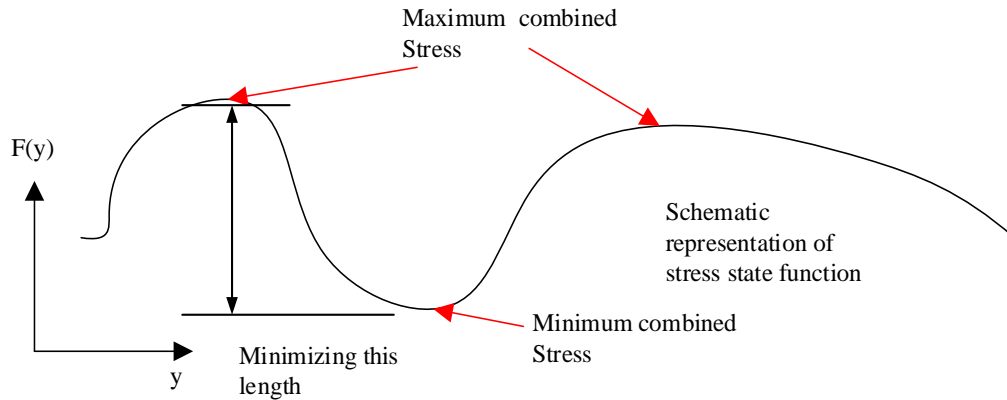


Figure 119. Mathematical concepts for uniform stress

To find the minimum and maximum values of the stress state function indicated in Eq. (72), the derivative of the above stress function should be equalized to zero, which eventually would lead to three real roots shown in Eq. (73), Eq. (74), and Eq. (75)

$$F(y) = \sqrt{\frac{1}{2} \left[ \left( \frac{\frac{PL}{4}}{\frac{1}{12} \left[ \frac{b+a}{2} \right]^3 t} \left( \left[ \frac{b+a}{4} \right] - y \right) \right)^2 + 6 \left( \frac{Py \left( \left[ \frac{b+a}{2} \right] - y \right)}{\frac{1}{12} \left[ \frac{b+a}{2} \right]^3 t} \right)^2 \right]} \quad (72)$$

The three roots are as follows:

$$\text{I:} \quad \frac{a}{4} + \frac{b}{4} \quad (73)$$

$$\text{II:} \quad \frac{a}{4} + \frac{b}{4} - \frac{\sqrt{3}(\sqrt{3a^2 + 6ab + 3b^2 - L^2})}{12} \quad (74)$$

$$\text{III:} \quad \frac{a}{4} + \frac{b}{4} + \frac{\sqrt{3}(\sqrt{3a^2 + 6ab + 3b^2 - L^2})}{12} \quad (75)$$

Therefore, the following criteria should be approaching zero for having the same stress state for all the points along the length of the link.

$$f(II) - f(I) \approx 0 \quad (76)$$

$$f(III) - f(II) \approx 0 \quad (77)$$

$$f(III) - f(I) \approx 0 \quad (78)$$

Eq. (77) is equal to zero and the results of Eq. (78) and Eq. (76) is the same. Eq. (79) is obtained based on the simplification of the results. The results in Eq. (79) could even be stated in a more simplified format as indicated in Eq. (80).

$$\frac{3P^2(3a^2 + 6ab + 3b^2 - L^2)^2}{32t^2(a + b)^6} = 0 \quad (79)$$

Therefore, the appropriate geometrical condition for having the happen at the quarter point and having uniform yielding over the depth of the section,  $y$  is summarized as shown in Eq.(80).

$$a + b = \frac{L}{\sqrt{3}} \text{ in which } \frac{a}{b} = \frac{1}{3} \quad (80)$$

Therefore,

$$b = \frac{\sqrt{3}}{4}L \text{ and } a = \frac{1}{4\sqrt{3}}L \quad (81)$$

To understand the effect of the proposed geometry on the behavior of the links, two different variations of  $(a + b)/\sqrt{4}$  and  $(a + b)/\sqrt{2}$  are considered for the comparison purposes. According to the stress function indicated in Eq. (72), the stress component variation is as shown

in Figure 120. It is concluded that the proposed geometry to consider the effect of shear and flexural stresses together for having the inelasticity located in quarter points would have less variations over the section. At the end of the Chapter 7, the results of the FE analysis on the proposed geometry would be investigated, and it will be shown that this geometry has better performance in terms of plastic distribution of the stresses, equivalent strain accumulation, and maximum displacement over yielding displacement values compared to the rest of the models.

Figure 120 shows that the stress function over the section length for the proposed geometry based on the Von-Mises criterion has uniform stress distribution compared to other cases. The vertical axis shows the stress function results summarized in Eq. (72) for comparison between the proposed geometry and other cases. The horizontal axis is different  $y$  values, for which the stress function is calculated. It is noted that the  $y$  values consider the quarter points of the butterfly-shaped link, and typically these links at the quarter point are less than 25 cm. In later chapter, computational models are shown to compare the behavior of this model with other geometrical shapes.

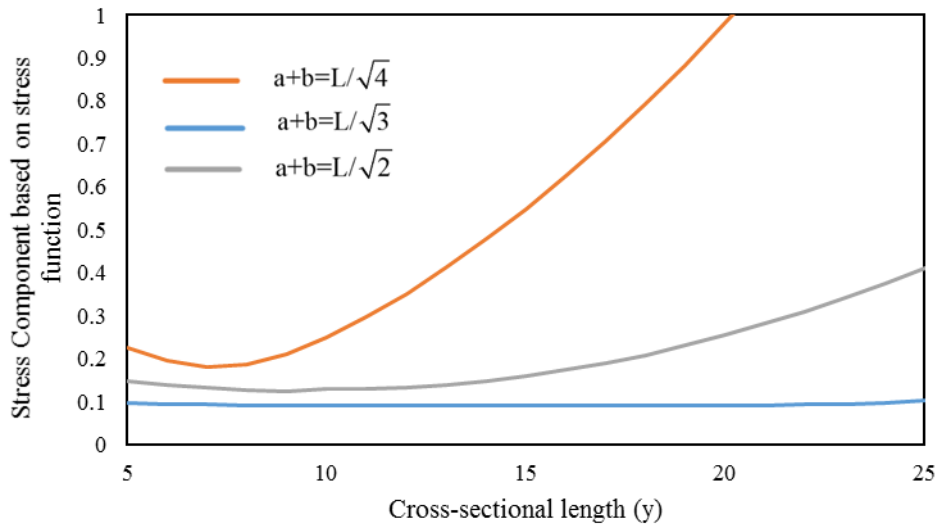


Figure 120. The stress component variation along the half-length of the section

### 4.3. Straight seismic shear link's yielding investigations

#### 4.3.1. Straight link strength formulation

##### 4.3.1.1. First yield and capacity strength corresponding to flexural limit state:

The straight fuses shear and flexural limit states are investigated in this section. The equations developed for estimating the straight links' flexural and shear strength indicated in Figure 121. To evaluate the strength of a yielding straight fuse, hinges at the end of the link length would be developed Eq. (82) indicates the shear yielding force, and Eq. (83) indicates the shear capacity. Following the same lines, To develop the capacity equation for straight links, the coefficient of 3/2 is used

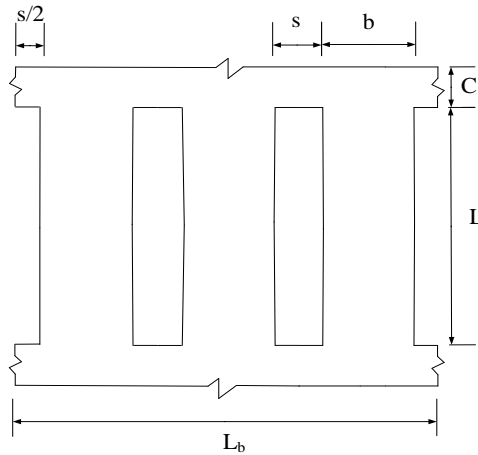


Figure 121. The straight panel

$$P_y = \frac{nb^2t}{3L} \sigma_y \rightarrow P_y = \frac{nb^2t}{3L} \sigma_y \quad (82)$$

$$P_p = \frac{nb^2t}{2L} \sigma_y \rightarrow P_p = \frac{nb^2t}{2L} \sigma_y \quad (83)$$

##### 4.3.1.2. First yield and capacity strength corresponding to shear limit state:

For the shear limit state, the first yielding and capacity of the straight link are indicated in Eq. (84) and Eq. (85).

$$P_y = \frac{2\sigma_y}{3\sqrt{3}}bt \quad (84)$$

$$P_p = \frac{\sigma_y}{\sqrt{3}}bt \quad (85)$$

### 4.3.2. Shear yielding or flexural fielding controlling the behavior

The shear and flexural limit state are formulated in this section. The shear stress could be formulated as follows:

$$\sigma^{shear} = \frac{\frac{3}{2}P}{bt} < \frac{\sigma_y}{\sqrt{3}} \quad (86)$$

Along the same lines, the flexural stresses could be formulated as follows. For flexure:

$$\sigma^{flexure} = \frac{\frac{PL}{2} \left(\frac{b}{2}\right)}{\left(\left(\frac{1}{12}\right)b^3t\right)} < \sigma_y \quad (87)$$

To have a criterion for shear or flexural limit state governing the following equation is derived.

$$\frac{\frac{PL}{2} \left(\frac{b}{2}\right)}{\left(\left(\frac{1}{12}\right)b^3t\right)} < \frac{\frac{3}{2}P}{bt} (\sqrt{3}) \quad (88)$$

By simplifying the Eq. (88), Eq. (89) is obtained.

$$1.15 < \frac{b}{L} \quad (89)$$

Therefore, as it is expected width of the link (b) should be less than 1.15 L to have the flexure governed over shear. The double flexural beam behavior was commonly observed in a number of studies on straight links (Ma et al., 2011; Lee et al., 2015; Hitaka and Matsui, 2003; Hitaka and Matsui, 2006; Cortes and Liu, 2008). The reason for such observation is analytically explained with the Eq. (89) which is a geometrical condition that imposes flexural limit state. The flexure and shear capacity of the straight links are also provided in Eq.(90) and Eq. (91).

The flexural capacity is:

$$P_p^{flexure} = \frac{\sigma_y t b^2}{4z} \quad (90)$$

The shear capacity is:

$$P_p^{shear} = \frac{\sigma_y}{\sqrt{3}} b t \quad (91)$$

If it is needed to have the straight link to be yielded fully in shear before flexure, it is concluded that:

$$\frac{\sigma_y}{\sqrt{3}} b t < \frac{\sigma_y t b^2}{4z} \quad (92)$$

Therefore:

$$1.15 < b/L \quad (93)$$

If the  $b > 1.15 L$  the shear capacity would be governing, however if the  $b < 1.15 L$  the flexure hinging would dominate. It is noted that the  $b/L$  ratio for having the first hinge developed in shear, or the whole section to be plastic in shear or flexure is the same.

### 4.3.3. Straight link stiffness formulation

To derive the stiffness of the straight, a uniform shear load would be applied on one end of the straight, which behaves as a flexural beam. The part from the fixed part to the hatched line (indicated as C or band zone) has a considerable effect on overall stiffens of the straight links; however, this part has not any significant effect on the overall strength of the plate.

Therefore, the total displacement is comprised of flexural displacement, shear displacement, and banding zone.

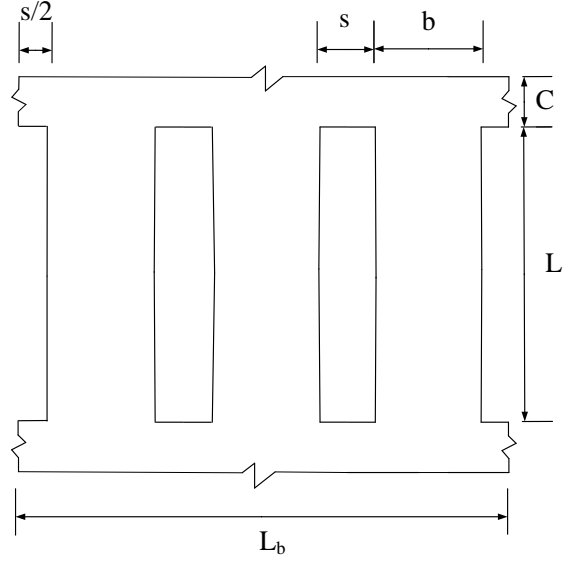


Figure 122. Number of straight links in a row

$$\delta_b = \frac{PL^3}{12EI} = \frac{PL^3}{Et b^3} \rightarrow K_b = \frac{nEt b^3}{L^3} \quad (94)$$

$$\delta_v = \frac{\frac{6}{5}PL}{Gta} \rightarrow K_v = \frac{5 Gtb}{6 L} \quad (95)$$

$$\delta_c/L = \phi C \rightarrow \delta_c = \frac{M}{EI} CL = \frac{P \left(\frac{L}{2}\right)}{Et L_b^3/12} CL = \frac{6cL^2}{Et b^3} \rightarrow K_c = \frac{Et L_b^3}{6cL^2} \quad (96)$$

Where  $L_b = n(s + b)$

$$\delta_d = \frac{\frac{6}{5}PL}{Gtb} \rightarrow K_d = \frac{5 GtL_b}{6 L} \quad (97)$$

$$K_T = \frac{K_b K_v K_c K_d}{K_b K_v K_c + K_b K_v K_d + K_b K_c K_d + K_v K_c K_d} \quad (98)$$

# 5. LATERAL TORSIONAL BUCKLING INVESTIGATION

## 5.1. Introduction

Butterfly-shaped links, which have linearly varying width between larger ends and a smaller middle section, have been shown in previous research to possess substantial ductility and stable energy dissipation capability, but can be prone to other limit states such as lateral torsional buckling (LTB) or shear yielding. In this chapter, the lateral torsional buckling of a butterfly-shaped link subjected to shear loading is conceptualized, and differential equations governing the links' buckling behavior are formulated. The resulting buckling strength is calculated using the shooting method and the results are explored for varying geometric parameters. Regression analysis is used to fit a relatively simple predictive equation to the results.

## 5.2. The governing differential equation for butterfly-shaped links

In this section, a differential equation is formulated with a twist about the longitudinal axis as the variable (Figure 123). It is noted that the cross-section is rectangular with varying width along the length of the link. Figure 124 (a) indicates the local axes from an edge view. The inset of Figure 124 (a) represents the projection of the moment over three local axes considering the related deformation variables based on which the differential equations would be derived. Figure 124 (b) represents the section view, as well as the situation of local axes with an applied moment on the section. The torsional effect of the applied loading is considered as it is represented in Figure 124.

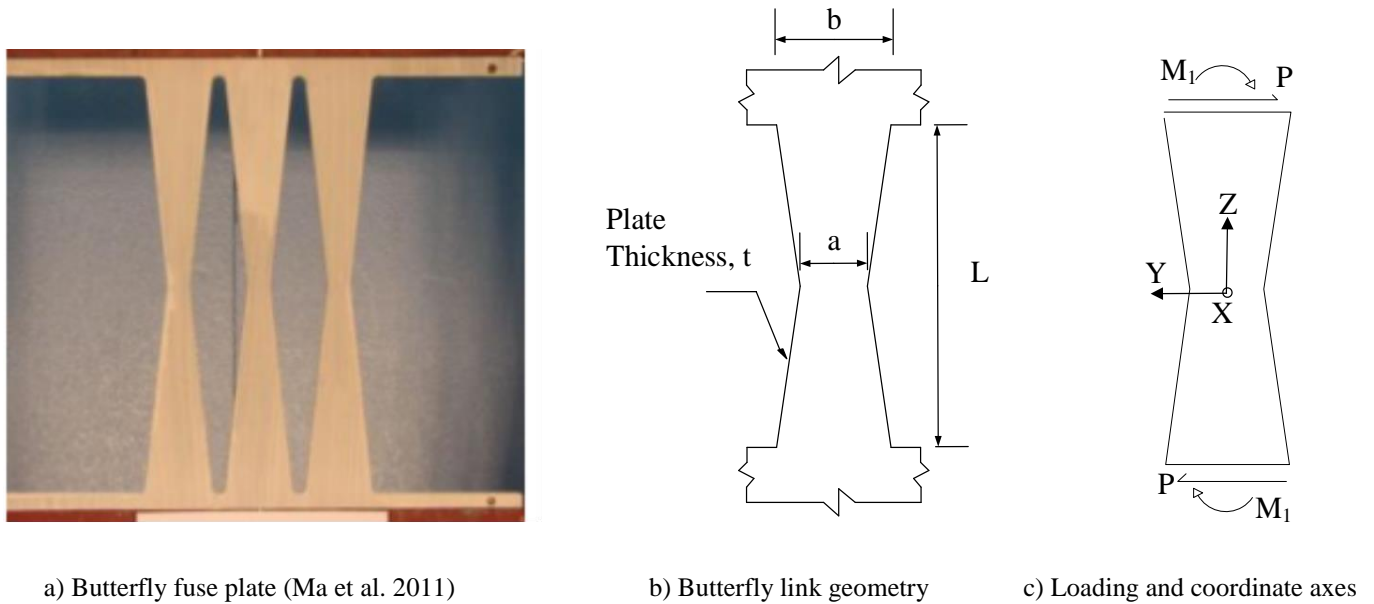


Figure 123. The butterfly fuse, link geometry, and loading

The differential equations are derived based on the assumptions associated with the governing basic differential equations of equilibrium (Timoshenko 1938). It is assumed that the link is free to warp which is a common assumption in lateral torsion buckling analysis of a beam (Timoshenko 1938). It is noted that only uniform torsion or St. Venant's is applied to the section and the ends are free to warping.

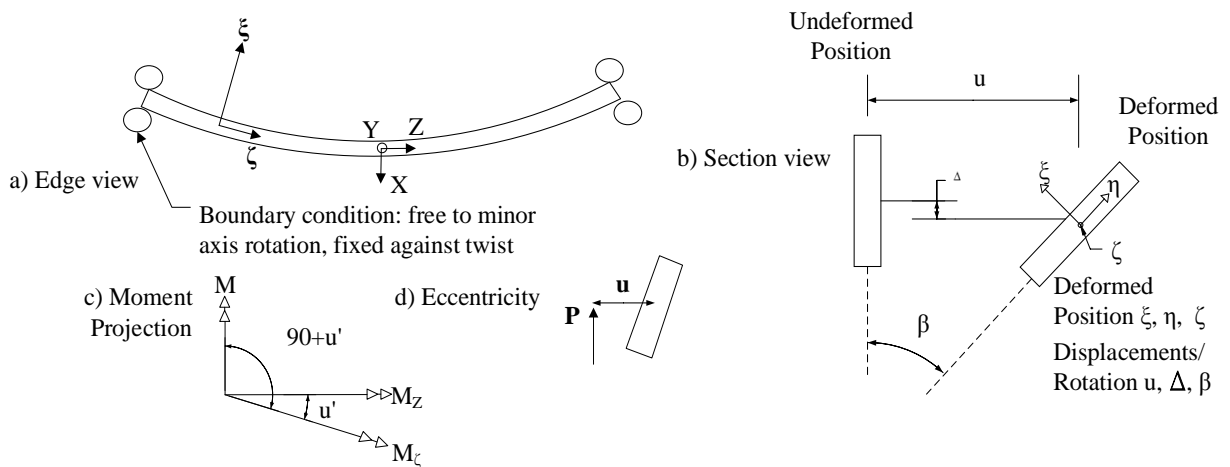


Figure 124. Defining local axes and displacement variables

Since the objective is to derive the critical buckling moment in terms of  $M$ , the local moments are put in terms of  $M$ . From the Figure 124(a), the projection of  $M$  on local axis,  $z$ , would result in Eq. (99). It is noted that rotation is considered small; hence, the Sine of terms having would be approximately equal to itself. Eq. (99) considers the  $M_z$ , projection of  $M$  against the axis  $z$ , the torsional moment along the length of the link, and the end torsional moments as well.

$$\begin{aligned} GJ\beta' &= -\cos\left(\pi - \left[\frac{\pi}{2} + u'\right]\right)M - Pu + M_{end} = -\sin(u')M - Pu + M_{end} \\ &= -Mu' - Pu + M_{end} \end{aligned} \quad (99)$$

in which,  $P$  and  $M$  are the shear and moment along the length of the link, respectively.  $M_{end}$  is the fixed torsional moment in the end. The variables  $u$  and  $v$  are the horizontal and vertical displacements as indicated in Figure 124(b),  $\beta$  is the rotation about the longitudinal axis (twist), and  $\beta'$  is derivative of rotation with respect to  $z$ .  $GJ$  is the torsional rigidity of the strip along the butterfly link. The width of the butterfly link,  $w$ , could be formulated as Eq. (100) which is valid for  $0 < z < l/2$ .

$$w(z) = a + 2(b - a)z / L \quad (100)$$

The angle of twist is small; therefore,  $\sin\beta$  and  $\cos\beta$  are approximately equal to  $\beta$  and 1, respectively. According to Young and Budynas (2002), the exact equation of torsional constant,  $J$ , for a rectangular section is indicated in Eq. (101).

$$J = \left(\frac{w}{2}\right)\left(\frac{t}{2}\right)^3 \left[ \frac{16}{3} - 3.36 \frac{t}{w} \left( 1 - \frac{t^4}{12w^4} \right) \right] \quad (101)$$

According to Figure 123(c),  $M_1$  is the end flexural moment at the end of the butterfly link. The derivative of the moment along the butterfly link length,  $M'$ , is obtained with the assumption of having the moment distribution linear. Therefore, the derivative of the moment is equal  $-P'$  which is  $2M/l$ . The torsional moments can then be assumed for an arbitrary section along the length due to the load  $P$  acting at an eccentricity,  $u$ .

Eq. (102) indicates the projection of the moment against the  $\eta$  axes based on Figure 124. Taking the derivative of Eq. (99) and plugging the Eq. (102), Eq. (103) would be obtained after simplification. It is noted that in Eq. (103),  $J$  is a function of  $z$ , so the left side is not simplified beyond what is represented.

$$EI_y u'' = M_\eta = M \sin \beta \approx \beta M \quad (102)$$

$$(GJ\beta')' = -\frac{\beta M^2}{EI_y} \quad (103)$$

$EI_y$  is the flexural rigidity about the weak axis. From the moment loading distribution, along with the length of the beam, the moment for the right half of the link can be rewritten as:

$$M = -\frac{2M_1}{L} z \quad (104)$$

Therefore, Eq. (103) could be rewritten as follows which is the governing differential equation regarding butterfly-shaped link lateral torsional buckling as indicated in Eq. (105):

$$(GJ\beta')' + \frac{4M_1^2}{L^2} z^2 \frac{\beta}{EI_y} = 0 \quad (105)$$

The governing equation on lateral torsional buckling behavior of the butterfly-shaped fuses is shown in Eq. (105). It is noted that the method for evaluating LTB for the butterfly-shaped links could be extended to any fuses with any linearly varying geometry as well.

The solution for the DE associated with LTB would not be direct due to the reason that all the other parameters in the governing equation are complex functions of the LTB angle, which makes the whole equation significantly nonlinear; therefore, for finding answers for a differential equation, mathematical methods are implemented. In later chapters, a new method is proposed, programmed and explained for solving such equations. Ultimately, this method is verified with the results extracted from different models in the FE program.

It is noted that the warping condition for this work is assumed to be free along the length of the link and at the boundaries. As it is mentioned in literature, warping does not allow a plane section to remain as plane after twisting. The warping is the predominant mode of behavior in thin walled sections; therefore, it does not significantly change the butterfly-shaped results since the sectional properties would remain rectangular along the length.

### 5.3. Solution assessment using parameter non – dimensionalization for governing differential equations

The buckling equation for butterfly-shaped links could not directly be solved due to high nonlinearity of the differential equations. In this part, a new mathematical method is proposed to find the solutions for the mentioned differential equation. To get all the differential equations in an appropriate format to be solved to be useful to solve, first, the parameters reformulate to be non-dimensional. This would eliminate the need for another extra variable, which means less analysis cost. A way to do so is to divide all the dimensions by the length of the link. In what follows, each equation is non-dimensionalized. The results are shown in Eq. (106), Eq.(107), Eq. (108), and Eq. (109). The Poisson's ratio is assumed to equal to 0.3.

$$A = a/l \quad B = b/l \quad G = 1/2.6 \quad \Omega = M_1 / El^3 \quad K = \frac{J}{l^4} \quad L = l/l = 1 \quad Z = z/l \quad (106)$$

$$W(z) = A + (2(B - A)Z) \quad (107)$$

$$K = \frac{1}{3} T^3 W \left( 1 - \left( \frac{0.63T}{W} \right) \left( 1 - \left( \frac{T}{W} \right)^4 \right) \right) \quad (108)$$

$$I_y = \frac{1}{12} t^3 w \rightarrow \phi_y = \frac{1}{12} T^3 W \quad (109)$$

The non-dimensionalized version of the differential equation could be written based on the non-dimensionalized parameters stated above, which is shown in Eq. (110).

$$\left( \frac{K\beta'}{2.6} \right)' + 4(\Omega)^2 (Z)^2 \frac{\beta}{\phi_y} = 0 \quad (110)$$

### 5.3.1. Solving the differential equation using MATHEMATICA implementing the shooting method

The non-dimensionalized differential equation from the previous section was used as an input for the software Mathematica. The resulting buckling modes represented by the twist angle,  $\beta$ , can be either symmetric or anti-symmetric. The symmetric mode with no nodes will give the lowest buckling moment (i.e., the critical moment).

Since the problem is linear and homogeneous, one can choose an arbitrary value for  $\beta(0)$ . The shooting method is used to solve the differential equation, in which a guessed value would be assigned to the moment, and the program varies it automatically until the boundary condition at  $z$  equal to 0.5 is satisfied. If the plot of  $\beta(z)$  looks like a symmetric buckling mode (e.g. Figure 125), the result is taken as the critical moment. If not, the initial guess for the moment is revised until a symmetric buckling mode is obtained.

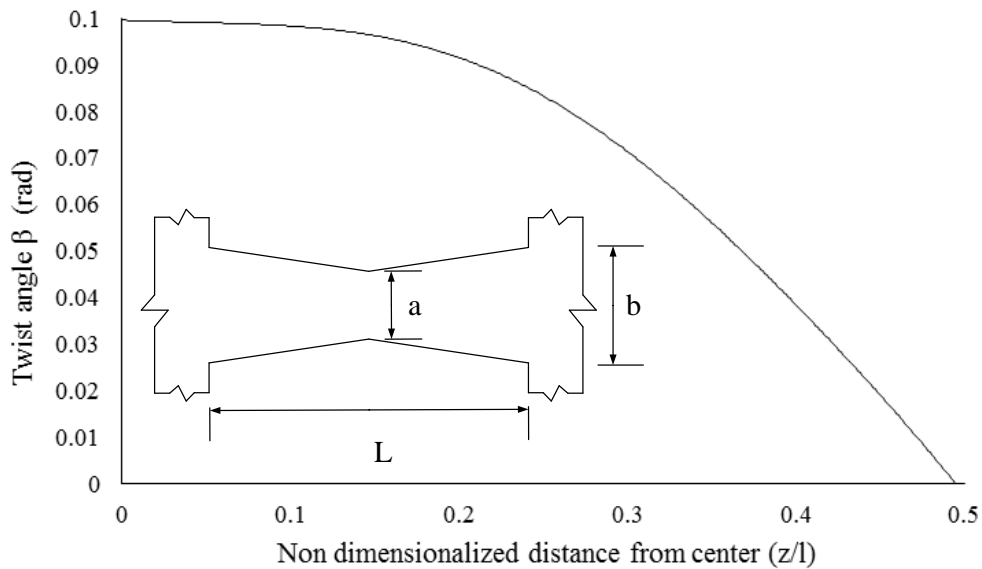


Figure 125. The first mode for  $\beta$  to show a symmetric mode with assumptions of  $\beta'(0) = 0$  and  $\beta(0.5) = 0$

### 5.3.2. Establishing lateral torsional buckling equation based on the parametric study on geometrical properties of the butterfly-shaped links

To further analyze the obtained methods, the parametric study on the buckling behavior of the butterfly-shaped links is done to understand the effect length over thickness ratio ( $L/t$ ), mid-width to bottom width ratio ( $a/b$ ) and bottom-width over the length ( $b/L$ ) on the buckling condition of the link. The result of this part would be summarized as a lateral torsional function describing the link behavior. Sixty-four models are chosen to be studied in this section. Table 5 indicates all the variations considered for the purpose of the parametric study.

Table 5. Parametric study values associated with each of parameters

<i>For L=0.5</i>				
<b><i>L/t</i></b>	10	20	40	60
<b><i>a/b</i></b>	0.1	0.33	0.75	1
<b><i>b/L</i></b>	0.1	0.2	0.3	0.4

The following criteria are proposed to compare the different butterfly-shaped link configuration with each other as indicated in Eq. (111). The results as indicated in Figure 126 would represent that the best geometry to be used to have the best efficiency of the amount of steel used with respect to highest critical buckling moment is  $a/b=0.1$  and  $a/b=0.33$ . Further FE analysis also indicates that the butterfly-shaped link with a narrower middle width (e.g.  $a/b=0.1$ ) or wide middle width ( $a/b=1$ ) are prone to highest accumulation of plastic strain; therefore, the best geometry recommended for the butterfly-shaped link would be  $a/b$  equal to  $1/3$ .

$$\frac{M_{cr}}{Volume} \tag{111}$$

Figure 127 indicates the trends critical buckling moment variation based on the  $b/L$ . It is concluded that the trends are similar; however, the thickness has a significant effect on the overall results.

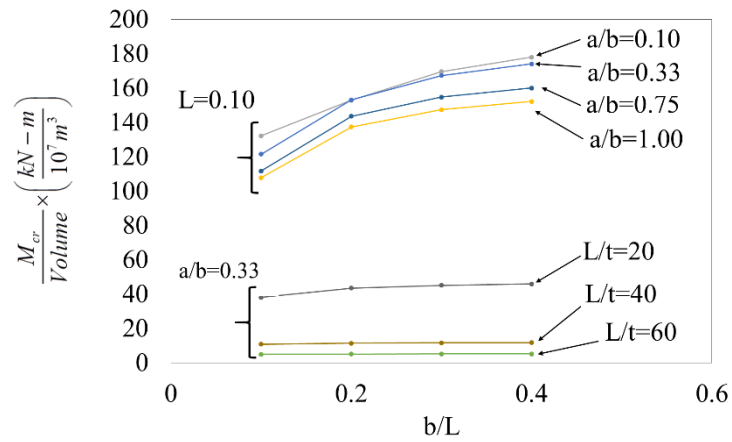


Figure 126. The parametric study results and the effect of the variation of  $a/b$ ,  $b/L$  and  $L/t$  on critical buckling moment

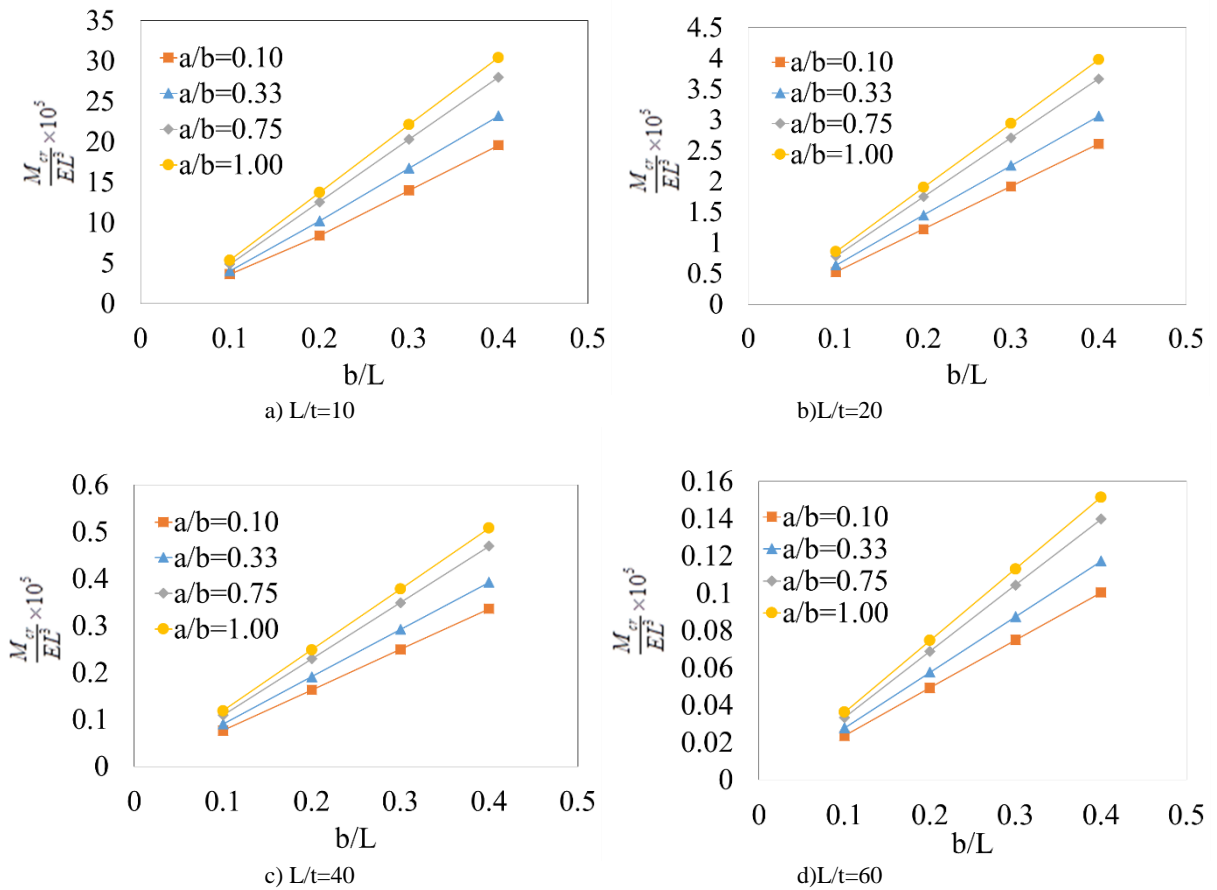


Figure 127. The parametric study results and the effect of the variation of  $a/b$ ,  $b/l$  and  $L/t$  on critical buckling moment

The important conclusion from the Figure 127 is that the effect of  $L/t$  ratio is significantly more noticeable than  $a/b$  ratio on critical buckling moment for butterfly-shaped links.

### 5.3.2.1. Regression Analysis on Data from the Critical Buckling Moment Analysis

To precisely estimate the shooting method results with analytical equations, regression study with different parameters has been done. In this study, the main parameter is  $a/b$  ratio. The following equations indicate the proposed equation for critical buckling moment. Eq. (112) would assess the critical moment with high accuracy. The accuracy of the proposed equation is examined in Figure 128, which represents the proposed critical moment equation regression line, and the actual data obtained from the shooting method. The  $R^2$  value is about to be 1 and the slope of the trend line is equal to 1, which shows that the regression equation has satisfactory accuracy.

$$\frac{M_{cr} L \sqrt{1+\nu}}{E b t^3} = [0.533 + 0.547(a/b) - 0.281(a/b)^2 + 0.096(a/b)^3] \quad (112)$$

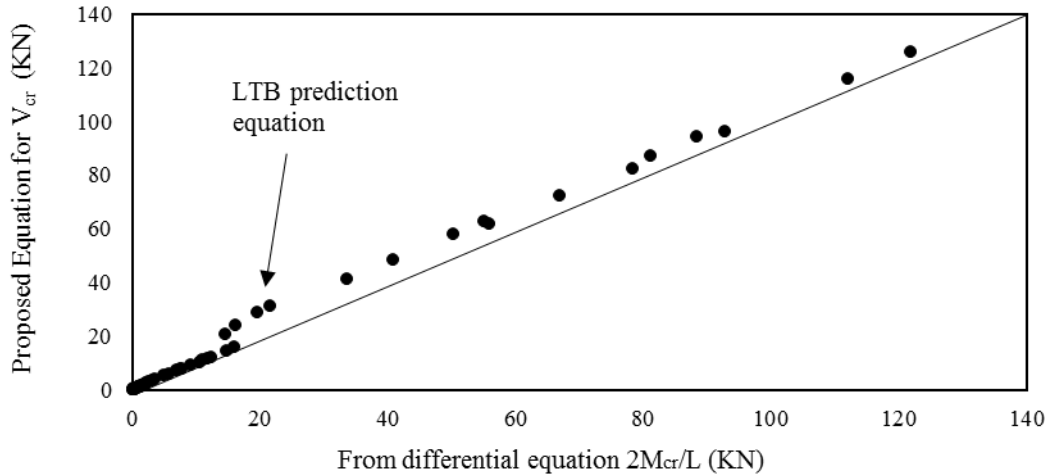


Figure 128. The accuracy of the proposed equation in assessing the critical buckling moment

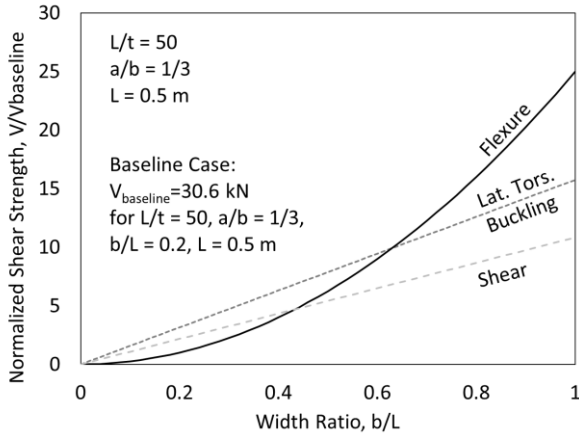
In addition, the linear regression shows a jump at 20 kN which is related to the set of models with lowest  $L/t$  values or higher thicknesses. These models compared to other models are subject to yielding limit states rather lateral torsional buckling due to higher thickness of the plate. Figure 129a shows that the lateral torsional buckling strength and shear yielding strength vary linearly with the width ratio,  $b/L$ , while the flexural yielding strength experiences quadratic growth. At a

width ratio,  $b/L=0.44$ , the baseline case switches from flexural yielding controlled to shear yielding controlled. This demonstrates the intuitive concept that links that are wide relative to their length are more prone to shear yielding or shear related failure (e.g. see El-Bahey and Bruneau 2012). For a fixed link length,  $L$ , varying the slenderness ratio,  $L/t$ , such as done in Figure 7b, has the effect of varying the thickness,  $t$ . Flexural yielding and shear yielding are both linear functions of the thickness, while the lateral torsional buckling is a cubic function of the thickness as shown in Eqn. (9). This is demonstrated in Figure 129b as decreasing the thickness (increasing  $L/t$ ) results in a greater loss in lateral torsional buckling strength. At a slenderness ratio,  $L/t=88$ , the lateral torsional buckling strength falls below the flexural yielding strength and starts to control for this baseline case.

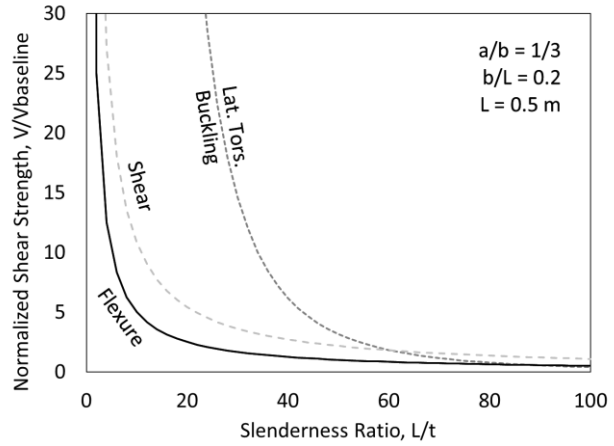
The variation in link shear strength with changing taper ratio,  $a/b$ , is shown in Figure 129c. With the fixed values for  $b/L$  and  $L$ , varying the taper ratio,  $a/b$ , from 0 to 1 has a linear effect on the width at the middle of the link,  $a$ , and thus a linear effect on the shear yielding strength. The lateral torsional buckling strength, on the other hand, is a cubic function of the taper ratio. The two parts of flexural yielding strength in Eqn. (12) are clearly demonstrated in Figure 129c. For  $a/b \leq 0.5$ , the plastic hinge forms along the link length interior. For  $a/b > 0.5$ , the plastic hinge forms at the ends of the link and thus flexural yielding strength is no longer affected by taper ratio (given a fixed width at the ends,  $b$ ). The link length,  $L$ , is varied in Figure 129d. In this case, with fixed characteristic ratios  $L/t$ ,  $a/b$ , and  $b/L$ , varying the link length,  $L$ , has the effect of linearly scaling the entire geometry of the link. As is shown in Figure 129d, the relationship between the strength for the three limit states stays constant as the geometry is scaled because all three equations are quadratic functions of the scale factor. This indicates that the scale of the link is not important when determining which limit state controls. Scale sets the magnitude of the link strength but otherwise is not expected to affect the behavior or progression of limit states. This observation reinforces the importance of the nondimensional ratios,  $L/t$ ,  $a/b$ , and  $b/L$ . It is noted that the conclusions in this chapter are summarized in Farzampour and Eatherton (2017), and Farzampour and Eatherton (2019) articles.

In addition, the warping condition for this work is assumed to be free along the length of the link and at the boundaries. As it is mentioned in literature, warping does not allow a plane section to remain as plane after twisting. The warping is the predominant in thin walled sections; therefore,

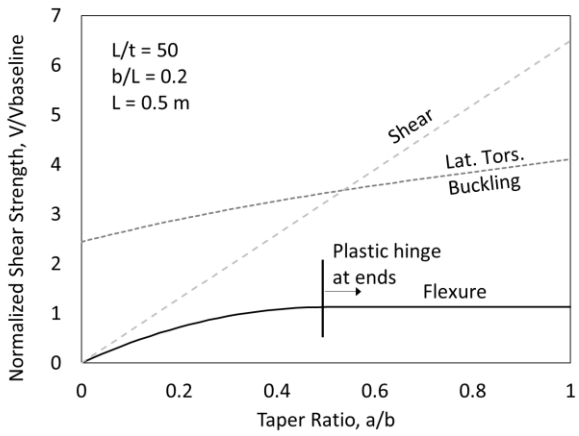
it does not significantly change the butterfly shaped results since the sectional properties would be rectangular along the length of the shear link.



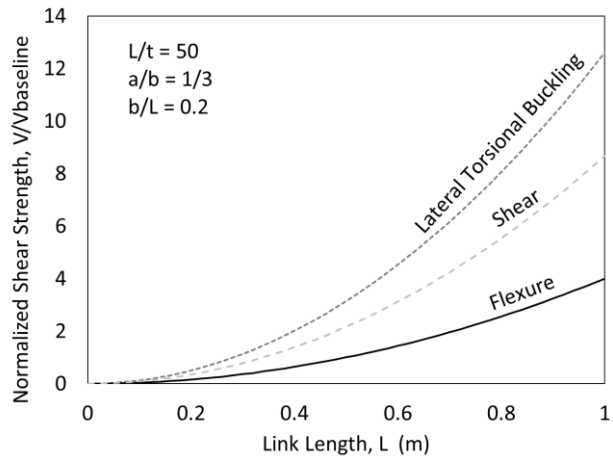
a) Effect of Link Width



b) Effect of Link Thickness



c) Effect of Taper Geometry



d) Effect of Link Length

Figure 129. Moment strength based on three limit states

# **6. COMPUTATIONAL STUDY ON LINKS, STRATEGY, AND VERIFICATION OF THE METHODOLOGY**

## **6.1. Introduction**

In this section, the computational approaches for analyzing the butterfly-shaped links would be delineated. The assumptions and modeling procedure are investigated in details. The modeling methodology for computational study is verified under a monotonic and cyclic loading conditions for laboratory tests done by Ma et al. (2011), Lee et al. (2015), Driver et al. (1998), and Ascheim et al. (2002). The modes of behavior of the experimental studies are captured with computational modeling methodology. Along the same lines, the imperfections study, which is related to initial condition of steel plates deformed out-plane, is investigated and the appropriate values for imposing imperfection are mentioned.

## **6.2. Computational study**

The models are made with aid of the finite element software ABAQUS FE program. The boundary conditions and the loading are assumed as it is indicated in Figure 130 and Figure 131 . The displacement controlled loading is assumed to be applied on the edge of the butterfly-shaped link. The properties of the steel material are chosen from the typical properties of the steel with strength hardening (Ma et al., 2011) which is shown in Table 6. An elastic perfectly plastic constitutive model was used for the steel with elastic modulus,  $E=200$  GPa and yield stress,  $F_y=273$  MPa, based on coupon tests reported in Ma et al. (2011). The dynamic explicit module is chosen as the main solver used for analysis purposes. It is noted that other solvers such as static general are used for analysis and verifications as well.

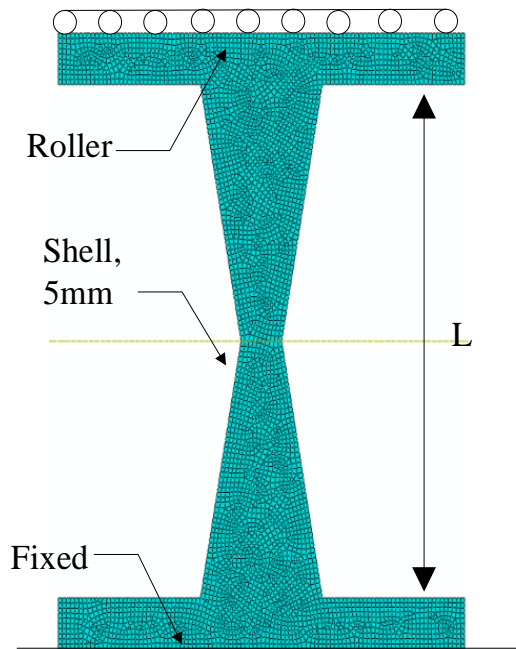


Figure 130. General properties of a model in ABAQUS

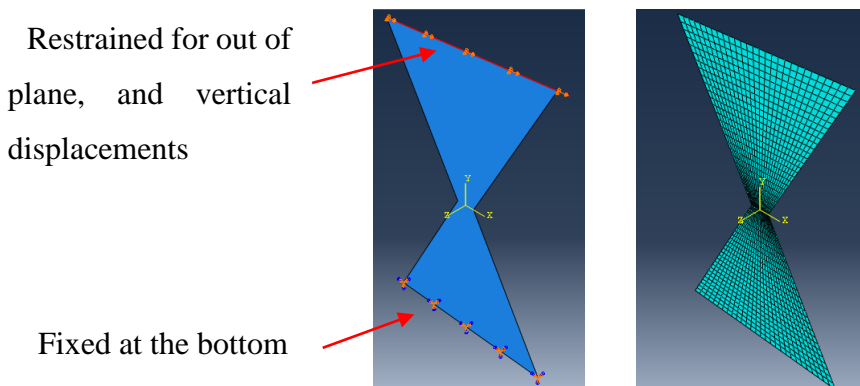


Figure 131. The butterfly-shaped link modeled in FE program

The shell element with four nodes with reduced integration condition is chosen (S4R). The S4R element is checked to avoid any hour glassing or shear locking issues affecting the output parameters. The mesh size for finest mesh size would be less than  $b/60$ . The mesh sensitivity analysis is conducted on the mesh size and the results are shown in the Appendix A. The boundary condition is fixed at the bottom and restrained out-of-plane at the top. It is noted that the procedures included in the Appendix A and Appendix B are implemented for modeling the structural fuses in

this study. The imperfection of  $L/250$  is considered based on the recommended values for the links in general (Egorova et al., 2013). It is noted that the study on imperfection for butterfly-shaped links are included in the Appendix B. The constitutive model is generally used as it is reported by Ma et al. (2011).

Table 6. The constitutive model used for modeling purposes

	$\sigma_y$	$\sigma_u$	Elongation
<b>Fuse</b>	273	374	0.32

### 6.3. Validation of numerical results

To validate the modeling methodology, four different laboratory experiments are investigated. The accuracy of modeling methodology has been established through verifying the laboratory tests. The pushover curves, failure modes and the general behavior of the models are verified against the corresponding experimental tests.

#### 6.3.1. Stanford test by Ma et al. (2011) on butterfly-shaped links (B10-36)

Specimen B10-36W is one of the butterfly-shaped structural fuses tested by Ma et al. (2011) and is shown in Figure 8a. The specimen had six links with length,  $L=229$  mm, width at link ends,  $b=64$  mm, width at link middle,  $a=25$  mm, and thickness,  $t=6$  mm. This specimen had a slenderness,  $L/t=36$  that was in the middle of the range tested by Ma et al. (2011) which went from  $L/t=14$  up to  $L/t=56$ .

A three-dimensional computational model, shown in Figure 132, was created in the commercial software package Abaqus (Simulia 2016). To more accurately capture the boundary conditions, part of the reaction frame is included in the model. Vertical struts were located on either side of the experimental specimen and were connected to the horizontal loading beam at the top and the reaction frame at the bottom with steel pins in double shear. The loading beam, vertical struts, and butterfly-shaped fuse plate were modeled using four-node reduced integration shell elements with 5 integration points through their thickness. The mesh was relatively coarse for the loading beam at approximately 30 mm on a side, and refined for the fuse plate at approximately 10 mm on a side. This results in approximately six elements along the width of the butterfly-shaped link at its

narrowest point and forty-six elements along the link length. A mesh sensitivity analysis showed negligible variation in the cyclic load deformation behavior with a reduction in mesh size of 50%. Initial imperfections were neglected.

In the test setup, the bottom of the butterfly-shaped fuse plate was sandwiched between two thick angles that were bolted to a rigid reaction beam as shown in Figure 132. This was simulated in the model by fixing all degrees of freedom at the bottom of the plate at the line of bolts. The nodes of the cross-section at the ends of the loading beam were tied to a single reference node which was in turn pinned (translational degrees of freedom constrained) to the top of the vertical strut. The bottom of the vertical strut was also pinned against translation, but rotationally free. The loading beam was constrained against out-of-plane translation at all locations. The band zones above and below of the links are modeled to account for their influence on stiffness mainly. The multi-purpose interaction (MPC) is used between the columns to beam connection. The bottom of the columns are considered as hinges, and the bottom of the butterfly-shaped links are assumed as fixed. The pushover curves are extracted based on the force at the bottom of the link and displacement at the top of the beam.

An elastic perfectly plastic constitutive model was used for the steel with elastic modulus,  $E=200$  GPa and yield stress,  $F_y=273$  MPa, based on coupon tests reported in Ma et al. (2011). A cyclic displacement history was applied to one end of the loading beam to match the experiment. The FE analysis was run using a dynamic explicit solver and considered geometric nonlinearity.

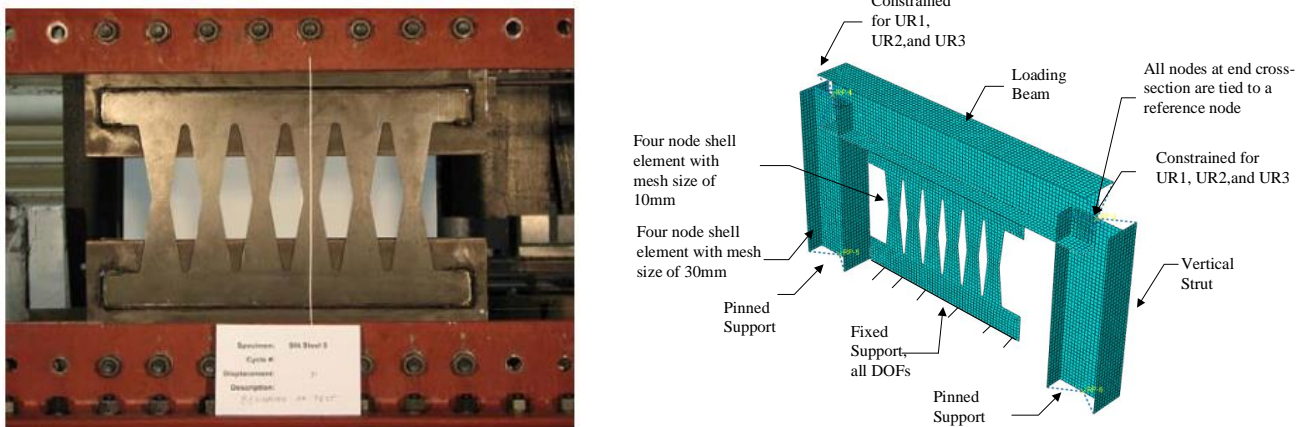


Figure 132. Specimen B10-36 and the model constructed in FE software

The initiation of the buckling has happened at 2.4% drift ratio according to Ma et al. (2011) as indicated in Figure 133. The FE model was able to capture the buckling. At a drift ratio of 2.4%, the buckling is observed which is captured in FE model shown in Figure 133 and Figure 134.

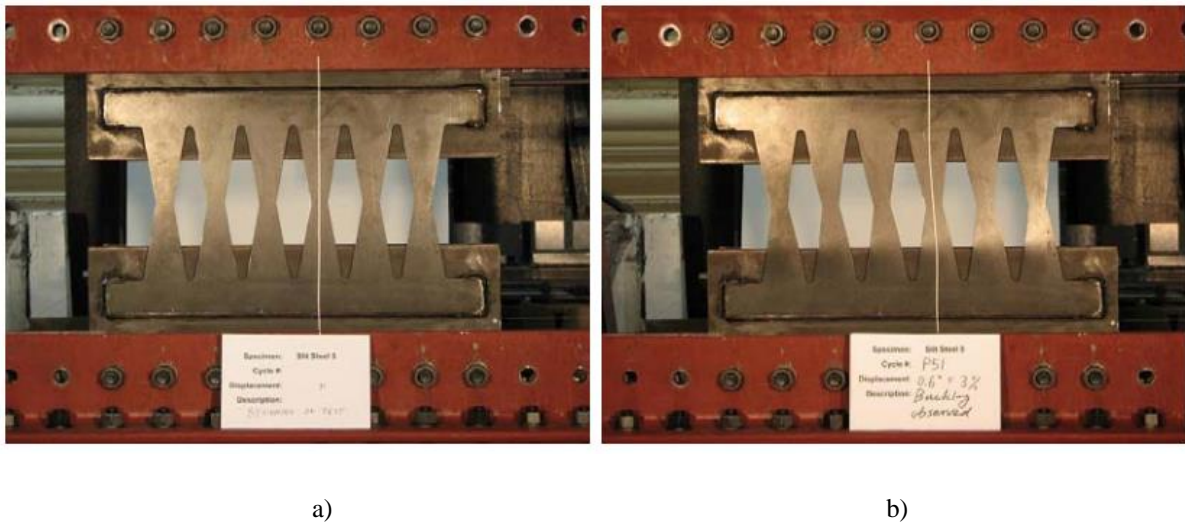


Figure 133. Specimen B10-36 a) beginning of the test; b) buckling initiation at 2.4% drift ratio

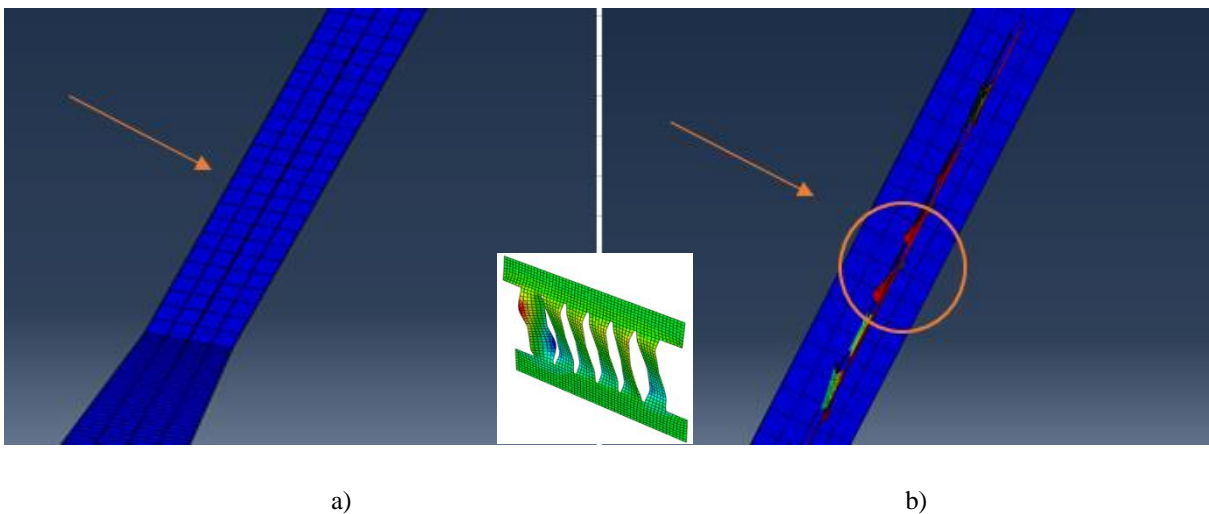


Figure 134. Specimen B10-36 a) beginning of the FE modeling; b) buckling initiation at 2.4% drift ratio in the FE model

Figure 135 shows a comparison of the hysteretic behavior obtained from the FE model as compared to the experiment. The model peak strength was within 15% of the experiment and the shear force as yielding developed was well captured. Ma et al. (2011) reports that specimen B10-36W underwent controlled flexural yielding until a story drift of 2.4% when the beginning of lateral torsional buckling was visually observed. The computational model captured the relatively full hysteretic behavior up to approximately 5% drift ratio at which time lateral torsional buckling started causing noticeable pinching in the hysteretic behavior shown in Figure 135 and Figure 136. The computational model captured the lateral torsional buckling shape and the subsequent geometric hardening associated with link tension. However, the computational model slightly over-predicts the strength during unloading and reloading, likely because the idealized boundary conditions in the model cause the links to resist more compression than the experimental boundary conditions (pinned connections, additional flexibility) allow.

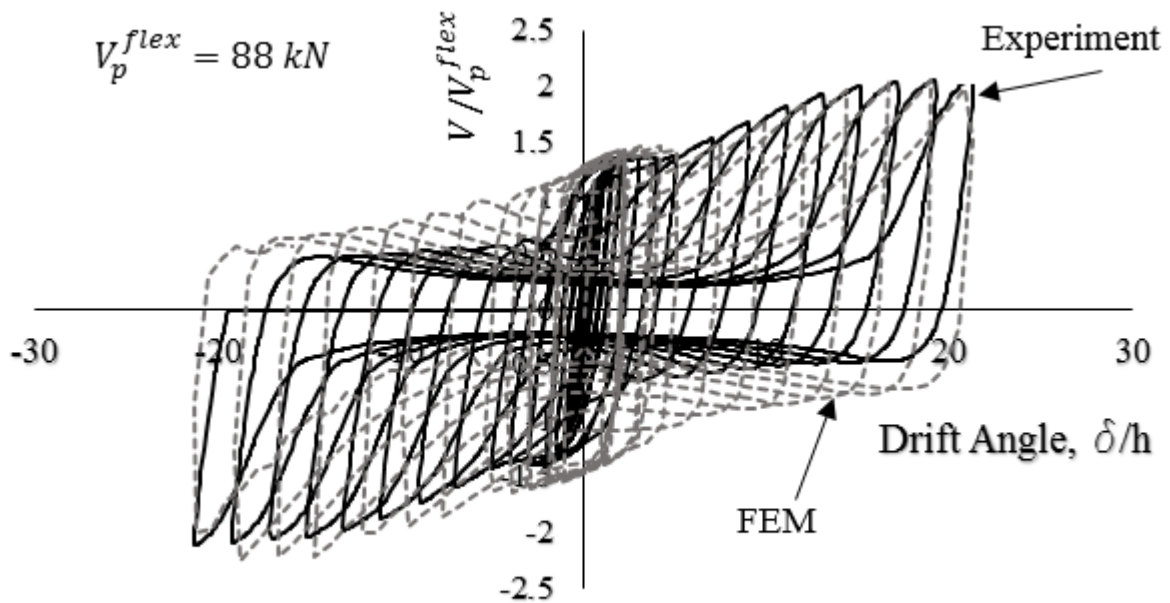


Figure 135. The verified curves experiment and FE model under cyclic loading

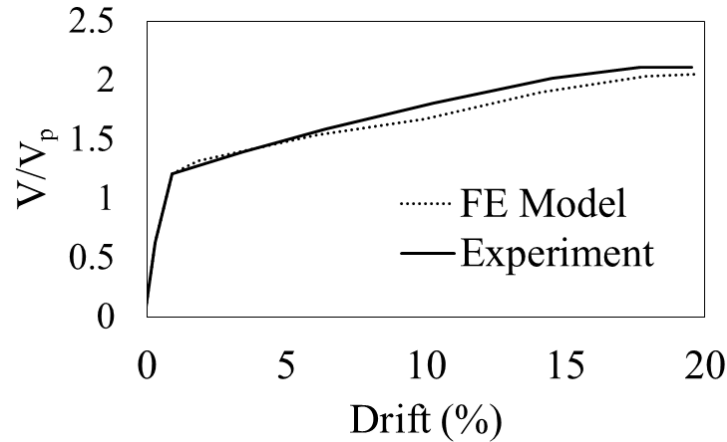


Figure 136. The verified curves experiment and FE model for monotonic loading

### 6.3.2. Four-story steel plate shear wall by Driver et al. (1998)

A four-story steel plate shear wall tested by Driver et al. (1998) has been modeled in finite element software. The overall width of the specimen is 7.4m, and the typical story height is 1.83m, and the first story is 1.93m. The columns are 3.05m apart center-to-center which represents the half scale specimen for an office building condition. The columns are W 310×118 that are the same over the four stories. The beam section for level 1, 2, and 3 are W12×40 and the beam at the fourth level is W21×55. The mean static yield strength was 341 MPa for panels 1, 2, 257MPa for panel 3, and 262 for panel 4. The monotonic and cyclic loadings based on the ATC 24 according to actual experimental test were applied and the backbone and hysteric pushover curves were achieved. In this study, the behavior of the multi-story structure made from the steel plates is investigated and validated.

The results, as represented in Figure 137 and Figure 138, show a satisfactory agreement between laboratory test results and the numerical models presented in this study. The hysteric behavior of the FE model, and the monotonic behavior of the FE reaches to the same strengths at the specified displacements reported based on the experimental test. The strength and stiffness degradation is captured after cycle 22 which is captured in FE model. The results indicate that the modeling methodology for verifying Driver et al. tests is accurate within 98% and 95% for monotonic and cyclic loading conditions. In addition, the buckling of the left column reported as the limit state of this shear wall specimen at the base is captured with the FE models as it is shown in Figure 139.

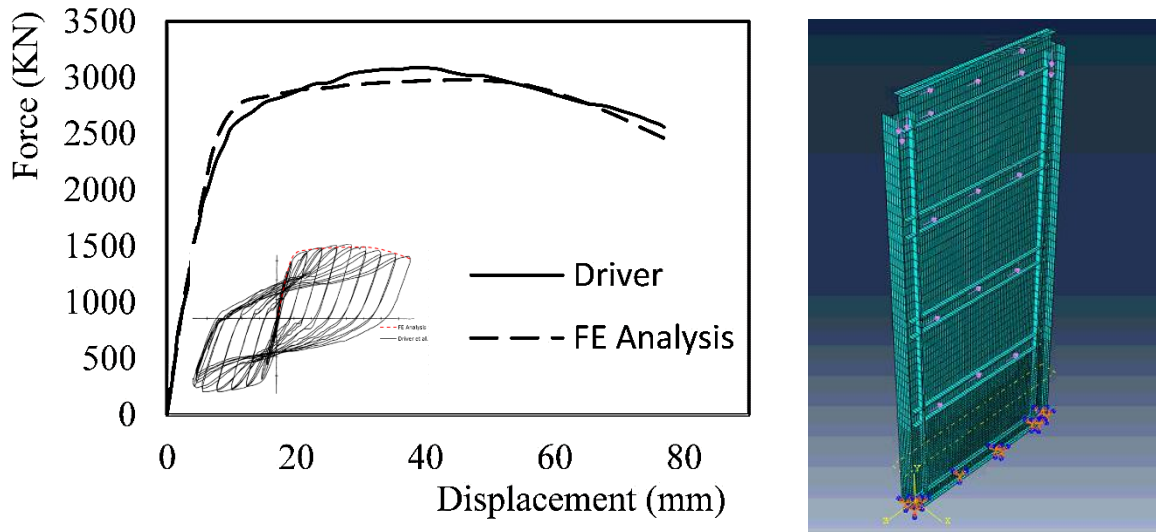


Figure 137. . The verification of the test results with FE methodology for monotonic loading condition

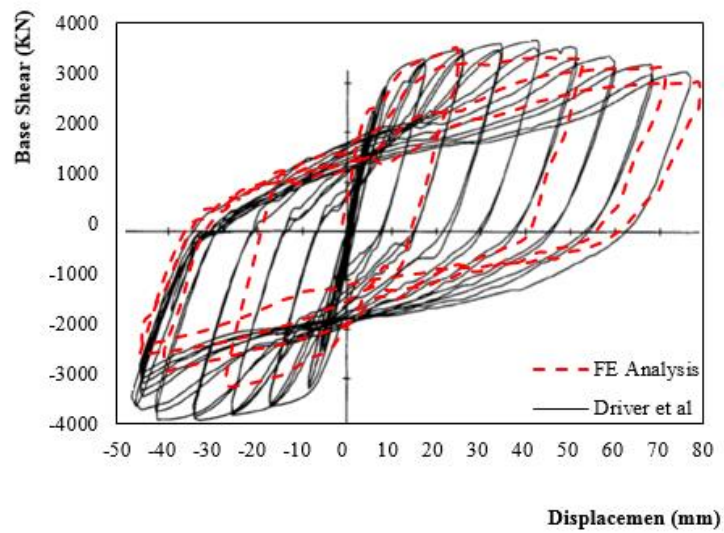


Figure 138. The verification of the test results with FE methodology for cyclic loading condition

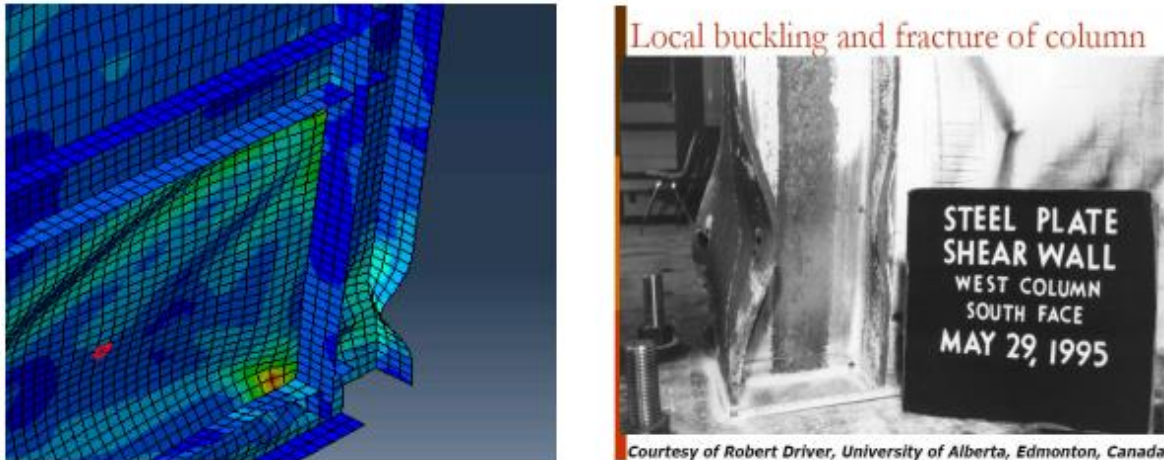


Figure 139. The compatibility of the limit states, buckling at the bottom of the column in laboratory test and in the FE model (Driver et al. 1998)

### 6.3.3. Links inside of the beam web from Ascheim and Halterman (2002)

This work is verified for checking the ability to capture the buckling behavior of the links. To simulate only the beam in the numerical model, one end of the beam was fully restrained against both translation and rotation, while the other end was released for translation only in the direction transverse to the longitudinal axis of the beam. Then, the loading was applied along the released direction at this end as indicated in Figure 140.

No initial out-of-straightness was modeled based on the authors' recommendations. The nominal specimen dimensions considered. The clear span length between columns is 3350 mm according to the test. A general purpose quadratic brick element, with reduced integration (2x2x2 integration points-C3D20R) is implemented for modeling purpose. A bilinear stress-strain relationship was assumed for the steel, with the yield strength of 379 MPa, elastic modulus of 200 GPa, and strain-hardening modulus of 1.38 GPa. The top beam is made of TS 14×10×5/8, the base beam was made of the TS16×12×5/8, and the columns are made of W14×176 shapes. The center to center distance between pins is 4.50m horizontally and 3.15 m vertically.

Figure 141 plots the computed story shear-story drift responses of the specimens; based on the geometry of the loading frame, the story shear is taken as 1.43 times the beam shear acquired from the FEA, and the story drift is taken as the beam chord rotation divided by 1.34, in which the chord rotation is the transverse displacement divided by the clear span length of the beam. In addition, to understand the effect of initial imperfection, first buckling mode is considered and the

imperfection of  $L/250$  is applied. The results show that this amount of imperfection slightly changes the curves and the overall values for strength of the links would not be different. The point at which a drop in strength happens is investigated (Figure 142). It is confirmed that the buckling has been occurred by having as the significant out-of-plane displacement represented in Figure 142. The strength values mentioned by authors are 76 (KN) and 57.4 (KN) for before and after buckling occurred. While, the FE model strength values are 73.2 (KN) and 52.7 (KN), respectively.

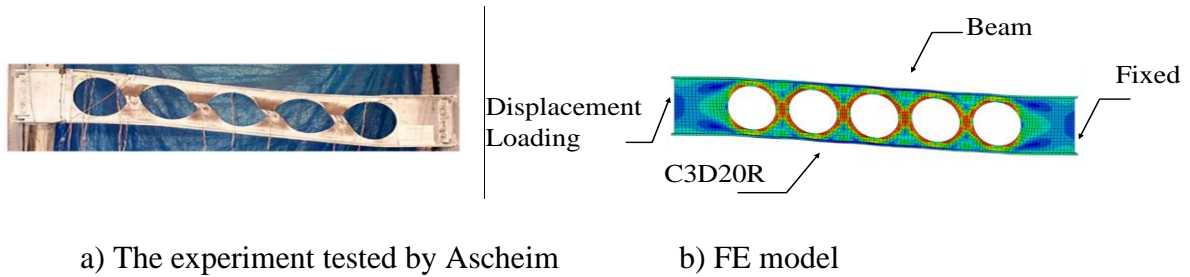


Figure 140. The verification study

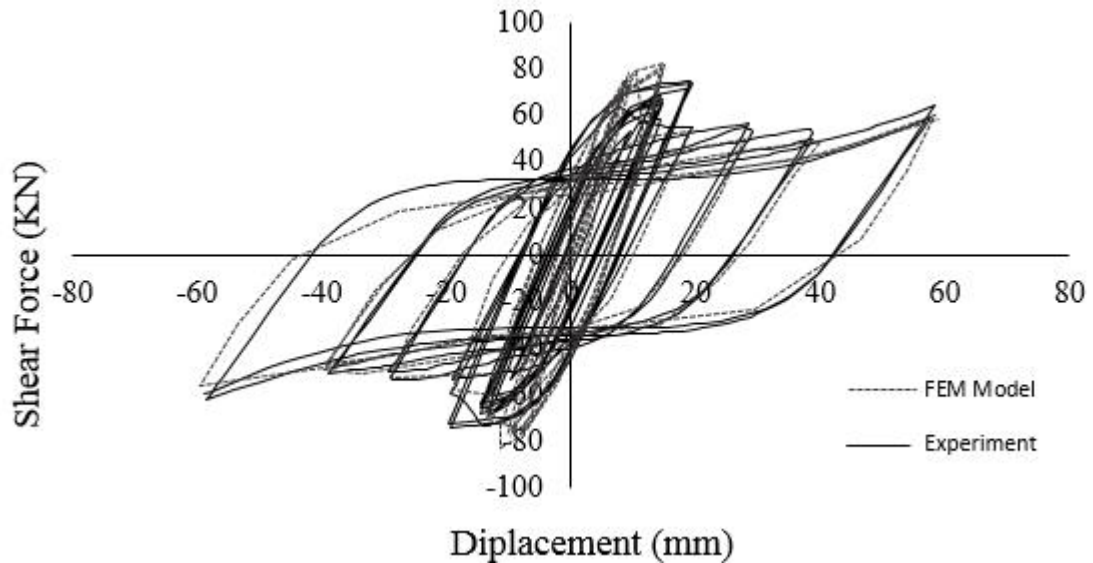
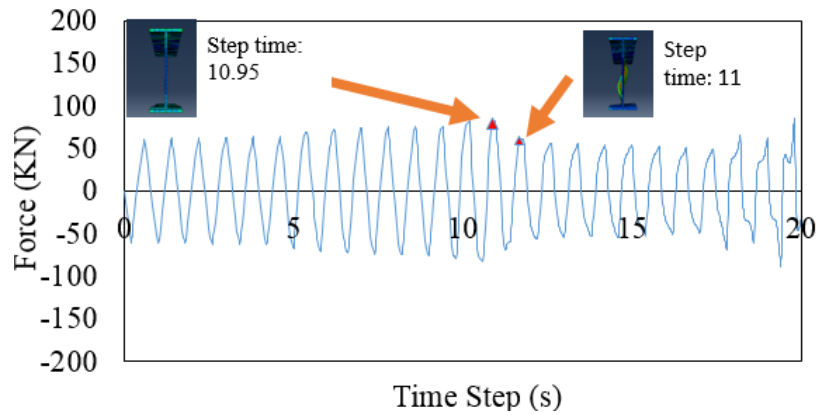
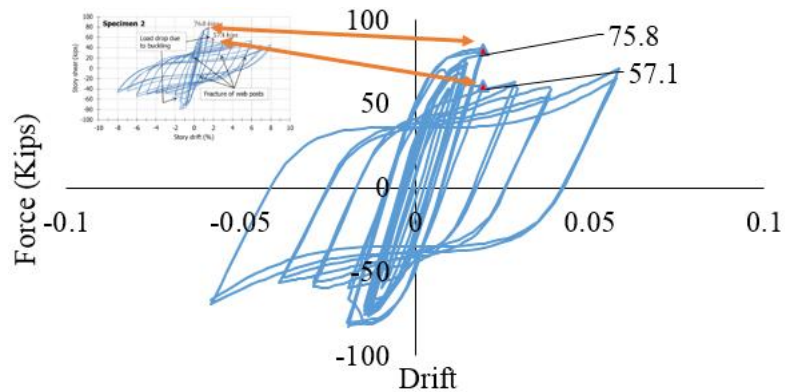


Figure 141. The cyclic pushover curve verified with an actual laboratory test, and the buckling points



a) The before and after buckling in FE analysis shown in step 10.95 and step 11



b) The forces associated with step 10.95 and 11 in the FE model

Figure 142. The buckling point captured by the FE software

### 6.3.4. Straight shear links done by Lee et al. (2015)

The strip dampers are tested by Lee et al. (2015) to reduce the stress concentration subject to cyclic loading condition. Several dampers are tested and hysteric motion is effectively distributed with the specimens. For this study, SS400 was selected as the material for the damper with 245 MPa yielding stress. The total length of the specimen is 540 mm by 360mm, and the thickness of the plate was 10mm. The straight links have 10mm width center-to-center, width a 180mm length. The plate containing the steel shear link are attached to the boundary elements with aid of the 22mm bolts.

In this study, the whole frame is modeled with the aid of the finite element software. The different type of link, the staright link has investigated the behavior of these links under cyclic loading is

verified. The displacement control loading is applied on the horizontal beam based on the protocol used by the authors for the laboratory test. The four nodes shell element, reduced integration (S4R) element is utilized with an appropriate mesh size of 10 mm. The top and bottom of the damper are restrained against vertical displacements which is considered within the FE models. The pushover curves are obtained by monitoring the fixed base forces at the bottom edge of the frame, and the loading points for the displacements (Figure 145). According to authors, the flexural yielding of the straight links was the major limit state of the mentioned specimen, the FE models were able to capture the strengths with each cycle of loading and the mode of behavior.

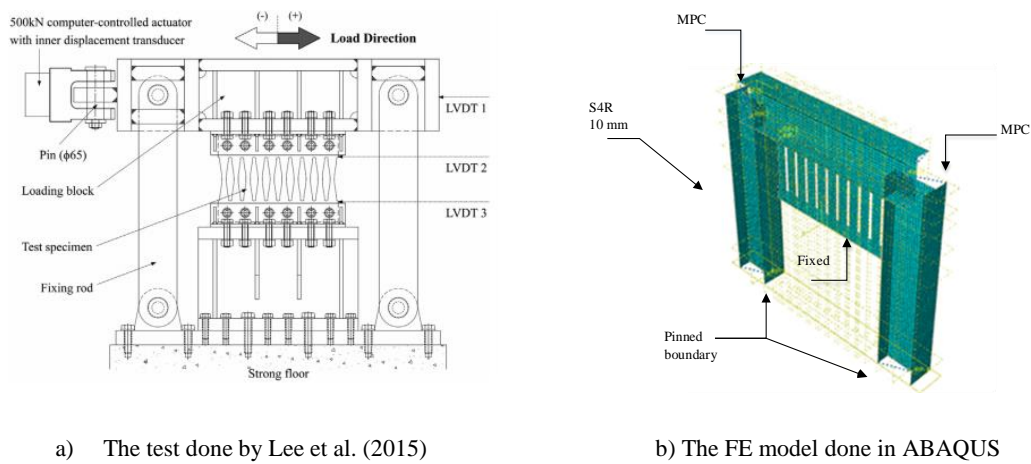


Figure 143. The whole model in ABAQUS

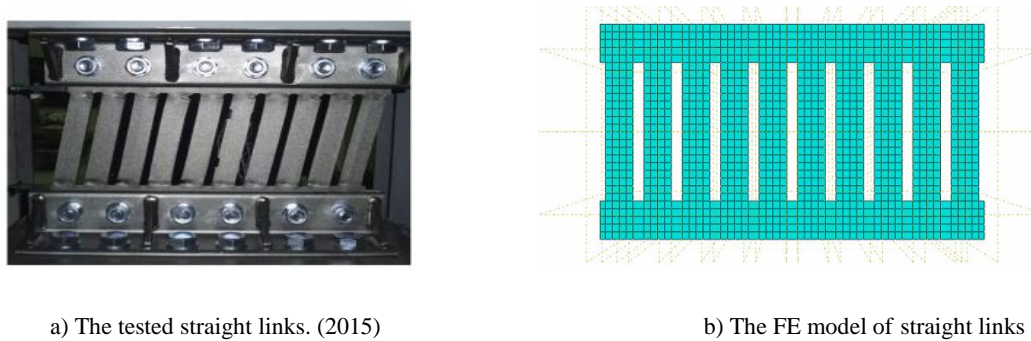


Figure 144. The straight model which the pushover curves are obtained from

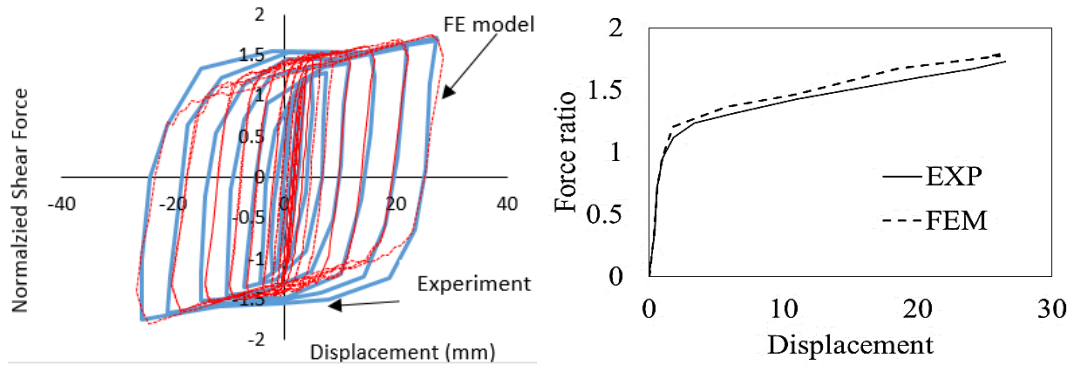


Figure 145. Pushover curves experimental and FE model

# **7. COMPUTATIONAL STUDY TO COMPARE TO BUCKLING, SHEAR AND FLEXURE LIMIT STATE EQUATIONS**

## **7.1. Introduction**

In this section, the equations provided for shear and flexural limit states represented in chapter 4 is investigated and validated against the models made computationally. The finite element modeling methodology elaborated in chapter 6 is implemented for finite element modeling purposes. The governing buckling equations explained in chapter 5 is investigated, and mathematical method to capture the data in previous chapters will be validated. The elastic lateral torsional buckling analysis is considered initially to investigate the buckling behavior of the links. Then, the models with inelastic behavior as well, are considered to study the brittle and ductile limit states. All the data from FE analysis is used to study the proposed equations and the accuracy of the formulas are estimated.

## **7.2. Comparison of the elastic results in finite element analysis software with the proposed lateral torsional buckling method results**

In this section, the links are modeled in the FE program to verify the analytical solutions generated by solving the governing LTB differential equation as well as plastic strength equations. The verified modeling methodology in chapter 6 is considered for investigating the butterfly-shaped links. For each one of the links' geometries with  $a/b=1/3$ ,  $t/L=0.01$  or  $0.03$ , link length  $L=1\text{m}$  and specified  $b/L$ , a model was constructed and subjected to monotonically increasing lateral displacement along the top edge. The general shape of a single butterfly-shaped link is shown in Figure 146 . The boundary conditions are fully fixed constraints at the bottom edge, and the vertical as well as out of plane displacement are fixed at the top edge of the links. The mesh sensitivity analysis is conducted but not shown here. The mesh sensitivity analysis method is elaborated in Appendix A. The approximate mesh size of 5mm is implemented as represented graphically in Figure 146.

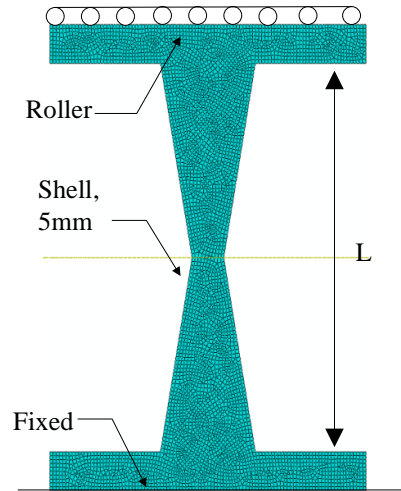
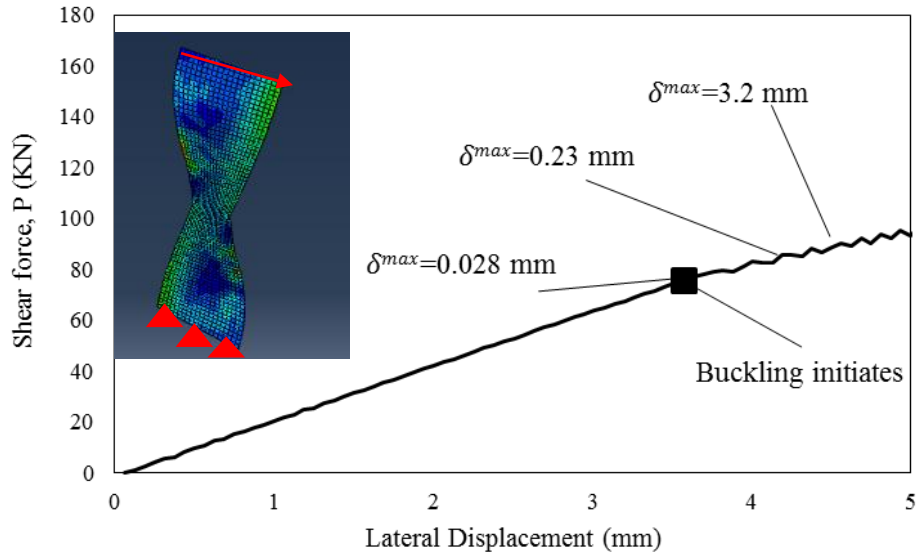
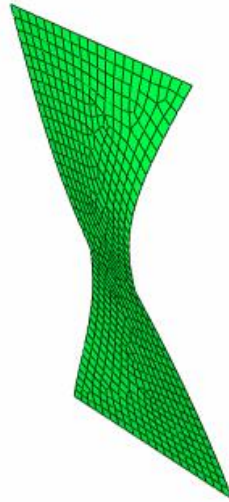


Figure 146. General properties of a model in ABAQUS

A four-node reduced integration element (labeled as S4R in ABAQUS) is chosen as a suitable element type to obtain buckling and the spread of inelasticity. The initiation of buckling was obtained from the shear force versus lateral displacement response as shown in Figure 147 . Fluctuations observed in shear force occurred during the explicit analysis were correlated with a slight reduction in stiffness and a substantial increase in out-of-plane displacement, labeled as values for  $U$  in Figure 147. These fluctuations in shear force were therefore taken as indicating the initiation of the buckling. It is noted that by using elastic buckling analysis directly in FE software, similar buckling results are obtained which is shown in Figure 147. It also shows an example of butterfly shaped link with buckling load of 280 kN from the elastic buckling analysis. This value is similar to the method used previously to capture the buckling load of each model which shows that both methods will have the same results.



a) The meshed butterfly-shaped link elastic response for  $a/b=0.33$ ,  $b/L=0.3$ ,  $t/L=0.01$ ,  $L=1\text{m}$  ( $U$  is out-of-plane displacement indicating buckling phenomena)



b) The buckling analysis for shape with  $b/L=0.5$ ,  $L/t=100$ ,  $a/b=0.33$ , and  $L=1\text{m}$

Figure 147. General output parameters based on the buckling analysis and pushover analysis

First, the FE models ran with an elastic material constitutive model to examine elastic lateral torsional buckling. The shear load at buckling was obtained as described above and the associated moment was calculated as given in Table 7. Figure 148. indicates the comparison between computational simulation and analytical equations. The associated critical moment initiating the lateral torsional buckling of the link is calculated. Table 7 indicates an average of 3.2% difference

between the estimation of LTB of butterfly links by comparing the general differential equations results and the FE model results.

Table 7. Comparison of ABAQUS results with MATHEMATICA

b/L	a/b	t/L	ABAQUS		MATHEMATICA		error%
			P (N)	Moment (kN.m)	Moment $\times 10^7$ (Non-dimen.*)	Moment (kN.m)	
0.1	0.3	0.01	25.2	12.6	0.6	13.4	5.8
0.2	0.3	0.01	55.5	27.7	1.3	28.0	1.0
0.3	0.3	0.01	79.0	39.5	1.9	41.9	5.9
0.4	0.3	0.01	105.2	52.6	2.5	55.9	5.8
0.5	0.3	0.01	139.3	69.7	3.2	70.9	1.7
0.6	0.3	0.01	158.6	79.3	3.8	84.4	6.0
0.7	0.3	0.01	197.9	98.9	4.5	98.3	0.6
0.8	0.3	0.01	228.1	114.1	5.1	113.0	1.0
0.9	0.3	0.01	261.7	130.8	5.8	126.9	3.1
1.0	0.3	0.01	285.1	142.6	6.4	140.8	1.3

\*Non-Dimensionlized Moment equal to  $M_{cr}/EI^3$

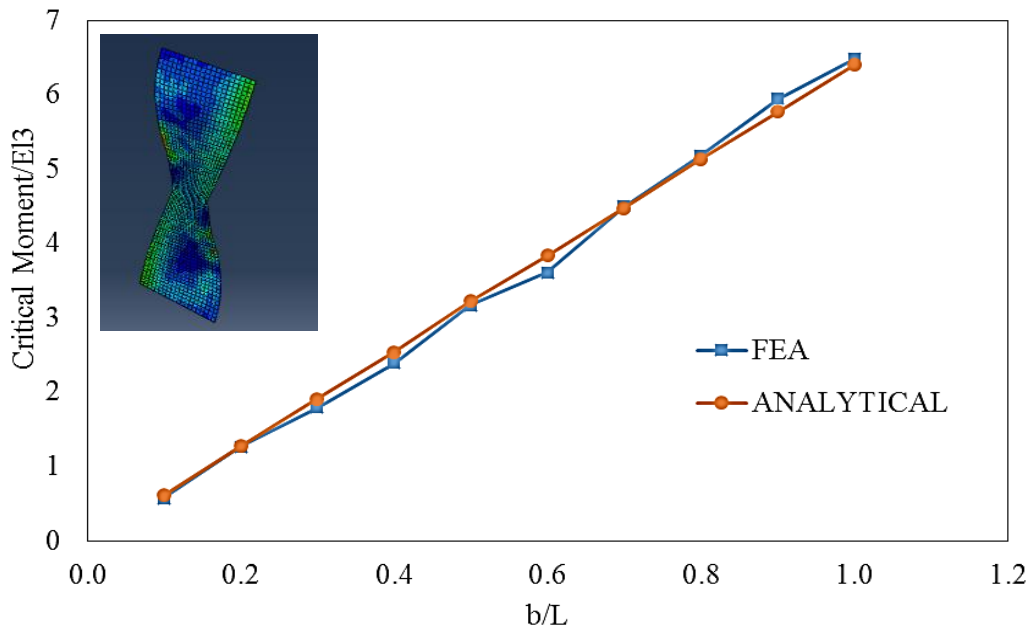


Figure 148. Comparison of buckling differential equations' results with elastic buckling FE models for t/l=0.01

### 7.3. Non-dimensionalization of the shear and flexural limit state and comparison with LTB equation

Before presenting results for the critical buckling moment, inelastic limit states are discussed. Two inelastic limits states, namely plastic shear yielding and plastic flexural hinging limit the strength of butterfly links. The domination of each mode depends on the geometry of the links. Eq. (113) gives the end moment corresponding to shear yielding at the middle of the butterfly link. The end moment associated with plastic flexural strength is calculated based on finding the maximum values corresponding to flexural force indicated in Eq. (114), and further simplified for the ratio  $a/b=1/3$ , which results in plastic flexural hinging at the quarter points of the links as indicated Eq. (115). Eq.(116) and Eq. (117) indicate the moments associated with the non-dimensionalized version of shear and flexure limit states.

$$M_p^{shear} = \frac{at(\sigma_y / \sqrt{3}) l}{2} \quad (113)$$

The capacity of the butterfly link is established before (Eq. (114)). Back-calculating the force will lead to:

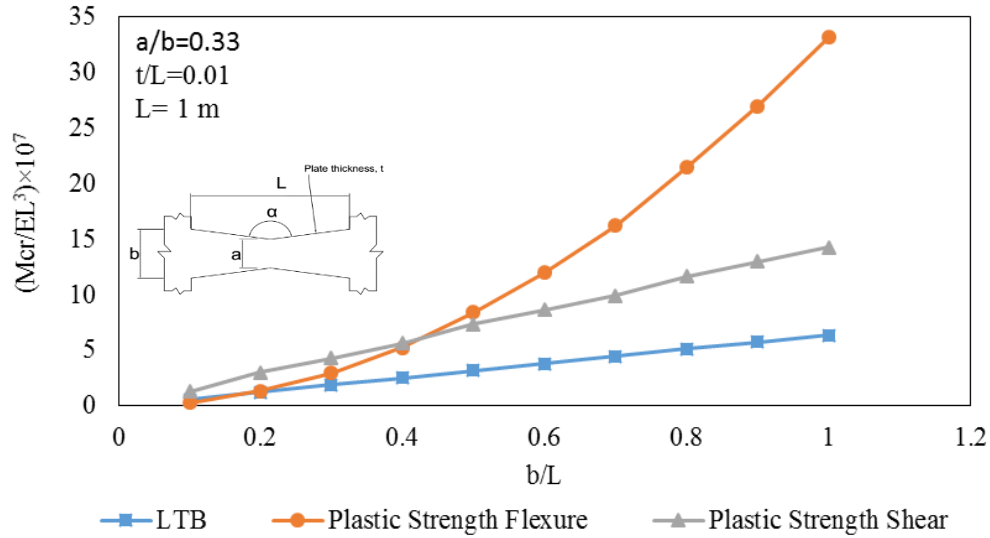
$$M_p^{end} = \frac{Pl}{2} = a\sigma_y nt(b-a) \quad (114)$$

$$M_p^{flexure} = 2a^2 t \sigma_y \quad \left(\text{for } \frac{a}{b} = \frac{1}{3}\right) \quad (115)$$

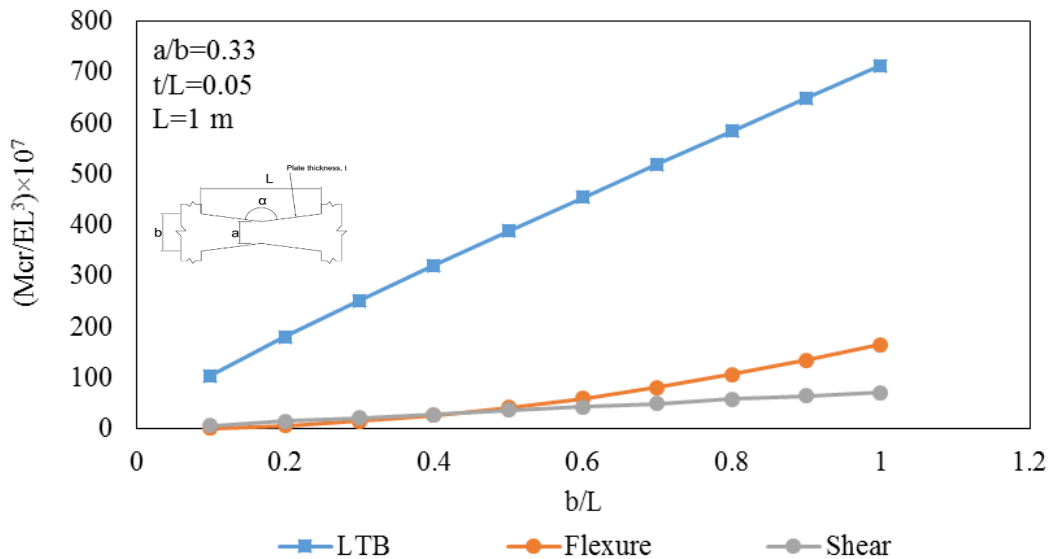
$$\frac{M_p^{shear}}{El^3} = \frac{AT(\sigma_y / \sqrt{3})}{2E} \quad (116)$$

$$\frac{M_p^{flexure}}{El^3} = \frac{2A^2 T \sigma_y}{E} \quad \left(\text{for } \frac{a}{b} = \frac{1}{3}\right) \quad (117)$$

Figure 149 shows the plastic capacity and lateral torsional buckling critical moment for a butterfly link with  $a/b=1/3$ ,  $t/L=0.01$  and the results for a thicker plate with  $t/L=0.03$ . It is shown that for all thin plate configurations ( $t/L=0.01$ ) except the least wide configuration ( $b/L=0.1$ ), that LTB is the governing limit state. For thicker plates ( $t/L=0.03$ ), it is shown that the plastic section capacity leads to the smallest moment and thus controls the moment strength. In addition, it is concluded that the narrower links (smaller  $b/L$ ) experience flexural hinging and wider links experience shear limit state will be governing.



a) Butterfly link with  $a/b = 0.33$ ,  $t/L=0.01$ , and  $L=1\text{ m}$



b) Butterfly link with  $a/b = 0.33$ ,  $t/L=0.05$ , and  $L=1\text{ m}$

Figure 149. The capacity and LTB curves

## 7.4. Comparison of the inelastic and LTB results in FE analysis software

In this section, 10 different models with thin fuse plate and 10 models with thicker plate are modeled and analyzed in the FE program. In all of these models, the  $a/b$  ratio is equal to  $1/3$ . The purpose of this study is to first confirm that the shooting method results are valid and reliable. Second, to confirm that the developed equation for shear and flexural limit state are precise and applicable. Third, to verify that the FE software is able to capture the torsional buckling as well as other limit states associated with each one of the fuses.

The links are modeled in the FE software with inelastic material constitutive to compare moments associated with inelastic limit states with proposed equations for flexure and shear capacity. The buckling initiation and the ultimate points are indicated in Figure 150.

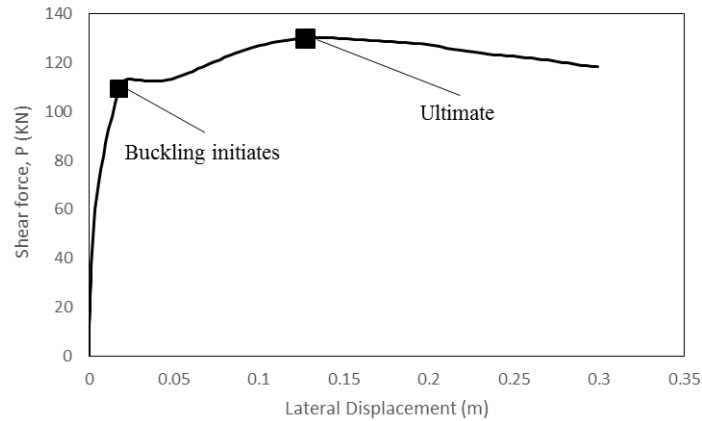
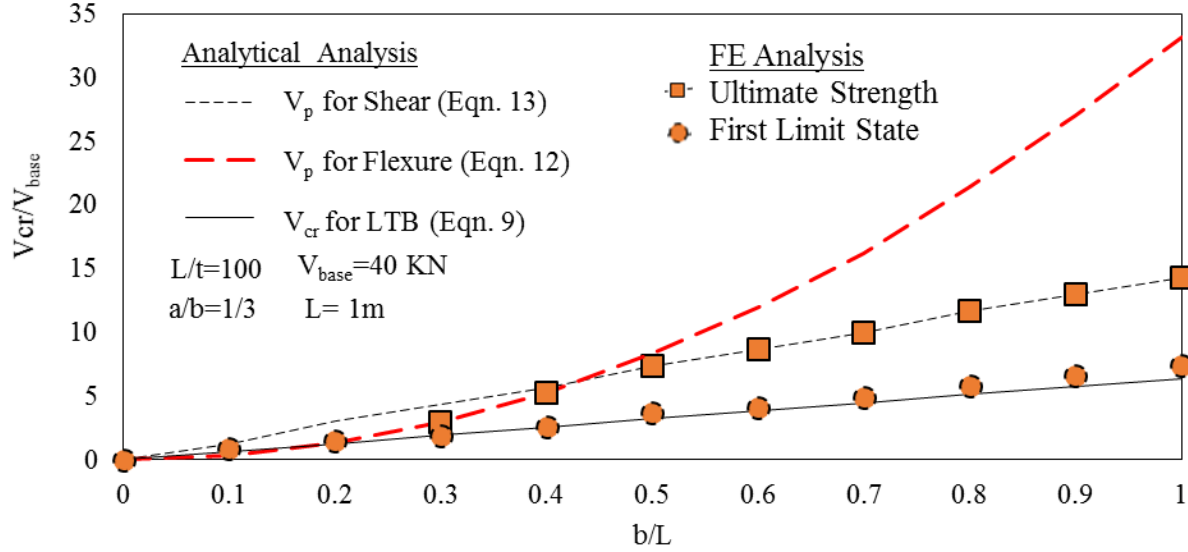


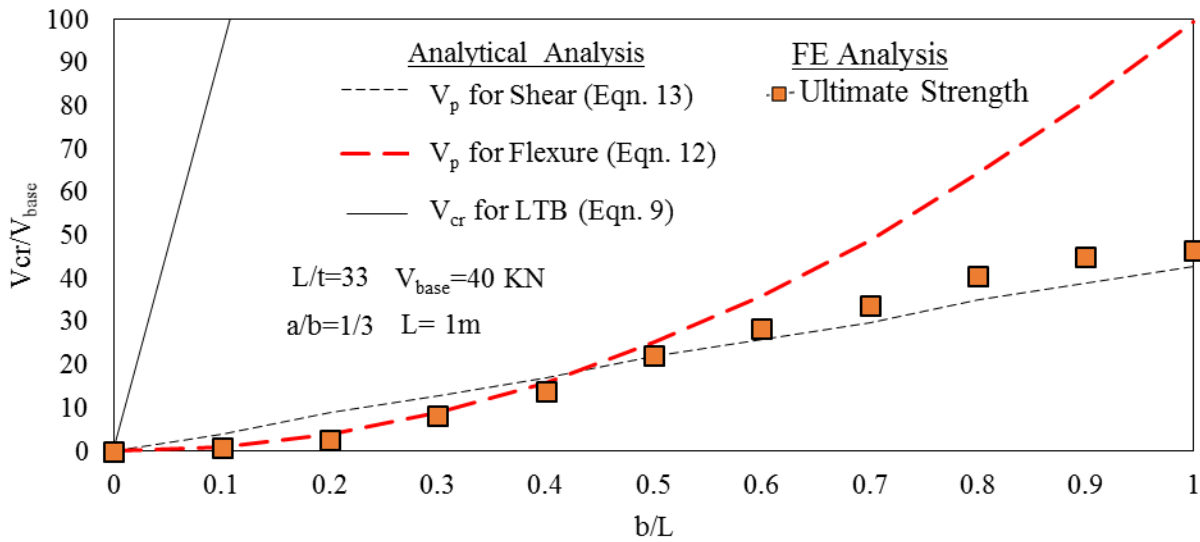
Figure 150. Schematic representation of the buckling initiation and ultimate points

To compare the results from analytical, FE and mathematical studies together, all the limit states associated with BF links are shown in Figure 151, which indicates three lines representing the LTB moment capacity from the differential equation and plastic moment capacity for shear and flexure. The circles indicate the initiation of the buckling while the squares represent the ultimate strength of the link. The FE models capture the domination of elastic lateral torsional buckling capacity of thinner links as well as the plastic shear and plastic flexural capacity of the links. Figure 151 does not show circles associated with buckling in the FE model because out-of-plane buckling was not observed. The elastic lateral torsional buckling of the links are shown in an inset for the thicker fuse to show how large the elastic lateral torsional buckling moment is related to the plastic moments for thicker plates. In general, the FE results are within 5% of the predicted analytical

values.



a) Butterfly link with  $a/b = 0.33$ ,  $t/L=0.01$ , and  $L=1$  m



b) Butterfly link with  $a/b = 0.33$ ,  $t/L=0.03$ , and  $L=1$  m

Figure 151. Comparison of FE results to analytical equations for elastic and inelastic limit states

Figure 151a shows that the initiation of buckling in the inelastic FE models compared well with the moment predicted using the elastic differential equation. The ultimate moment strength of the links obtained from FE analysis compared well with the plastic strength equations in both Figure

151a and Figure 151b. In addition, the effect of thickness of the butterfly link on the lateral torsional buckling is demonstrated. As the thickness increases (Figure 151b), the butterfly-shaped link will reach to shear or flexure hinging capacity while elastic lateral torsional buckling governs for thinner links (Figure 151a).

Figure 152 shows load-drift plots for three example configurations that demonstrate each of the three limit states while Figure 153 shows related deformed shapes. The configuration with  $L/t=100$ ,  $a/b=1/3$ , and  $b/L=0.5$  is a relatively slender and wide butterfly-shaped link that is expected to undergo lateral torsional buckling based on the computed strengths  $V_{cr}=150.4$  KN,  $V_p^{flexure} = 336.4$ KN, and  $V_p^{shear}=290.4$  KN. As shown in Figure 153a, this configuration undergoes lateral torsional buckling deformations. The onset of these deformations is associated with a drop in shear load at approximately 0.02 rad. drift angle. At a large drift angle of approximately 0.13 rad, the shear strength of the link reaches a peak value as the observed stress distribution (not shown here) indicates shear yielding at the narrowest part of the link. The peak shear strength from the FE model is within 3% of the computed shear yield strength. It is noted that although the curve for lateral torsional buckling in Figure 152 appears to be relatively similar to the flexural and shear yielding curves, that buckling may not be desirable in some cases because 1) fracture may occur at smaller drifts for buckling configurations due to localized inelastic strains at link ends (fracture not included in these models), 2) buckling configurations will be prone to hysteretic pinching which limits energy dissipation during cyclic loading, and 3) strength is reduced for configurations undergoing buckling (not shown in Figure 152 due to normalized vertical axis). The configuration with  $L/t=33$ ,  $a/b=1/3$ , and  $b/L=0.6$  is also a relatively wide link compared to its length, but the thickness has been increased by a factor of three relative to the previous configuration. In this case, the deformed shape and Von Mises stress distribution is shown in Figure 153b are consistent with shear yielding. The peak shear force is within 8% of the computed shear yield strength of  $V_p^{shear} = 1039.2$  KN, which was the smallest of the computed link strengths ( $V_{cr}=1132$  KN, and  $V_p^{flexure} = 1440$  KN).

The third and final configuration keeps the same thickness and taper ratio as the previous configuration  $L/t=33$ ,  $a/b=1/3$ , but reduces the aspect ratio to  $b/L=0.3$ . The stress distribution shown in Figure 153c shows large stresses at the extreme fibers at the quarter points along the link length which is consistent with flexural hinging.

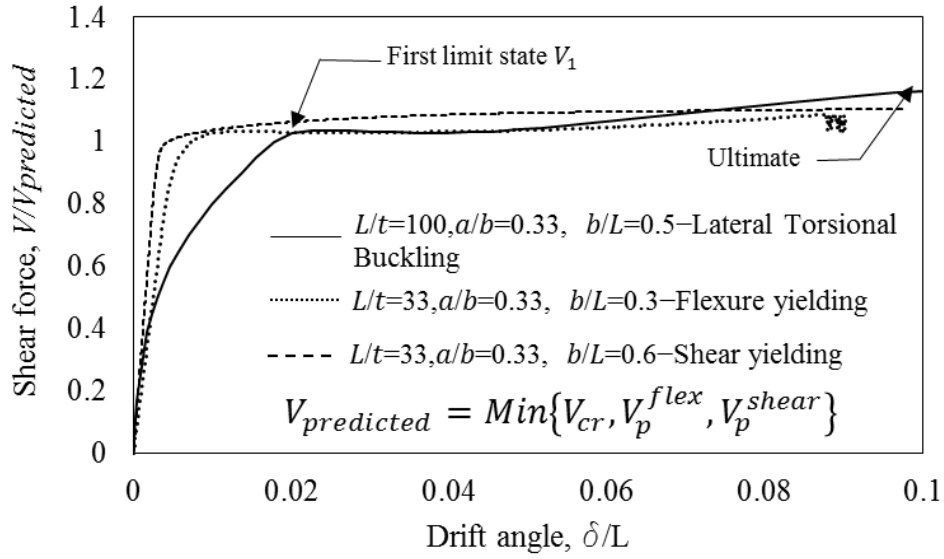


Figure 152. Schematic representation of the buckling initiation and ultimate points

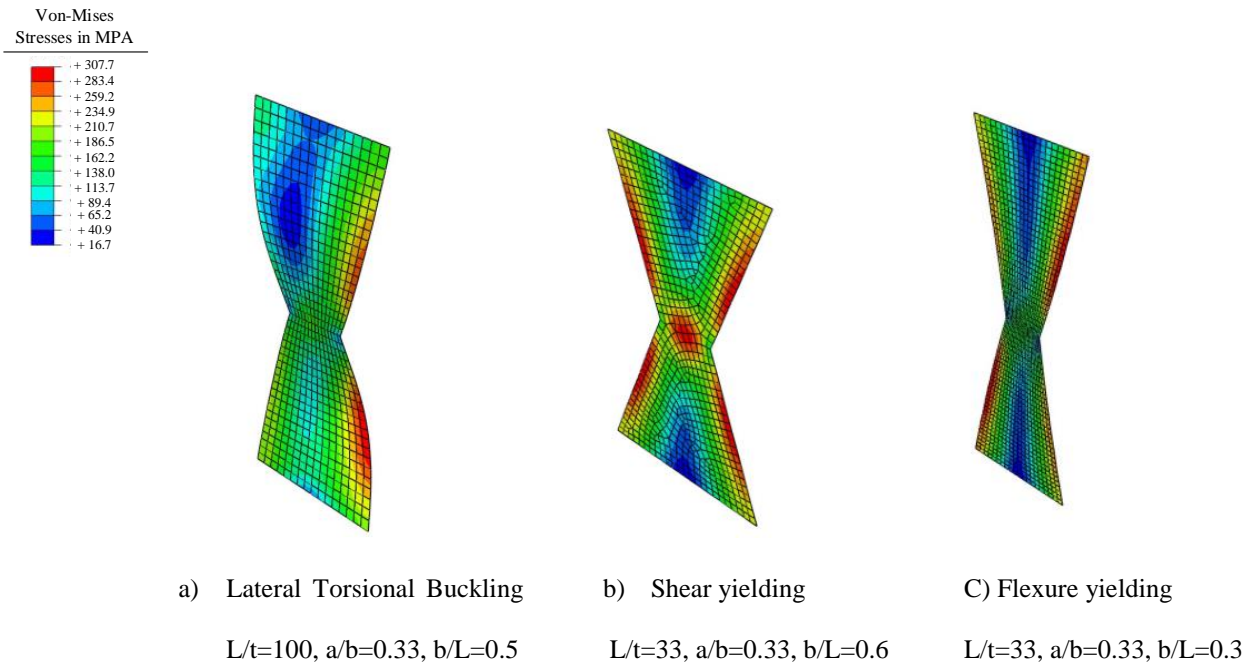


Figure 153. Deformed Shapes of three models demonstrating three limit state

## 7.5. Investigation of the combined effect of shear and flexural stresses simultaneously on the behavior of the BF links

To investigate the effect of having a uniform distribution of the stresses over the length of the link from the section 4.2.4, three different models are conducted in FE software. For these models,  $a+b$  is equal to  $L/\sqrt{4}$ ,  $L/\sqrt{3}$ , and  $L/\sqrt{2}$ . For investigating the three models, two displacements of  $U_{max}$ , and  $U_y$  are identified.  $U_{max}$  shows the displacement in which the strength degradation and stiffness degradation starts to happen generally due to occurrence of inelastic buckling. In addition,  $U_y$  shows the displacement in which element within the model starts to yield. The results indicate that having the uniformed stress distribution based on mathematical concepts will improve the accumulation of plastic strains and higher  $U_{max}$  over  $U_y$  ratios as it is shown in Table 8. The larger  $U_{max}/U_y$  shows that the models will start to lose their lateral load resistance capability in larger displacement after initiation of yielding. In addition, Table 8 indicates that the stress distribution based on the proposed concept works and if the  $a + b$  is equalized to  $L/\sqrt{3}$ , the total stress distribution is uniform and almost the whole section reaches to the plastic level as compared to other geometries that only some portions plastify.

Table 8. The comparison of Equivalent Plastic Strain (PEEQ) and  $U_{max}/U_y$

$(a+b)/L$	$1/\sqrt{4}$	$1/\sqrt{3}$	$1/\sqrt{2}$
$U_{max}/U_y$	4.81	5.76	5.41
<b>EQUIVALENT PLASTIC STRAIN (PEEQ) at 0.01%</b>	0.1520	0.0068	0.0078
Von-Mises Stresses in MPA 			

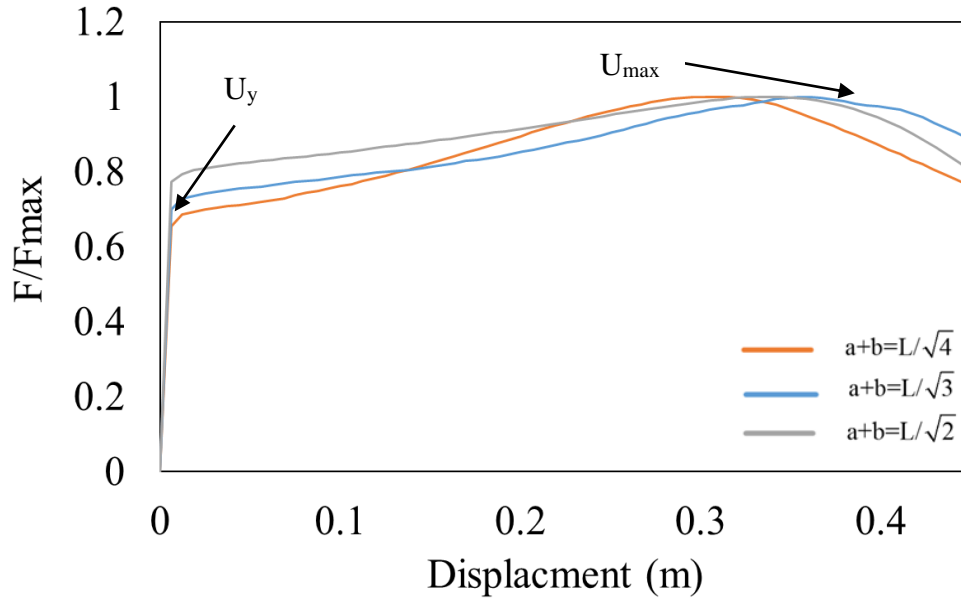


Figure 154. The pushover curves associated with three models with different geometries

## 7.6. Verification of the yielding limit states equations with FE software

To compare the results obtained from the proposed mathematical yielding limit state equations with FE models, a specific model is made and analyzed. The modeling methodology would be explained and validated in Chapter 6. The push over curve is extracted and the results are represented. The first model done in FE program which had properties of  $a=10\text{cm}$ ,  $b=30\text{cm}$ ,  $L=100\text{cm}$ ,  $t=20\text{mm}$ . This model is chosen to have the flexural limit state governing the shear limits state. To check the flexure would happen before shear, Eq. (46) is used which identifies the ductile mode of behavior.

$$\frac{b-a}{L} = \frac{30-10}{100} = 0.2 < 0.28 \text{ or } \alpha = 157^\circ > 148^\circ \quad (118)$$

Therefore, the flexure hinges would dominate before shear since the butterfly angle is more than  $148^\circ$ . The limit state prediction equation for yielding and total capacity represented for this model predicted the behavior as it is expected. The flexural stresses initially are occurred within the model, which is predicted by the limit states equations as the mode of behavior is identified in Eq.(118). It is shown that the critical butterfly angle is more than 148, which results in the flexural limit states to be occurred before shear limits state. This phenomenon has been observed in FE results accordingly.

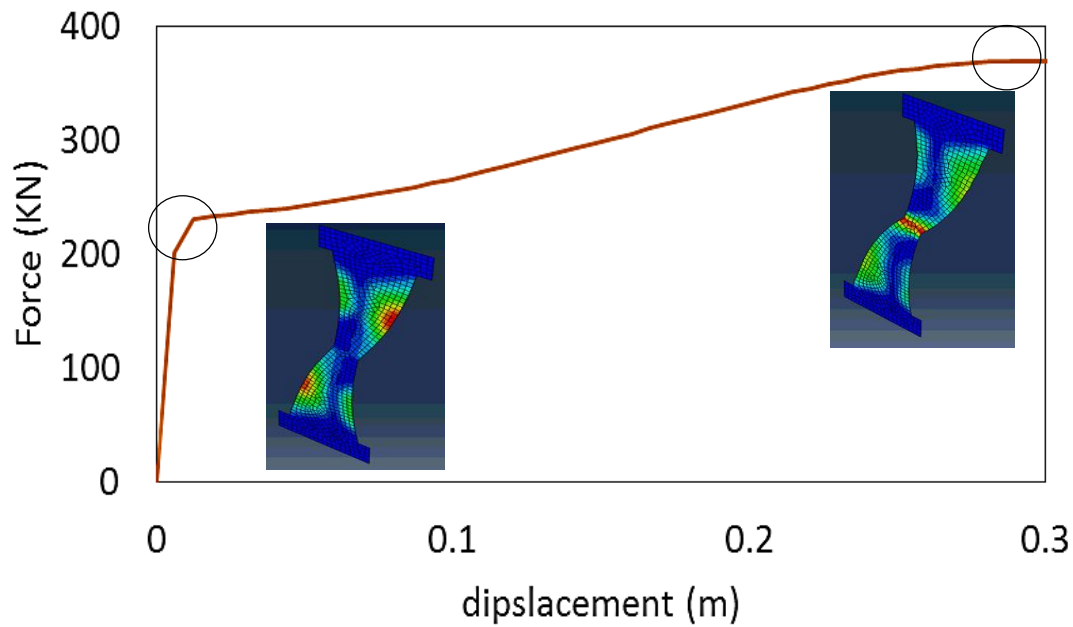


Figure 155. Occurrence of flexural yielding limit states before shear yielding limit state

Table 9 indicates the comparison of the results associated with the FE analysis and analytical equations for flexural BF link. The Eq. (32), and Eq. (41) are used to calculate the ductile limit states for flexure and shear, which is captured with the FE model as well. Eq. (63) is used for comparing the butterfly-shaped prediction equation for stiffness with FE model.

Table 9. The comparison between equations and FE model for flexural dominated BF

<b>a=10cm, b=30cm L=100cm, t=20mm</b>	<b>P<sup>P</sup><sub>FLEXURE</sub></b>	<b>P<sup>P</sup><sub>SHEAR</sub></b>	<b>STIFFNESS</b>
	<b>(KN)</b>	<b>(KN)</b>	<b>(KN/MM)</b>
<b>PREDICTION EQUATION</b>	230.1	368.7	19166.7
<b>FE</b>	240.2	346.7	19714.3
<b>ERROR (%)</b>	4.2	6.3	2.7

As given in Table 9 the errors are less than 5% in average limit state prediction equation and less than 3% for the stiffness; therefore It is concluded that the general equations provided to

describe the pushover behavior of butterfly-shaped links appropriately estimate the actual behavior of the specimens.

Along the same lines, to compare the results for the shear limit state, a specific model is made and analyzed. The model done in FE program had properties of  $a=10\text{cm}$ ,  $b=50\text{cm}$   $L=100\text{cm}$ ,  $t=20\text{mm}$ . This model is chosen to have the flexural limit state governing the shear limits state. To check the shear would happen before flexure, Eq. (46) is used which identifies the ductile mode of behavior. The shear yielding over flexure will be verified with Eq.(119):

$$\frac{b-a}{l} = \frac{50-10}{100} = 0.4 > 0.28 \text{ or } \alpha = 136^\circ < 148^\circ \quad (119)$$

Therefore, the shear yielding limit state would dominate before flexure since the butterfly angle is less than  $148^\circ$ . The limit state equations for yielding limit state at different parts of the pushover curve are incorporated. It is shown that for this model, in which the critical angle is less than  $148^\circ$  or  $\frac{b-a}{L} > 0.28$  then the shear limit states will be occurred before flexure limits state. This phenomenon has been observed in FE results accordingly.

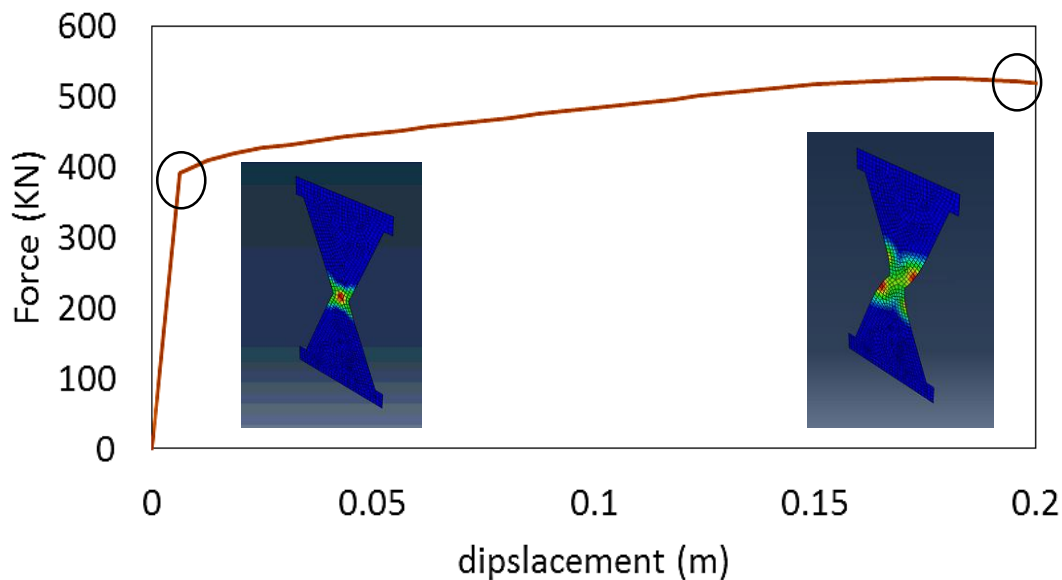


Figure 156. Occurrence of shear yielding limit states before flexural yielding limit state

Table 10 indicates the comparisons of the result associated with the FE analysis and analytical formulation for shear type BF link. The Eq. (32), and Eq. (41) are used to calculate the ductile limit states for flexure and shear, which is captured with the FE model as well. Eq. (63) is used for comparing the butterfly-shaped prediction equation for stiffness with FE model.

Table 10. The comparison between Equations and FE model for shear dominated BF

<b>a=10cm, b=50cm L=100cm, t=20mm</b>	<b>P<sup>P</sup><sub>SHEAR</sub></b> <b>(KN)</b>	<b>P<sup>P</sup><sub>FLEXURE</sub></b> <b>(KN)</b>	<b>STIFFNESS</b> <b>(KN/MM)</b>
<b>PREDCITION EQUATION</b>	390	517	63934.5
<b>FE</b>	388	482	59538.5
<b>ERROR (%)</b>	0.5	7.2	7.3

As given in Table 9Table 10 the errors are less than 5% in average for limit state prediction equation and less than 8% for the stiffness; therefore, it is concluded that the general equations provided to describe the pushover behavior of butterfly-shaped links appropriately estimate the actual behavior of the modeled specimen. As it is indicated in FE analysis for the two separate cases which flexure and shear govern the behavior of the butterfly-shaped links, the equations in elastic and plastic regions are capable of predicting the actual limit states within less than 5% error.

In the next section a set of models will be considered to compare the total backbone behavior of the links with FE models

### **7.7. Geometrical hardening investigation, formulation, and concepts**

It is noted that, for the earthquake design, the second-order effects in the yielding links should be expected and must be considered in the response of the links. The geometric hardening that is developed in each of the links when they are subjected to significant bending deformation will result in post-yield stiffening that can be observed in the load-displacement response of the links. The post-yield stiffening of the links is relevant to the capacity design of the remaining elements and whole LRF system. As it is mentioned before the shear force (here indicated as P) is the same along the beam. In addition, the moment in inflection point is zero. Therefore, we are able to cut the length to the half and put the shear load on the top.

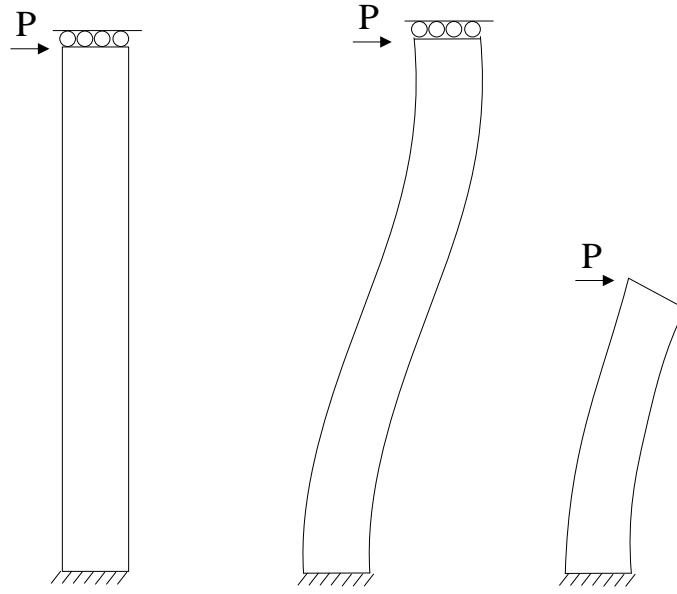


Figure 157. The general link configuration and applied loading for the full length and half length

The amount of horizontal shortening shown in Figure 158, is calculated based on the horizontal displacement difference before and after applying the load. The variables used for studying the post-yielding behavior of the butterfly-shaped links are identified in Figure 158. In which,  $L$  is the total length of the link,  $R$  is the radius of curvature,  $\delta$  is the displacement under the loading direction,  $\rho$  is the horizontal displacement,  $2\Theta$  is the angle associate with the half deformed length of the butterfly-shaped link, and  $P$  shows the applied load. It is noted that the total shortening, along the dashed line in Figure 158 is calculated based on the horizontal shortening and corresponding angle.

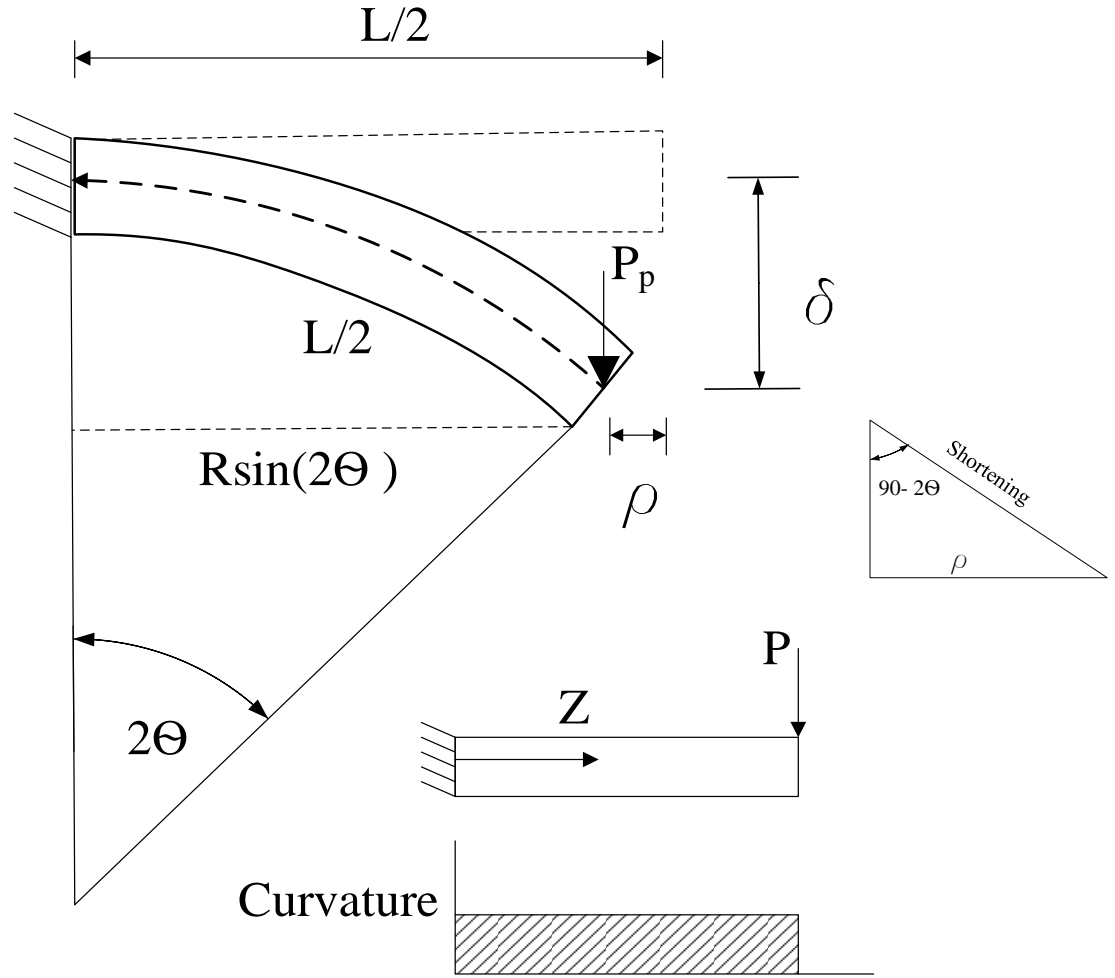


Figure 158. Geometrical link properties

From the Figure 158, the following geometrical equation for  $\rho$  is obtained.

$$\rho = \frac{L}{2} - R \sin(2\theta) = \frac{L}{2} - R \sin\left(\frac{2\delta}{\frac{L}{2}}\right) \quad (120)$$

$$R(2\theta) = \text{Arc length} = \frac{L}{2} \rightarrow R\left(\frac{2\delta}{\frac{L}{2}}\right) = \frac{L}{2} \rightarrow R = \frac{L^2}{8\delta} \quad (121)$$

$$\rho = \frac{L}{2} - \frac{L^2}{8\delta} \sin\left(2\left(\frac{\delta}{\frac{L}{2}}\right)\right) = \frac{L}{2} - \frac{L^2}{8\delta} \sin\left(\frac{4\delta}{L}\right) \quad (122)$$

The amount of shortening could be estimated from the following equation.

$$shortening = \frac{\rho}{\sin(90 - 2\theta)} = \frac{\rho}{\cos(2\theta)} = \rho / \cos\left(\frac{4\delta}{L}\right) \quad (123)$$

It is worthy of notice that the  $P_p$  (a shear force which is compatible with the force associated with FEM models) consists of two components of tension and flexural/ shear mechanisms. The axial load in the format of tension is estimated as follows:

$$T_{shortening} = K_{avg} \frac{\left(\frac{L}{2} - \frac{L^2}{8\delta} \sin\left(\frac{4\delta}{L}\right)\right)}{\cos\left(\frac{4\delta}{L}\right)} \quad (124)$$

In which the  $K_{avg}$  is calculated based on the plastic axial stiffness of the link. The stiffness is evaluated based on the assumption of the nonlinearity of the link section, which is indicated as follows:

$$K_{avg} = \frac{E_p A_{avg}}{L} \quad (125)$$

$A_{avg}$  is the average area between the middle and end sections, and  $E_p$  is the hardening factor which should be calibrated with FEM models. The component associated with flexural/shear parts could be estimated from the following equations: and,  $P_p$  is defined based on the minimum of the forces associated with flexural and shear yielding.

$$P_{flx-bf} = \frac{2n(b-a)at\sigma_y}{L} \quad (126)$$

$$P_{shr-bf} = \frac{n\sigma_y at}{\sqrt{3}} \quad (127)$$

Therefore,  $P_p$  is defined as follows:

$$P_p = \min\{P_{flx-bf}, P_{shr-bf}\} \quad (128)$$

The total force is equal to the summation of the axial, shear or flexural components, which lead to the following equation:

$$P = P_p + K_{avg} \frac{\left(\frac{L}{2} - \frac{L^2}{8\delta} \sin\left(\frac{4\delta}{L}\right)\right)}{\cos\left(\frac{4\delta}{L}\right)} \sin\left(\frac{4\delta}{L}\right) \quad (129)$$

To verify the proposed equations, FEM study on three models with different material hardening is conducted. The hardening ratio values have a significant effect on the pushover curves specifically the post-yield condition.

The models used for this study has a=10cm, b=30cm, L=100 cm and t=2cm. Since the proposed equation only cover the geometrical hardening and the material hardening is dependent on the material properties and strain hardening slope, it is expected that the perfect match would be achieved for the models with zero strain hardening slope. However, for the models with strain hardening slope, the effect of material hardening would show the difference and importance of material hardening as compared to geometrical hardening. Figure 159 shows that the geometrical equations appropriately predict the behavior of the BF link as it is observed with orange line and dashed blue line. The prediction of the BFs with higher strain hardening would be approximate since the equations are based on the geometrical hardening prediction and it is expected that the material hardening should be addressed with additional material factors needed to be experimentally calibrated. The calibrated  $E_p$  factor for the FEM models with  $E_h$  equal to 0.0, 0.01, and 0.03 are 0.027, 0.075 and 0.20 respectively. In addition, the three models with different hardening modulus shown in Figure 168 are considered, and the post-yielding behavior is obtained (dashed lines) and compared with FEM analysis.

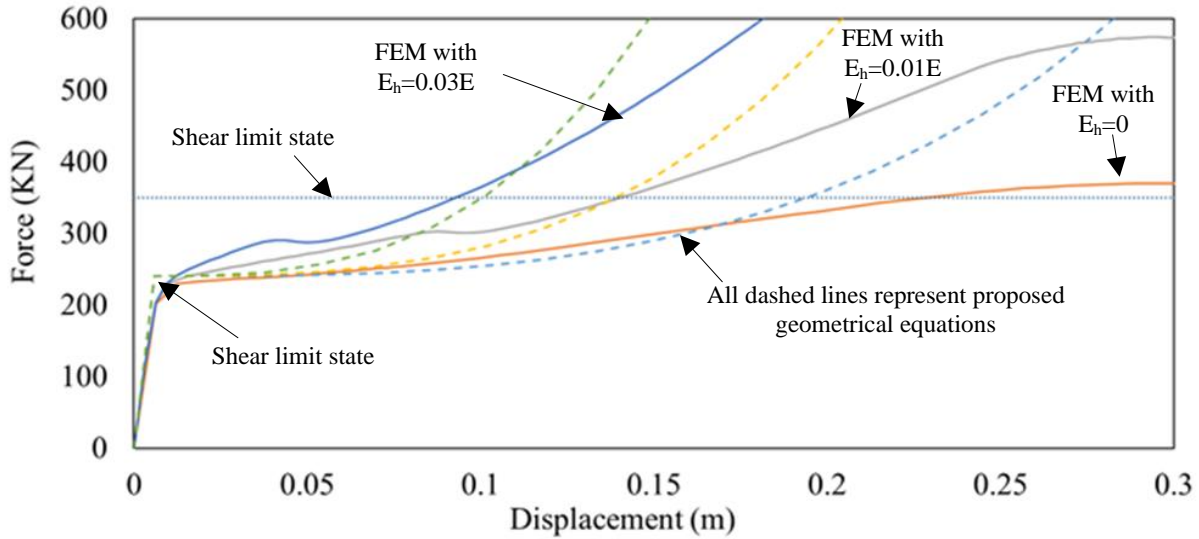


Figure 159. The FEM analysis, and geometrical equation

The models with higher strain hardening are investigated after occurrence of second limit state point which is identified with constant dotted line. It is observed that in both of the models the strain hardening at middle happens and the links act as axial members experiencing significant material hardening shown in Figure 160.

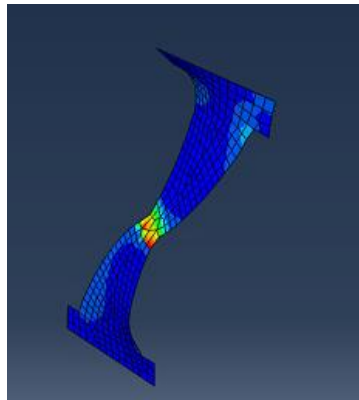
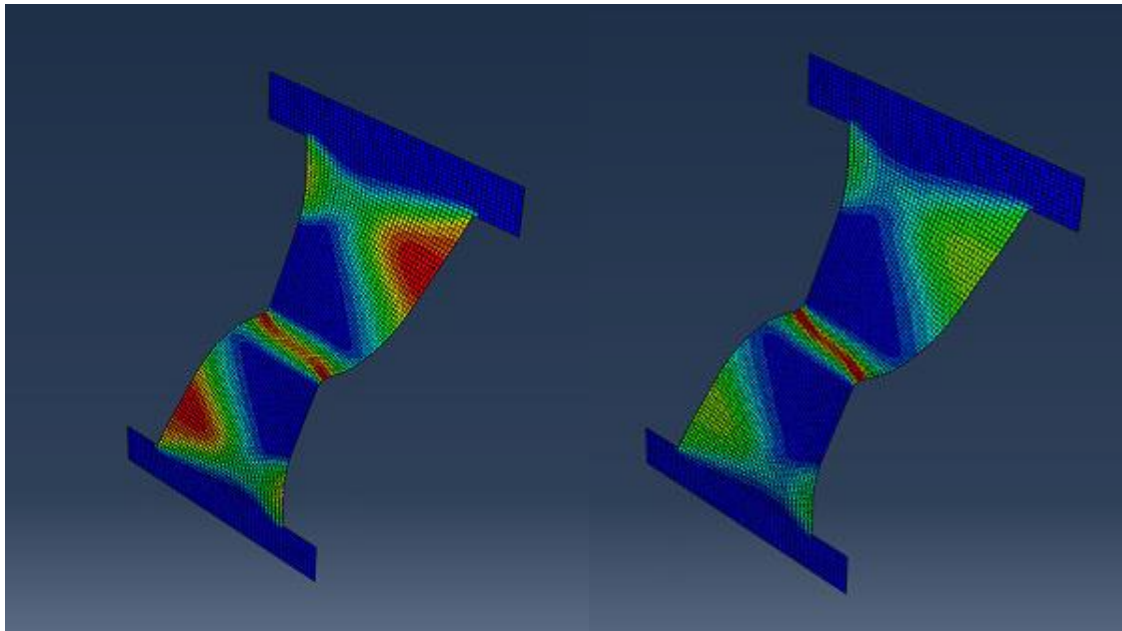


Figure 160. The strain hardening at the middle of the model with 3 percent hardening

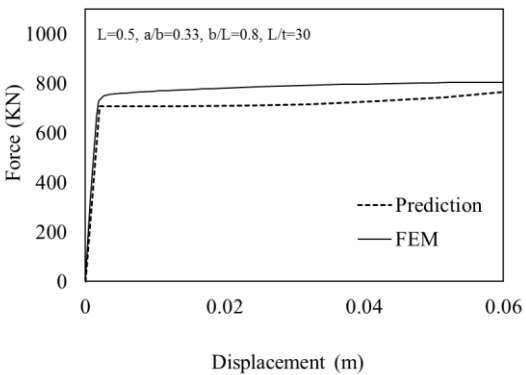
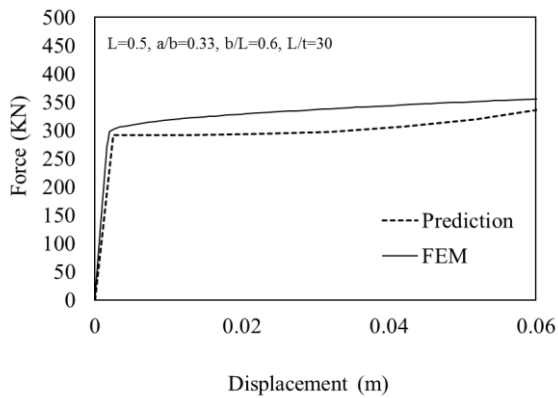
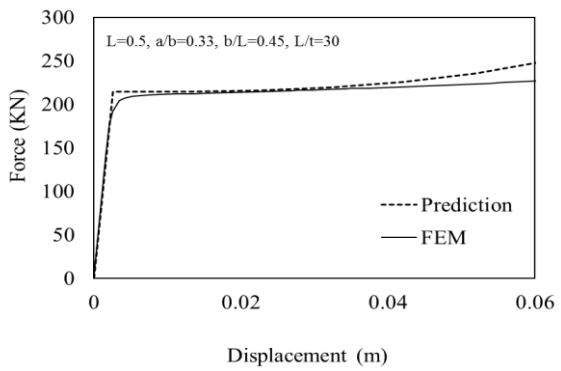
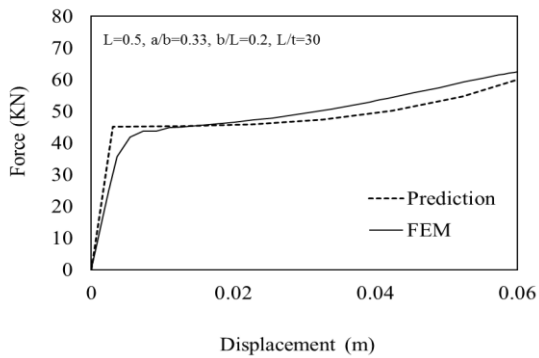
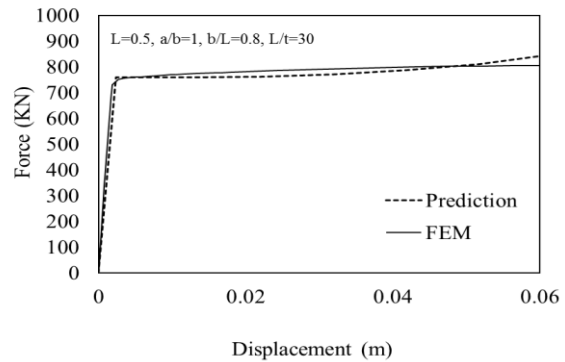
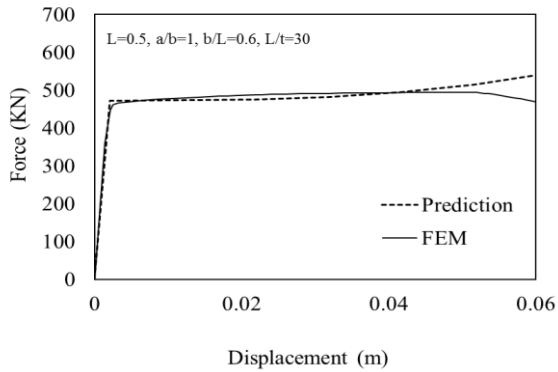
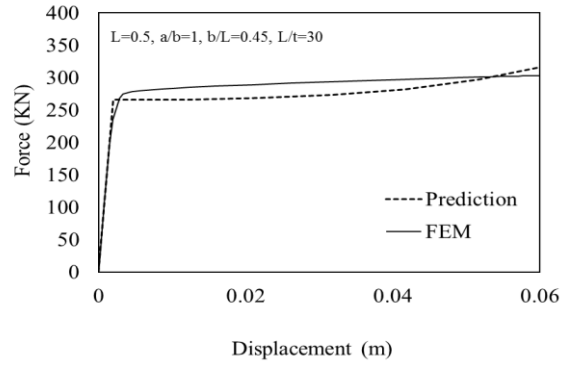
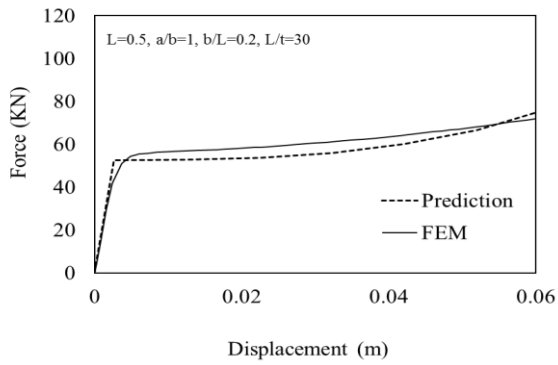
The necking occurs at the maximum load-bearing capacity of a link. The material would be outperformed when the inter-granular cracks coalesce to the point that effective cross sectional area is decreased and the stresses would be concentrated on the sound areas.

Figure 161 shows a specimen with a high value of thickness (10 cm). For this specimen, the possibility of buckling is prevented and it is tried to only have the yielding limit states occurred within the model as the pushover displacement loading starts to be increased. At displacement of 0.43m, or step 68, the significant sudden reduction in load-bearing capacity is observed. The reason for observation of such phenomena is the necking at the middle part where we are dealing with the second yielding limit state. The peak associated with this model occurs at step 67 or displacement of 0.43m. It is noted that the hardening value of steel is 0.07%. As long as the rate of change in stress due to a change in area is lower than the rate of increase in strength because of work hardening, a metal sample will elongate uniformly and will not neck. In addition, to compare the derived equations of predictions accuracy, the finite element pushover curves for 24 models are extracted. The push over curve is then compared to pushover curves based on the proposed equation shown in Figure 162. It is shown that the accuracy of the prediction equation is more than 92% on average for total pushover behavior of the specimens up to 6% drift angle. The conclusions in this chapter are summerized in Farzampour and Eatherton (2018a).



a) Before the occurrence of necking at step 67 in the analysis b) After Occurrence of necking at step 68

Figure 161. Occurrence of necking within the FEM models



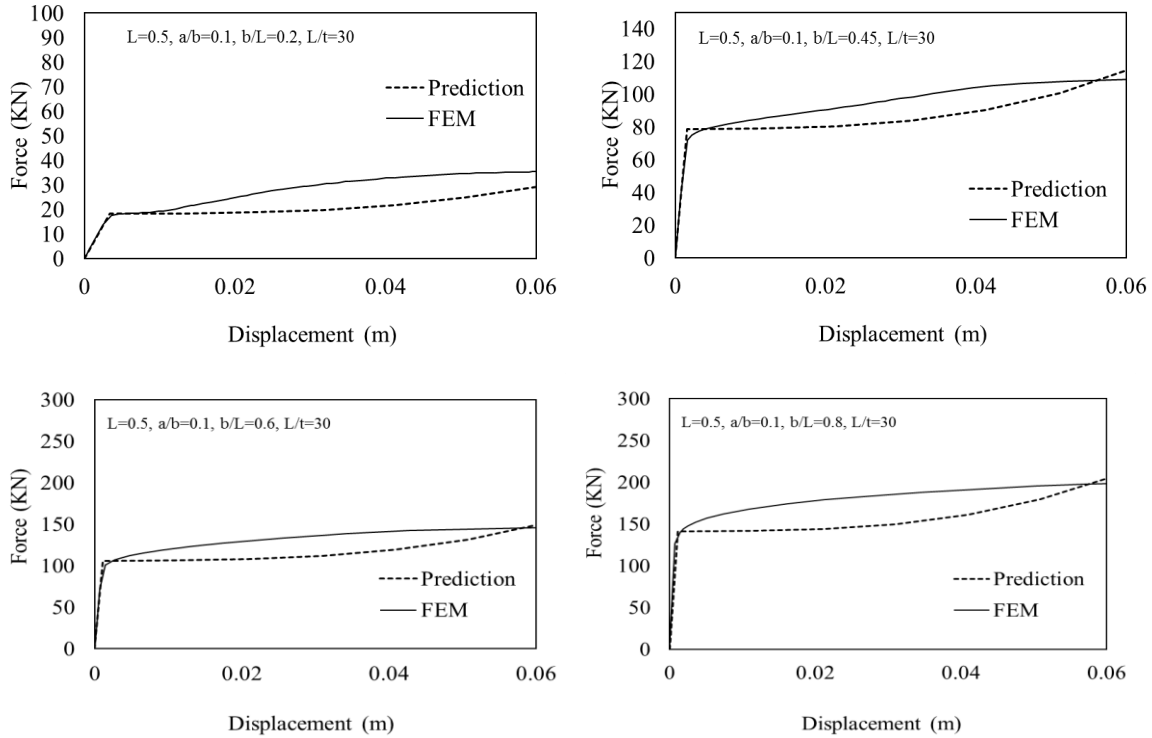


Figure 162. Pushover analysis based on the ABAQUS models and validation with proposed equations

## 7.8. Guideline to design butterfly-shaped links

This guideline is proposed to delineate the procedures to design the butterfly-shaped links for use in seismic structural fuses. This section is drawn based on the summary of the previous chapters investigating the shear, flexural and lateral torsional limit states. The stiffness equations provided in this guideline would summarize the implementation of the BF links in frames and the requirements to satisfy drift ratios.

*1. Understanding the effect of limit state and designing based on the ductile limit state:*

The general energy dissipation analysis indicated that the capability of energy dissipation for those links having flexural limit state as the governing ductile mode of behavior would be the ones with desirable behavior and the better capability in dissipating the energy and being able to have the inelasticity location far from the discontinuity area. The design procedure is an iterative procedure in which the geometry should be updated to avoid the brittle modes to occur.

In general, the flexure limit state is preferred over the shear limit state because of two reasons. First, the inelasticity location would be far from the discontinuity areas, which reduces the chance of having a fracture. Next, the energy dissipation studies show that the capability of flexural dominated butterfly-shaped links in dissipating the energy would be higher than shear dominated ones. However, in some cases, it is not possible to have the flexural dominated links due to the limitation of the geometry; therefore, the shear limit state should be considered for the design purposes.

The transitional equation for having the first yielding and ultimate capacity in flexure would be estimated by what follows:

For  $a < b/2$ :

For the purpose of having flexure mode to be governed over the shear mode it is required that the geometry satisfy the following equations:

$$\frac{b-a}{L} < 0.28 \text{ (or } \alpha > 148^\circ) \quad \text{Flexure dominated} \quad (130)$$

The shear and flexure capacity limit states are assessed as follows:

It is noted that if multiple links are used the number of the links (n) should be considered for the total plastic strength force which is shown in Eq. (131) and Eq. (132).

$$P_p^{flexure} = \frac{2n(b-a)at\sigma_y}{L} \quad (131)$$

$$P_p^{shear} = n \frac{\sigma_y at}{\sqrt{3}} \quad (132)$$

For  $a > b/2$  or straight ( $a=b$ ):

$$b/L < 1.15 \quad \text{Flexure dominated}$$

It is noted that if multiple links are used the number of the links (n) should be considered for the total plastic strength force which is shown in Eq.(133) and Eq. (134).

$$P_p^{flexure} = \frac{nb^2t}{2L} \sigma_y \quad (133)$$

$$P_p^{shear} = n \frac{\sigma_y bt}{\sqrt{3}} \quad (134)$$

2. Controlling the brittle mode, while having the ductile limit state as the predominated mode:

To avoid buckling, and have flexure or shear the following equations should be satisfied.

$$P^p = \min\{P_p^{flexure}, P_p^{shear}\} \quad (135)$$

$$P_{cr}^{LTB} = \frac{2nE[0.533+0.547(a/b)-0.281(a/b)^2+0.096(a/b)^3]bt^3}{L^2\sqrt{1+\nu}} \quad (136)$$

Therefore, the maximum forces from the brittle limit state should have lower values compared to minimum force from shear and flexure limit states. To avoid the chance of buckling occurrence right after the first limit state, the effect of overstrength factor should be considered. Based on the parametric study, the Over strength factor could be extracted. The numbers more than b/L equal to 0.4, could be conservatively taken from whatever is proposed for b/L equal to 0.4.

Table 11. The overstrength factor

BF LINKS		b/L	Overstrength $\Omega$
a/b	0.1	0.1	4.1
		0.2	3.3
		0.3	2.8
		0.4	1.8
	0.33	0.1	2.3
		0.2	1.65
		0.3	1.35
		0.4	1.3
	0.75	0.1	4.13
		0.2	3.18
		0.3	2.51
		0.4	1.95
	1	0.1	4.35

		0.2	3.35
		0.3	2.75
		0.4	2.45

$$\Omega P^p < P_{cr}^{LTB} \quad (137)$$

It is worthy of notice that the occurrence of the buckling in monotonic condition would be identical with the occurrence of buckling under cyclic condition. Table 12 shows average normalized equivalent plastic strain values with respect to minimum equivalent plastic strain values for butterfly-shaped links. It is concluded that the implementation of a/b equal to 1, or 0.1 would have high equivalent plastic strain values which makes the links highly prone to fracture. However, the equivalent plastic strain values of 0.33 and 0.75 would have low equivalent plastic strain values, which could be recommended for design purposes. It is noted that high-normalized equivalent plastic strain values indicate less ductility, potential to fracture and less resistance against load reversals.

Table 12. The overstrength factor

Normalized equivalent plastic strain at 5%	a/b			
	b/L	0.1	0.33	0.75
0.1	5.82	2.35	2.59	5.18
0.2	8.41	6.18	5.47	15.94
0.3	16.35	1.03	1.00	16.76
0.4	20.71	1.29	1.24	21.76

### 3. Controlling the drift ratios, and stiffness equations requirement:

The stiffness of the butterfly-shaped link could be evaluated based on the equations provided in previous chapters:

$$K_T = \frac{K_b K_v K_c K_d}{K_b K_v K_c + K_b K_v K_d + K_b K_c K_d + K_v K_c K_d} \quad (138)$$

In which  $K_b$ ,  $K_v$ ,  $K_c$ , and  $K_d$  could be evaluated as follows:

$$K_b = nEb^3t \left( \frac{2 \left( \frac{a}{b} - 1 \right)^3}{3 \left[ 2Ln \left( \frac{a}{b} \right) + \left( \frac{a}{b} - 1 \right) \left( \frac{a}{b} - 3 \right) \right] L^3} \right) \quad (139)$$

$$K_v = \frac{\frac{5nGt}{6L} (b - a)}{\text{Ln} \left( \frac{b}{a} \right)} \quad (140)$$

$$K_c = n \frac{P}{\delta_c} = \frac{EtL_b^3}{6C(L)^2} \quad (141)$$

$$K_d = \frac{5}{6} \frac{GtL_b}{L} \quad (142)$$

For the straight links the criteria for stiffness is as follows:

$$K_T = \frac{K_b K_v K_c K_d}{K_b K_v K_c + K_b K_v K_d + K_b K_c K_d + K_v K_c K_d} \quad (143)$$

In which  $K_b$ ,  $K_v$ ,  $K_c$ , and  $K_d$  could be evaluated as follows:

$$K_b = \frac{nEt b^3}{L^3} \quad (144)$$

$$K_v = K_v = \frac{5n}{6} \frac{Gtb}{L} \quad (145)$$

$$K_c = \frac{EtL_b^3}{6cL^2} \quad (146)$$

$$K_d = \frac{GtL_b}{L} \quad (147)$$

Therefore, the residual displacement for the links should less than what is specified for specific lateral resisting systems.  $P_{\text{loading}}$  is the amount of load associated with the link.  $\delta_{\text{specified}}$  is estimated based on the requirements associated with specific lateral resthe isting system.

$$\frac{p_{loading}}{K_T} < \delta_{specified} \quad (148)$$

In addition to the first group of applications (e.g. EBFs), the drift limit stats is needed to be checked. Taking into account the Example 5 of the 2012 IBC SEAOC Structural and Seismic Design Manual (SEAOC, 2012), the maximum typical displacement of the stories are about 1 inch for 12ft height building. Therefore,

$$\delta_{up} - \delta_{down} \leq 1 \text{ inch} \quad (149)$$

Therefore, the maximum rotational angle ( $\gamma_p$ ) inside of the link could be calculated from Eq. (150).

$$\gamma_p = \frac{L}{e} \theta_p \text{ where } \theta_p = \frac{\delta_p}{h_{story}} \quad (150)$$

$$\theta_p = \frac{1}{144} = 0.007 \quad (151)$$

For a 30ft span we would have:

$$\gamma_p = \frac{30}{4} (0.007) < 0.2 \sim 0.3 \quad (152)$$

The requirement for  $\gamma_p$  is based on what Ma et al. (2011) mentioned about the ductility of the butterfly-shaped links, which should be less than 0.2 up to 0.3 rad.

# 8. PARAMETRIC STUDY ON BUTTERFLY AND STRAIGHT LINKS

## 8.1. Introduction

A parametric computational study is conducted to investigate the shear yielding, flexural yielding, and lateral torsional buckling limit states for butterfly-shaped links. After validating the accuracy of the finite element (FE) modeling approach against previous experiments, 112 computational models with different geometrical properties were constructed and analyzed including consideration of initial imperfections. The resulting yielding moment, corresponding critical shear force, the accumulation of plastic strains through the length of links as well as the amount of energy dissipated are investigated.

The results indicate that as the shape of the butterfly-shaped links become too straight or conversely too narrow in the middle, peak accumulated plastic strains increase. The significant effect of plate thickness on the buckling limit state is examined in this study. Results show that overstrength for these links (peak force divided by yield force) is between 1.2 - 4.5, with straight links producing larger overstrength. Additionally, proportioning the links to delay buckling and designing the links to yield in the flexural mode are shown to improve energy dissipation.

## 8.2. The parameters study variable investigation and general backbone behavior of butterfly-shaped links

The effect of varying geometries on the location of the hinges, the accumulation of strains, the buckling limit state and the capability of dissipating energy are in need of more investigations. Parametric computational study to investigate the shear and flexural limit states, as well as the buckling behavior of the different butterfly-shaped link geometries, is conducted. The parametric study is conducted on a set of 96 models. Each model is constructed based on the modeling methodology investigated previously in chapter 6. analysis software twice (Figure 163). First, the buckling analysis is done to extract the modal shapes of the butterfly-shaped links, and then push

over analysis would be done. The first mode as the dominant mode is chosen for applying initial imperfection displacement of  $L/250$ .

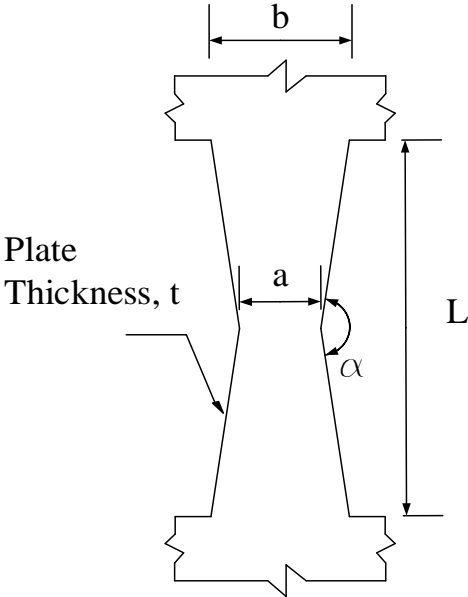


Figure 163. The general butterfly-shaped with the geometry indicated

Table 13 is the summary of the models developed in FE software. The summary and detailed plan for the different cases of the parametric study is determined. About 112 models are indicated to be analyzed and the data would be extracted from them accordingly. The  $L$  value is set to be 0.5m. The  $L/t$  is chosen to have the values of 10-20-40-60. The  $a/b$  values are 0.1, 0.33, 0.75, and 1.0. The  $b/L$  values are 0.1, 0.2, 0.3 and 0.4.

Table 13. The summary of the models analyzed in ABAQUS

<b>L=0.5</b>	
<b>L/t</b>	10
	20
	40
	60
	80
	100
<b>a/b</b>	0.1
	0.33
	0.75
	1
<b>b/L</b>	0.1
	0.2
	0.3
	0.4

For the sake of better organization, each model is identified with four different parameters A, B, C, and D. A is the length of the butterfly-shaped link, B shows the a/b ratio. C shows the b/l ratio. and D shows the L/t ratio.

Mainly two types of pushover behaviors are observed, which would be elaborated in details. The first type of pushover curve is indicated in Figure 164, Figure 165 and Figure 166. At the point one the flexural limit states govern the behavior the system, while for the point 2, the next limit state would be observed, which is shear limit states. Between these two limit states, the second order action occurs. In addition, the amount of out-of-plane ( $U_3$ ) is equal to 5mm. The initial imperfection is assigned based on the first mode of the structure with L/250 value. The procedures to make links in the shop could affect the magnitude of imperfections. Therefore, some other manufacturing methods may result in more imperfections. It is worthy of notice that for the models that experience buckling, the load-bearing capacity would be reduced. In addition, the imperfections are applied by changing the coordinates of the elements without inducing any stresses.

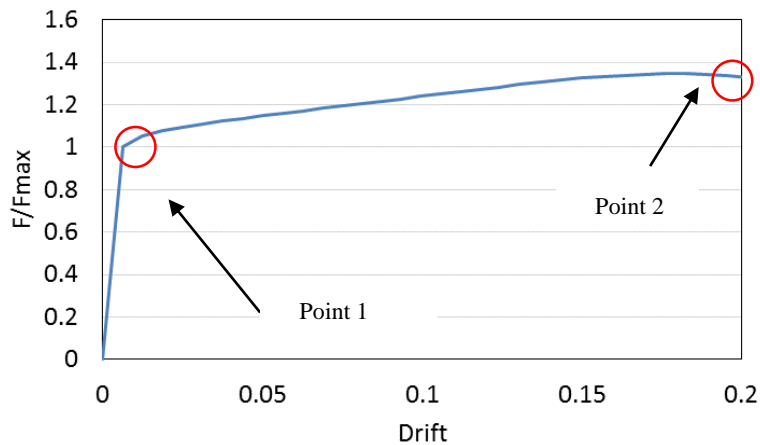


Figure 164. General pushover behavior for 1-0.33-0.3-50



Figure 165. The behavior of the model with 1-0.33-0.3-50 at point 1

At point 2, the equivalent plastic strain is concentrated in the middle and the shear hinge at the mid-point length of butterfly-shaped. From this point on the whole link acts as a mechanism and the strength and stiffness degrade significantly. By acquiring the second limit state, the butterfly-shaped link does not have the capability to resist the load. The  $U_3$  at point 2 is about 7.5mm.

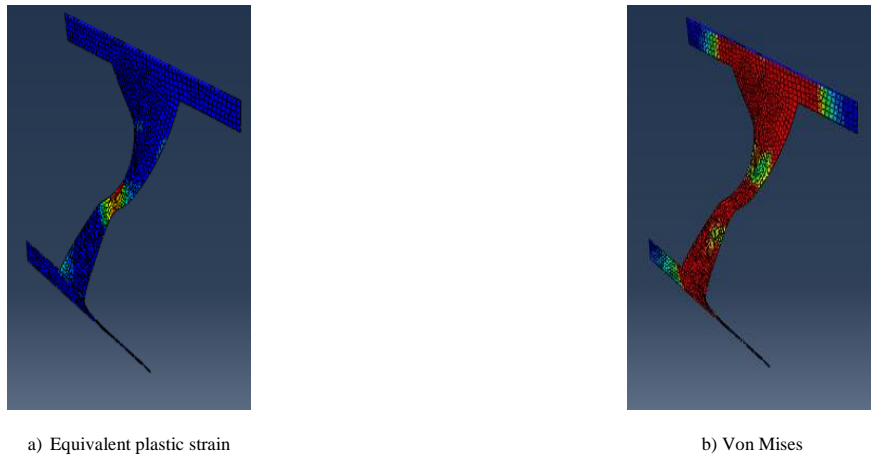


Figure 166. The behavior of the model with 1-0.33-0.3-50 at point 2

The second type of the pushover curves is the occurrence of shear limit state first (Figure 167). It is observed that the butterfly-shaped link has experienced shear limit state at point 1. The second-order action occurs after that, and that is because of the fact that the membrane effect due to elongation of the link would take place. The second limit state, flexure limit state, occurs after this part and the link strength and stiffness degrades afterward.

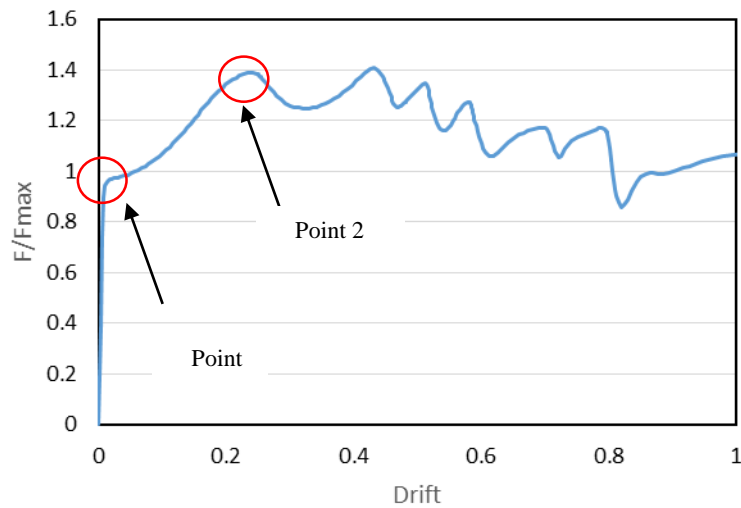


Figure 167. Pushover curve for 0.5-0.33-0.3-20

It is noted that the buckling due to the geometry of the butterfly-shaped link is possible to occur which is highly dependent on the thickness of the link. If the link is not thick enough, the buckling would take place and prevent from reaching to ductile limit states. However, it does not mean that buckling would never happen for a thicker plate since the other geometrical properties are important in buckling occurrence.

Based on the geometrical properties of each model indicated in each model is identified. The associated geometrical properties and the predicted values for shear yielding and flexural yielding limit states are indicated in each table for each set of butterfly-shaped links (e.g. Table 38). The forces associated with flexure and shear limit states, based on the previously derived equation are calculated for each model. The total capacity, which is the minimum of the shear or flexure forces, is also added to the tables.  $P_{max}$  is the maximum value extracted from the pushover curves and the moment ( $M_{end}$ ) is obtained based on  $P_{max}$ .

The rest of the output parameters for each set of models are summarized (e.g. Table 39). The equivalent plastic strain is monitored at the specified drift of 5 percent for all the models. For this case at the specified displacement, the highest equivalent plastic strain on the whole model would be identified first. The equivalent plastic strain values are based on the average method, in which the elements in the neighborhood of the maximum equivalent plastic strain would be identified.

The average distance of the elements, which have somehow the same values of equivalent plastic strain (less than 5% margin with the maximum equivalent plastic strain) would be assumed as the target element for hinging location. Accordingly, the pushover curve forces associated with each model is normalized based on the minimum value of the shear and flexural capacity. The displacements are normalized also based on the total height of the link. The buckling output indicates that at what displacement ( $U_1$ ) buckling happens. For determination of the buckling, any abrupt change in out-of-plan displacement would be considered as the buckling initiation and the  $U_1$  associated with that is monitored

In addition, the normalized parameters are extracted based on the pushover curves.  $F_s/F_{pred}$  ratio is the first point's force where a change in stiffness and strength is observed.  $\delta_s/L$  ratio is the first point's associated displacement where a change in stiffness or strength is observed.  $F_u/F_{pred}$  ratio is the second point's force where a change in stiffness or strength is observed. It is the point that in some models one of the limit states occurs.  $\delta_u/L$  ratio is the second point's displacement where a change in stiffness or strength is observed. Energy index is the area under the pushover curve up to 0.2 of drift over the total rectangular area, which is shown in Figure 168.

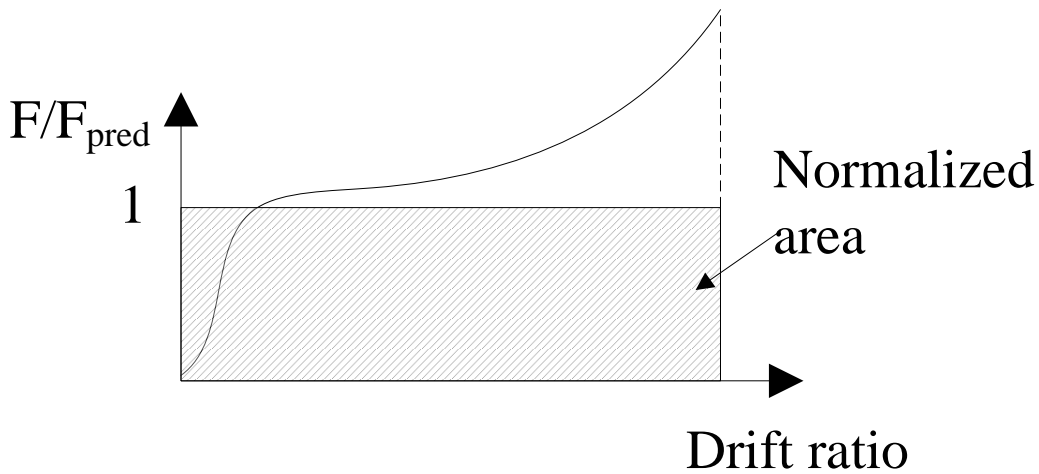


Figure 168. The normalized energy dissipation concept

It is noted that the energy dissipation capability and damping ratios will be investigated in a separate section in details. In what follows, the results of the parametric study are delineated. For all the models the initial imperfection is applied by changing of the coordinate without inducing

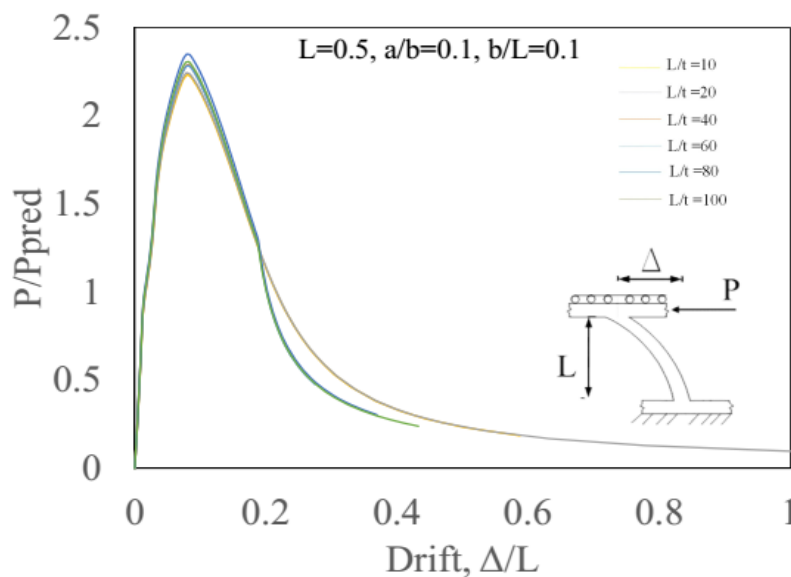
any stresses in the models. The magnitude of initial imperfection is  $L/250$ . It is worthy of notice that the imperfection values are highly dependent on the manufacturing methods which may result in more imperfections.

### 8.3. The results of the parametric study:

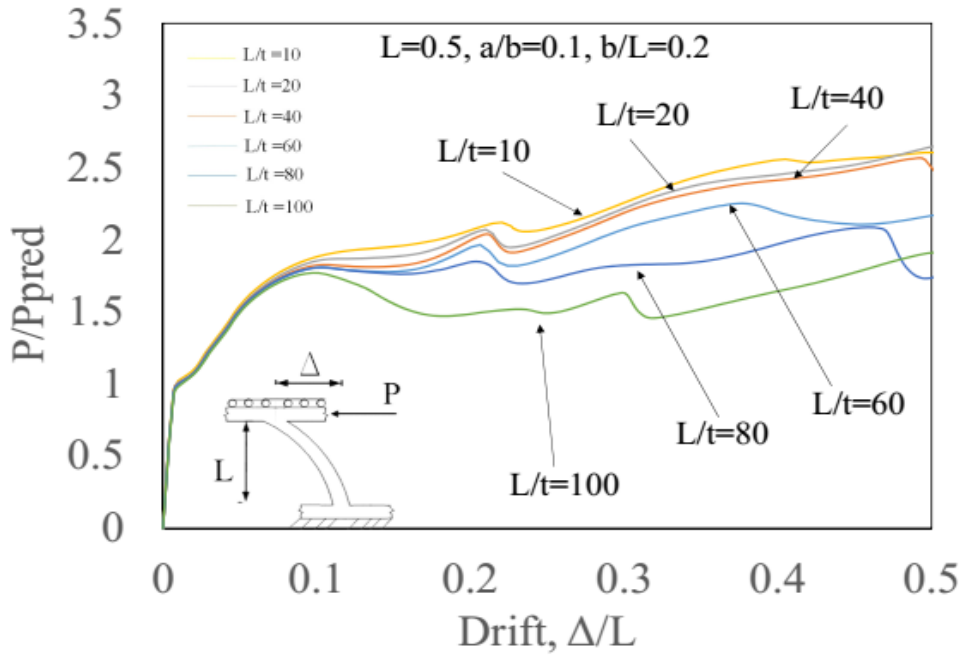
In this section, the results of the parametric study described. The detailed summary of the work is included with tables in Appendix showing the calculated and monitored parameters as well as explanations of the behavior. The pushover curves are included in Appendix as well.

#### 8.3.1. The group of butterfly-shaped links with $L=0.5$ , and $a/b=0.1$

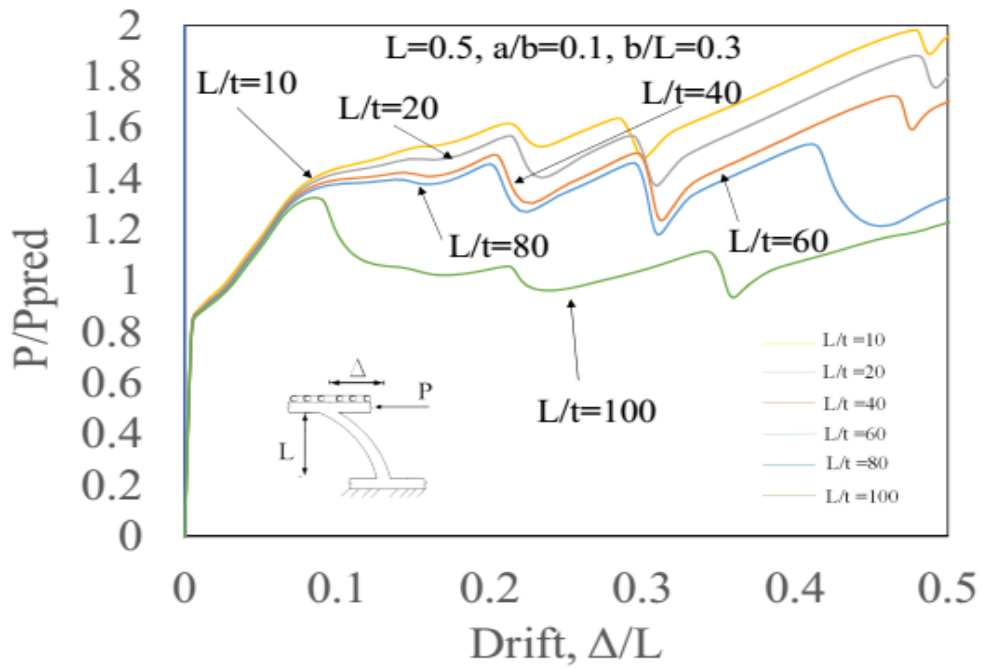
This group of models shows four different sets, in each set the  $b/L$  varies based on the different values for  $L/t$ . However, the  $L$  and  $a/b$  are fixed and equal to 0.5, and 0.1, respectively. Compared to the greater values of  $b/L$ , elaborated in next sections, the second-order behavior is generated much faster. The considerable out-of-plane buckling limit state has happened before reaching to the shear limit state for this type of butterfly-shaped links. After the occurrence of buckling large degradation of strength and stiffness was happened. It is concluded that the effect of end width on the possibility of the buckling occurrence is significant. The buckling capacity, shear and flexural capacity of the links are improved compared to lower end width cases.



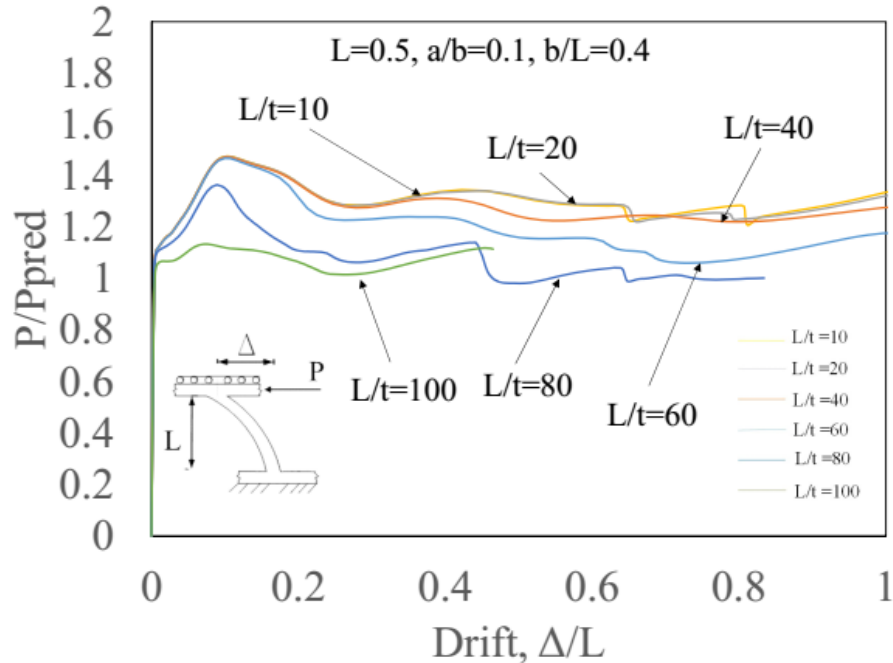
a)  $L=0.5, a/b=0.1, b/L=0.1$



b)  $L=0.5, a/b=0.1, b/L=0.2$



c)  $L=0.5, a/b=0.1, b/L=0.3$

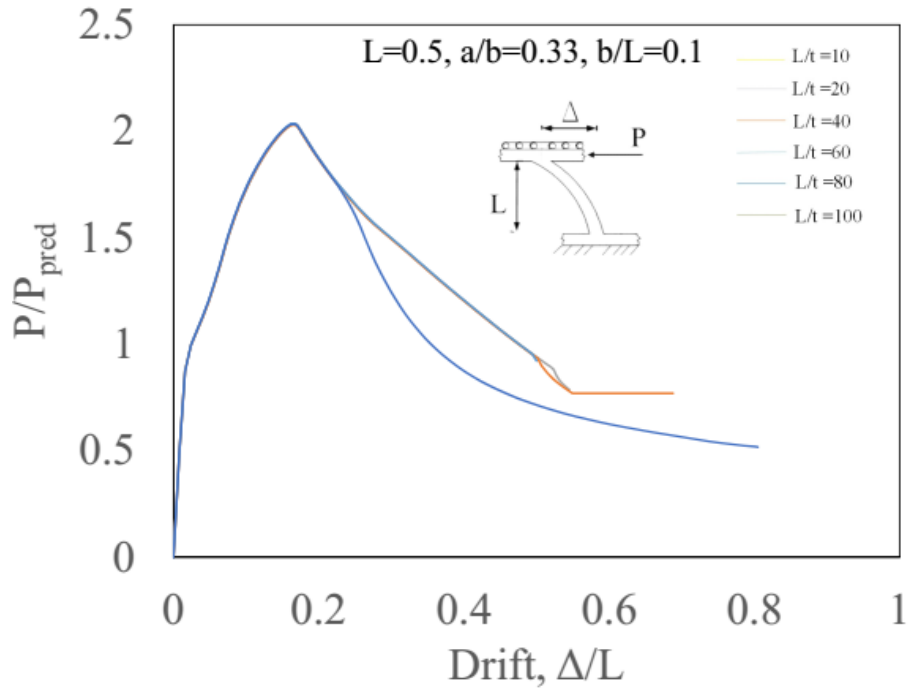


d)  $L=0.5, a/b=0.1, b/L=0.4$

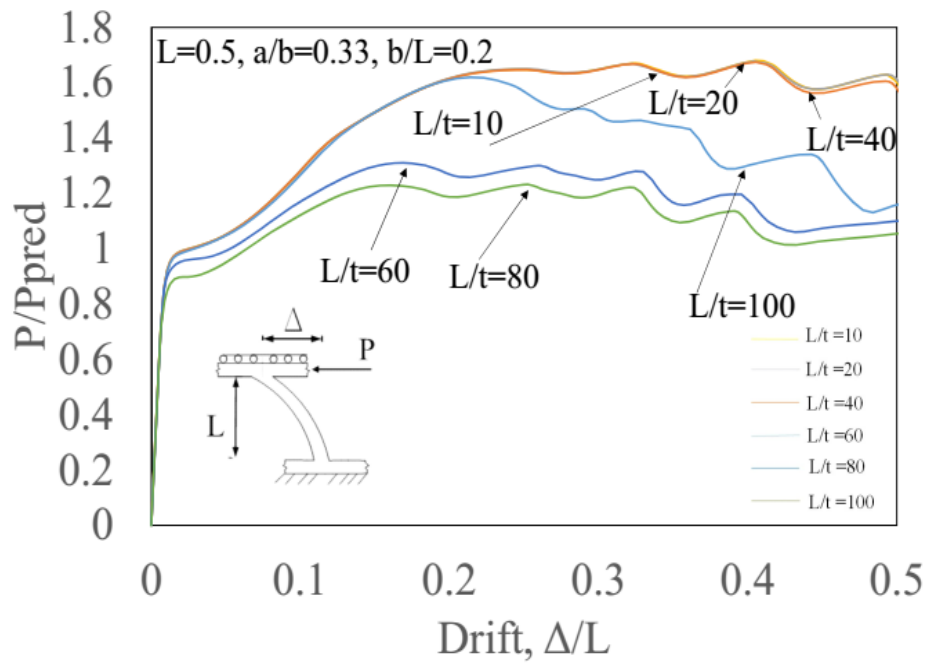
Figure 169. The group of  $L=0.5, a/b=0.1$

### 8.3.2. The group of butterfly-shaped links with $L=0.5$ , and $a/b=0.33$

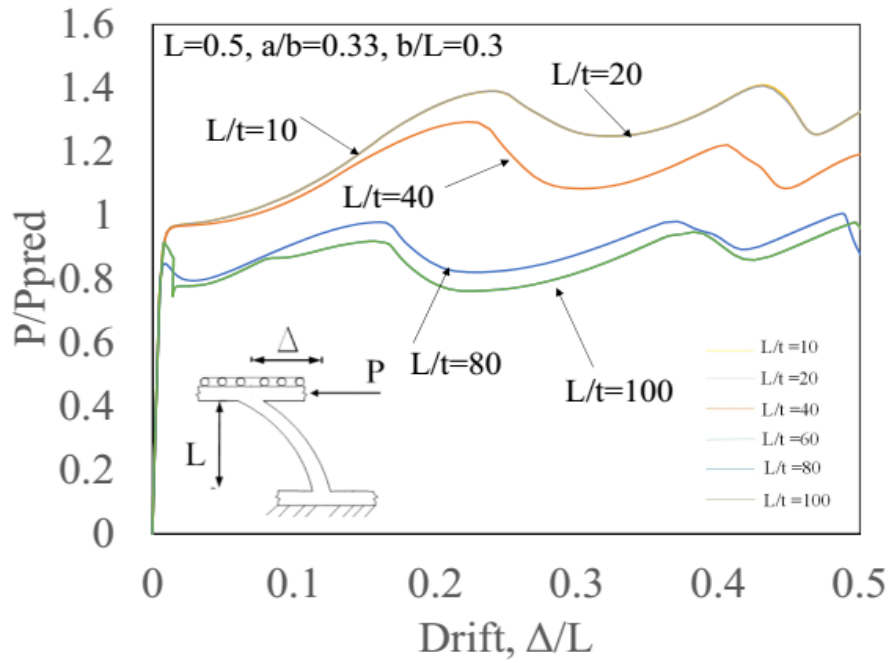
This group of models shows four different sets, in each set the  $b/L$  varies based on the different values for  $L/t$ . However, the  $L$  and  $a/b$  are fixed and equal to 0.5, and 0.33, respectively. The hinge location is far from the sharp ends because of the  $a/b$  ratio, and the fact that these links are flexural governed. The flexural limit state has been occurred in the initial stages of pushover analysis, by increasing the load values, the second order effect takes off, this effect is occurred with less rate compared to the corresponding  $a/b$  equal to 0.1 the buckling limit state have been occurred in almost all of the thicknesses before having shear limit state governing the behavior. The equivalent plastic strain values indicating the accumulated plastic strain in models are less than other geometrical properties; due to the fact, the hinges are located in quarter points far from the sharp edges.



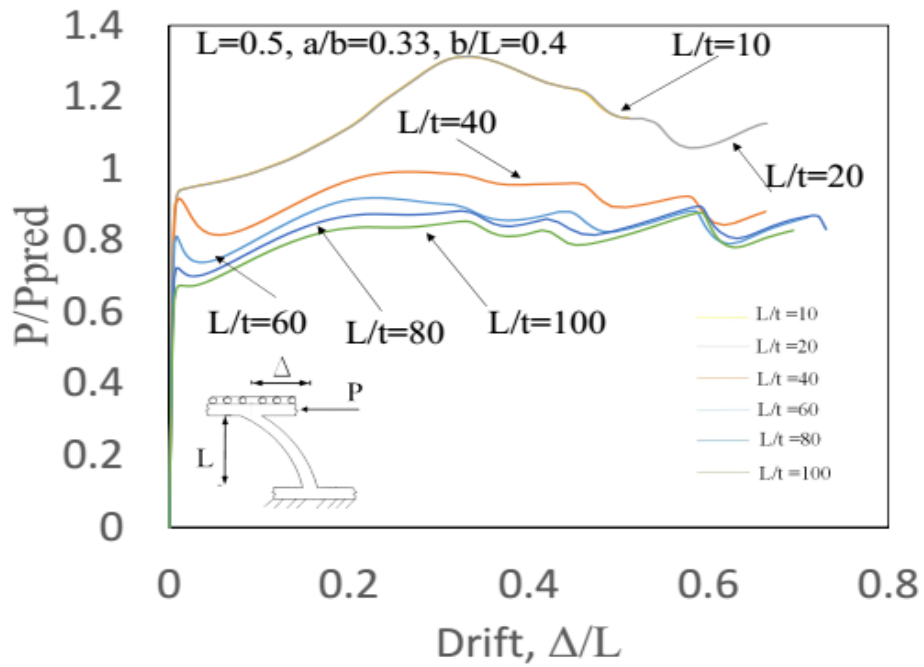
a)  $L=0.5, a/b=0.33, b/L=0.1$



b)  $L=0.5, a/b=0.33, b/L=0.2$



c)  $L=0.5$ ,  $a/b=0.33$ ,  $b/L=0.3$

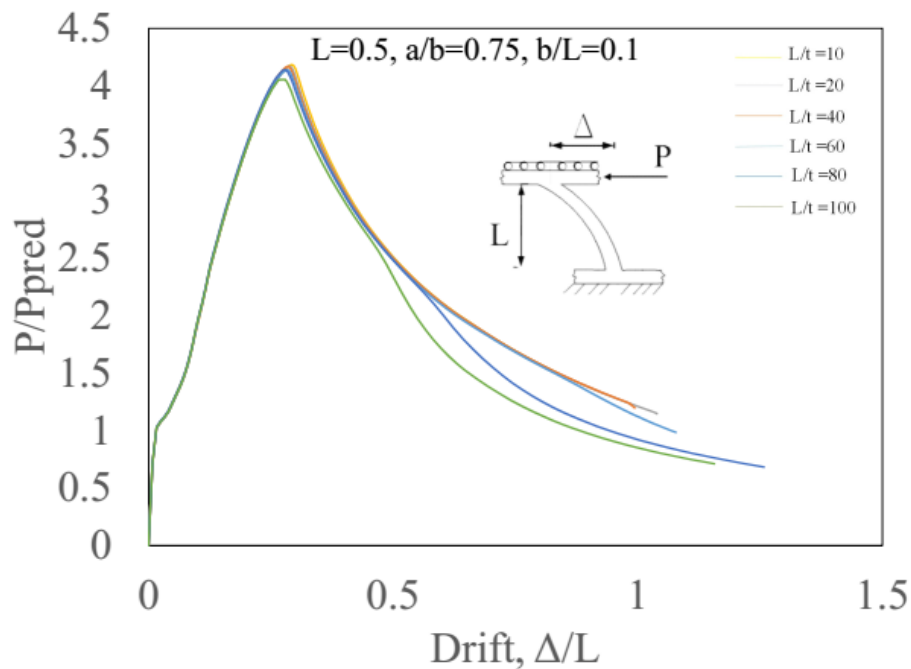


d)  $L=0.5$ ,  $a/b=0.33$ ,  $b/L=0.4$

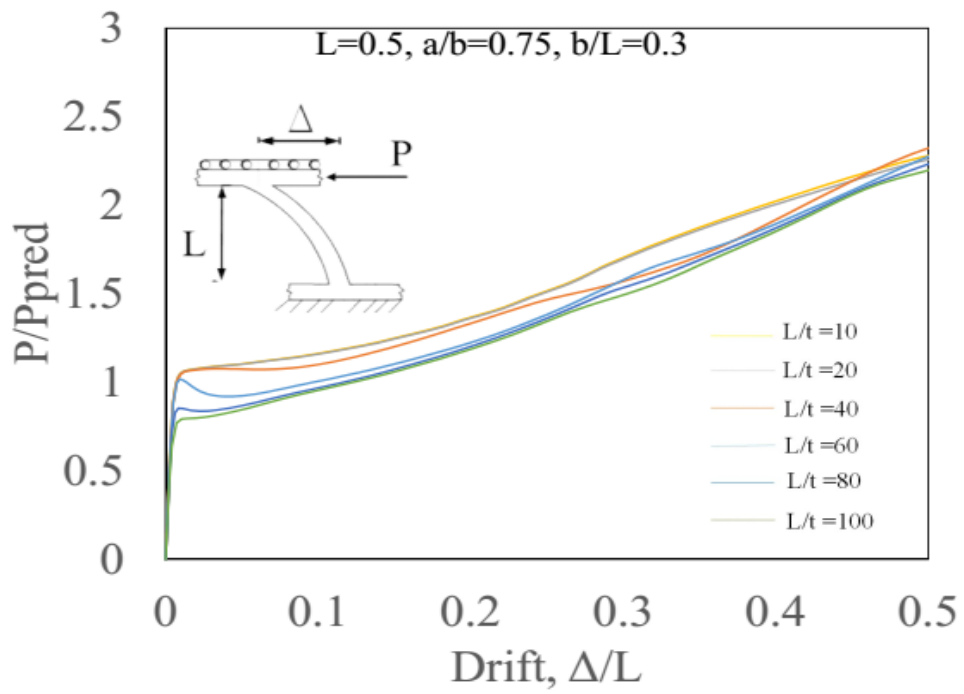
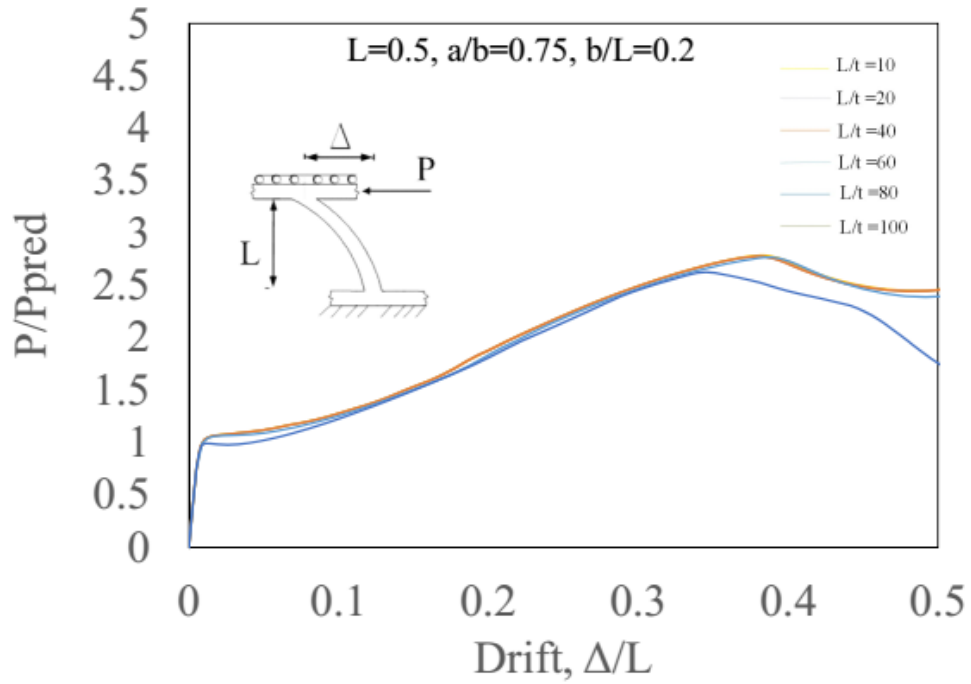
Figure 170. The group of  $L=0.5$ ,  $a/b=0.33$

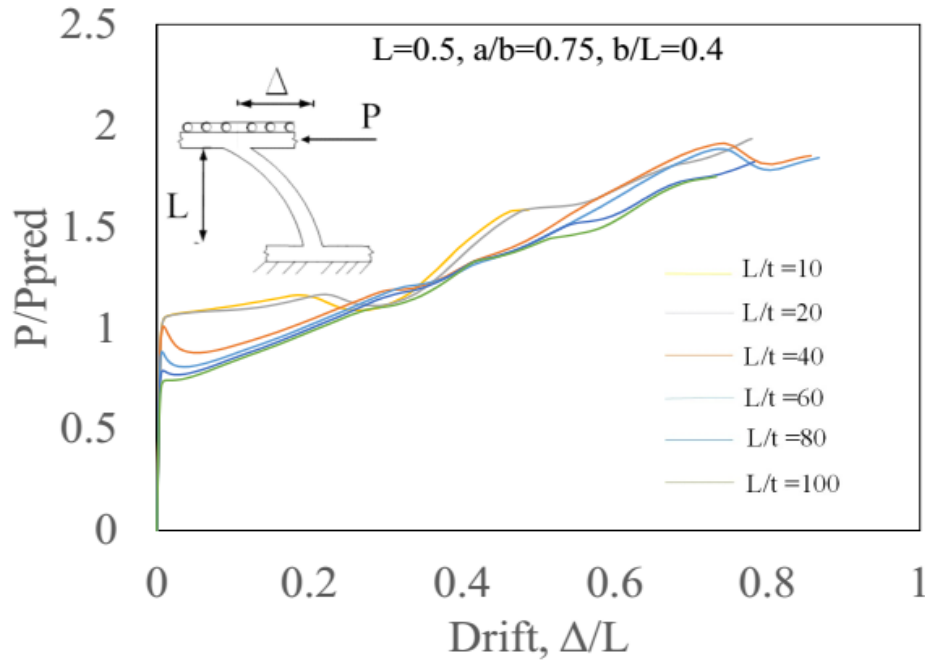
### 8.3.3. The group of butterfly-shaped links with $L=0.5$ , and $a/b=0.75$

This group of models shows four different sets, in each set the  $b/L$  varies based on the different values for  $L/t$ . However, the  $L$  and  $a/b$  are fixed and equal to 0.5, and 0.75, respectively. The hinge location is at the end of the butterfly-shaped link, indicating that the flexure hinging is the governing limit state. The flexural limit state has happened in all the models at first, and then the second order behavior takes off rapidly, and well before the shear limit state, the buckling was occurred to greatly reduce the load-bearing capacity of the links. The normalized curves show that the almost two limit states have happened models with higher  $b/L$  ratios. In this group of models, flexural yielding has been occurred at first, the second order behavior takes place but with a fast rate compared to the previous set of models. The occurrence of buckling kept the models from fully experiencing the shear limit state; hence, the peak occurs in fewer values the shear strength.



a)  $L=0.5, a/b=0.75, b/L=0.1$



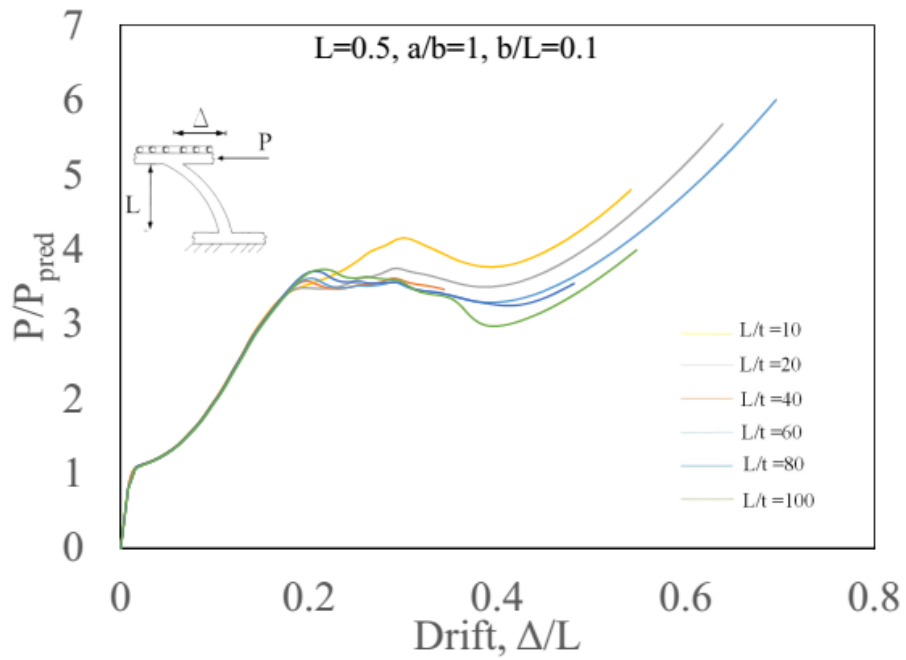


d)  $L=0.5, a/b=0.75, b/L=0.4$

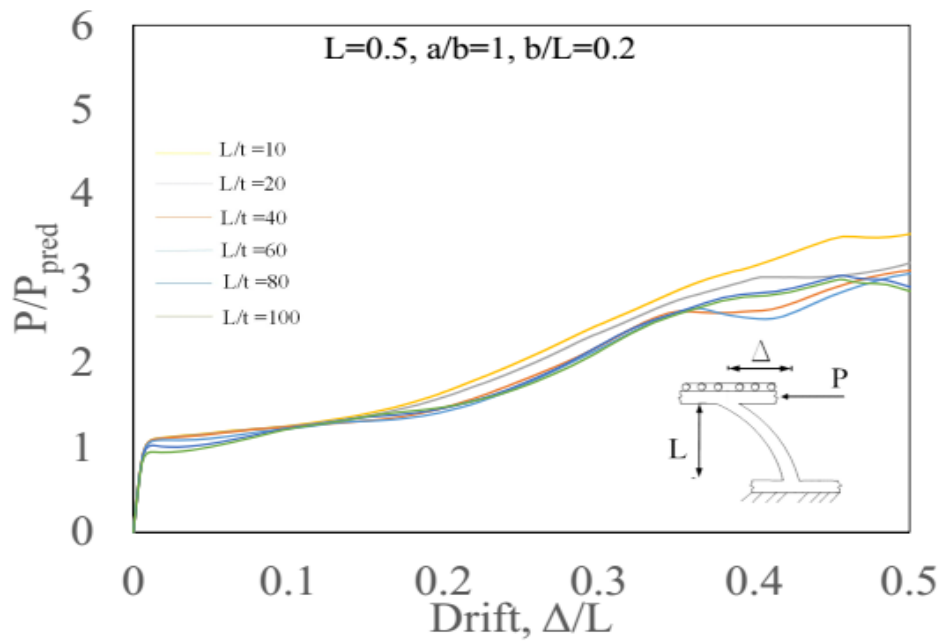
Figure 171. The group of  $L=0.5, a/b=0.75$

### 8.3.4. The group of butterfly-shaped links with $L=0.5$ , and $a/b=1$

This group of models shows four different sets, in each set the  $b/L$  varies based on the different values for  $L/t$ . However, the  $L$  and  $a/b$  are fixed and equal to 0.5, and 1, respectively. The hinges happened at the end of the link. For these links, the flexural hinges would always govern the limit state behavior. Since the  $a/b$  is equal to 1, these links generally behave as flexural dominated links. The flexural limit state has occurred in the initial stages, the buckling limit state has been occurred after having second-order behavior. These links which are commonly known as straight links, which would generally show the flexural hinging at the end. Chapter 4 indicates the mathematical concepts for justifying the behavior of these links. In addition, Lee et al. (2015) and Ma et al. (2010) observed the same behavior from the experimental models. It is noted that the considerable amount of equivalent plastic strain values have happened within these models by increasing  $b/L$  since the accumulation of plastic strains are concentrated at the end of the links where the shape angles exist. Another issue with these links is an observation of the considerable overstrength factor. If these links are used in the seismic application, the design should account for the over the strength of more than 2 for other elements structure.



a)  $L=0.5, a/b=1, b/L=0.1$



b)  $L=0.5, a/b=1, b/L=0.2$

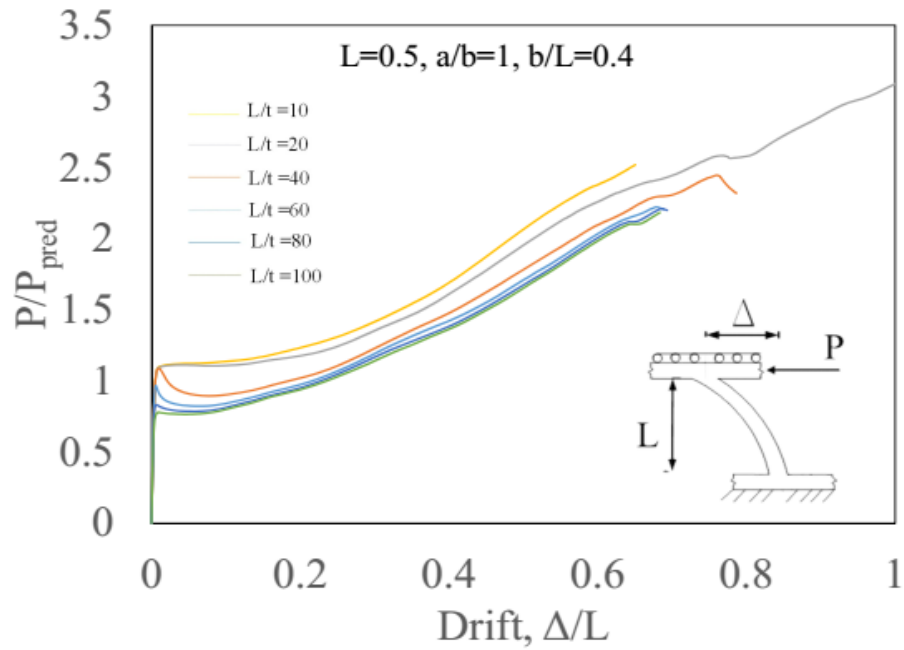
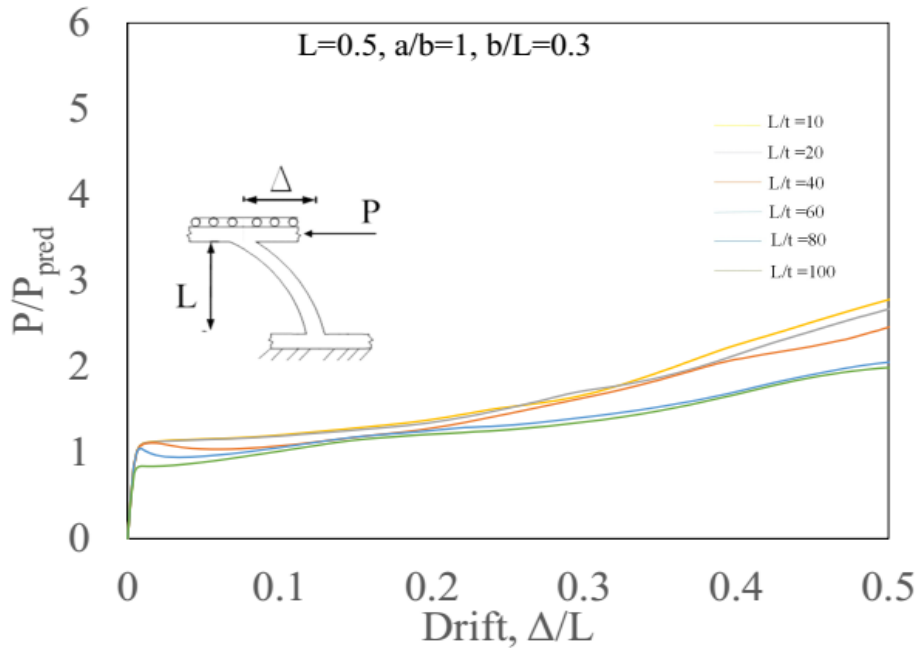


Figure 172. The group of  $L=0.5, a/b=1$

From the parametric study, the amount of over strength proposed by the Lee et al. (2015) and Ma et al. (2011) could be observed the models, which averagely have over the strength of 2-3. Along the same lines, the parametric study on the modeled BF link indicates that if the links with narrow mid-width ( $a/b$  equal to 0.1) the membrane effect would take off faster at initial stages of the pushover analysis. The second-order behavior would be happening at initial displacement. Figure 2 shows that for narrower BF in the middle part the membrane effect would be happening clearly as compared to strain-hardening effect, while for wider links the strain-hardening and membrane effect happen simultaneously. It is noted that as Figure 173 shows, the first limit state is captured well with aid of the equations.

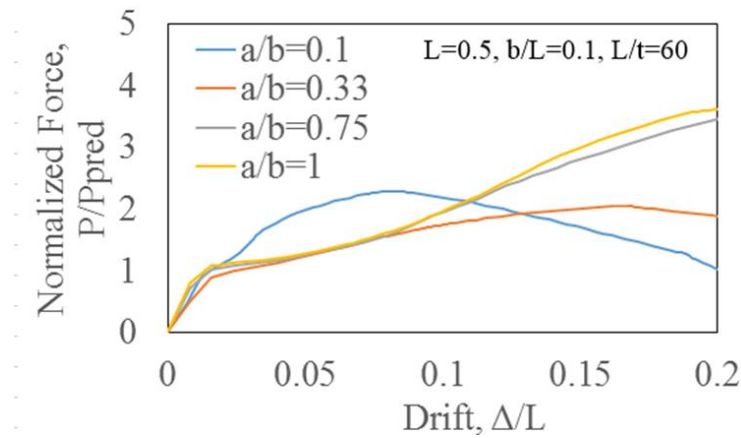


Figure 173. The comparison between the normalized curves

The flexural limit state is observed for the set of models computationally investigated and shown in Figure 173. Table 1 represents the fact that the flexural limit state would be governing first based on critical butterfly-shaped equation. For narrower mid-width BF, the membrane effect takes off at initial stages while the other BFs the material strain-hardening would be controlling the pushover curves at lower deflection values after the occurrence of first limit state, and the membrane effect would be incorporating to the hardening at larger drift values.

Table 14. The comparison between the normalized curves

L (m)	a/b	b/L	L/t	$(b-a)/L < 0.28$	The flexure governs
0.5	0.1	0.1	60	0.09	Yes
0.5	0.33	0.1	60	0.067	Yes
0.5	0.75	0.1	60	0.025	Yes
0.5	1	0.1	60	0	Yes

### 8.4. Investigation of the output parameters

It is observed that the hinge location with is independent thickness values. The hinge location would be approaching the middle part if the  $b/L$  increases. Which essentially is compatible with fact that the inelasticity would approach the shear yielding at the middle. The provided equation for flexural and shear limit state governing are confirmed with computational FE analysis. For instance, the equations showing the shear limit state governing is indicated Chapter 4. Therefore, for the group of models with  $L=0.5$ ,  $a/b=0.33$  and  $b/L=0.1-0.2-0.3-0.4-0.5-0.6-0.7-0.8-0.9$ , the  $\alpha$  values are 172.37, 164.81, 157.38, 150.13, 143.12, 136.39, 129.96, 123.85, 118.02, which shows that the inelasticity goes toward the middle link as the equation predicted as it is shown in Figure 174.

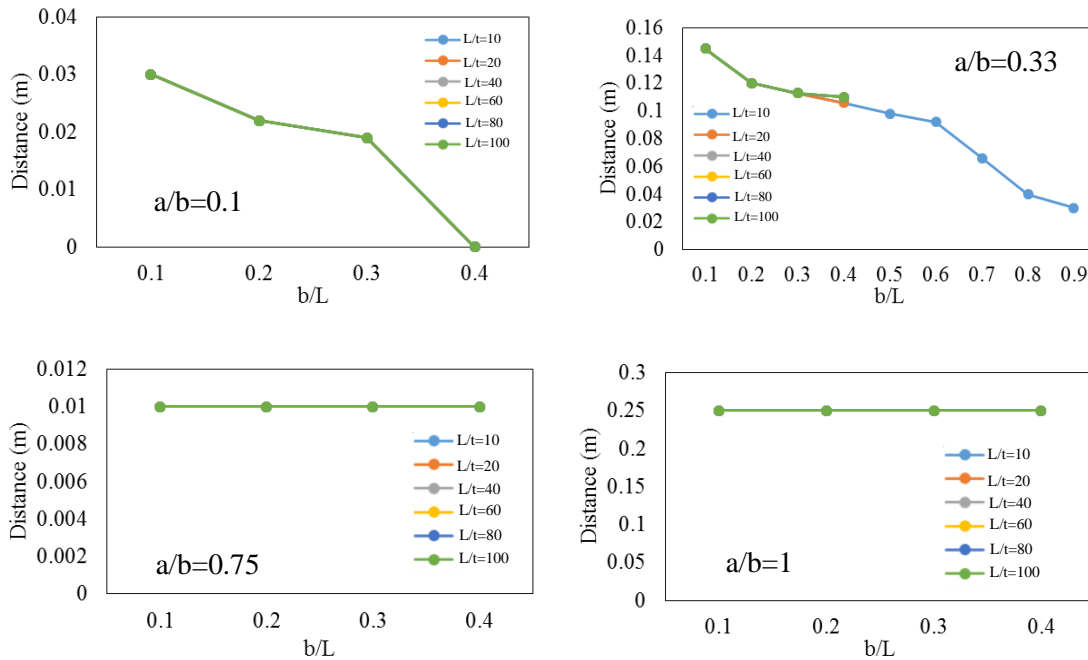


Figure 174. The hinge location from the top of the butterfly-shaped link

The general values of the equivalent plastic strain are low for all the groups except for  $a/b$  equal to 1, which justify the reason that in previous literature the possibility of fracture for these links, especially with thicker plates is high. This further represents the fact that the straight links could be highly prone to fracture compared to corresponding butterfly-shaped links. The light change about  $b/L$  0.2 for  $a/b=0.33$  and  $a/b=0.75$  series could be due to slight changer in mesh generation procedure.

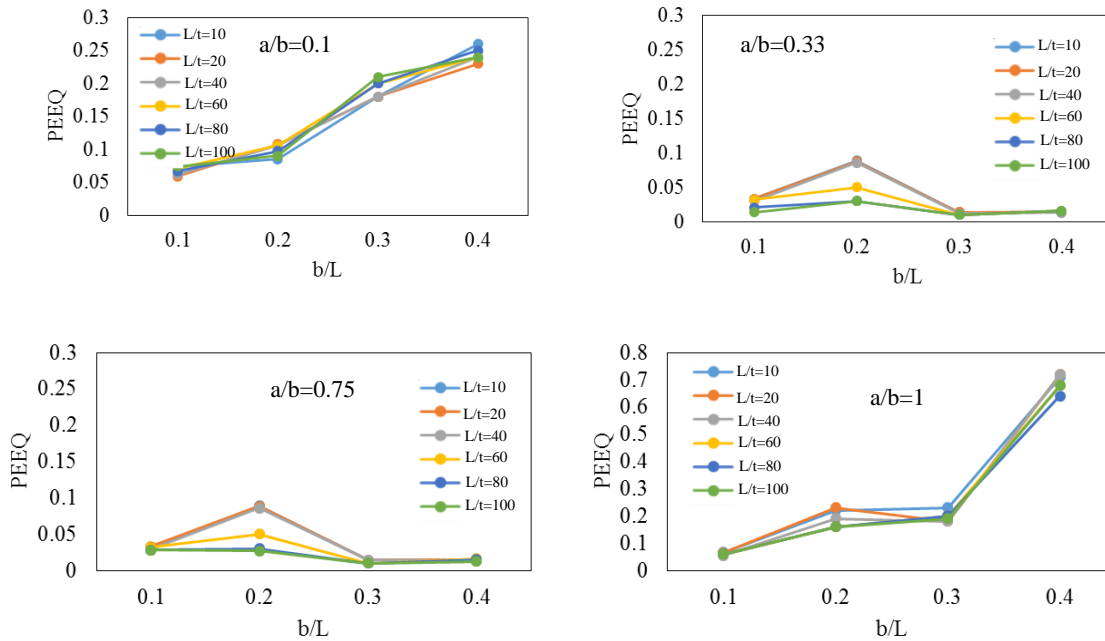
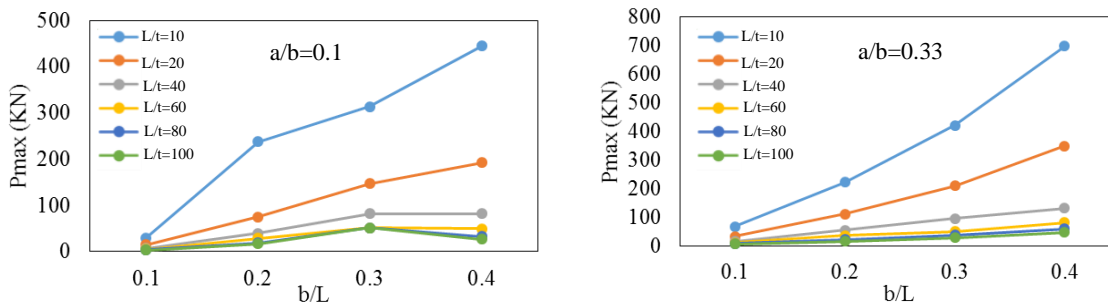


Figure 175. The summary of equivalent plastic strain (PEEQ) results

As far as the shear limit state is concerned, the equivalent plastic strain results get higher. The reason for that could be the fact is that the middle part the geometry get to be sharper compared to the rest of geometry, specifically for  $a/b=0.33$  which the flexural hinges are supposed to be developed in quarter points. Therefore, equivalent plastic strain seems to be increased in the middle if the inelasticity is supposed to be generated there Figure 175.

The general trend of  $P_{max}$  and  $M_{max}$ , which are taken directly from the pushover analysis, would be increased by an increase in thickness (Figure 176 and Figure 177). In general, any increase in thickness would lead to nonlinearly increase in ultimate results for force and moments. The trend shows that the strength majorly comes from the flexural strength compare to shear strength.



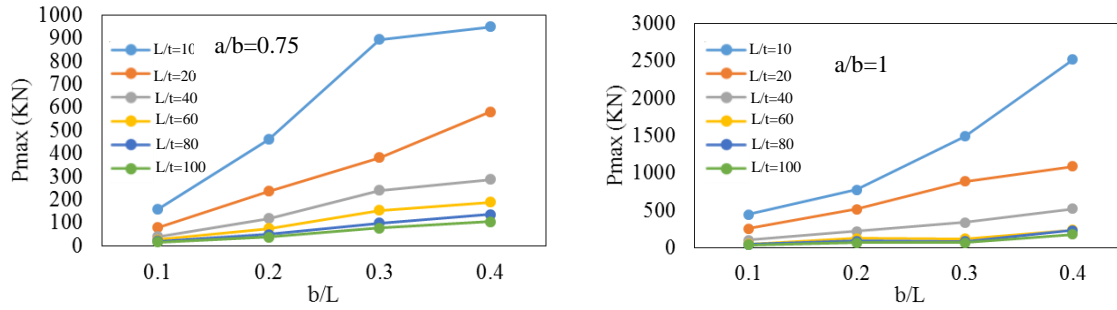


Figure 176. The maximum force extracted from pushover analysis

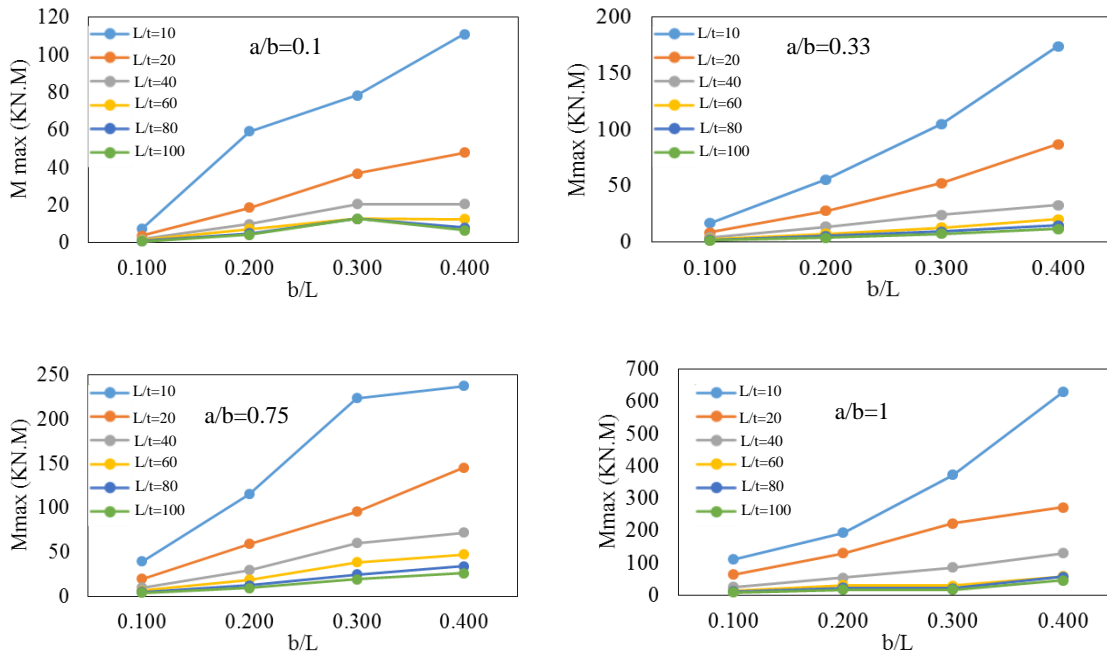


Figure 177. The maximum moment extracted from pushover analysis

The normalized energy index is affected by how thin the butterfly-shaped link is. If the plate is thin enough, it means that it is more prone to buckling, ultimately less capacity to dissipate energy, which is observed in Figure 178. For all of the butterfly-shaped links, the increase in  $b/L$  would decrease the energy dissipation capability which means that the shear governed link would not be as effective as flexure governed link.

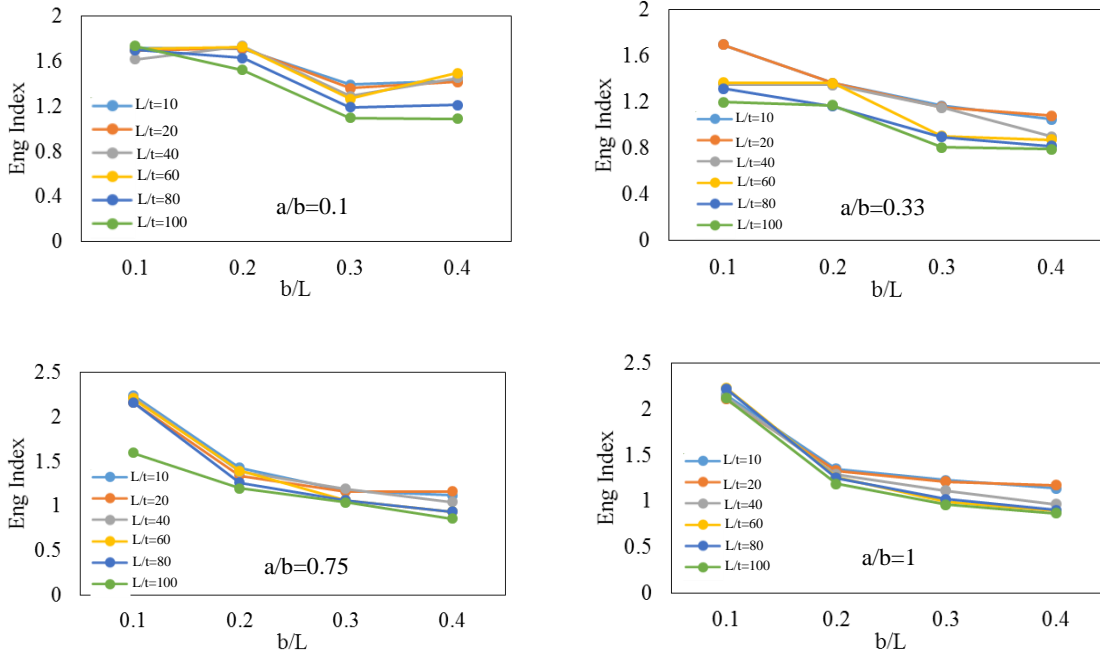


Figure 178. The energy index

If the shear and flexure limit states considered, the force would be being increased by any increase in thickness, but the rate of increase would be higher for flexural limit states in higher  $b/L$  (Figure 179 and Figure 180).

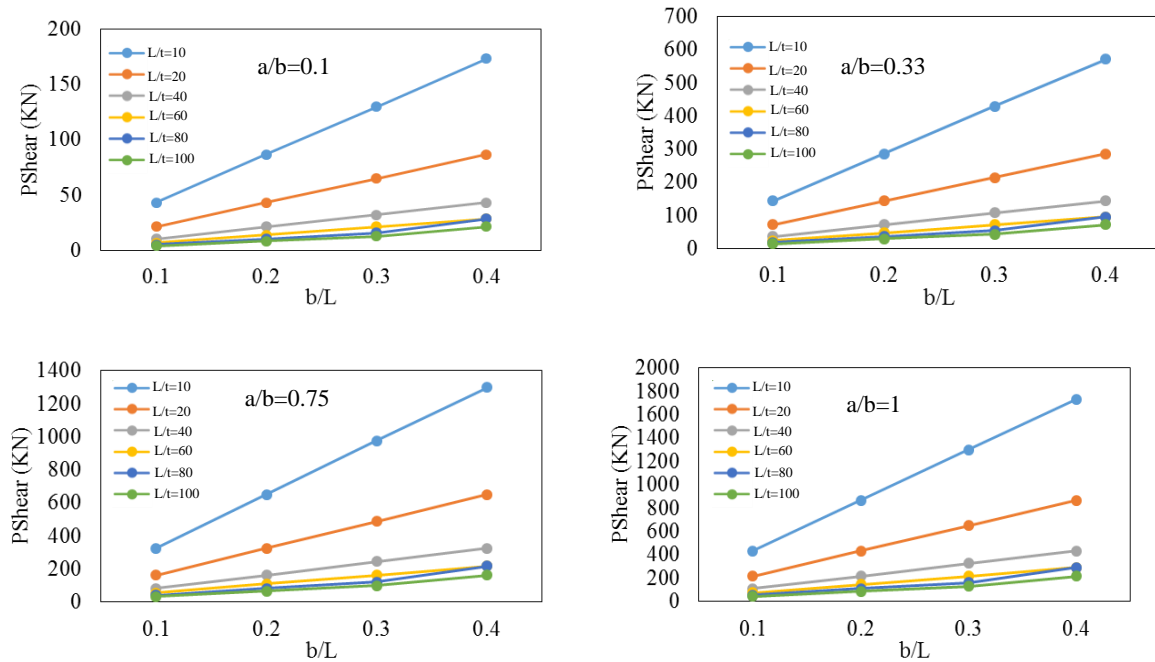


Figure 179. Shear limit state based on the equations

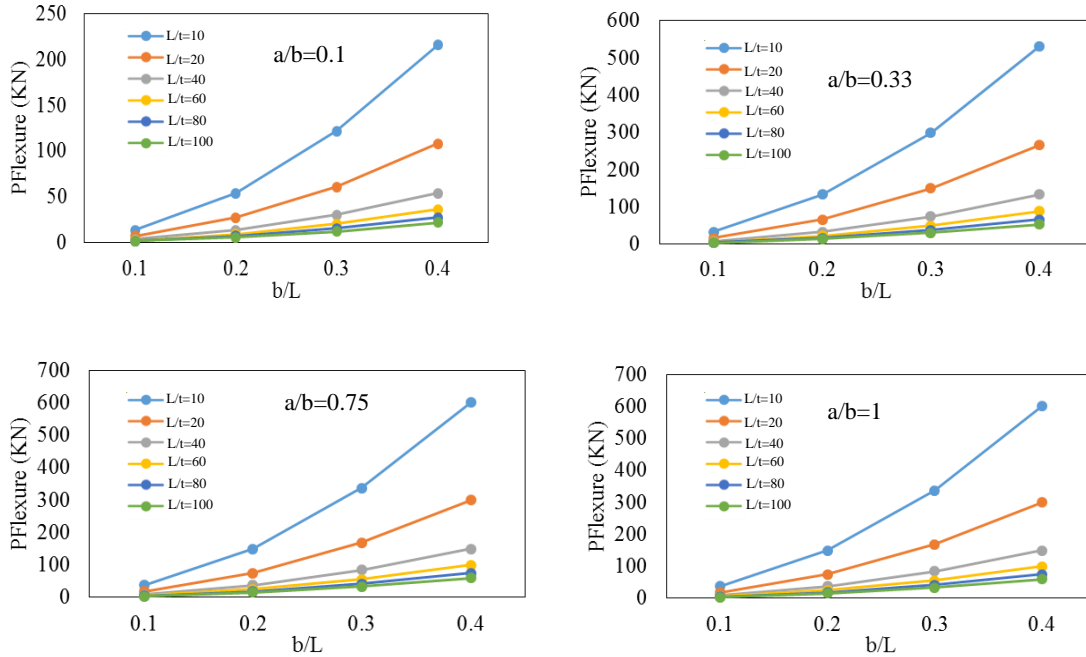
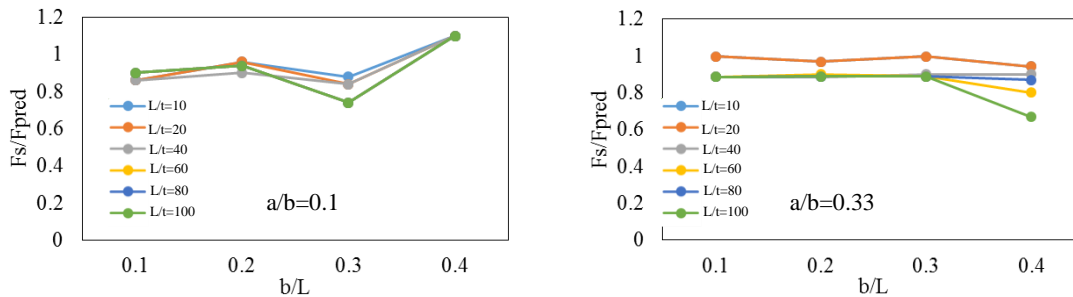


Figure 180. Flexure limit state based on the equations

Figure 181 indicates the actual force over predicted force, which is affected by how thin the butterfly-shaped link is. In which, the thinner the butterfly-shaped link, the lower the actual force would be which practically due to the initiation of buckling at some point along the pushover behavior. In significantly narrow width in the middle, the  $F_s$  is generally less than  $F_{pred}$  compared to rest of the models. Therefore, from the whole analysis, it is concluded that narrow butterfly-shaped links would not be useful due to the buckling issue.



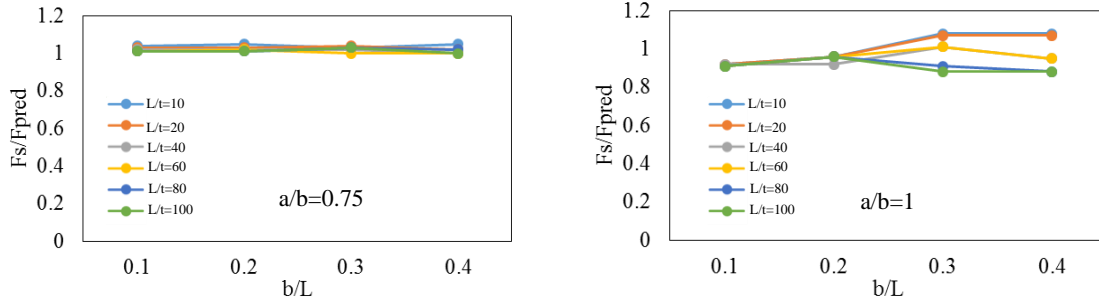


Figure 181. Indication of buckling occurrence before shear or flexure limit state

### 8.5. Overstrength Evaluation:

Figure 182 shows that for narrower BF in the middle part the membrane effect would be happening clearly as compared to strain-hardening effect, while for wider links the strain-hardening and membrane effect happen simultaneously.

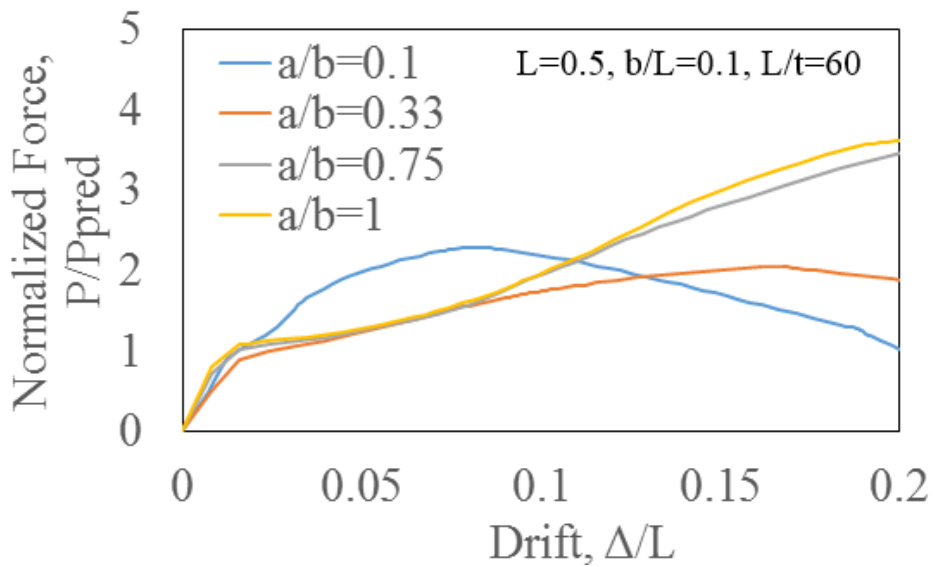


Figure 182. The comparison between the normalized curves

In all the models shown in Figure 182, the flexural limit state would be governing first. Table 15 represents the fact that the flexural limit state would be governing first. For narrower mid-width

BF, the membrane effect takes off at initial stages while the other BFs the material strain-hardening would be controlling the pushover curves at lower deflection values after the occurrence of first limit state, and the membrane effect would be incorporating to the hardening at larger drift values.

Table 15. The comparison between the normalized curves

L (m)	a/b	b/L	L/t	(b-a)/L<0.28	The flexure governs
0.5	0.1	0.1	60	0.09	Yes
0.5	0.33	0.1	60	0.067	Yes
0.5	0.75	0.1	60	0.025	Yes
0.5	1	0.1	60	0	Yes

### 8.6. Energy dissipation and Damping ratio:

The energy dissipation could be assessed by the estimation of the area under the hysteric curves. For this purpose 16 models are used as the representative of the models from the parametric study to evaluate the energy dissipation capability. Different drift ratios of .005, 0.008, 0.012, 0.015, 0.025, 0.035, 0.045 and 0.05 are examined to evaluate the area under the curves and damping coefficient ratios. In addition, the effect of buckling which significantly decreases the energy dissipation capability and increases the pinching effect, as shown in Figure 183, is investigated within this section.

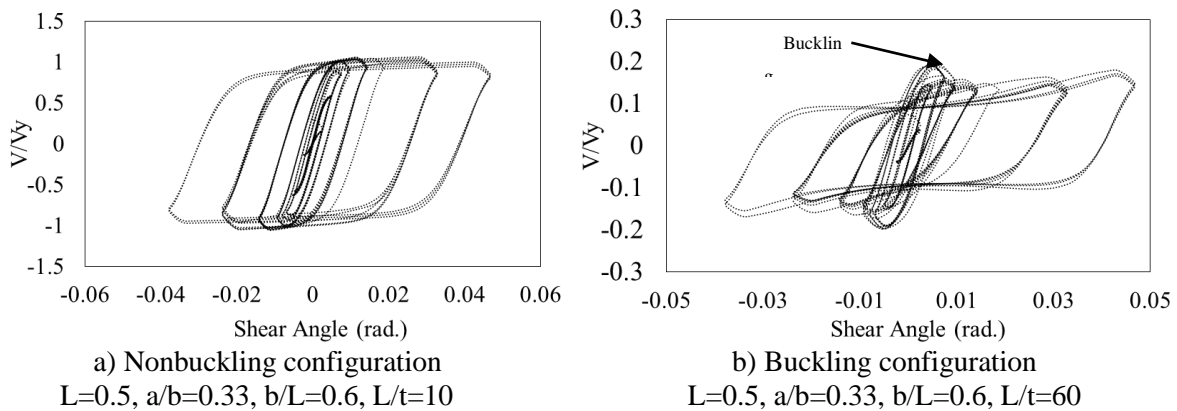
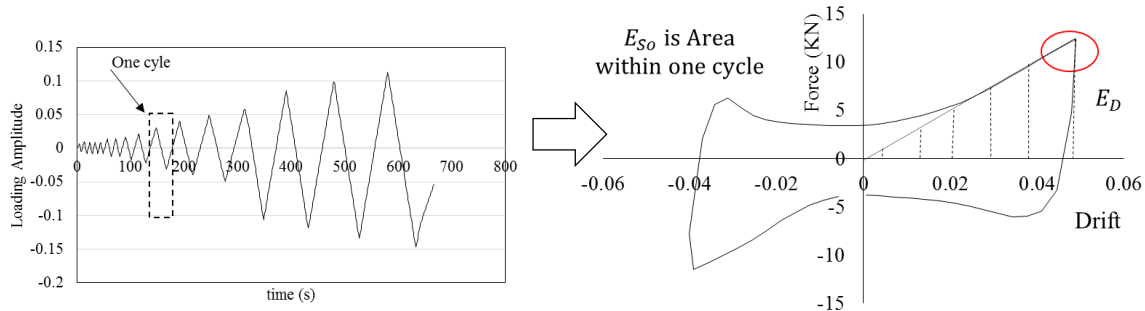


Figure 183. Effect of buckling on butterfly-shaped link hysteric behavior

One of the common methods for defining equivalent viscous damping is to equate the energy dissipated in a cycle of loading applied to the structure and equivalent viscous system. The hysteric behavior would be arbitrarily shaped indicated schematically. The indicated damping ratio would be useful for those structures with high damping [Chopra, 2011; Farzampour et al., 2017]. The damping ratio at other amplitude frequencies would be approximated to the damping ratio in resonance condition ( $w=w_n$ ) according to Chopra (2011). This damping would be useful for a system with a number of degrees of freedom. According to Chopra (2011) this damping derivation methodology is mostly related to systems acting in elastic zones, a number of studies specifically in passive-controlled systems suggested similar procedures for damping estimation with regard to the inelastic behavior of the structure as well (Lee et al., 2015; Teruna et al., 2015; Soong, 1990). It is noted that the damping evaluation methods previously studied are used in the study.

$$4\pi\varepsilon_{eq} \left( \frac{W}{W_n} \right) E_{S0} = E_D \quad (153)$$

$$\varepsilon = \frac{1}{4\pi} \left( \frac{E_d}{E_{S0}} \right) \quad (154)$$



a) Load amplitude and definition of a cycle  
b) The hysteric response behavior  
Figure 184. Definition of areas used to calculate the equivalent viscous damping

The equivalent damping would be calculated with the aid of average equivalent stiffness (ASCE 7-10, FEMA 356; Lee et al., 2016; Ternuna et al., 2105).

$$K_{eff} = \frac{(|P^+| + |P^-|)}{(|\delta^+| + |\delta^-|)} \quad (155)$$

$$\varepsilon_{eq} = \frac{1}{2\pi} \left[ \frac{E_{loop}}{K_{eff}(|\delta^+| + |\delta^-|)^2} \right] \quad (156)$$

In which,  $\delta^+$ , and  $\delta^-$  are the displacements associated with maximum and minimum values of force ( $P^+$ , and  $P^-$ ), respectively.  $E_{loop}$  is the energy dissipated within one complete cycle of force-displacement. This method of damping evaluation is used to consider the fact that in the unloading parts, and the loading reversal, there is always a chance that the absolute loading values would not be equal to the loading part; hence, it would be more accurate to consider the effect of loading and unloading together.

The effect of the thickness and mode of behavior on damping is investigated for butterfly-shaped links subjected to cyclic loading. Models with a/b equal to 0.33, 0.75 and thicknesses of L/t equal to 10 and 60 are considered first to understand the effect of the thickness on damping capability of the butterfly-shaped links, and then to investigate the mode of behavior (e.g. shear or flexure dominated) on damping ratios. All the models are subjected to cyclic loading confirmed by AISC 2005 which is adopted due to having similarities in links functionalities with EBF and fuses in dual rocking system (Ma et al., 2011). The damping then is calculated for a handful of drift ratios of 0.005, 0.008, 0.012, 0.015, 0.025, 0.035, 0.045 to understand the damping trends with increasing drift ratios. The results are summarized in Table 16 and Table 17 for damping and energy dissipation investigations. Figure 185 represents that for all the models the trends with lower thickness specimens, the damping capability in smaller drift ratios is high and after the occurrence of the buckling, the damping ability decreases significantly. Along the same lines, the damping of buckling prevented models in smaller drifts is not significant; however, by increasing the drift ratios the damping capability gets larger and the system would be able to dissipate energy more efficiently.

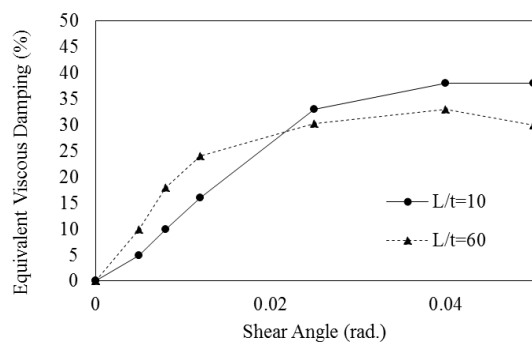
Table 16. The damping ratio

	Geometry			Damping at a drift ratio						
	a (m)	b (m)	t (m)	0	0.005	0.008	0.012	0.025	0.04	0.05
<b>ENG-05-033-06-10</b>	0.099	0.3	0.05	0	0.1195	0.39	0.3	0.4	0.43	0.43
<b>ENG-05-033-06-60</b>	0.099	0.3	0.008333	0	0.23	0.31	0.29	0.333	0.34	0.35
<b>ENG-05-033-02-10</b>	0.033	0.1	0.05	0	0.0004	0.12	0.16	0.36	0.38	0.38

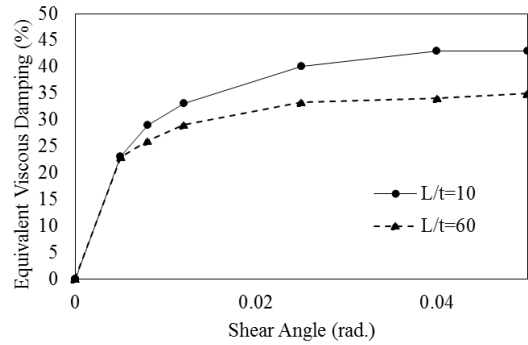
<b>ENG-05-033-02-60</b>	0.033	0.1	0.008333	0	0.02	0.23	0.24	0.30	0.31	0.31
<b>ENG-05-075-02-10</b>	0.075	0.1	0.05	0	0.047	0.24	0.28	0.35	0.4	0.45
<b>ENG-05-075-02-60</b>	0.075	0.1	0.008333	0	0.14	0.25	0.28	0.37	0.4	0.41
<b>ENG-05-075-06-10</b>	0.225	0.3	0.05	0	0.1	0.2	0.26	0.39	0.45	0.48
<b>ENG-05-075-06-60</b>	0.225	0.3	0.008333	0	0.16	0.34	0.24	0.26	0.21	0.23

Table 17. The energy dissipation

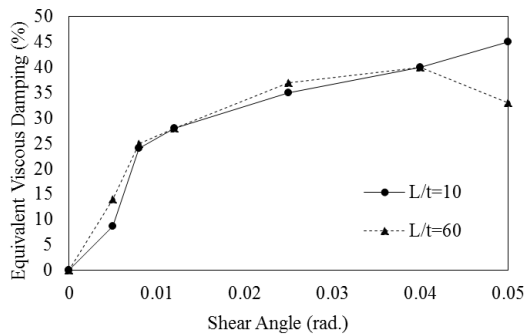
	<b>Energy dissipation at drift ratio/10<sup>3</sup> [N.m/10<sup>3</sup>]</b>					
	<b>0.005</b>	<b>0.008</b>	<b>0.012</b>	<b>0.025</b>	<b>0.04</b>	<b>0.05</b>
<b>ENG-05-033-06-10</b>	2.378	10.8	13.12	37.74	55.749	53.4
<b>ENG-05-033-06-60</b>	0.852	1.6	1.713	3.895	5.83	6.674
<b>ENG-05-033-02-10</b>	0.001	0.421	0.934	4.131	4.1295	2.46
<b>ENG-05-033-02-60</b>	0.007	0.091	0.16	0.661	0.436	0.330
<b>ENG-05-075-02-10</b>	0.127	1.116	1.424	4.167	7.048	9.73
<b>ENG-05-075-02-60</b>	0.043	0.228658	0.269	0.687	1.043	1.175
<b>ENG-05-075-06-10</b>	2.61	14.3	15.4	39.4	65.1	88.6
<b>ENG-05-075-06-60</b>	1	1.82	1.84	3.09	3.793	5.75



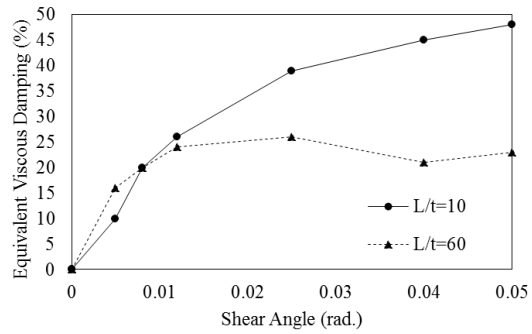
a) a/b=0.33, b/L=0.2



b) a/b=0.33 b/L=0.6



c) a/b=0.75, b/L=0.2



d) a/b=0.75, b/L=0.6

Figure 185. The effect of thickness on the damping ratio capability of BF links

In addition, the mode of behavior effect (e.g. shear dominated or flexure dominated) on damping trends is investigated in Figure 186 and it is shown that for the specific amount of steel the shear-governed models would have less capability in damping the applied forces compared to those models with flexure-governed mode of behavior in larger displacements, which once again confirms the results of the monotonic parametric study in previous sections.

In addition, the shear governed models would dissipate energy better at the initial stage and lower displacements, while the flexural dominated butterfly-shaped links would dissipate energy through cyclic loading reversals, especially in larger displacement values. According to guidelines provided in chapter 7, for the design of butterfly-shaped links, the equivalent plastic strain and fracture possibility would be significantly higher for shear dominated links which could significantly reduce the energy dissipation capability of such links. This phenomenon is observed in the works done by Luth et al. (2008) and Hitaka and Matsui (2006) previously. The conclusions in this chapter are summarized in Farzampour and Eatherton (2018b).

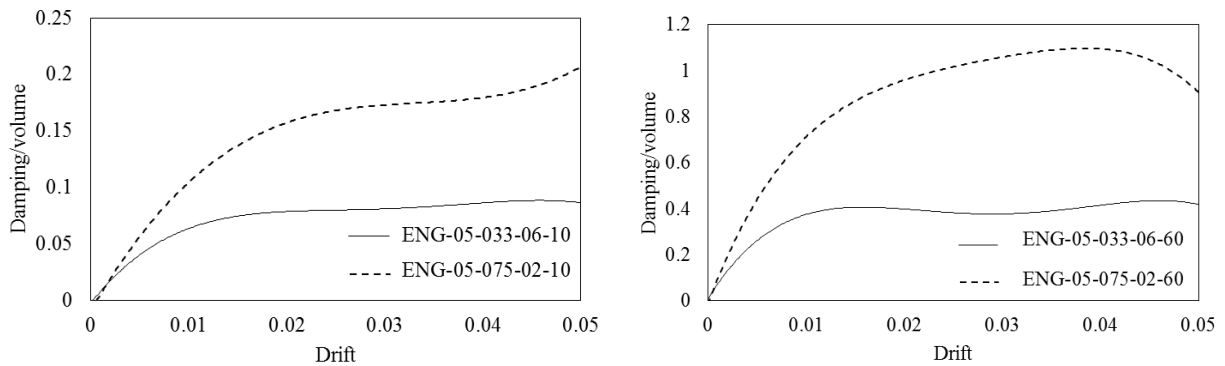


Figure 186. The effect shear dominated and flexure dominated links on damping

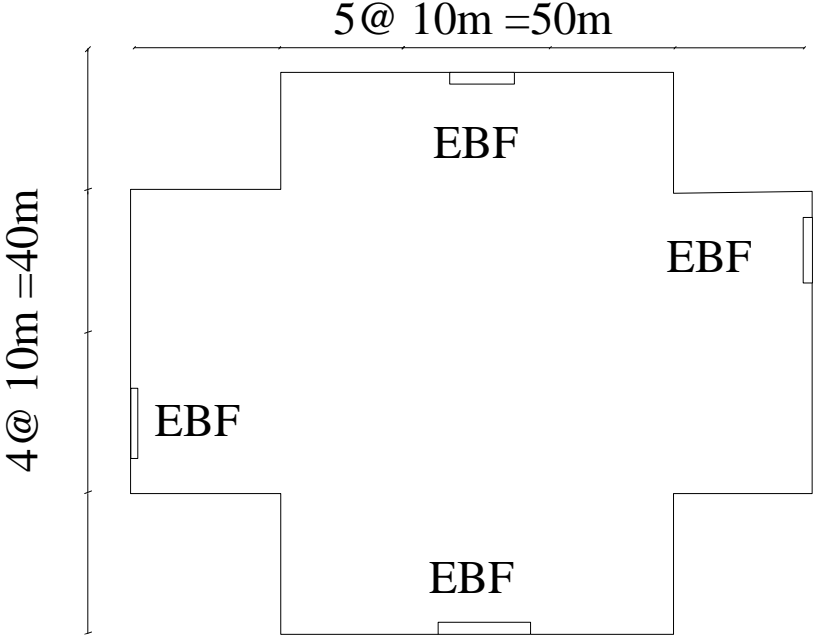
## **9. EXPLORATION OF SHAPES FOR THREE STRUCTURAL APPLICATIONS**

In this chapter, based on the previously studied structural applications in chapter 2 and chapter 3, the concepts provided are considered, and the links are designed accordingly. The applications are categorized into three groups: First, the groups with single row of links which could be used in coupling beams and eccentrically braced frames. Second, the multiple rows of links which could be used in bridges, or coupled steel shear walls. Third, the perimeter perforated links that could be used in steel plate shear walls. Different systems are designed based on the developed design criteria for seismic shear links. For each group, different structural links are designed and incorporated. The designed shapes are modeled with finite element software for further investigation on the seismic performance. Subsequently, the models designed with seismic fuses are compared to conventional systems and advantages of use is delineated.

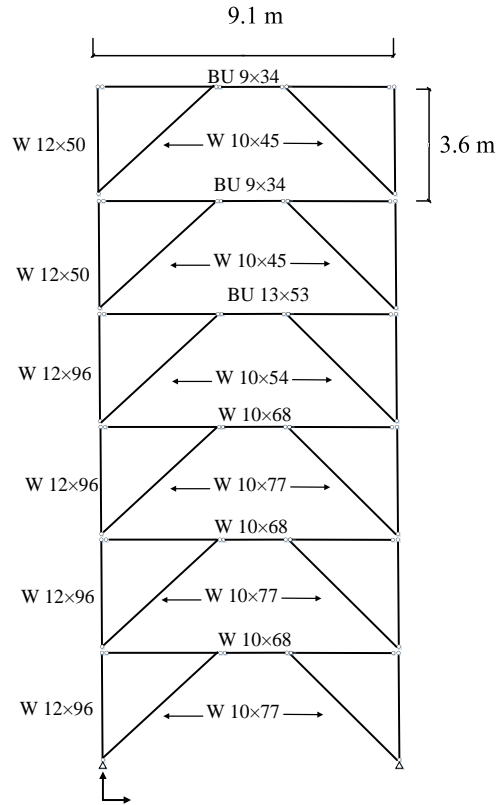
### **9.1. Single Row of Links (SRLs)**

In this section, SEAOC example (SEAOC, 2012) for EBF system is considered and redesigned with regard to developed concepts. The design algorithms are elaborated in Chapter 7. Different cut-out shapes are taken into account and for each one of them, the appropriate shapes with specific geometrical properties are designed to meet the demand force requirement. The geometrical properties used for EBF systems are compatible with what is mentioned in the SEAOC example (SEAOC, 2012). Flexurally dominated butterfly-shaped link (named FBF) is studied in this research, and it is basically used for spreading out the inelasticity within the seismic link. The circular (named Circle) and shear dominated butterfly (named SBF) shaped links are generally used to accumulate the stress with the middle section of the seismic link. The oval shape models (Oval) are studied in chapter 3 and chapter 4 based which the uniform curvature concept in which the inelasticity would spread through the more uniformly. The straight links (named Slits) is a straight shear links used in shear walls and seismic systems to generate the hinges at the ends of the links due to flexural stresses. The simple solid plate (named solid) is the conventional shape with which different coupling beams and EB systems are designed and incorporated in structures.

It is noted that for all the sharp geometrical change, a fillet radii is used which is explained in details in Appendix A, and Appendix B. Figure 187 shows the plane view and elevation view related to first group of application for which SRLs are designed.



a) The plan view of the structure with EBF system shown on the perimeter of the building (SEAOC, 2012)



b) The EBF system with columns, beams and braces sectional properties

Figure 187. The SEAOC Example for EBF system with six stories

### 9.1.1. Model description

The design is basically done for the force of 530 KN based on the EBF system Example. The finite element modeling methodology is based on chapter 7. The selected beam is located at the story one of the six story building. Based on the Figure 187, the designed beam is W10×68. The 322 MPa steel with 1% hardening is used to establish the mode. The demand force for which the modes are designed is related to first story of EBF system, which was 530 KN (SEAOC, 2012). The mesh sensitivity analysis is conducted to reach to the appropriate mesh size based on the procedures explained in Appendix A and Appendix B.

### 9.1.2. Design and results of analysis for single row of links

The SBF-SRLs are designed based on the shear yielding of the mid-point of the link. The Straight-shaped SRLs are designed based on the yielding of the endpoints. The Oval-shaped SRLs are designed based on the constant curvature concept discussed in chapter 3. The solid link is designed

based shear buckling and yielding of steel plates and the Circle-SRLs are designed based on the mid-point yielding of the links. The Figure 188 shows the designed links, based on the guidelines provided in previous chapters. It noted that the models containing oval shaped cut-out and circle shaped cut-outs are designed based on the flexure dominated and shear dominated structural butterfly shaped links. In which the oval shaped is designed based on the flexurally dominated link with two sections of  $z=0$  and  $z=3L/8$  (shown in Figure 103), and for the circle shaped link the middle section of the links are considered for design purposes.

It is noted that the fillet radii are used for the middle and end sharp angles to reduce the effect of the plastic strain accumulation. Based on Chapter 2, the  $L/60$  and  $L/15$  are used for the end angle and middle angle radii sizes, respectively.

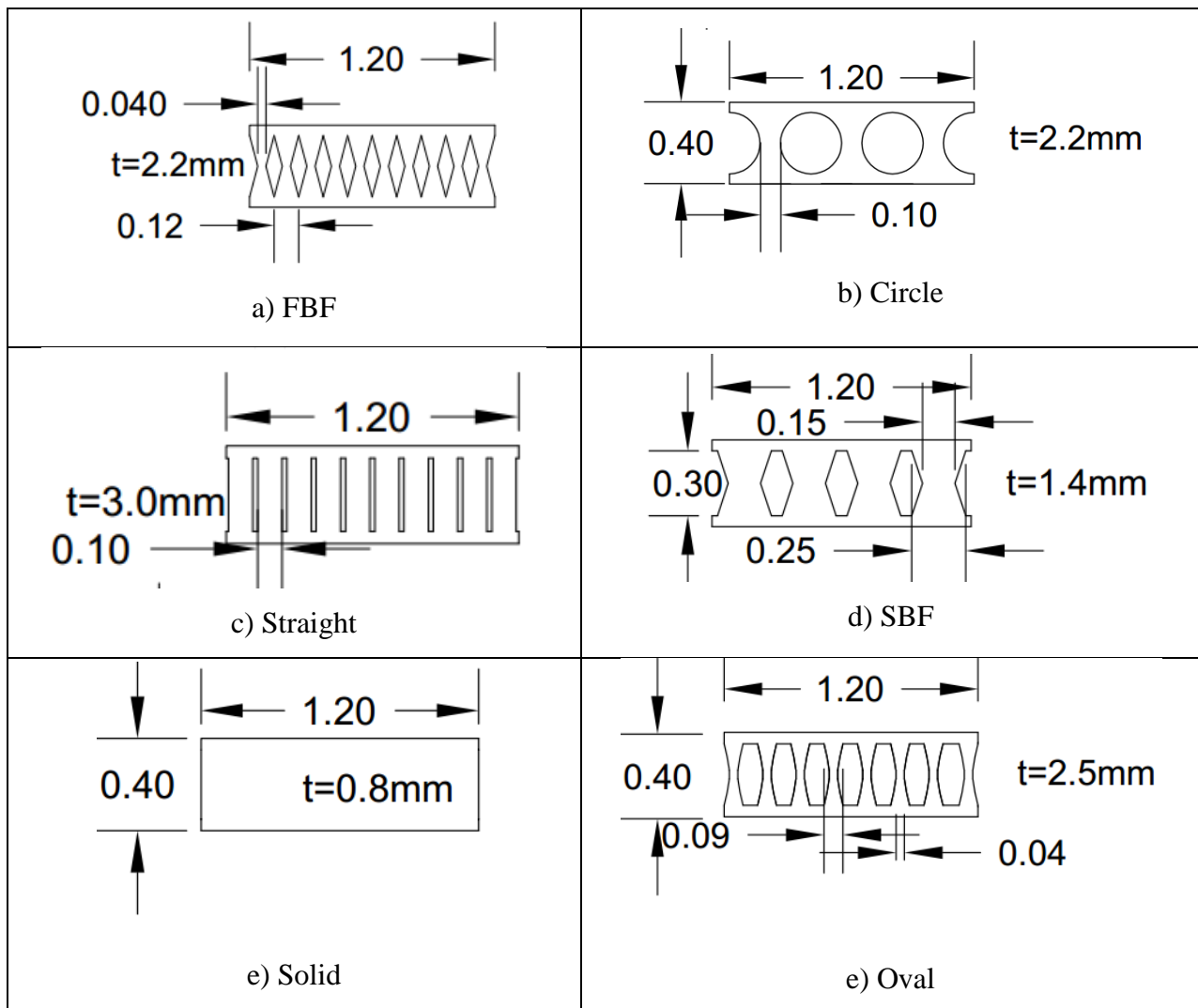


Figure 188. The designed models For single row of links (all the units are in meters, except thickness which is in millimeters)

Figure 189 shows the push over behavior of the system with seismic links, as it is designed for the single row of the links application, the system strength is about 530 KN. The result for SRLs is summarized in Figure 189. In general, the links were resisting the loading up to the yielding point, and then undergo geometrical hardening up to the point the large out of plane buckling is observed or excessive rotation within elements are occurred. The detailed behavior of the models are summarized in Table 18 and Table 19.

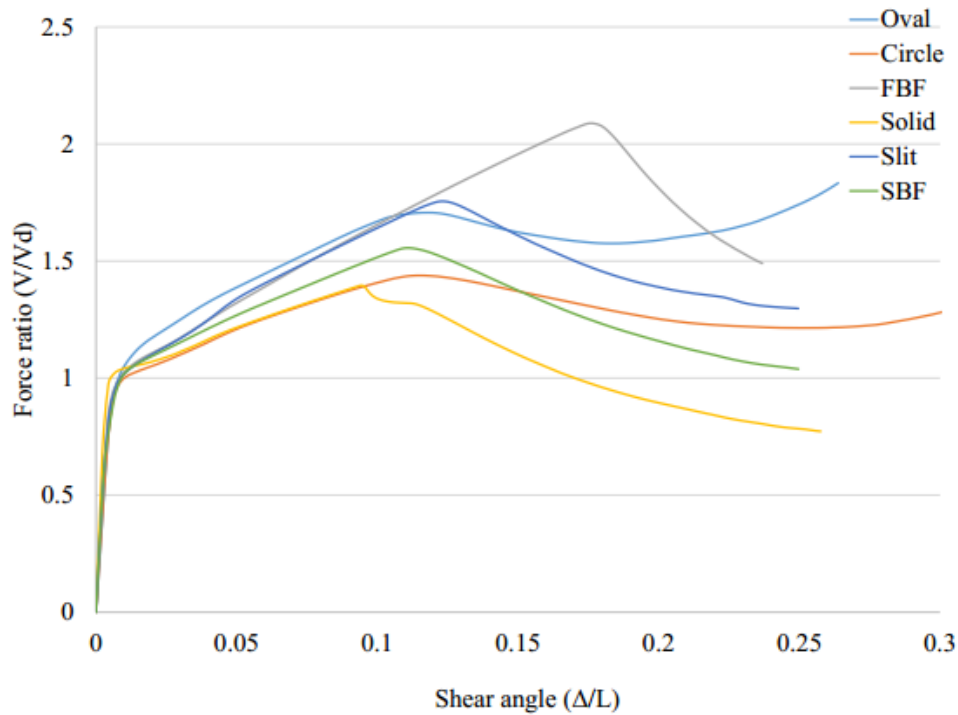


Figure 189. Pushover curves associated with SRLs

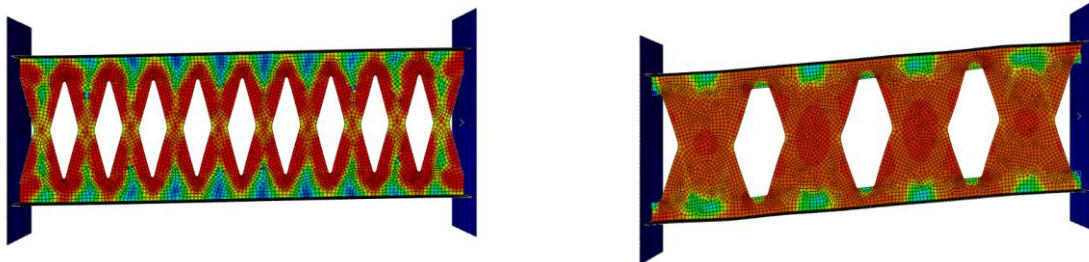
Based on the shown Figure 189, it is indicated that the pushover curves based on which the yielding strength, ultimate strength, initial stiffness, over strength and displacement ratio are calculated. The equivalent plastic strain for 0.08 drift ratio, which is recommended as the drift ratio for ultimate displacement of EBF system based on the AISC 341 provisions, are monitored for different models to investigate the possibility of the fracture.

Table 18 shows the results associated with single rows of links (SRL). The post-processing is done based on the parameters of interest associated with behavior and pushover curves of the models.

Table 18. The post-processing results in SRLs

	Oval	Circle	FBF	Simple	Straight	SBF
Equivalent plastic strain at 0.08	0.22	0.25	0.28	0.68	0.61	0.26
Yielding displacement, $\Delta_y$ (m)	0.012	0.008	0.0089	0.01	0.009	0.01
Ultimate displacement, $\Delta_m$ (m)	0.13	0.115	0.21	0.115	0.14	0.135
Displacement ratio ( $\Delta_m/\Delta_y$ )	10.8	14.4	23.6	11.5	15.6	13.5
Ultimate Strength (KN)	908	862	1037	767	802	808
Yielding Strength (KN)	561	582	496	577	450	520
Over strength	1.62	1.48	2.09	1.33	1.78	1.55
Stiffness (KN/m)	46750	72750	55730	57700	50000	52000

It is concluded that if the equivalent plastic strains (PEEQ) is a matter of interest the FBF, circle and oval shapes could be appropriate options. If the overstrength is considered, the circle and oval shapes could work better than the others. Figure 190 shows that the Von-Mises stress of each link, the type of the behavior is as expected. The FBF models developed the hinges at the quarter points indicating that the flexural yielding limit state occurred before the shear yielding limit state. The circle, and SBF models developed the maximum shear stress at the middle portion of the link which could be prone to strain accumulation points especially close to shaper geometrical changes. The simple model developed maximum stress at the boundary condition, and tension field action is shown within this model. The straight link developed the two flexural hinges at the ends of the links, where the strain values are large; hence, the fracture is possible. The oval shape shows a less strain values as it is expected from the constant curvature concepts an uniform distributed yielding, however, the stiffness of this model is lower than the rest modes.



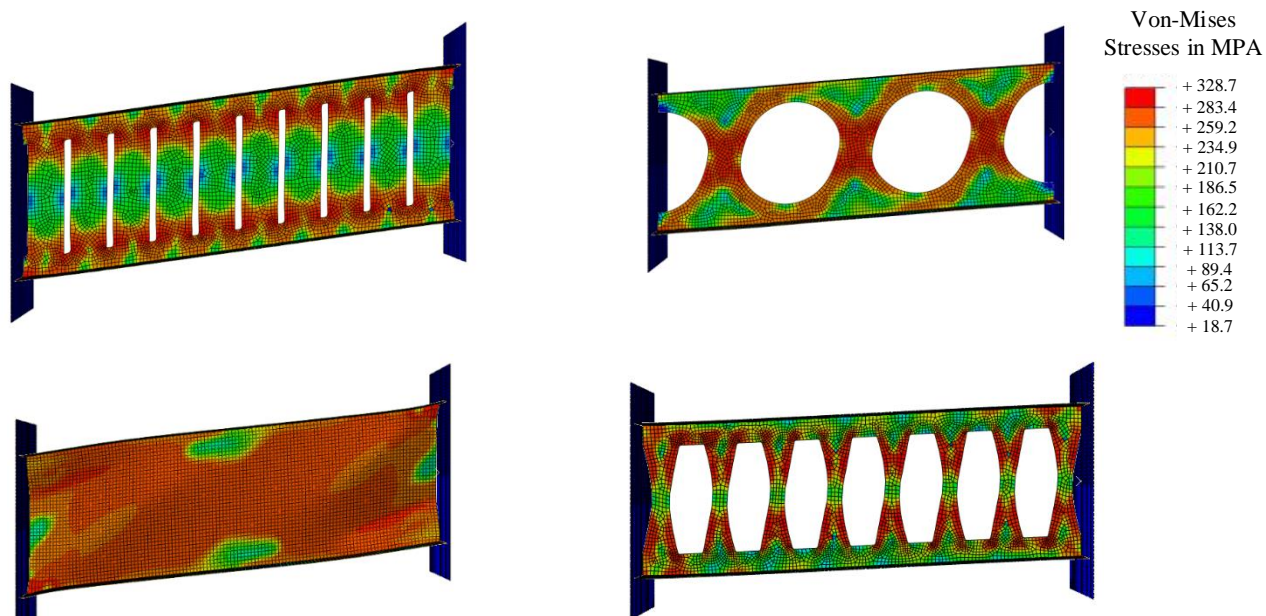


Figure 190. The Von-Mises stress, and stress concentration areas

In addition, Table 19 shows the general behavior of the model as the loading is applied.

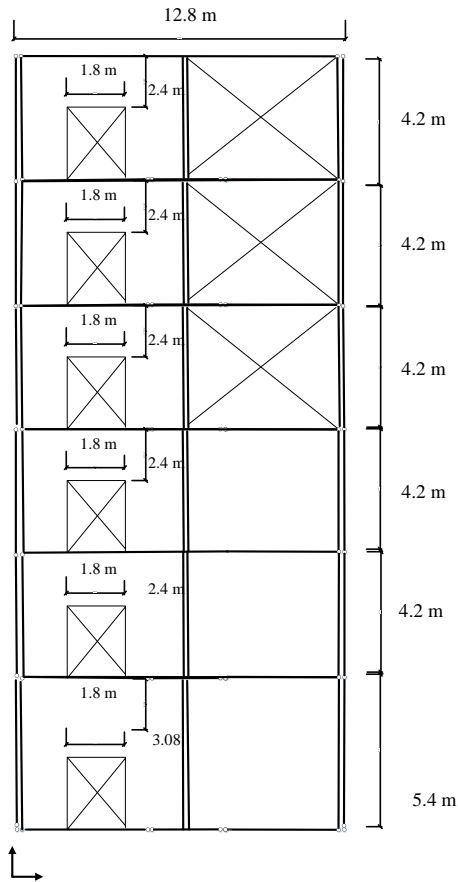
Table 19. The mode of behavior for SRLs

mode of behavior	<b>Oval</b>	End links elements have experienced excessive plasticity, and limited buckling are observed within the links.
	<b>Circle</b>	No buckling is observed., the inside links yielded, the end elements experience excessive rotation and plasticity. The middle section of the links are yielded initially.
	<b>FBF</b>	End elements start to yield. Yielding are distributed along the length of the link. No buckling is generally observed- inside links fully yielded due to uniform stresses under shear and flexure stresses.
	<b>Simple</b>	The buckling occurred, Tension Field Action (TFA) is observed clearly. The tension field action imposed a large force on the flanges of the beam.
	<b>Straight</b>	the yielding is at the end of the links, and at the ends, the elements at the end are plasticized due to constant width of straight links. The plasticity at the ends are large compared to other models, and buckling is not observed.
	<b>SBF</b>	initially, the links are yielded in shear at the middle, but ultimately at the end of links the elements show plasticity but less than other configurations.

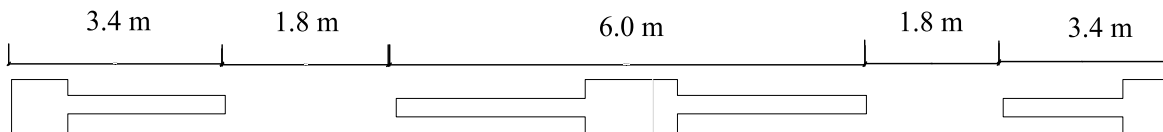
## 9.2. Multiple Rows of Links (MRLs)

In this part, SEAOC example (SEAOC, 2012) for coupled steel shear walls is considered and redesigned with regard to developed concepts for links. The design is based on the guidelines provided in Chapter 7. Different cutout shapes are considered and for this application, the appropriate shapes with specific geometrical properties are developed. The geometrical properties

used for the mentioned coupling beam systems are compatible with the example of coupled shear wall SEAOC (2012). This example is chosen because of having a coupling beam in coupled shear walls design procedure which could be designed with multiple rows of links. Figure 191 shows the elevation view and the plan view of the coupled steel shear wall. It is noted that the coupled shear wall is located at the fourth story which is used for design purposes due to largest shear values.



a) Coupled shear wall application elevation view



b) Plan view of the coupled shear wall application

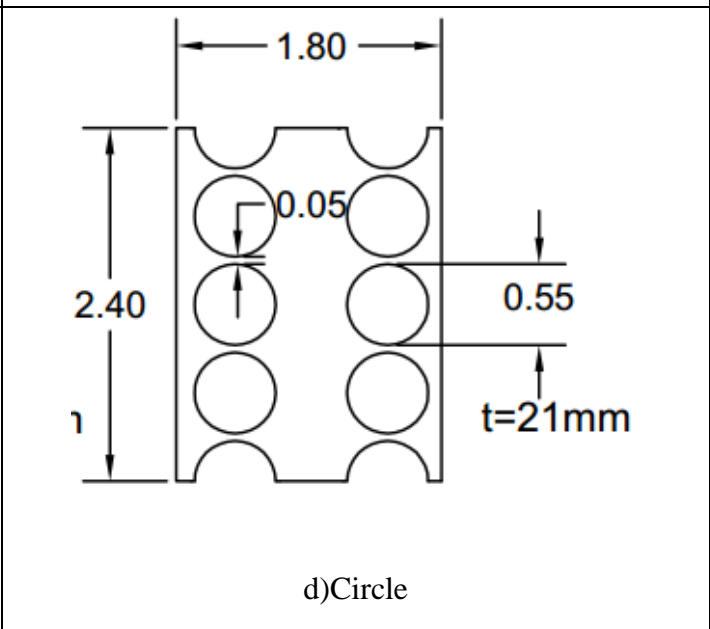
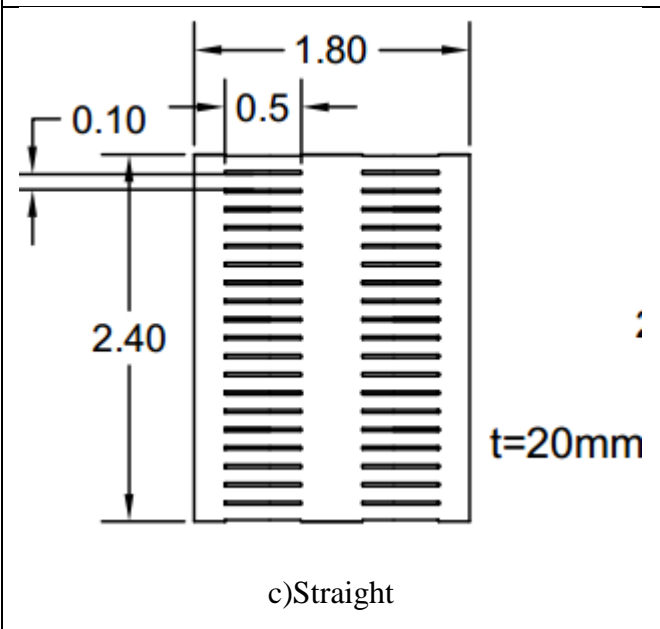
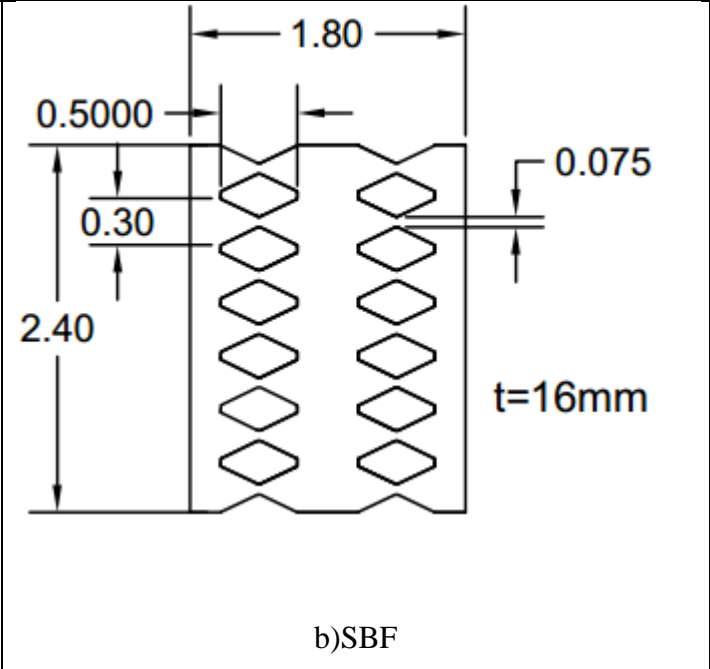
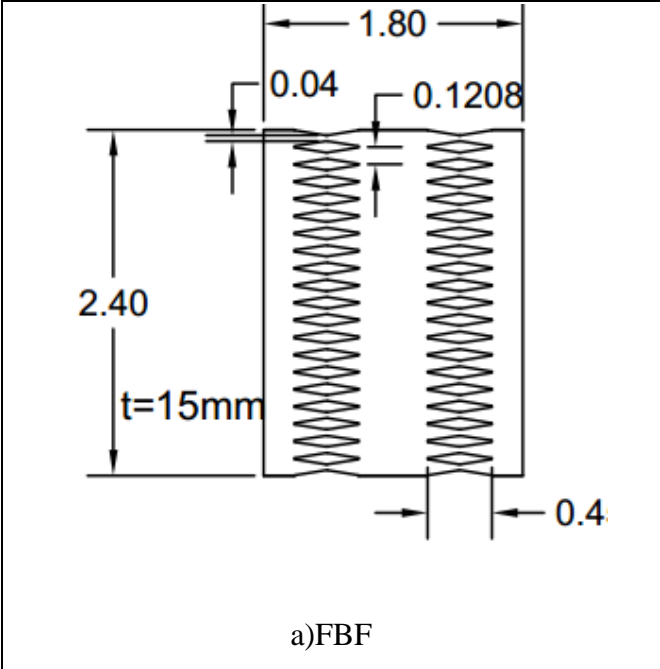
Figure 191. The coupled shear wall and implementation of MRLs for this application

### **9.2.1. Model description**

The design is done for the coupled steel shear wall with the demand force of 2200KN. This is the demand force for the fourth story, which has the most shear applied. The finite element modeling methodology is based on chapter 7. The 322 MPa steel with 1% hardening is used to establish the mode. The mesh sensitivity analysis is conducted to reach to the appropriate mesh size based on the procedures explained in Appendix A and Appendix B.

### **9.2.2. Design and results of analysis for multiple rows of links**

Figure 192 shows the designed links, based on the guidelines provided in previous chapters. Flexurally dominated butterfly-shaped link is studied in this research, and it is basically used for spreading out the inelasticity within the seismic link, and concentration of hinges far from the sharper areas. In addition, the occurrence of the rotation of the middle section prevented the links to perform as it is expected. The circular and shear dominated butterfly shaped links are designed to accumulate the stress with the middle section of the seismic link. The oval shaped models are studied in chapter 4 based on the uniform curvature concept in which the inelasticity would spread through the more uniformly. The straight links are straight shear links used in shear walls and seismic systems to generate the hinges at the ends of the links due to flexural stresses. The simple solid plate is the conventional shape with which different coupled steel shear wall systems are designed and incorporated in structures. Tension field action is even more obvious in this case compared to single row of links, which imposes a larger demand on the boundary elements. For all the models the rotation of the middle part of the plate prevented the system to perform as it is expected.



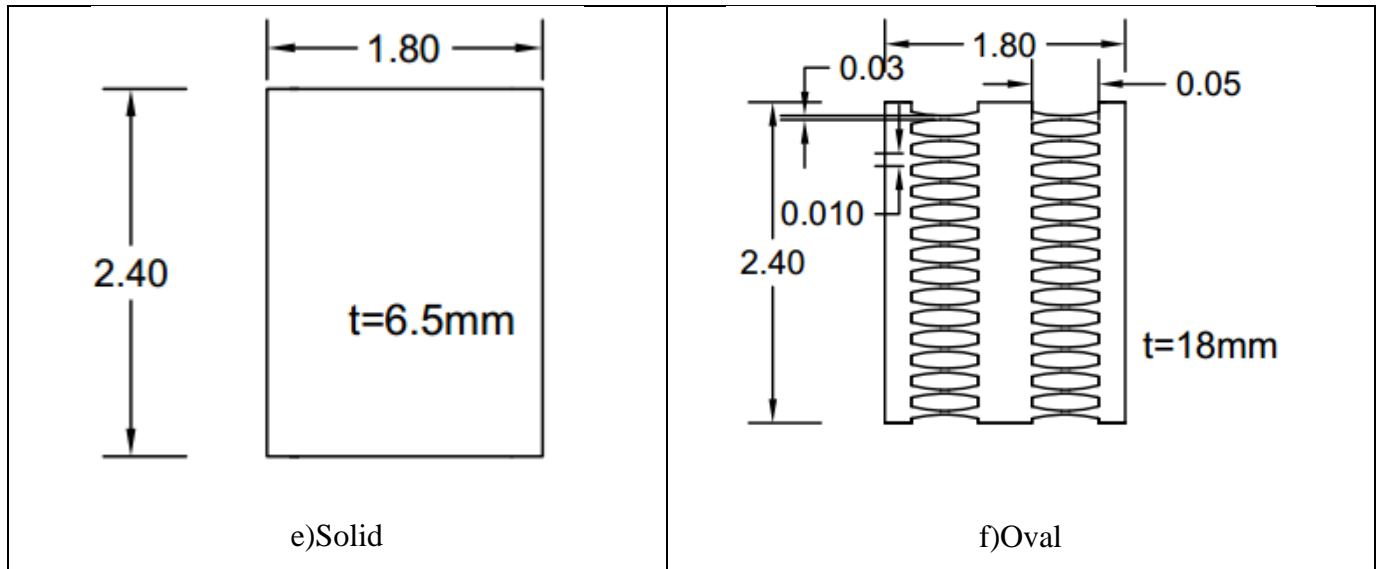


Figure 192. The designed models For SRLs

The design is basically done for the force of 2200 KN based on the coupled steel shear wall coupling beam (SEAOC, 2012). The design procedure associated with these MRLs follow the same path as SRLs with only a simple difference of the fact that two rows of links are supposed to be yielded. However, this idea has not happened since the rotation of the middle section prevented the system to perform well and reach to yielding stage.

Table 20 and Table 21 show the results associated with single rows of links (SRL). The post-processing is done based on the parameters of interest associated with behavior and push over curves of the models. It is shown that for Circle and FBF, the least equivalent plastic strain values are expected, while the straight links have the largest strain values and fracture possibility. Among all the models the Oval shape has the highest overstrength values.

Table 20. The post-processing results in MRLs

	<b>Oval</b>	<b>Circle</b>	<b>FBF</b>	<b>Simple</b>	<b>Straight</b>	<b>SBF</b>
Equivalent plastic strain at 0.03	0.055	0.084	0.044	0.14	0.09	0.09
Equivalent plastic strain at 0.08	0.065	0.137	0.12	0.47	0.51	0.11
Yielding displacement, $\Delta y$ (m)	0.011	0.0084	0.011	0.0078	0.008	0.0056
Ultimate displacement, $\Delta m$ , (m)	0.21	0.22	0.185	0.19	0.38	0.197
Displacement ratio, $\Delta m/\Delta y$	19.1	26.2	16.8	24.4	47.5	35.2
Ultimate Strength (KN)	4744400	3073650	2927600	2505050	7627150	3476550.0
Yielding Strength (KN)	1474840	1481370	1954400	2284580	2173440	2354480

Over strength	3.22	2.07	1.50	1.10	3.51	1.48
Stiffness (KN/m)	134076	176354	177673	292895	271680	420443

Table 21. The mode of behavior for MRLs

mode of behavior	<b>Oval</b>	The yielding happens along the length of the links, buckling is prevented and the equivalent plastic strain (PEEQ) value is low indicating appropriate behavior in terms of fracture control.
	<b>Circle</b>	The elements at the middle part of the links are yielded in shear. No buckling and the yielding is concentrated at the middle only.
	<b>FBF</b>	Almost all the elements along the length of the BF are yielded, the flexural mode is clear and observed. The buckling is completely prevented and the yielding is concentrated in the links uniformly over the length before mid-part rotating excessively.
	<b>Simple</b>	The TFA is observed, the buckling obviously appears which affects the total strength of the system. TFA is more obvious for this case compared to SRLS.
	<b>Straight</b>	The elements at the end of the links are yielded and no sign of yielding or buckling for other element is observed. It showed the high value of equivalent plastic strain (PEEQ) for the end elements and the possibility of fracture at the link ends.
	<b>SBF</b>	First, the yielding is observed at the middle of the links. By increasing the load, the flexural yielding and buckling are observed as the next limit state.

The rotation of the middle part of the MRLs significantly reduced the load-bearing capacity of the links. The rotation, however, is calculated for all of the MRLs with aid of the equation  $(U_2 - U_1)/L$  according to Figure 193.  $U_2$  is the displacement of upper side of the middle section at 0.08 drift, and  $U_1$  is displacement of middle section at 0.08 drift, and  $L$  is total length, which is shown in Figure 193.

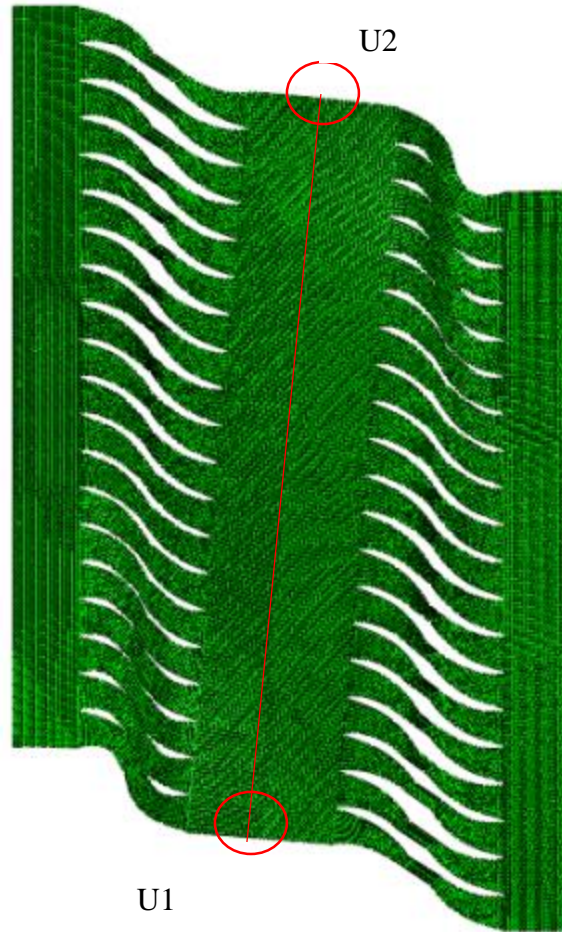


Figure 193. The rotation of the middle steel plate and prevention of the link to resist the load

Table 22. The rotation values for different MRLs

	<b>MRL-FBF</b>	<b>MRL-Circle</b>	<b>MRL-Straight</b>	<b>MRL-Oval</b>	<b>MRL-SBF</b>
<b>The rotation at drift rotation of 0.08 Drift</b>	0.0021802	0.00612	0.001881	0.000723	0.011117
<b>The normalized rotation to MRL/FBF</b>	1	2.81	0.86	0.33	5.10

Based on the previous study, it is shown that the SBF has the largest rotation compared to other shapes. The pushover curves for the MRLs are shown in Figure 194. The significant reduction in lateral load resisting capacity is observed which is basically due to the rotation of the middle steel plate, and changing the mode of behavior from flexure or shear yielding to axial yielding. This rotation prevents the links from working appropriately in the way that they would be able to resist the loading. Therefore the strength of the models with larger rotations at the middle are decreased.

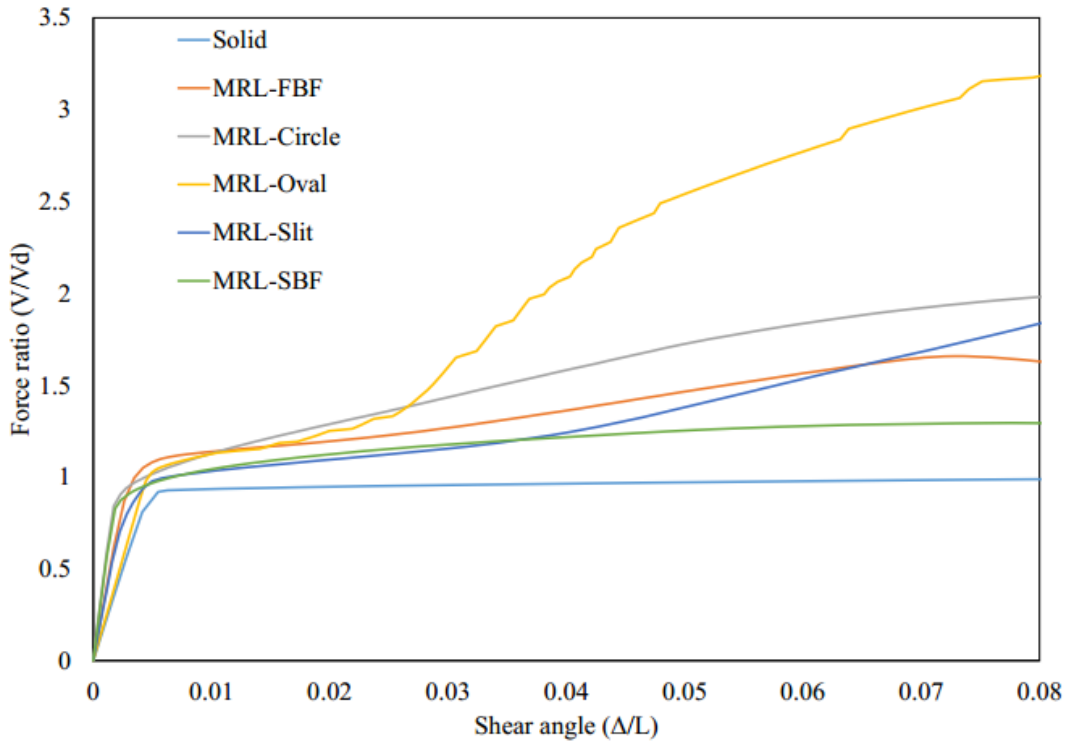
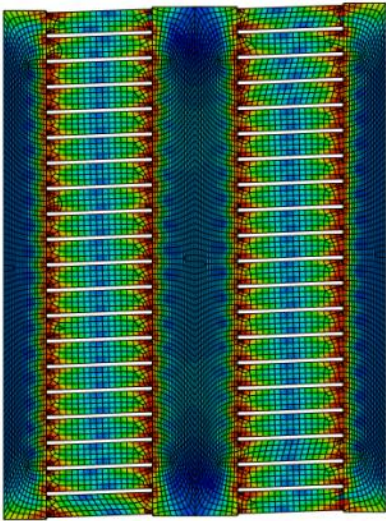
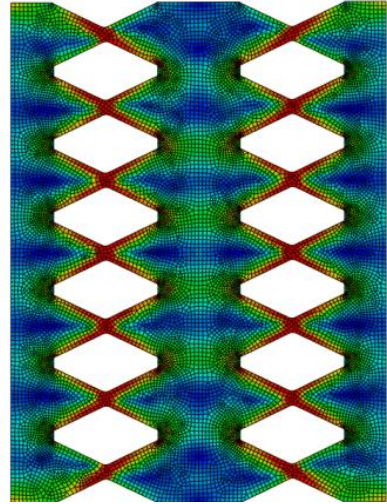
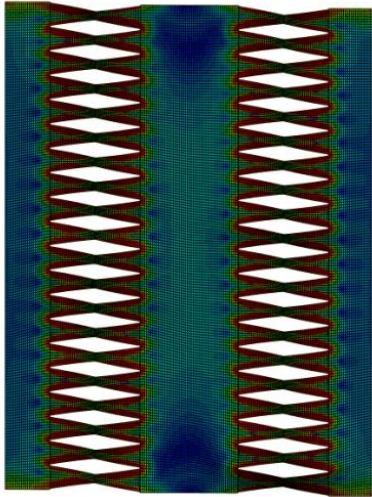


Figure 194. The pushover behavior of MRLS

The behavior MRLs due to a large reduction of the load-bearing capacity are not promising since in almost all of the models the expected mode of behavior has not happened and the inelasticity was not distributed uniformly. The Von-Mises stress condition is indicated in Figure 195. To address this issue, it is recommended to either use stiffener or implement SRLs instead of MRLs which is shown in Figure 196.



Von-Mises  
Stresses in MPA

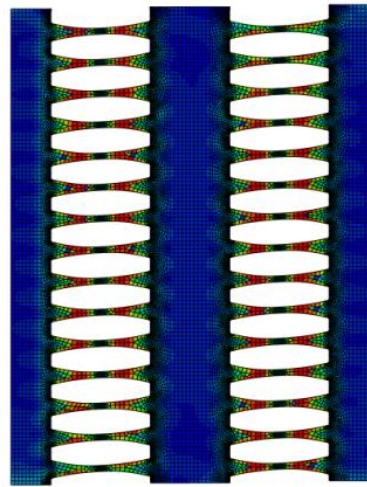
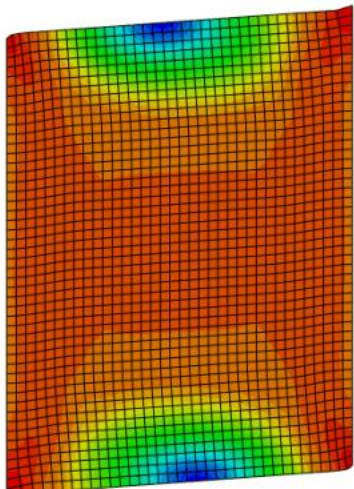
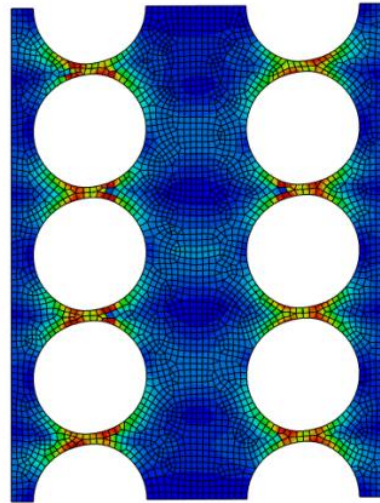
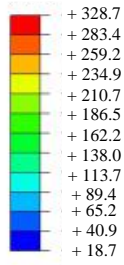


Figure 195. The Von-Mises stress distribution for MRLs and stress concentration areas

One of the applicable solutions for MRLs is to use SRLs instead but with appropriate geometrical properties which could satisfy the demands applied to the coupled steel shear walls.

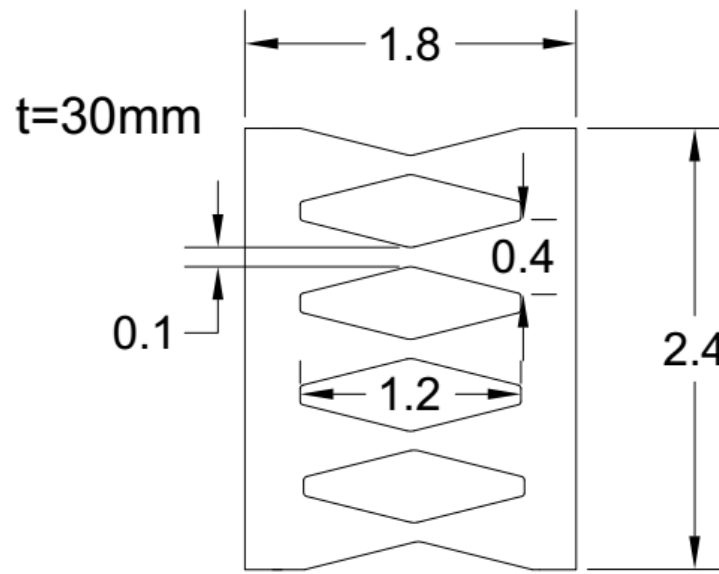


Figure 196. The corresponding SRL designed for the demand loading of 2200 KN

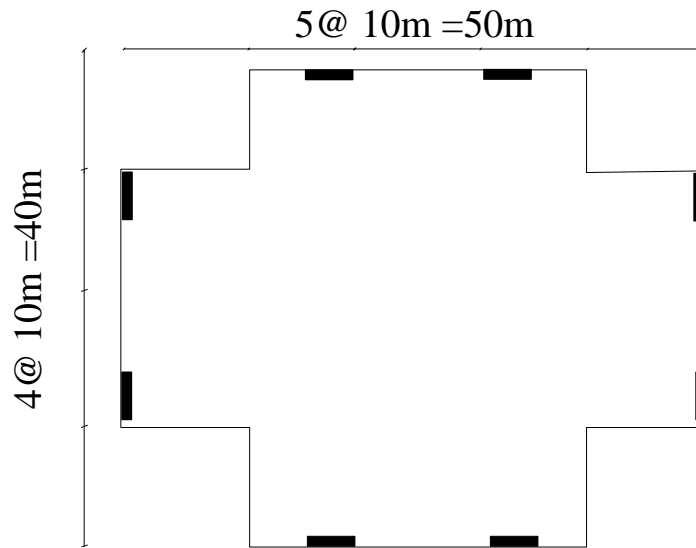
### 9.3. Perforated Rows of Links (PRLs)

In this section, SEAOC example for Steel plate shear wall system is considered and redesigned with regard to developed concepts (SEAOC, 2012). The design is based on guideline provided in Chapter 7. Different cutout shapes are considered and specific geometrical properties are derived to meet the design force requirement.

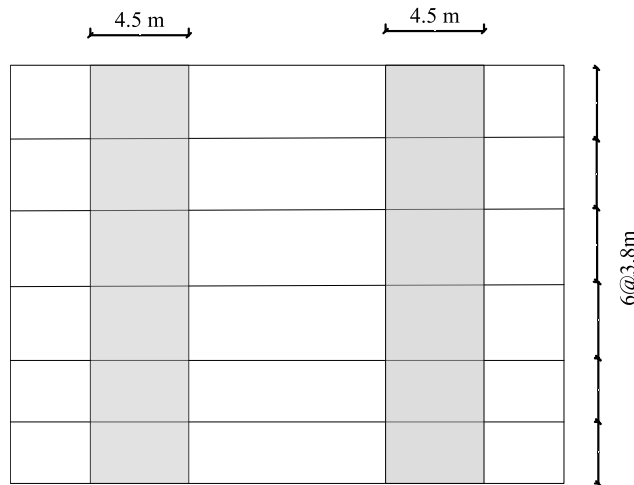
#### 9.3.1. Model description

The selected steel plate shear wall is located at the story one of the six story building. Based on the Figure 197, the story one shear wall with length of 4.2m and height of 3.3m is considered. The design is basically done for the force of 1300 KN based on the steel shear wall application Example. The finite element modeling methodology is based on chapter 7. The 322 MPa steel with 1% hardening is used to establish the mode. The mesh sensitivity analysis is conducted to

reach to the appropriate mesh size based on the procedures explained in Appendix A and Appendix B.



a)The plan view for steel plate shear wall system



b)The Elevation view for steel plate shear wall system

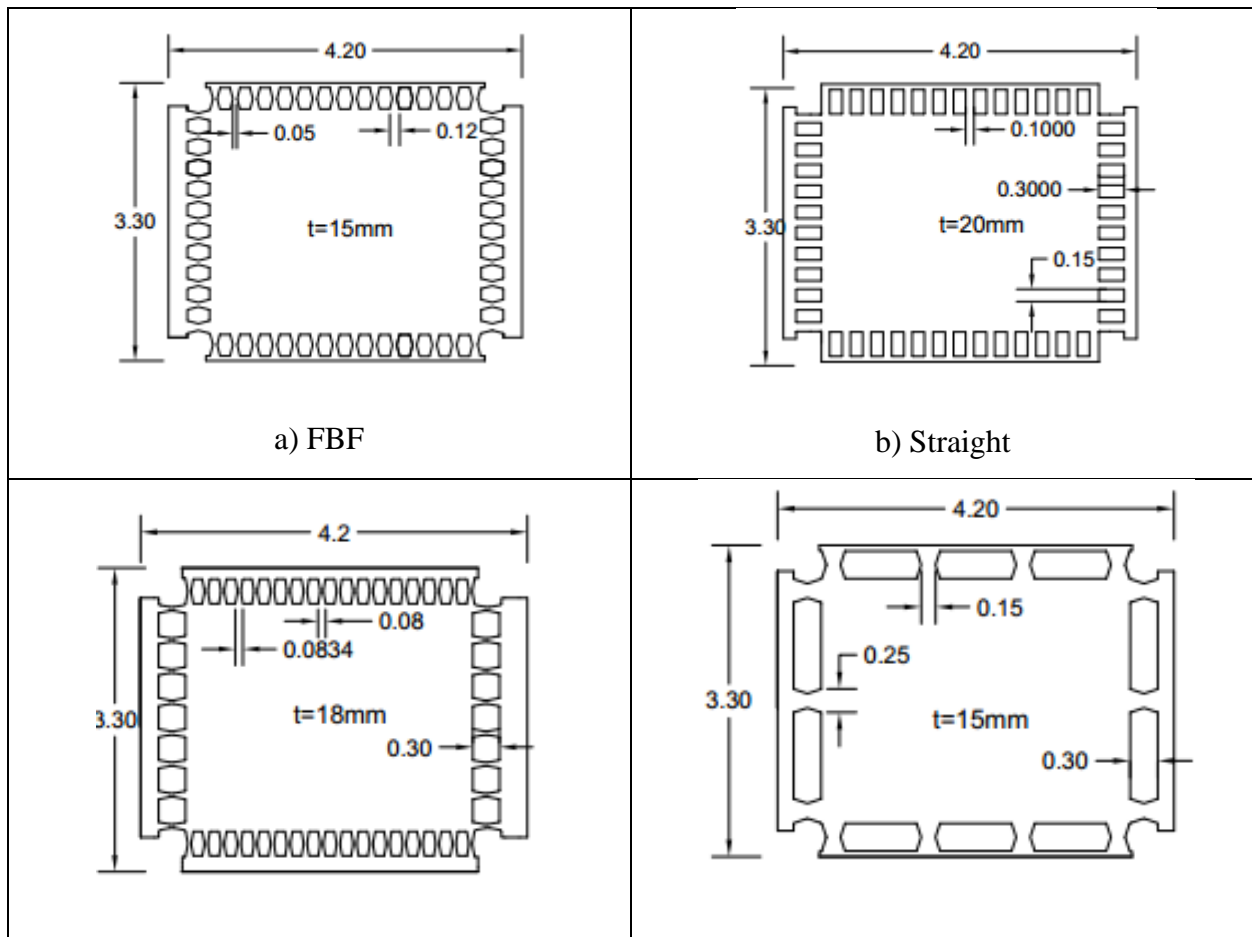
Figure 197. The steel shear wall example from SEAOC (2012)

### 9.3.2. Design and results of analysis for perforated rows of links

The design is basically done for the force of 1300 KN based on the SEAOC steel plate shear wall system example. The general dimension of steel plate is based on the SEAOC example for steel

plate shear walls. This example discusses the use of special steel shear wall and the demand designed force is about 1300KN.

Flexurally dominated butterfly-shaped link is considered to have the hinges far from the sharper areas. The circular and shear dominated butterfly shaped links are generally used to accumulate the stress with the middle section of the seismic link, the circle shaped link would have a better transition which led to better distribution of plastic strain compare to SBF. The oval shape model is studied in chapter 3 based on the uniform curvature concept in which the inelasticity would spread through the more uniformly. The straight links had hinges at the far ends to the highest moment demand at that point. The simple solid plate is the conventional shape with which different coupled steel shear wall systems are designed and incorporated in structures, this system showed a significant tension field action, which ended in large demand on the boundary elements. The design shapes are shown in Figure 198.



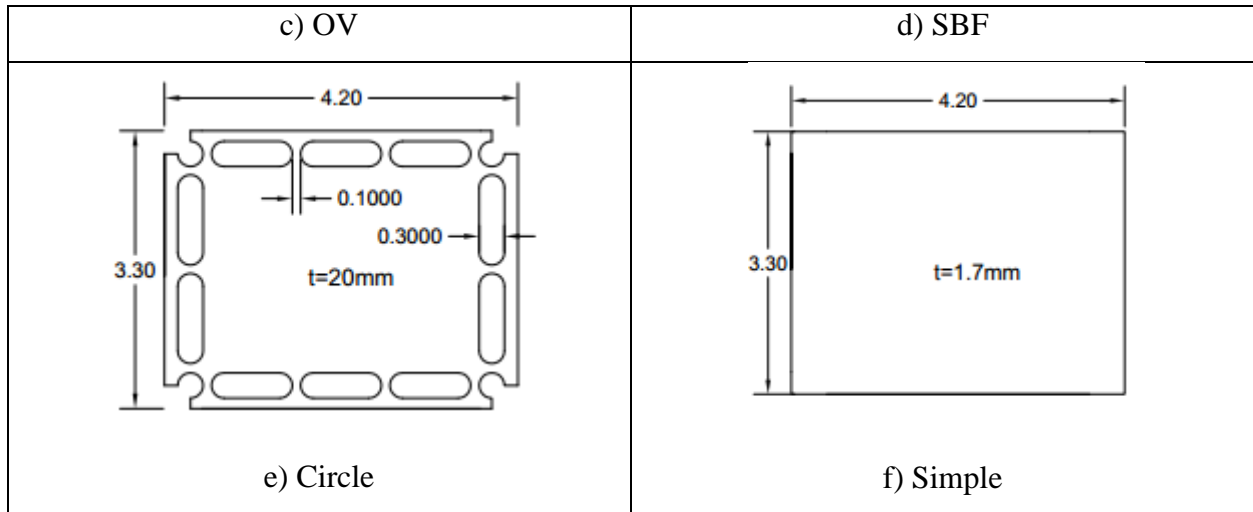


Figure 198. The designed models with seismic shear links for steel plate shear wall application

All the models reached to yielding approximately around 1300 KN which is the designed demand force as it is shown in Figure 199. The post-processing is done based on the parameters of interest associated with behavior and pushover curves, which is summarized in Table 23 and Table 24. It is concluded that the simple shear wall in which the tension field action is captured, the equivalent plastic strain values are less than other models. In addition, compared to the rest of the models this system has less overstrength values; however, the boundary element force are significantly larger than the rest of the models, which is elaborated in Table 25. The tension field action also specially for the first and last floor makes high demands on beams and columns which is necessary to be taken into account for design purposes.

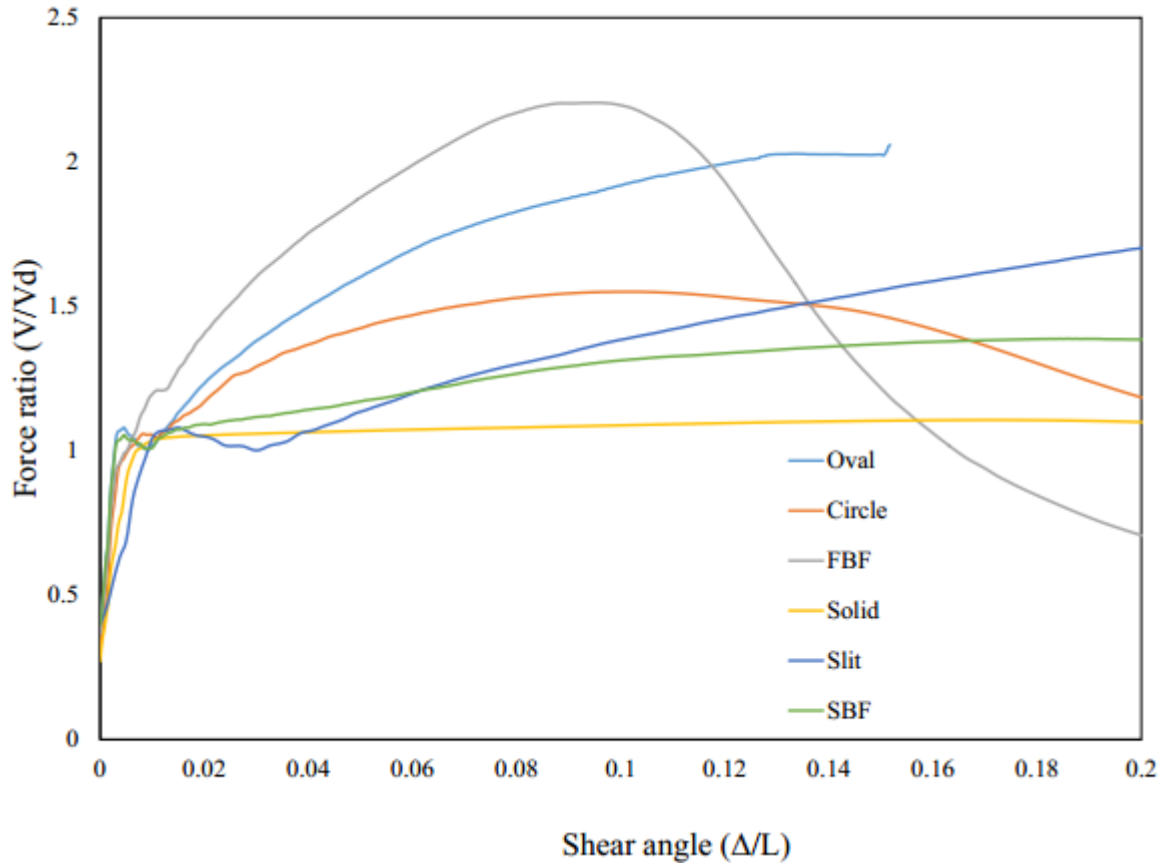


Figure 199. The comparison pushover curves PRLs

Table 23. The post-processing results in PRLs

	<b>Oval</b>	<b>Circle</b>	<b>FBF</b>	<b>Simple</b>	<b>Straight</b>	<b>SBF</b>
Equivalent plastic strain at 0.02	0.24	0.11	0.40	0.045	0.3	0.21
Yielding displacement (m)	0.0174	0.027	0.0162	0.0348	0.0099	0.023
Ultimate displacement (m)	0.478	0.349	0.332	0.61	0.468	0.62
Displacement ratio	27.47	12.93	20.49	17.53	47.27	26.96
Ultimate Strength (KN)	2916	2232	3158	1591	2915	1998
Yielding Strength (KN)	1526	1525	1435	1497	1503	1476
Over strength	1.91	1.46	2.20	1.06	1.94	1.35
Stiffness (KN/m)	87720	56483	88565	43009	151818	64156

Table 24. The mode of behavior for MRLs

<b>mode of behavior</b>	<b>Oval</b>	The corner links experience buckling and yielding while the panels start to buckle. The frame does not show any buckling at initial stages of deformation.
	<b>Circle</b>	The corner left top link experiences high inelasticity stress concentration, and the panel starts to buckling while the frameworks without buckling
	<b>FBF</b>	The bottom left-hand side and right-hand side links experience elongating and shortening ( in case of seismic loading) which is the main cause of the behavior, and the general buckling occurred for the plate, while the frame does not show any buckling whether locally or globally.
	<b>Simple</b>	TFA is observed which affects the strength capacity. TFA ended up imposing a very large demand on the boundary element members.
	<b>Straight</b>	The bottom corner links yield at the ends initially while the whole panels starts to buckle, also the link buckling is observed as well. The hinges are concentrated at the ends of each link.
	<b>SBF</b>	The yielding of the links especially at the mid part is observed, the system worked fine without occurrence of early buckling and the panel started to buckle

The behavior PRLs due to a large reduction of the resistance capacity are promising. The Von-Mises stress condition is indicated in Figure 200. It is concluded that for the most of the systems with links, the yielding is initiated within the link and plastic strain are accumulated within the links.

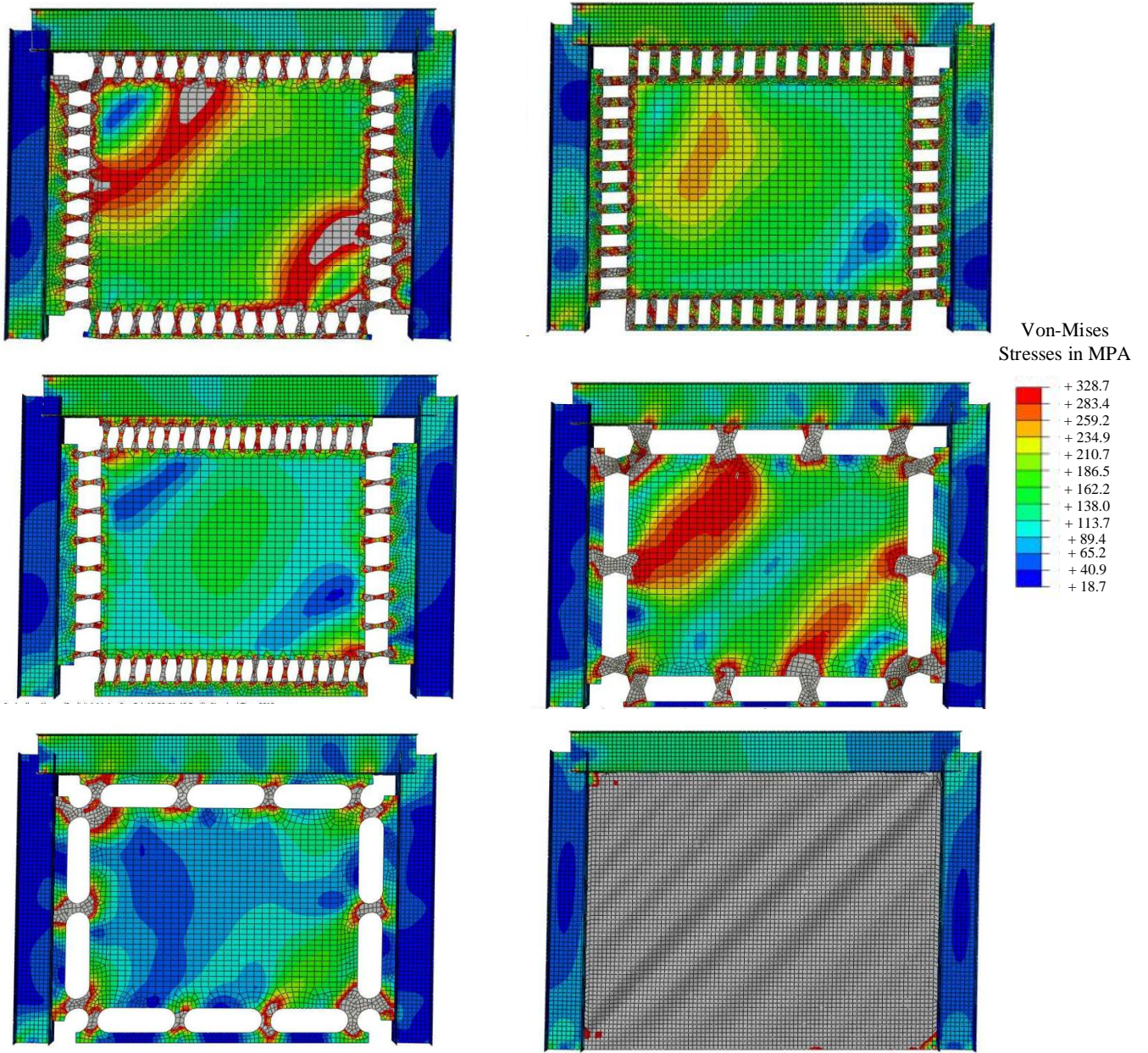


Figure 200. The Von\_Mises stress distribution for PRLs

In addition, the moment at the middle of the beam and at the middle of the column are calculated for all the models to understand the boundary element forces caused by the type of link. The moment is calculated by the average stress state of the flange elements multiplied by section modulus. The purpose of this study is to investigate the boundary element forces caused by the yielding of the links and compare them to the traditional solid plates. The flexural moment forces on the beam and the columns are estimated at mid-points, which are indicated in Table 25 . It is worthy of notice that the simple solid steel shear wall and the wall having straight links show significant demand on the beam boundary elements while the significant demand on the simple steel shear walls columns is observed. The reason for such observation is the tension field action, which is completely generated in solid steel shear walls, while for the shear walls enjoying the links, the beam, and columns experience less amount of force applied to them. The different demand moments on beams and columns for the solid plate and a plate with links could be assumed as one of the reasons for which the plate with links are chosen over the solid plate.

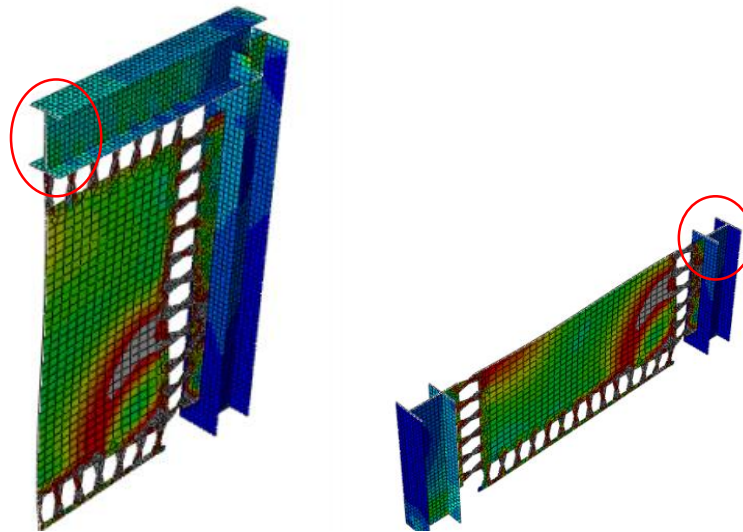


Figure 201. The column and beam section for evaluation of the moment at the middle

Table 25. The forces on the beam and column

	M (KN.m) at 0.02 drift		Type
	BEAM	COLUMN	
	447	125	Straight
	373	273	Simple
	378	50	Oval
	307	85	Circle
	373	72	SBF
	313	76	FBF
Mp (KN.m)	1288	2566.3	

Considering different output parameters and the moment demand along the length of the beam and column, it is concluded that different shapes could be used for different purposes. For instance, if the moment demand is considered the FBF could be an appropriate option, while if the equivalent plastic strain is considered the circle and oval could have better performance.

For investigating the effect of links on high rises, the rest of the study is done considering the flexural dominated links.

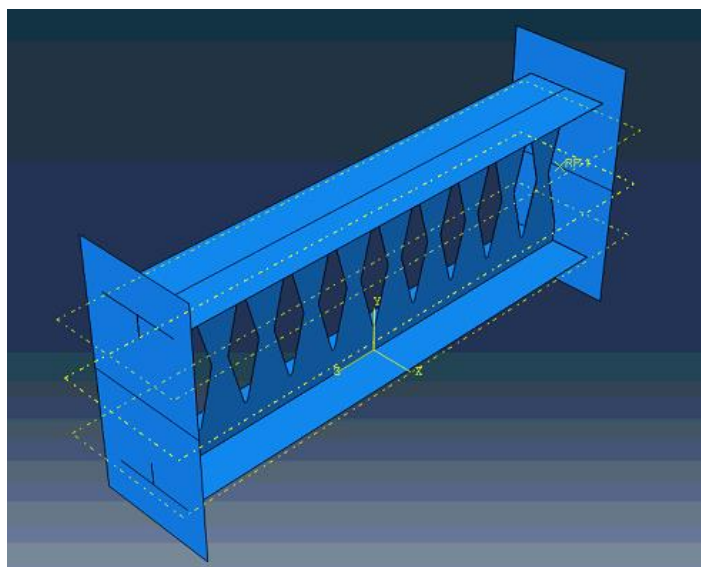
# 10. SEISMIC RESPONSE ANALYSIS OF MULTI-STORY BUILDINGS

In this section, the application of the fuse link structures is discussed. For this purpose, the reduced order models are initially generated in OpenSees, and verified with previous FEM models. After verification of the models, the reduced order models are used to build two prototype buildings with butterfly-shaped fuse links and conventional EBF link beam for comparison purposes. The pushover analysis and modal analysis are conducted to extract the features of the two mentioned lateral resistance systems. The fuse behavior, interstory drifts, stiffness, strength, and natural modes are investigated. The behavior of the two systems under two hazard levels of MCE and DBE for 44 ground motions are elaborated and discussed. The results of nonlinear response history analysis are summarized, and comparisons between the seismic behavior of the two system with and without structural shear links are explained.

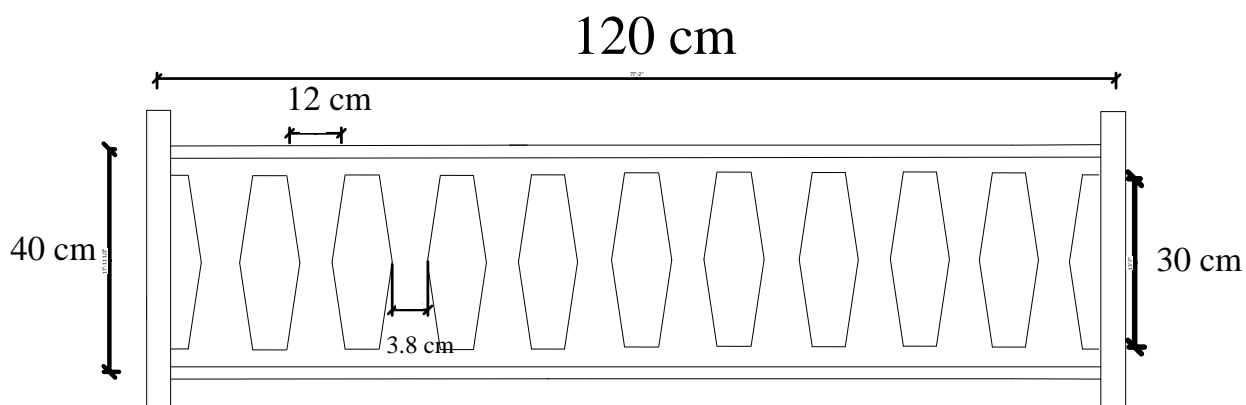
## 10.1. The validation of numerical modeling

To validate our modeling methodology with Openness software, a flexural dominated butterfly-shaped links are considered (FBF, please find in section 9.1). The model is previously described contains a set of flexural dominated butterfly-shaped links. This model, which is previously investigated in FEM, has a length of 120 cm, and 10 butterfly-shaped dampers.

The geometrical properties of the model are as follows. The height of the links is equal to 30cm, the mid-width length is equal to 3.8cm, and the end width length is equal to 12cm. The total length of the beam is equal to 120cm and the total height of the beam is equal to 40cm. This beam is based on the Figure 188, shown in chapter 9. The schematic representation of the model in ABAQUS and OpenSees are shown in Figure 202 and Figure 203. The design shear for this according to SEAOC was 530 kN (120 kips). In addition, the material model is based on the yielding stress of 250 MPa (36 Ksi), modulus of elasticity of  $2 \times 10^5$  MPa (29000 Ksi) and the strain-hardening ratio is 0.0005.



a) The model simulated in FE program



b) Details of the simulated model in FE program

Figure 202. The schematic representation of the FBF model (the details are given in the text)

The Figure 203 shows the schematic illustration of the Opensees reduced order model. For this model the beams (between node 20 and node 21, between node 21 and node 22, between node 23 and node 27, between node 24 and node 25, between node 25 and node 26) are model with element elastic elements, since the contribution of the upper and lower plates to the inelastic total inelastic behavior is negligible. The butterfly-shaped links are modeled with displacement based beam element (dispBeamColumn) with distributed plasticity and 5 integration points. The multi-point constraint (equalDOF) between the nodes 22, 23 and 26, 27 are in 1, 2, direction. The length of the beam is equal to 120 cm, and height of the beam is equal to 40 cm. The end width, middle

width and length of butterfly shaped links are 12cm, 3.8 cm and 30cm. The links are modeled with taper shaped with varying width shown in . The number of butterfly shaped links are 10 The boundary condition for nodes 20 and 24 are pinned. In addition, the geometrical properties of the model are as follows. The material model is Giuffr -Menegotto-Pinto Model with Isotropic Strain Hardening (Steel02 in Opensees) with yielding point of 36 Ksi (248 MPa), modulus of elasticity of 29000 Ksi (2e5 MPa) and the strain-hardening ratio is 0.0005 (CR1, CR2, a1, a2, a3, a4, and sigInt are 0.925, 0.15, 0.005, 1.0, 0.005, 1.0 and 0 respectively)

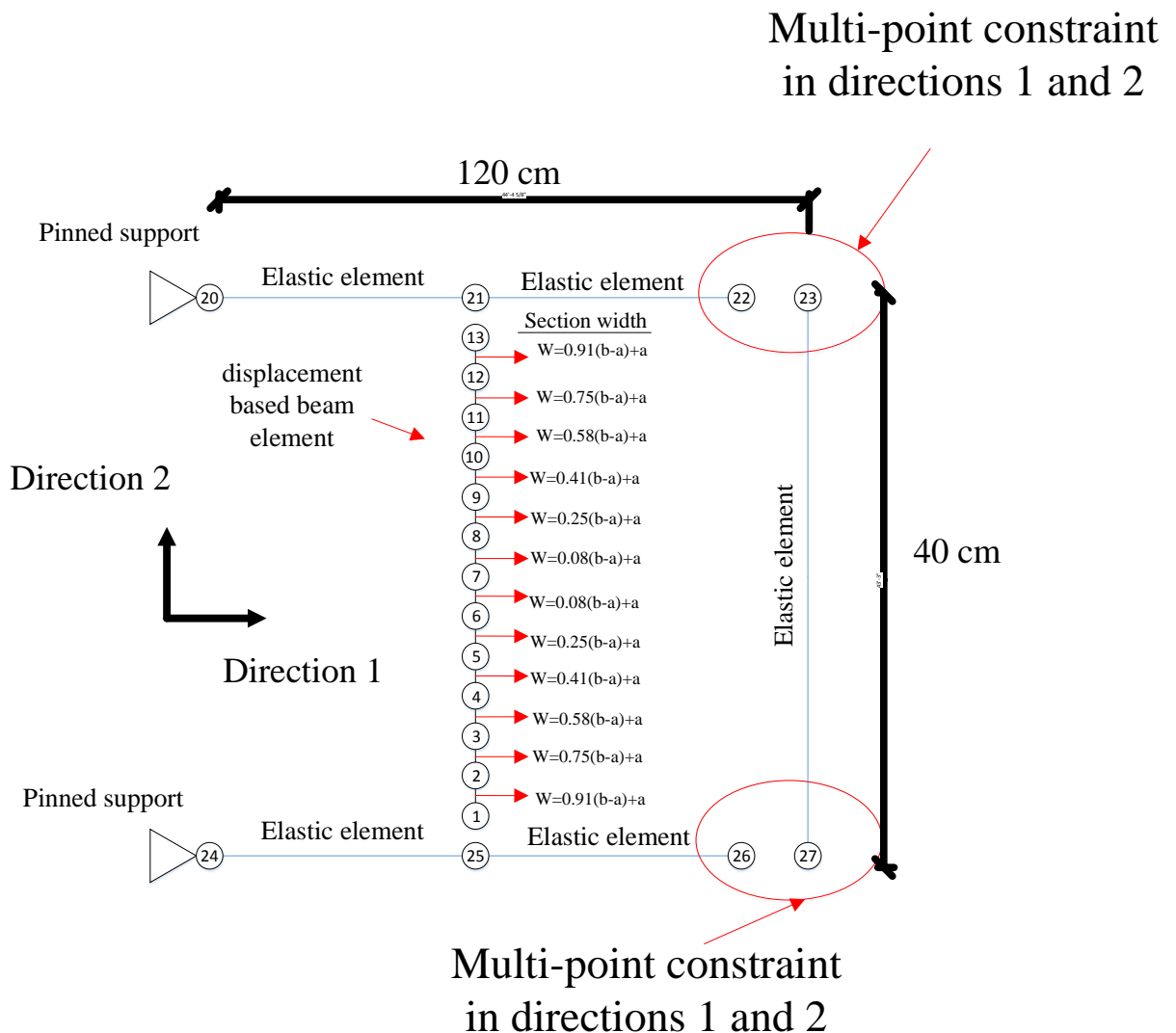


Figure 203. The schematic representation of the FBF model in Opensees (the details are given in the text)

It is noted that the modeling methodology in ABAQUS is shown in details in Chapter 7, in which the methodology is verified against four laboratory tests. The modeling methodology with Opensees is conducted through validating the cyclic behavior against the same model constructed in ABAQUS. For this purpose, a cyclic load suitable for EBF systems based on the general loading sequence protocol proposed by AISC is implemented. This protocol is used for link-column connections in EBF systems (AISC, 2005). This loading protocol is implemented because of the similarity in behavior of the EBF beams and butterfly-shaped links. The loading protocol is indicated in Table 26. The hysteric cyclic response of the ABAQUS FEM analysis and OPENSEES FEM analysis is summarized in Figure 204. The results show more than a 98% match between the two methods in both peak strength points in loading and peak strength points in unloading parts. In addition, from the ABAQUS model, it is observed that the flanges of the SRL model remains almost elastic under the cycle applied loading and the butterfly-shaped fuses are the only elements that contribute to the nonlinearity of the whole system. Hence, the model in the Opensees does not consider the contribution of the beam flanges.

Table 26. The loading protocol

Cycle #	Number of Cycles	$\gamma=\Delta/h$ (%)
1 - 6	6	0.0625
7 - 12	6	0.125
13 - 18	6	0.250
19 - 24	6	0.375
25 - 30	6	0.50
31 - 36	6	0.75
37 - 42	6	1.0
43 - 46	4	1.5
47 - 50	4	2.0
51 - 52	2	3
53	1	4
54	1	5
55	1	7
56	1	9
57	1	11
58	1	13
59	1	15
60	1	17
61	1	19
62	1	21
63	1	23
64	1	25
65	1	27
66	1	29

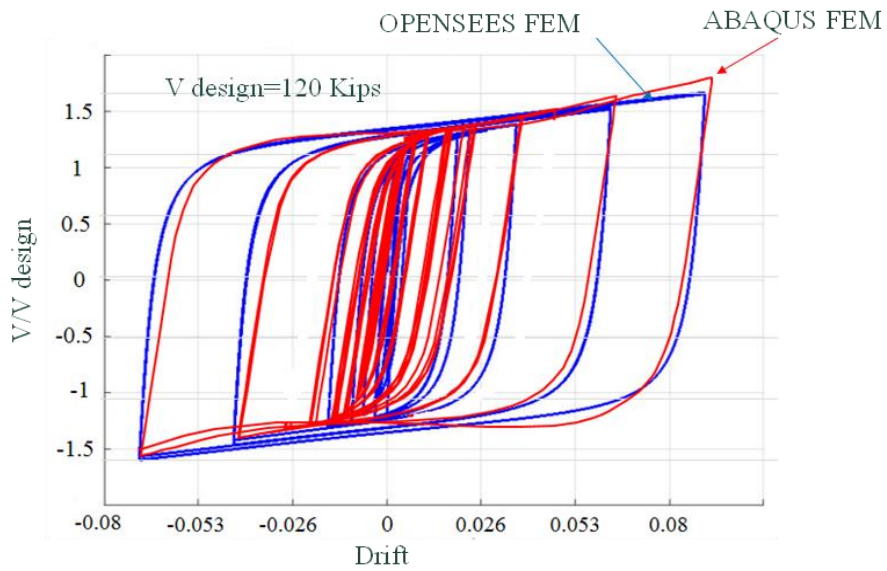


Figure 204. The verification of modeling methodology in Opensees ( 120Kips is equal to 530 KN)

## 10.2. Nonlinear Response History Analysis for multi-story building

To investigate the applicability of the fuses on structures, the example for EBF system from SEAOC is taken into account (SEAOC, 2012). Both six story conventional building and six story building with fuses are designed to be compared with aid of Opensees software. Table 27 shows the designed fuses based on the demand shear forces.

Table 27. The shear for which the building is designed

Level	Shear (kips)	Cumulative Force (kips)	Design force for the BF links with Eq.(159) (kips)		Design groups
Roof	60	60	244	244	III
6th	60	120	244		
5th	88	208	358	358	II
4th	125	333	508	508	I
3rd	125	458	508		
2nd	125	583	508		

In addition to satisfying equilibrium, and considering Figure 205, the following equations, Eq. (157) and Eq. (158) are derived for obtaining the force related to the butterfly-shaped link. The first equation could be derived from the equilibrium condition of the horizontal beam at the top of the butterfly-shaped damper. In addition, the second equation is derived based on the total equilibrium of the system over the point A in the middle of the vertical beam.

$$V_{BF} = \frac{2M}{H} \text{ \& } M = \frac{VL}{2} \quad (157)$$

$$2M - VL + HV_{BF} - V_{BF}H = 0 \quad (158)$$

Therefore, Eq. (159) could be derived based on the simplification of the previous equations.

$$V_{BF} = \frac{V \times H}{L} \quad (159)$$

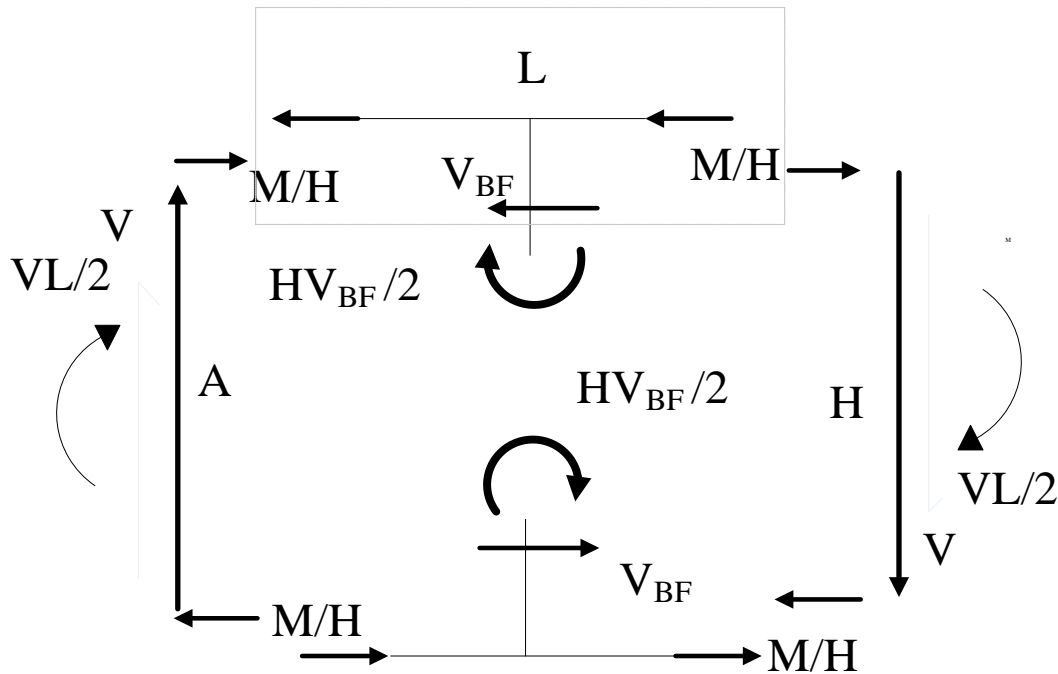


Figure 205. The forces applied to a typical butterfly-shaped damper system

The three design groups are categorized as shown in Figure 206. Based on the provided equation, the links are designed to resist the loading recommended by SEAOC (2012). The links shapes are as follows:

a) Category I, for lower story structural fuses based on W 10×68 beam dimensions.	b) Category II, for middle story structural fuses based on BU13×53 beam dimensions.	c) Category III, for upper story structural fuses based on BU 13×53 beam dimensions.

Figure 206. The three design groups used for designing the NRHA sample building (Thickness in centimeter, but the rest is in meter)

The flanges of the beams are designed based on the mentioned sectional properties shown in Figure 206. The model used to describe the effect of fuses on the mid-rise building includes six stories. In each story, the links with strategic cutout are implemented as the EBF connecting beam. The

fuses design are based on the guidelines provided in Chapter 7, and the demand force for each story level. The six-story model is shown in Figure 207. The leaning columns are considered within the study to have P-delta effect. In addition, the conventional model is developed to compare the EBF-BF fuse system with the corresponding EBF system, which is shown in Figure 208. It noted that all the models are considered with leaning columns to simulate P- $\Delta$  effect. The gravity force is calculated based on the seismic weight associated with each story and divided by two, to have the gravity load associated with leaning columns for each lateral resistance EBF system. The damping is applied based Raleigh method for the periods associated with first and second modes. The damping ration is considred to be 0.02 for which  $\alpha$  and  $\beta$  terms assoicated with Raleigh method are calcaulted and implemented within the models.

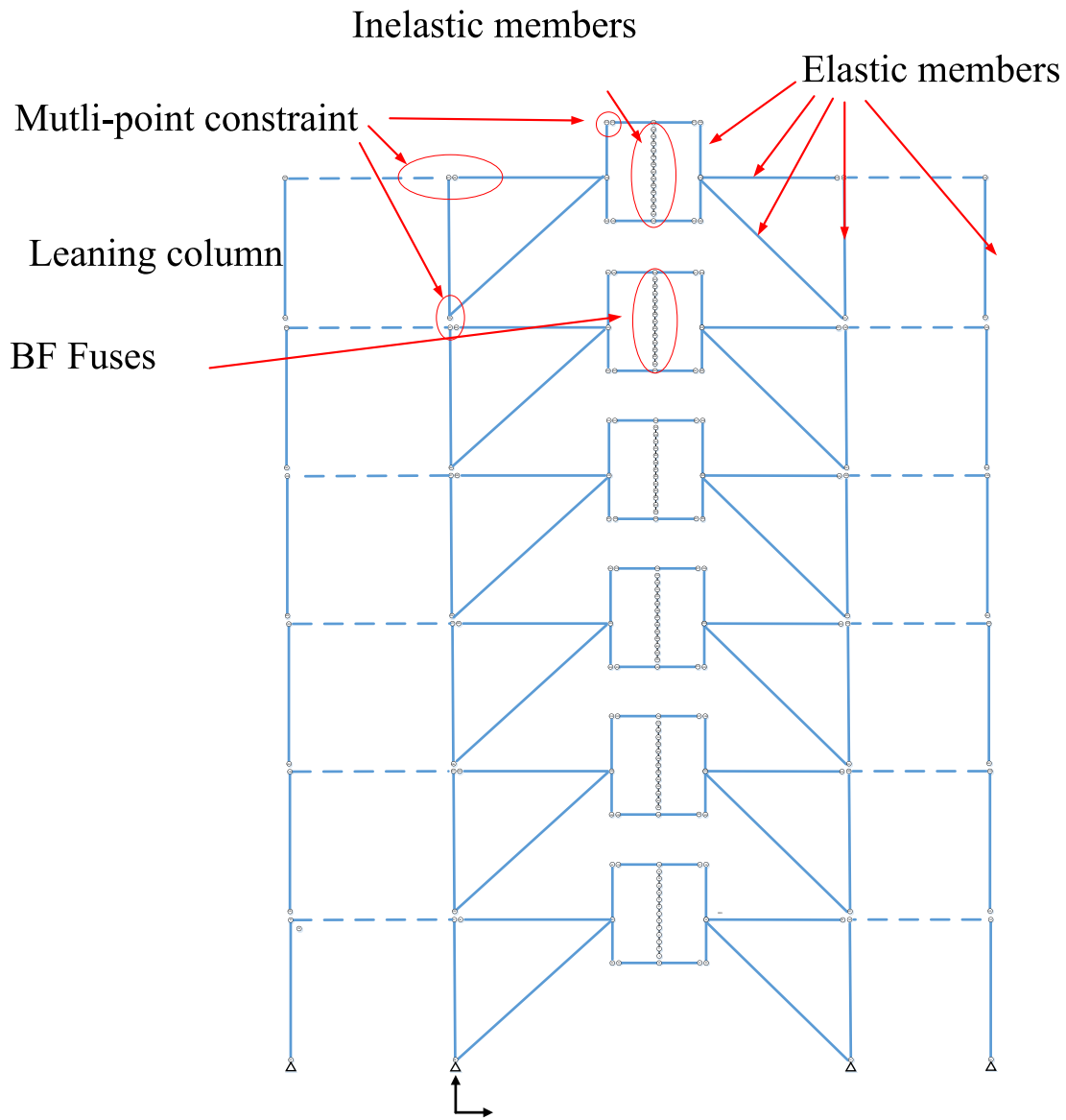


Figure 207. The model considered for NRHA studies

The model is checked within the Opensees once again to make sure all the nodes and elements are appropriately defined. The conventional model EBF system is designed in such a way that the linking element is yielded in shear. The EBF system is designed with the aid of the Zero-Length element since the shear is governed according to SEAOC (2012). The zero-length elements are used for y direction between the link beam and the point in which the brace and beam are

intersected. The purpose of zero-length element is to simulate the shear stiffness of a system; therefore, it yields when the vertical demand reaches toe specified force. This force is taken from the SEAOC (2012) EBF example.

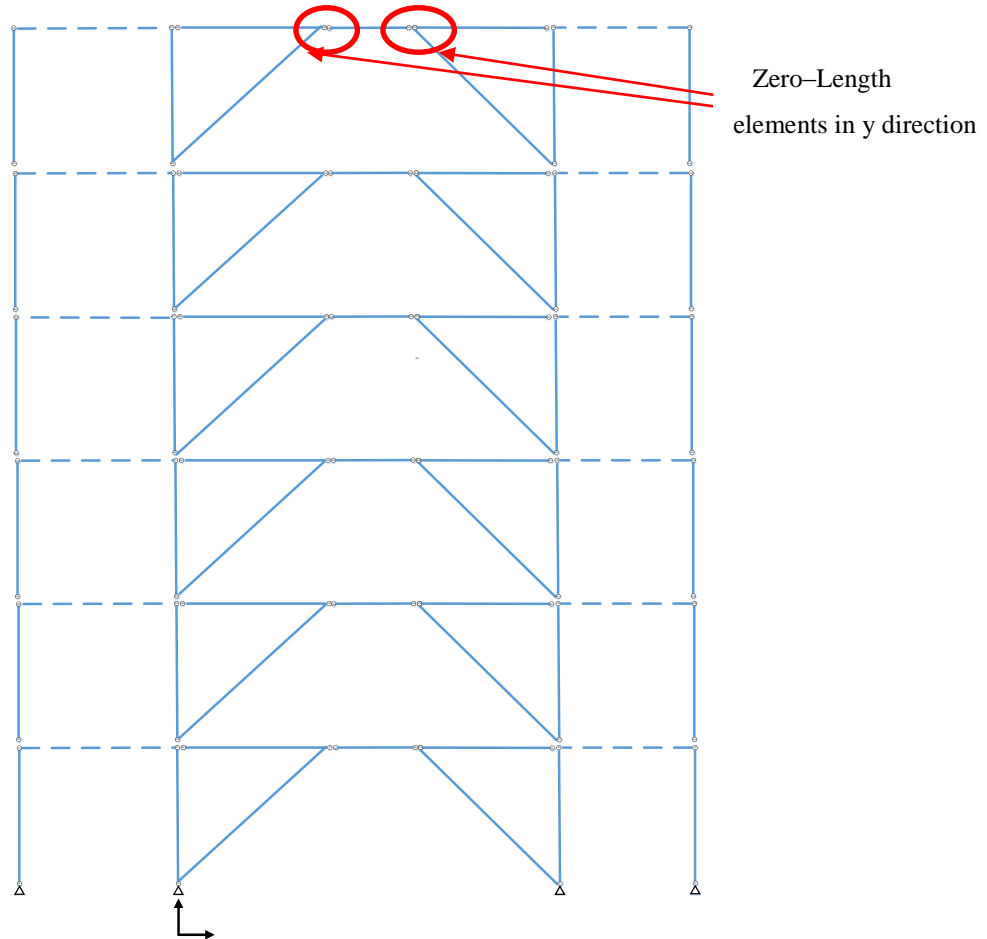


Figure 208. The conventional EBF model

### 10.2.1. The comparison of the monotonically loaded frames with conventional EBF system and BF fuses

The pushover analysis is conducted by applying displacement controlled loading monotonically on the two models. The displacement controlled loading applied as it is shown in Figure 209 ( in which H is a displacement load). The Pushover of the two systems indicates that both of the systems have approximately the same stiffness and both of them start the yielding at the same shear value, which is shown in Figure 210.

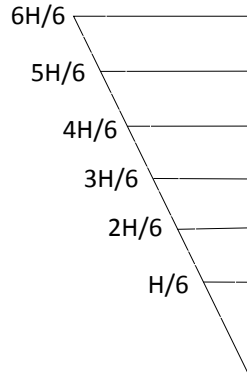


Figure 209. The monotonic loading applied for both models for obtaining pushover curves

It is noted that for all the stories of the two models, the allowable drift ratio is checked based on the design forces, and none of them pass 0.02 drift ratio limit, which is shown in Figure 211. Comparison of the two BF fuses and EBF systems show that both systems start to yield at the same strength level; however, the conventional EBF system is not able to experience higher drifts while the BF fuse system could experience higher drift which is observed from Figure 211 and Figure 212.

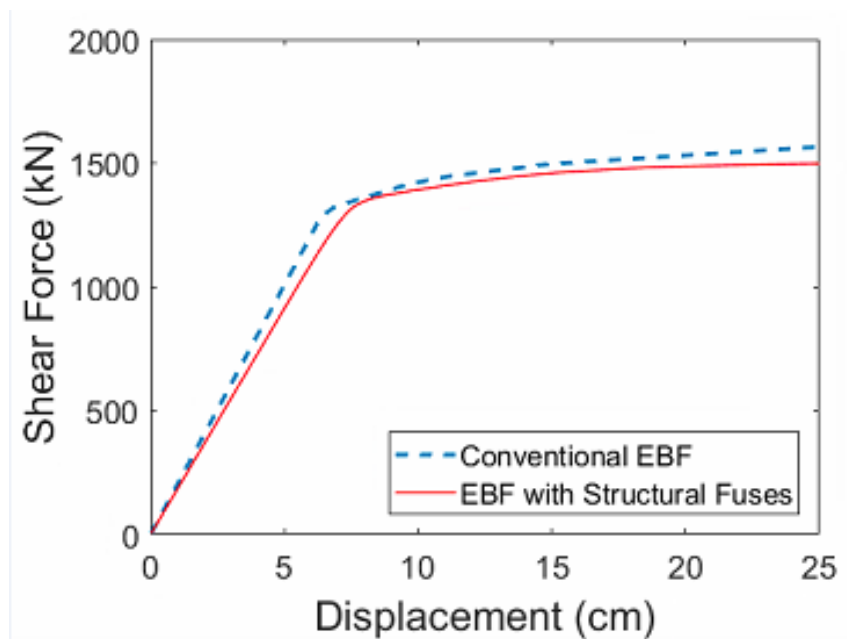
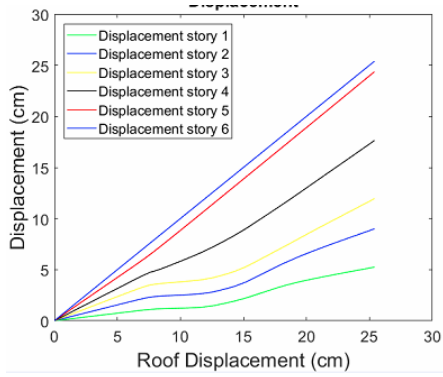
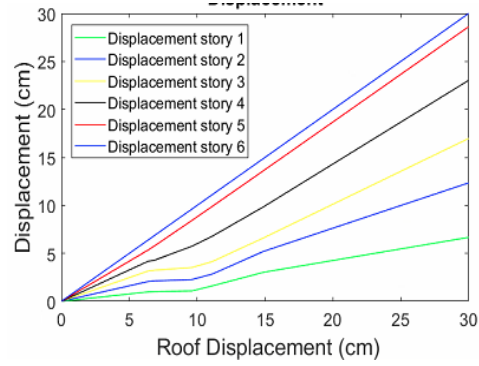


Figure 210. Pushover curves comparison



a) Six stories with BF fuses



b) Six stories with EBF system

Figure 211. Comparison of the two systems

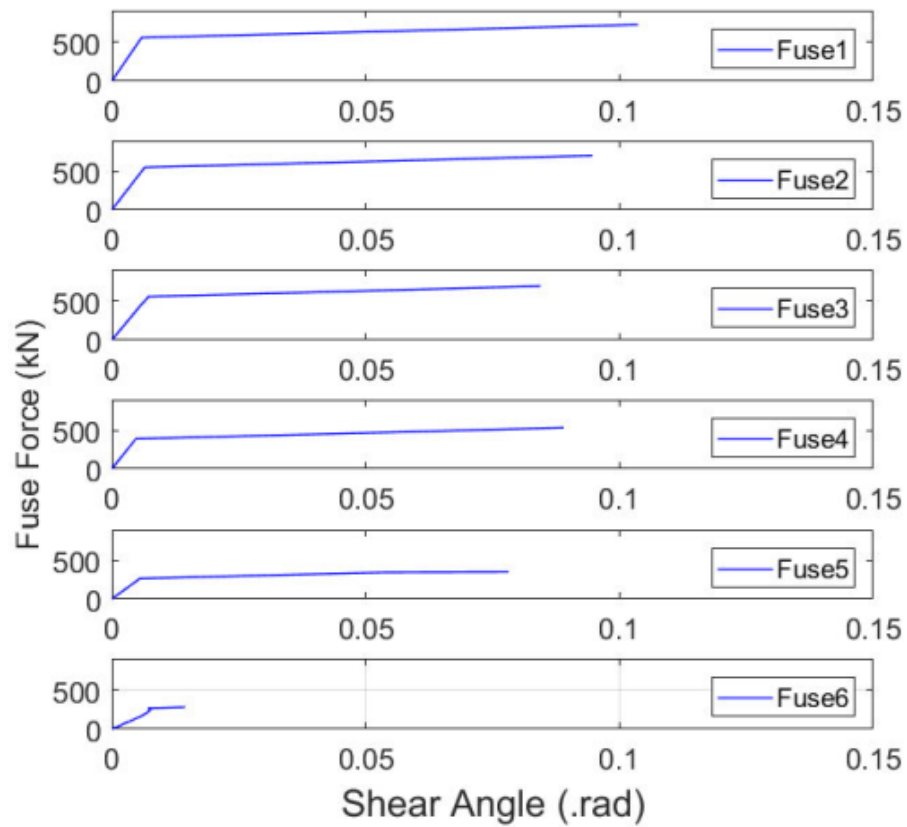


Figure 212. The fuse behavior under the pushover loading for six stories with BF fuses

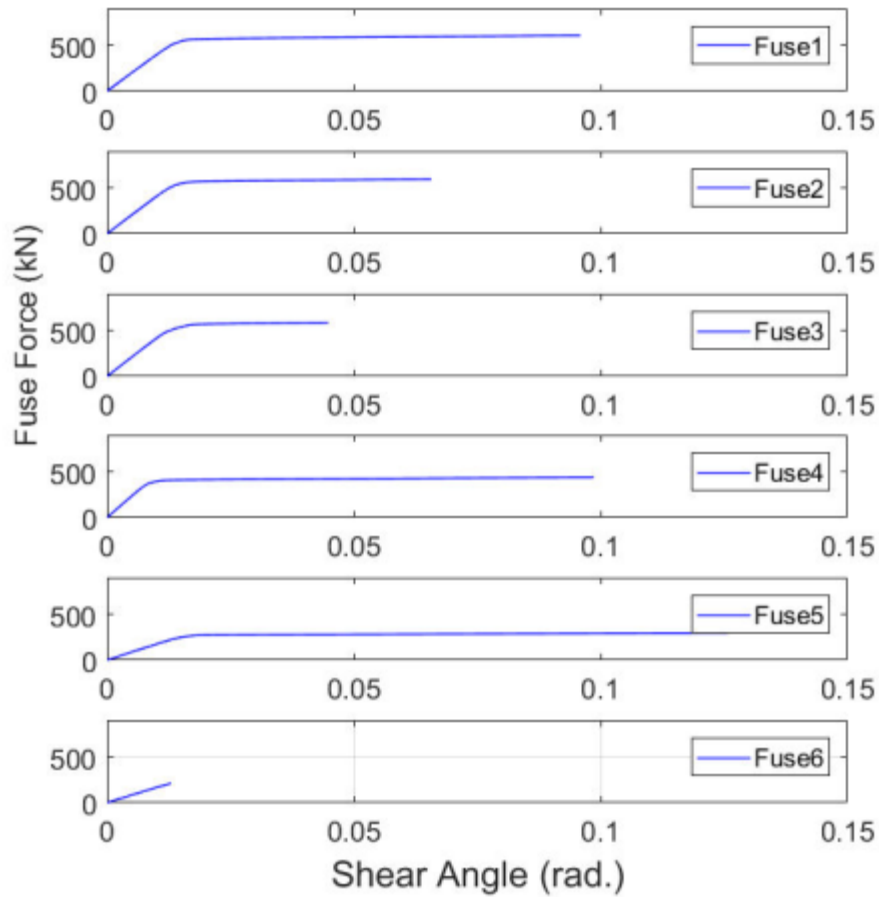


Figure 213. The fuse behavior under the pushover loading for six stories with conventional system

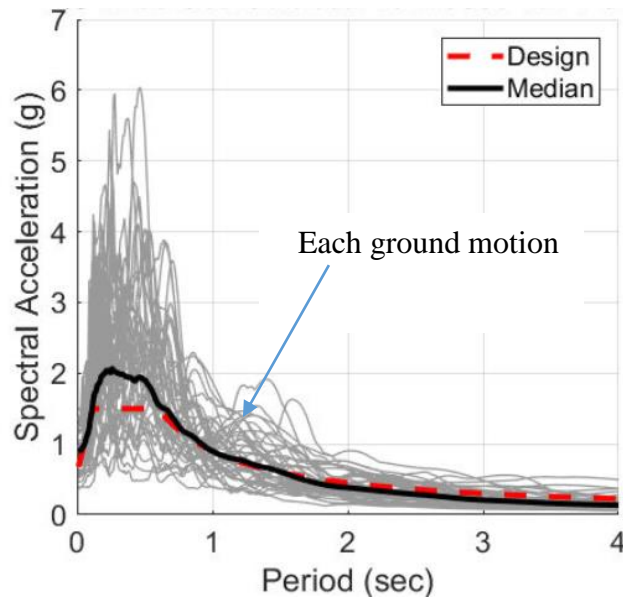
In addition, the Eigenvalues analysis summarized in Table 28, shows that for both of the system the first and second period are close. This will show that stiffness of the two systems are close since the mass is exactly the same and it is applied with aid of the seismic weight associated with each story.

Table 28. Comparison of the EBF building with BF fuse building

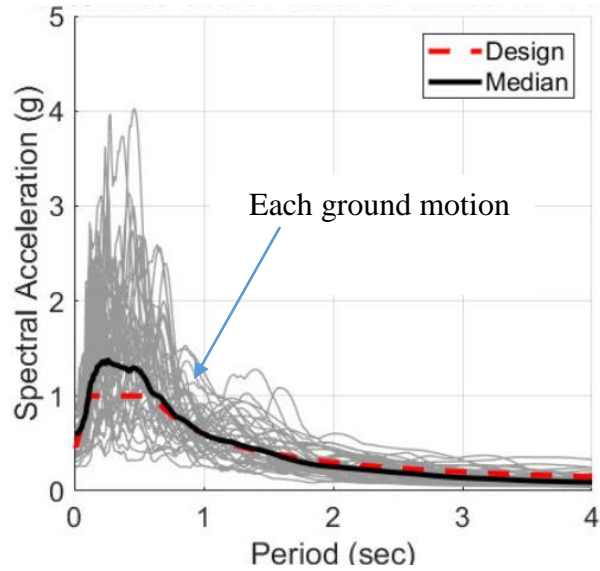
<b>MODE NO.</b>	<b>BF FUSE SYSTEM</b>	<b>CONVENTIONAL SYSTEM</b>
<b>1</b>	1.332	1.283
<b>2</b>	0.518	0.482
<b>3</b>	0.299	0.289
<b>4</b>	0.243	0.227
<b>5</b>	0.192	0.180

### 10.2.2. The scale factor analysis

In this part, the scale factor analysis is elaborated. Forty-four ground motions are considered for conducting the scale factor analysis. For each one of the ground motions, the associated spectrum is drawn and the average spectrum is shown. The grounds motions are once considered for two levels of MCE and DBE. The average of the 44 grounds motions spectrums is calculated and shown with a black line in Figure 214. Next, the design spectrum is illustrated with a red line based on the seismic codes. The studied systems have a period of more than one second, depending system stiffness and system mass. The scale factor for a period equal to one second is calculated based on design spectrum and 44 ground motions' average spectrum. The scale factor for the period one second is taken into account since the two curves of design and 44 ground motions' average spectrum matches well from period equal to one, and the periods higher than one second.



a) MCE level scale factor analysis, 2% in 50 scale factor is 2.58 for 1 sec

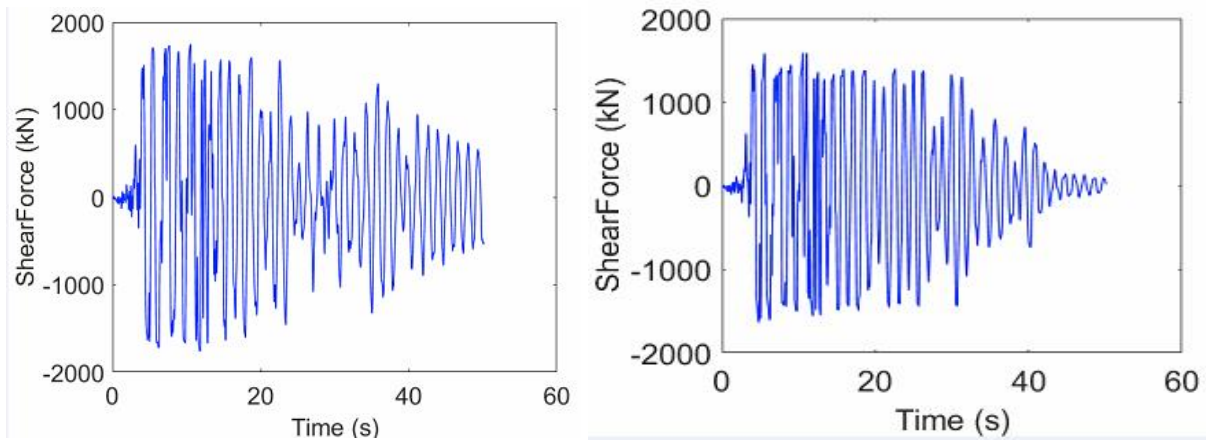


b) DBE level scale factor analysis, 10% in 50 scale factor is 2.58 for 1 sec

Figure 214. The scale factor assessment for two earthquake levels

### 10.2.3. The analysis of the frame for a specific ground motion

In this section, the behavior of the designed frames under a specific ground motion is considered. For both of the frames, the DBE considered and the same ground motion is applied with the aid of the openses software. Figure 215 shows the behavior of the two frames under earthquake loading. It is concluded that the maximum shear under the earthquake for both frames are the same; however, the contribution of the higher modes in the behavior of the conventional system is higher than the corresponding system with BF fuses.



a) Six stories with BF fuses

b) Six stories with EBF system

Figure 215. Shear Comparison of the two systems

In addition, due to a slight difference in initial stiffness of the EBF system with BF fuse system, the story displacements for six-story frames with BF are slightly higher than the corresponding conventional EBF system, which is shown in Figure 216. The difference between the story drift displacement, also confirms the behavior of the system (as it is shown in Figure 217).

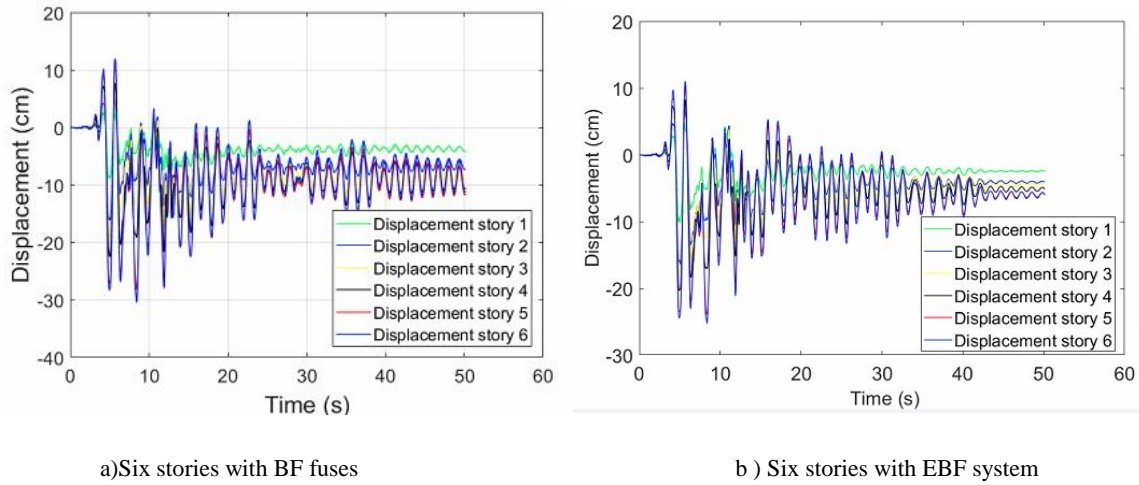


Figure 216. Story displacement comparison of the two systems under earthquake loading

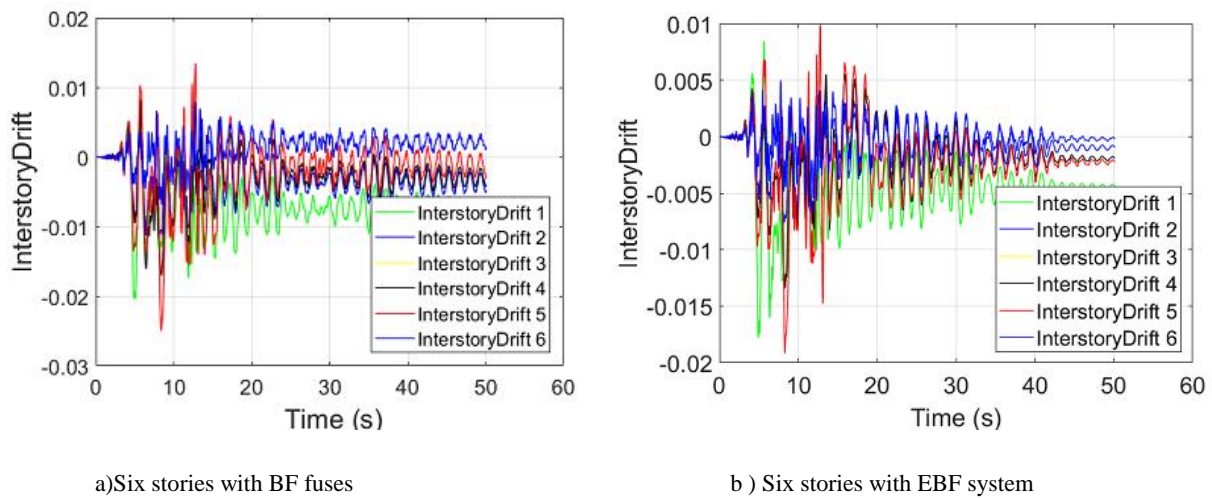


Figure 217. Inter-story displacement comparison of the two systems under earthquake loading

The energy dissipation of the two systems is significantly different. As it is shown in Figure 218 and Figure 219, the energy dissipated by each BF fuse, is several times larger than the corresponding EBF system. This could be verified by assessing the area under the curve. Fuses in lower stories have the highest contribution to energy dissipation of the system.

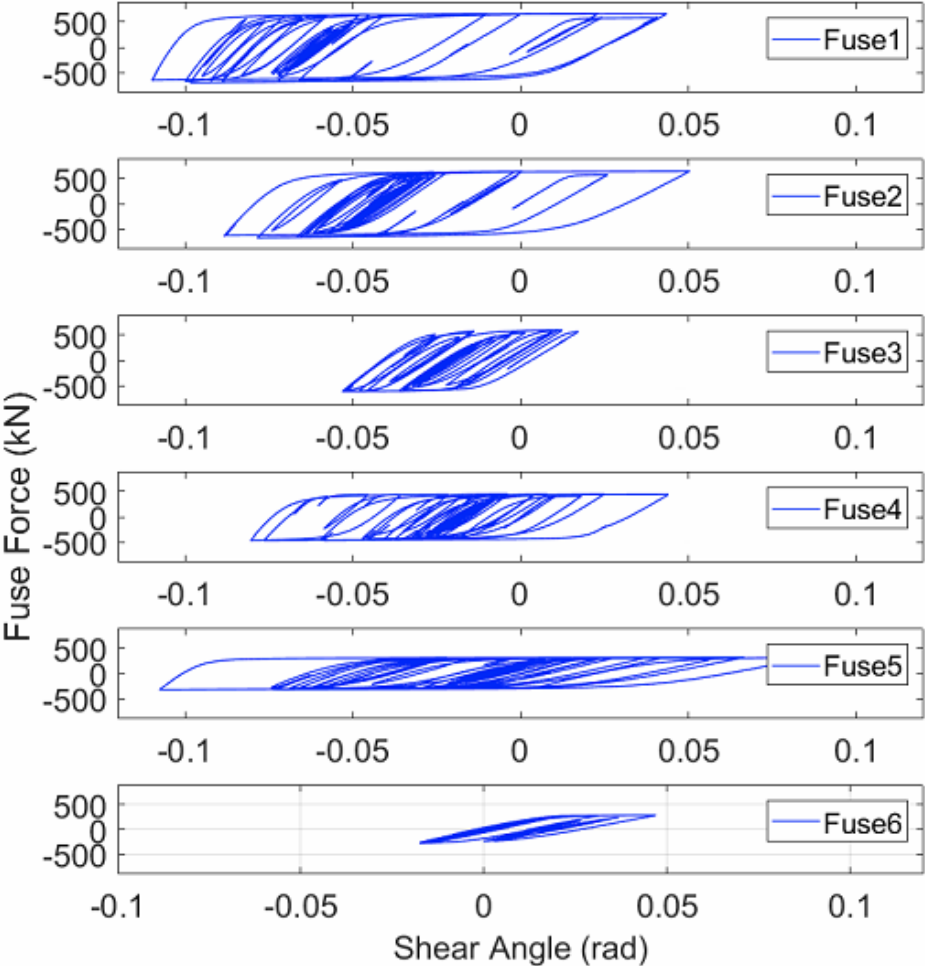


Figure 218. Fuse behavior for the six system with butterfly shaped fuses under an specific earthquake loading

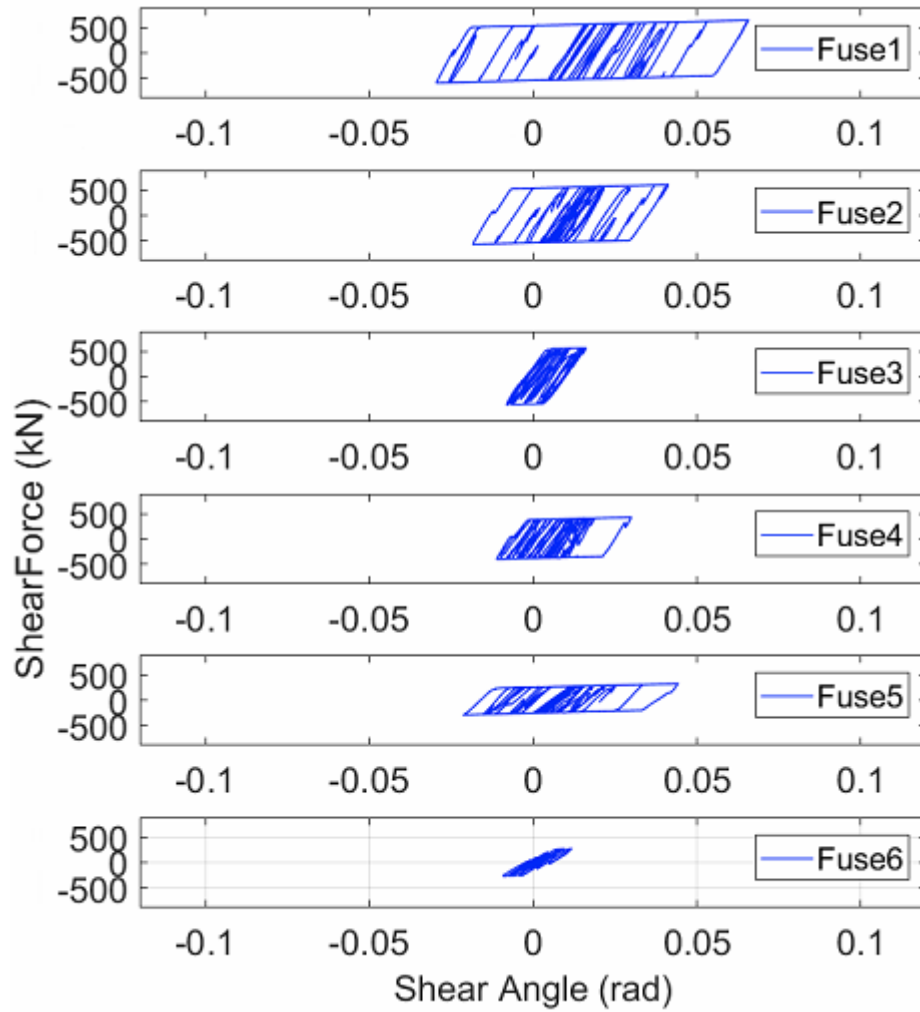
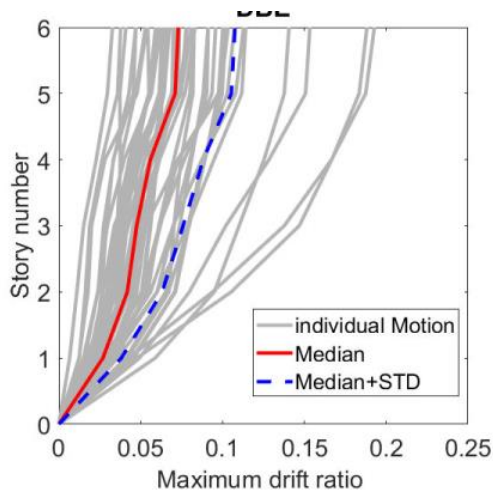


Figure 219. Link behavior for the six story system under an specific earthquake loading

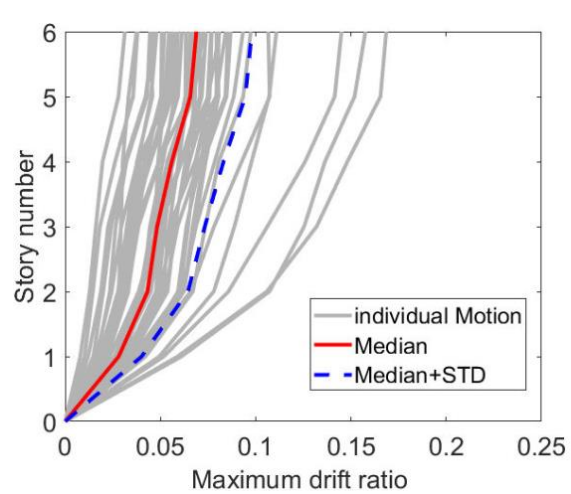
### 10.2.4. NRHA results for 44 ground motions

In this section, the performance of the two 6-story buildings is compared under two levels of ground motion scale factors for 44 ground motions. The 176 models are run and investigated. The scale factors are based on the period of a structure with one second natural period.

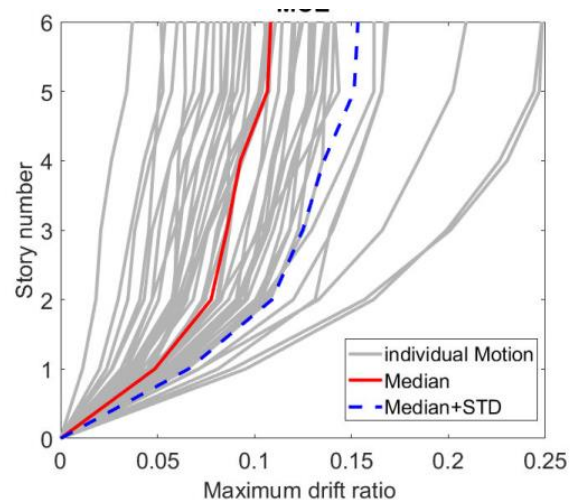
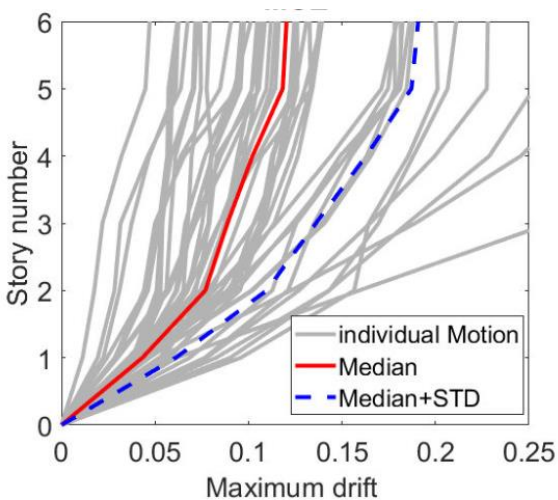
Figure 220 shows the behavior of butterfly-shaped and conventional systems for two levels of DBE and MCE under 44 ground motions. The median and median plus one standard deviation is conducted and incorporated in the graphs. It is concluded that total drift ratio of each story is slightly higher for butterfly-shaped system due to slightly lower stiffness. It is shown that the total story drifts for both systems are close, and butterfly-shaped link or simple link will have close total story drifts, which could be due to similar initial stiffness and mass of the system.



a) Butterfly-shaped fuse under DBE



b) Conventional System under DBE

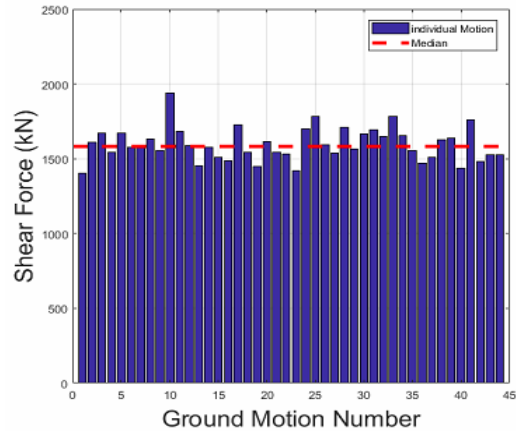
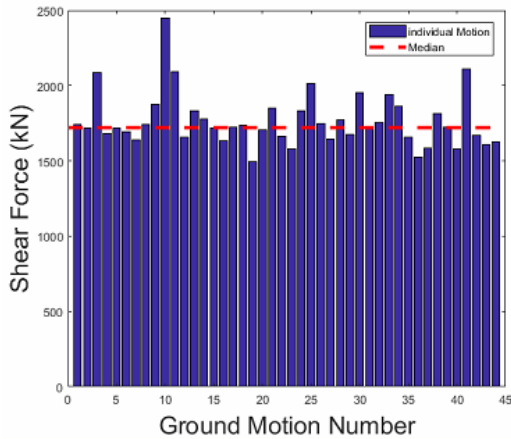


a) Butterfly-shaped fuse under MCE

b) Conventional System under MCE

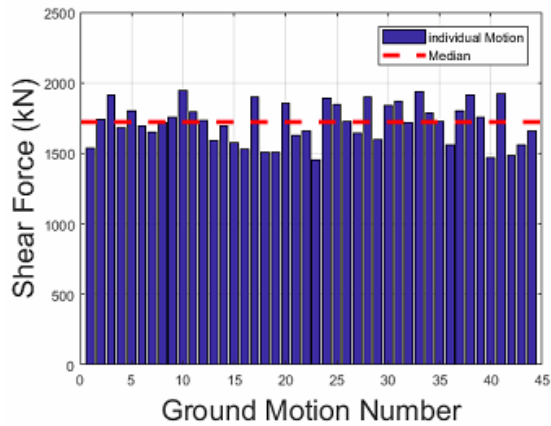
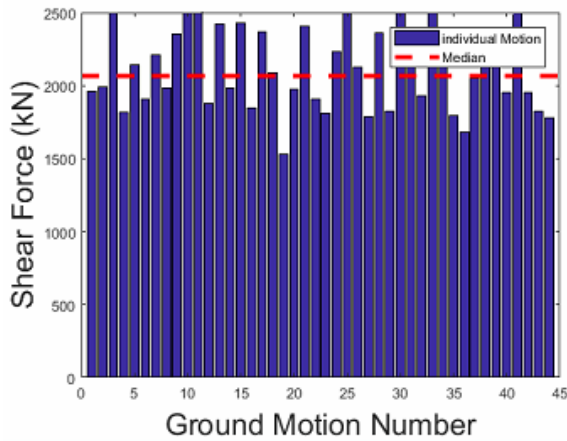
Figure 220. The comparison total story drift for two systems

Figure 221 shows the maximum shear at the bottom of the two systems, under 44 ground motion for two level of DBE and MCE. The shear under the DBE and MCE level for both systems are close since the two systems are designed in such a way that the fuse elements would yield about the same load value.



a) Butterfly-shaped fuse under DBE

b) Conventional System under DBE



a) Butterfly-shaped fuse under MCE

b) Conventional System under MCE

Figure 221. The comparison maximum total shear for two systems

The inter-story drifts for both systems are shown in Figure 222. It is concluded that the maximum inter-story is expected with the lower story levels, while the middle stories have the least inter-story drifts. The inter-story drift comparison of the butterfly-shaped system and conventional systems shows that the drifts are close, which is due to the close total stiffness of the structures. It is concluded that the system with butterfly-shaped link relatively reduces the inter-story drifts under both DBE and MCE hazard level especially for lower stories, which reduces the damage to secondary structural elements.

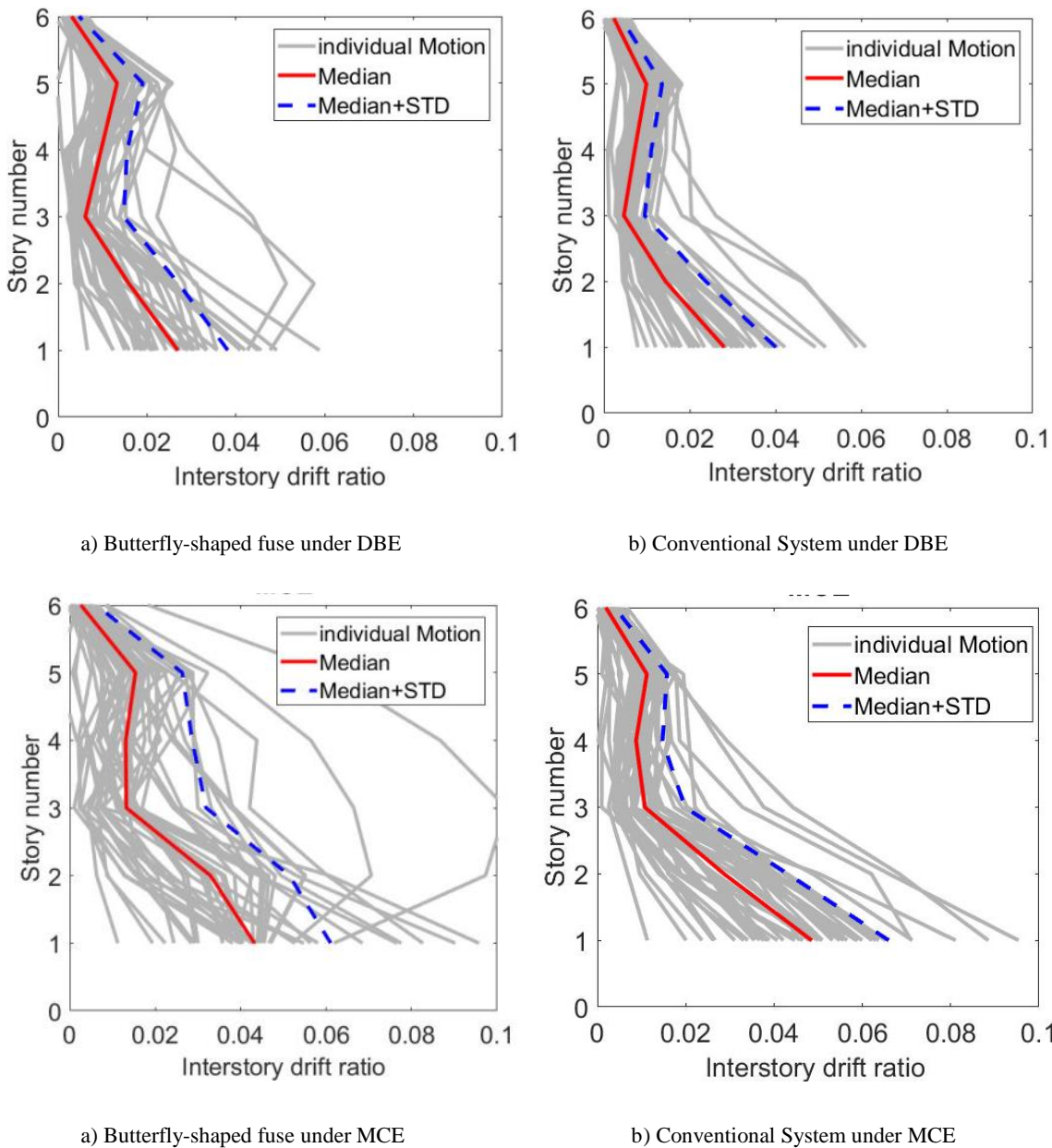


Figure 222. The inter-story drift for two systems

The fuse shear for both systems has the same trend with close values which is shown in Figure 223. This indicates that both systems which are designed based on the same fuse shear resistance are able to withstand the lateral load and yield at the same value. The fuse force shows that lower stories contribute more to total resistance of the structures, while higher stories have the least contribution to the total shear resistance of the system.

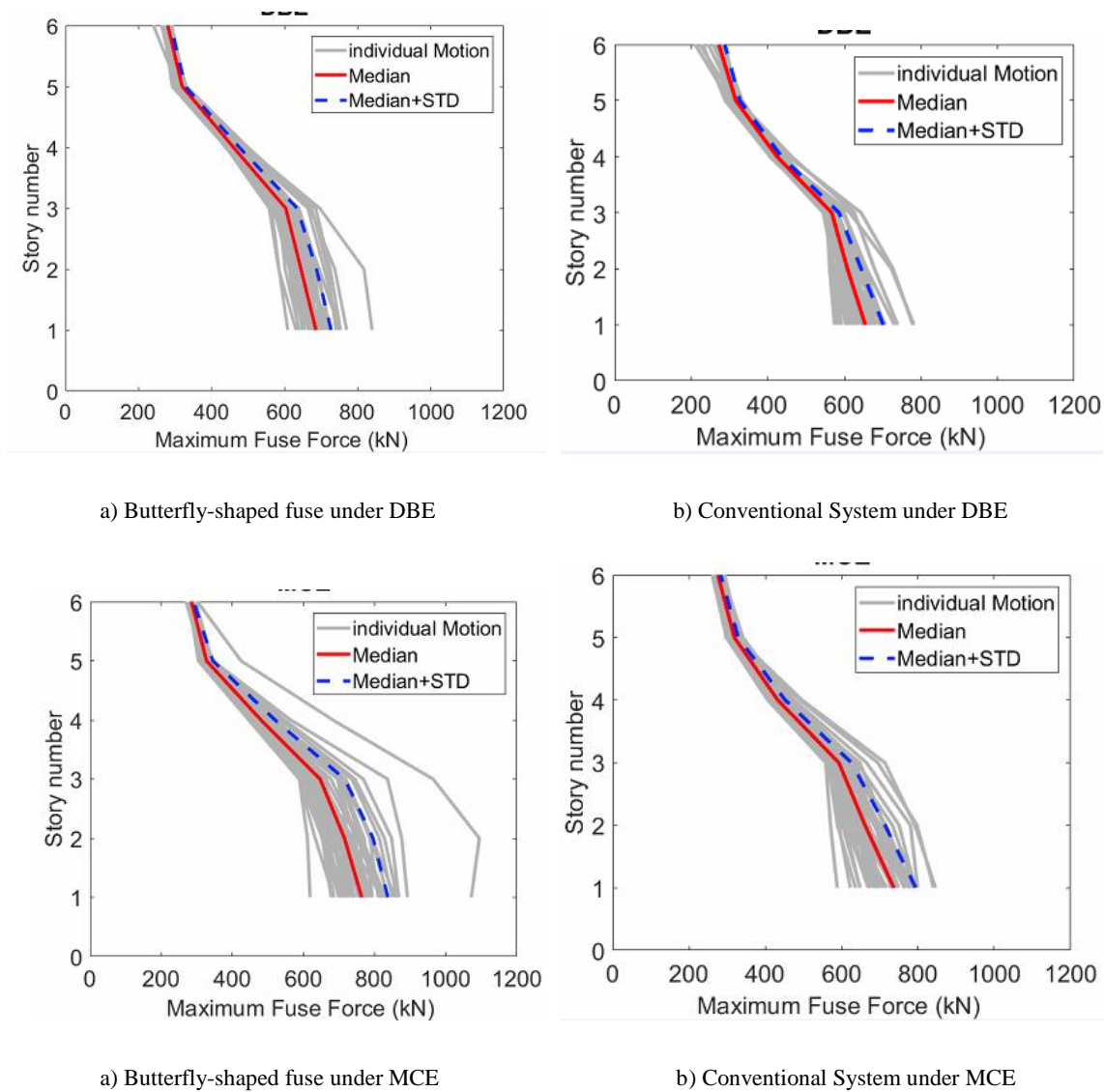


Figure 223. The fuse force for two systems

The shear angle for the conventional model would start from a constant value since these links are working in shear rather than flexure based on designed example from the SEAOC (2012) for

EBF systems. The constant value shown in Figure 224 for conventional model is related to zero-length element defined in the software to account for the shear behavior of the linking beam. The higher shear angle for conventional models compared to butterfly-shaped models indicate that the possibility of fracture for these models is high for a simple conventional link, which needs to be considered in the design, specifically for areas with high seismicity which corroborates the fact that the ductility of the system should be investigated elaborately.

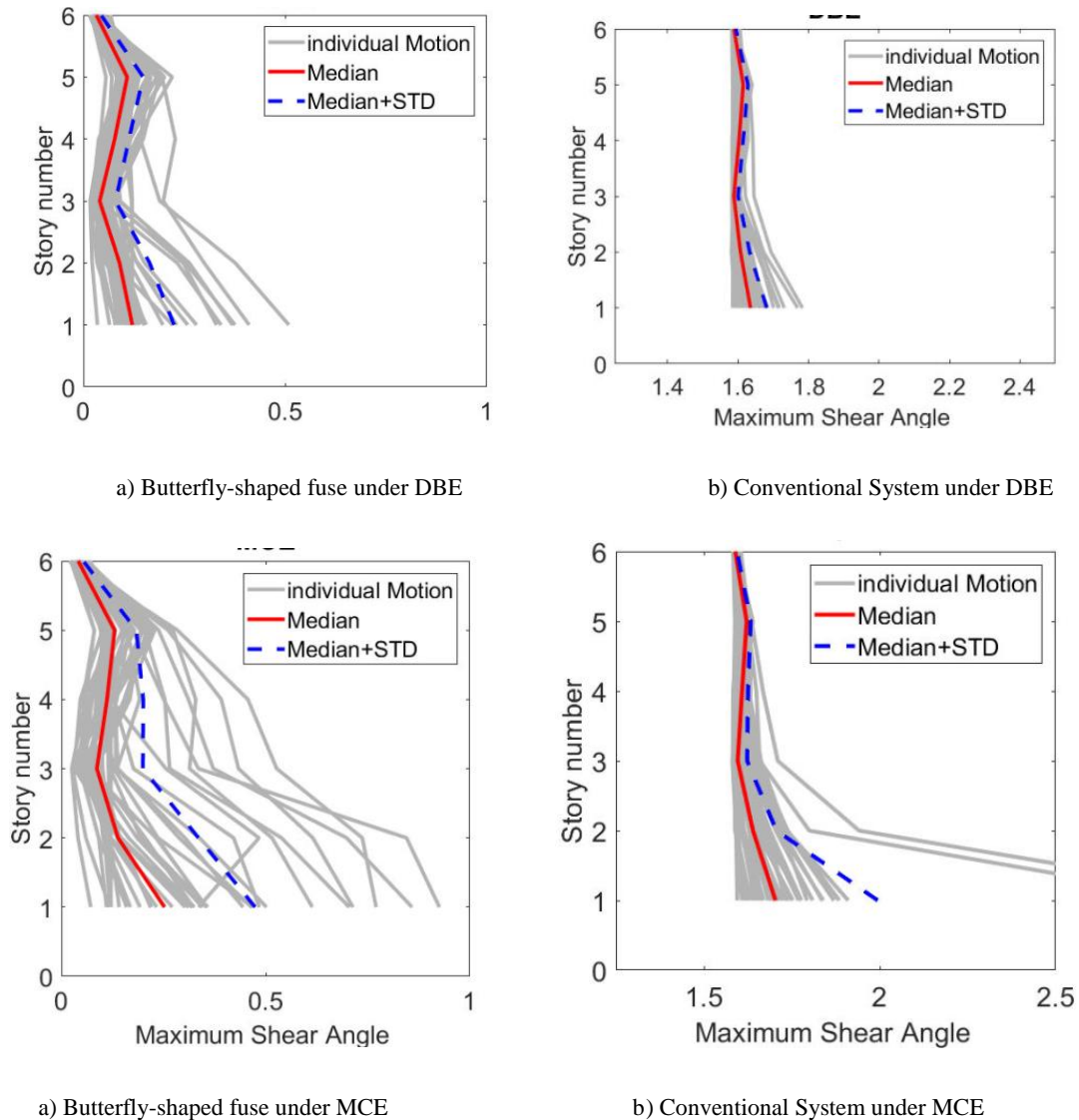


Figure 224. The shear angle for two systems

To further investigate the structure, as an example, two elements which The columns and the beam are checked against the maximum plastic moment in Figure 225. It is shown that the

assumption with which the models are generated are correct since under the majority of the earthquakes the beams and columns would not yield or plasticized. It is concluded that the conventional model has higher demands on the boundary elements, meaning that the boundary elements should be designed for larger loads, which is not economical. The general stiffness and strength of the system with the butterfly-shaped link is close to conventional models; however, the demands on the boundary elements are lower than the corresponding conventional model.

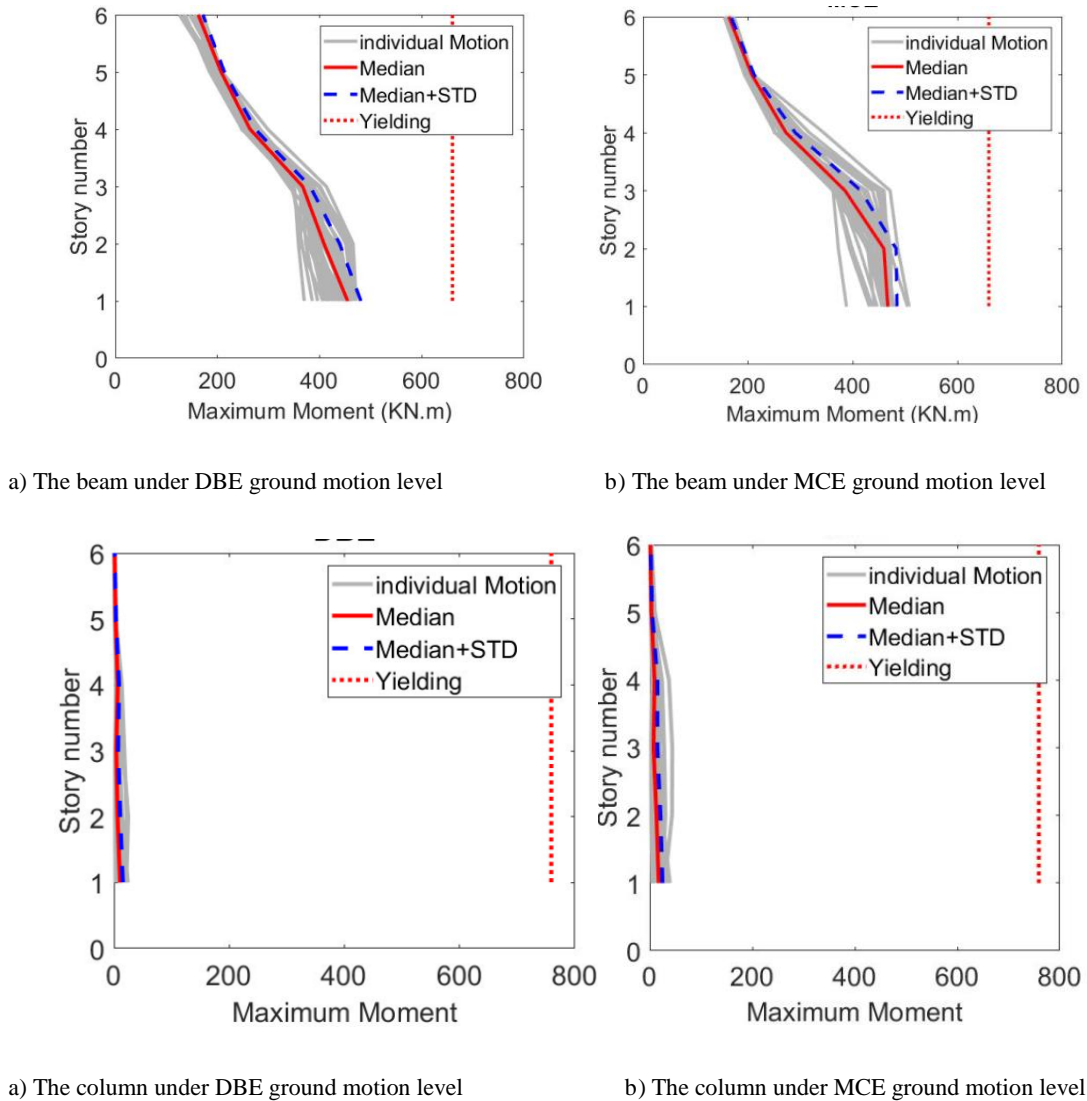
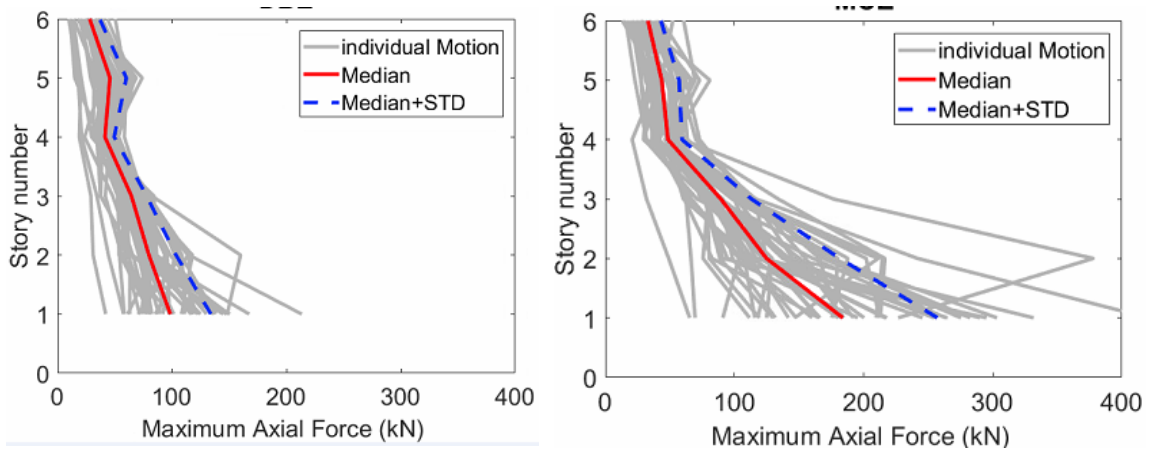


Figure 225. Investigation of beams and columns elastic behavior

In addition, the further analysis of the axial load indicates that the axial load in the system is approximately equal to 110KN and 185KN for DBE and MCE ground motion levels for the lowest story level, which has the highest axial load demand and is shown in Figure 226. It is concluded

that the axial load demand significantly less than the yielding strength of the links. From the NRHA analysis, it is concluded that the structure with shear links is able to dissipate more energy within each story level, have less shear angles values, and less beam demands for the lower stories compared to conventional systems. In addition, replaceability is another reason that shear links could be implemented within the structures.



a) The axial load under DBE ground motion level

b) The axial load MCE ground motion level

Figure 226. Investigation of the axial load within the fuse

# 11. Conclusions

Advances in structural systems that resist extreme loading such as earthquake forces are important in their ability to reduce damages, improve performance, increase resilience, and improve the reliability of structures. Buckling resistant shear panels can be used to form new structural systems, which have been shown in the previous analysis in this study to have improved hysteretic behavior including increased stiffness and energy dissipating ability. Both of these characteristics lead to reduced drifts during earthquakes, which in turn leads to a reduction of drift related nonstructural damage. Shear links are being used for seismic energy dissipation in structures. During a severe earthquake, inelastic deformation and damage would be concentrated in the shear link fuses, while the other normal steel elements would remain in the elastic state, which improves the structural performance under higher seismic loading conditions. In what follows, the general summary of investigations in this study on the seismic links is explained in more details.

## 11.1. Summary of the steps of this research and applications

The original contribution of the research is to establish a design methodology based on which the links would have ductile modes behavior instead of brittle ones. By understanding the load-resisting behavior of the links, it is tried to address the previous shortcoming associated with fuses in general. The mathematical concepts for describing the common limit state behavior of the links are developed in this research. The ductile limit states (e.g. shear and flexure) are investigated based on the general geometrical properties of the links, and the brittle limit state (e.g. lateral torsional buckling) is formulated based on the differential equation governing the behavior of the link.

Along the same lines, new structural fuses shapes are established based on the concepts provided in this research and previous studies for use not only for having an economical design, but also for improving the general seismic links behavioral aspects (e.g. strength, and stiffness). A common class of structural fuses is those consisting of a structural steel element deformed in shear. Links are defined here as relatively short lengths of steel that undergo shear or flexural yielding and are

utilized in the larger structural fuse panel. Links can be created through the strategic removal of material, which are essentially called “Strategic Cutouts”. Based on the common theories, the behavior of the links are established, and behavioral prediction equations are derived for general type butterfly-shaped links.

Next, the finite element (FE) methodologies are explained and the finite element modeling methodology of the links is confirmed with laboratory tests. The mathematical derivation methodologies for explaining the behavior of the links are shown to be accurate. The implementation of the links in prototype statures is delineated for use in areas with seismic potential. It is noted that in this work the geometrical solutions rather than material behavior are investigated for addressing the common issues associated with the links. The limit states and backbone behavior including the post-yielding behavior of the links are evaluated with prediction equations and then compared with results of FE analysis to verify the accuracy of prediction equations.

Two parametric computational studies were completed on butterfly-shaped links to study the effect of varying geometries on the shear yielding and flexural yielding limit states as well as the buckling behavior of the different butterfly-shaped link geometries and the results (e.g. over strength, dissipated energy, equivalent plastic strain) are summarized and interpreted. The work culminates in a system-level validation of the proposed structural fuses with the design and analysis of shear link structural fuses for application in three buildings with different seismic force resisting imperfection.

Based on the results of previous analysis and investigations, three different groups of structural of applications are selected, and for each one of them, a set of at least six models are designed and computationally analyzed to compare the seismic links implemented models with conventional structures. Subsequently, two multi-story structures are designed and developed for comparison of the building with seismic fuses to conventional structures. Ultimately, nonlinear response history analysis for 44 ground motions is further conducted on multi-story models to investigate the structural behavior of a system with and without structural seismic links under DBE and MCE hazard levels.

## **11.2. Summary the analytical investigations, prediction equation, and limit states investigations**

Common type of structural fuses is subjected to shear deformations. Links are chosen for use in the structural fuses to improve the overall behavior of the structure (e.g. strength, stiffness, ductility, and energy dissipation). There are many studies investigating the behavior of different links shapes and fuses. Use of strategic cutout would lead to the efficient implementation of the material and postpone or prevent the brittle limit states such as buckling. The butterfly-shaped links show four different categories of behavior based on the geometry of the link, which is concisely mentioned:

First, the pure flexural behavior, which would develop flexural hinges,  $M_p$ , could be occurred along the link length due to high flexural moment demands, compared to less shear forces. The energy dissipation would occur by developing of flexural yielding hinges.

Second, the pure shear behavior, developing shear forces,  $V_p$ , along the length of the links. The energy dissipation would occur by shear plastic rotations.

Third, the combination of flexural and shear stresses together. For this type of links, the shear and flexure both contribute to the energy dissipation.

Fourth, in addition to the flexural and shear limit states, which contributes to strength, stiffness, and ductility of the butterfly-shaped or straight link, the torsional buckling behavior represents a critical limit state, which has been observed in a number of studies. (Ma et al., 2010). This limit state would be considered brittle and could limit the load-resisting capacity and stiffness of the links significantly (Lee et al., 2016).

In general, any sacrificial structural elements with appropriate ductility and capability of energy dissipation used in the structure could be implemented as a fuse. These fuses studied in this research although have advantages over the conventional systems (e.g., buckling resistance); however, they could be employed with self-centering mechanisms for having approximately zero residual drifts, which allows replacing the links.

Butterfly-shaped structural fuses are a type of hysteretic damper used for seismic energy dissipation that consist of a set of butterfly-shaped links cut into a steel plate and subjected to shear

deformations. Previous testing has shown that these plates are capable of substantial ductility and energy dissipation, but can also be prone to multiple limit states. The investigations in this research developed equations to predict the shear strength of butterfly-shaped links associated with the three primary limit states of lateral torsional buckling, flexural yielding, and shear yielding.

For lateral torsional buckling, the governing differential equation was derived and a numerical solution method was used to obtain the critical buckling strength for 64 configurations with a range of geometric parameters ( $L/t=10$  to  $60$ ,  $b/L=0.1$  to  $0.4$ ,  $a/b=0.1$  to  $1.0$ ). Regression analysis was used to fit a closed-form cubic equation to the data to provide an easy means for calculating shear strength associated with lateral torsional buckling. The equation was shown to have 3.2% error compared to the differential equation over the range of parameters considered. Using the prediction equations, the effect of geometric variables on the expected behavior of the butterfly-shaped links was evaluated. It was found that since the predicted strengths associated with all three limit states vary quadratically with the scale factor, that the three nondimensional parameters (i.e. slenderness ratio,  $L/t$ , aspect ratio,  $b/L$ , and taper ratio,  $a/b$ ) are more important than the scale (i.e. overall size) in predicting which limit state controls and thus more important for predicting behavior.

Elastic finite element models with realistic boundary conditions were used to evaluate the accuracy of the lateral torsional buckling strength equation, which found an average difference of 1.3% for a set of 10 configurations. Finally, inelastic finite element models were used to evaluate the accuracy of the strength prediction equations. Three configurations were examined more thoroughly, while 20 configurations were evaluated in total and it was found that the prediction equations were capable of capturing the correct limit state and peak shear load within 0.6%. The buckling resistant design concepts include local yielding mechanisms that enhance the global seismic performance while improving the efficiency of the shear panel. This study would investigate the implementation of the links concepts provided in previous chapters in prototype buildings. The implementation of the extension of this study could directly improve the usage of steel plate in different applications (e.g. bay bridges, EBF link beam, linked column, and steel shear walls).

Equations for shear strength associated with flexural and shear limit states are proposed and a critical butterfly angle is derived to delineate the transition from the shear to flexure-controlled behavior. Similar equations are developed for straight links and a critical length is defined for the

transition between shear and flexure controlled behavior. Along the same lines, the geometrical post yielding hardening of the links are mathematically explained. In addition, the stiffness of panels with either butterfly-shaped or straight links is derived consisting of four contributing parts to deformation: link flexure, link shear, and end zone shear and flexure stiffnesses.

### **11.3. Summary of the finite element investigations**

The computational approaches for analyzing the seismic links are delineated. The assumptions and modeling procedure are investigated in details. To confirm the methodology for computational study, the tests done by Ma et al. (2011), Lee et al. (2015), Driver et al. (1998), and Ascheim et al. (2002) are verified under a monotonic and cyclic condition with FE results. The modes of behavior of the experimental studies are captured with computational modeling methodology. Along the same lines, the imperfections study are explained and the appropriate values for imposing imperfection are mentioned. The mesh type and mesh convergence studies are described and appropriate mesh size is reported in this part.

The equations provided for shear and flexural limits state were investigated and validated against the models made in the FE program. The governing buckling equations are investigated, and mathematical method to capture the data in previous chapters is validated. In addition, to validate the proposed equations, two example configurations, one flexure-dominated and one shear-dominated butterfly link were investigated using FE models after validation of finite element methodology against laboratory tests. The shear strength and stiffness from FE models were compared with the derived equations and it was shown that for two examples, the first limit state and stiffness were predicted within 3% and 5% error, respectively. The post-yielding behavior is investigated and by considering a sample of 16 FE models the validity of the proposed equations are compared for complete backbone behavior of butterfly-shaped links. It is shown that for the elastic behavior and the occurrence of first limit state the equations are accurate within 96%, while for the post-yielding behavior the equations predict the behavior with 91% accuracy up to 6 percent drift in butterfly-shaped and straight links. It is concluded that configurations that encourage flexural yielding at the quarter points (i.e.  $a/b=1/3$ ) have been shown to possess large ductility. However, configurations with flexural yielding at ends (i.e.  $a/b \geq 1/2$ ) or the ones dominated by shear yielding may not have as much ductility.

## 11.4. Summary of a computational parametric study on seismic links

Hysteretic dampers with butterfly-shaped shear links have been shown in past research to be an effective way to dissipate seismic energy. It has also been shown in previous research that the geometry of butterfly-shaped shear links can be characterized by three nondimensional ratios, namely the taper ratio ( $a/b$ ), the slenderness ratio ( $L/t$ ), and the width ratio ( $b/L$ ). This part of this research study investigated the effect of the three key butterfly-shape geometric parameters on link behavior. A parametric computational study using a validated computational modeling approach was conducted on 112 configurations to investigate the location of plastic hinges, accumulation of plastic strains, the occurrence of buckling, energy dissipation and equivalent viscous damping.

The three primary limit states for butterfly-shaped links are flexural yielding, shear yielding, and lateral torsional buckling. The trends in observed plastic hinge location show that for small taper ratios ( $a/b=0.1$ ), shear yielding occurs at the middle of the link and that for large taper ratios ( $a/b=0.75$  and  $1.0$ ), flexural hinges form at the ends of the link. The models also corroborate previously derived equations that predict that a taper ratio of  $a/b=0.33$  cause flexural plastic hinges to form at the quarter points midway between the middle and ends of the link since flexural stresses has significant contributions in hinge development locations. The magnitude of equivalent plastic strains can be an order of magnitude larger for straight links ( $a/b=1.0$ ) as compared to butterfly-shaped links that promote more distributed yielding along the link length (e.g.  $a/b=0.33$ ). This suggests that straight links will have less inelastic deformation capacity which is consistent with past testing. The results also suggest that having even a little taper (e.g.  $a/b=0.75$ ) causes a substantial reduction in equivalent plastic strains.

The taper ratio and width ratio were shown to control the amount of hardening and overstrength a butterfly-shear link will develop in which the overstrength was defined as the peak shear force from the FE model divided by the shear yield force and did not consider fracture. The configurations with taper ratio  $a/b=0.33$  led to smaller overstrength, between one and two whereas other taper ratios led to overstrength as large as four for width ratios of  $b/L=0.1$  and approximately two for width ratio of  $b/L=0.4$ .

It was shown that configurations with wide links (large  $b/L$ ) and thin plates (large  $L/t$ ) were susceptible to lateral torsional buckling which reduced the amount of energy dissipation and

equivalent viscous damping. However, these configurations produced larger equivalent viscous damping at small shear angles because they become inelastic at smaller drift angles. In general, the results of this study reinforce previous research that recommends  $a/b=0.33$  to create flexural plastic hinges at the quarter points, promote inelasticity away from geometric discontinuities (i.e. corners), and thus resist fracture. The  $a/b=0.33$  geometry was also found to limit the amount of hardening and overstrength which is expected to lead to the more economical design of the surrounding frame. If larger hardening is desirable to encourage the spread of inelasticity to as many structural fuses as possible, then smaller width ratio (e.g.  $b/L=0.1$ ) and larger taper ratio (e.g.  $a/b=0.75$ ) are recommended. In some cases, thinner links that experience lateral torsional buckling may be desirable to produce inelasticity at small drift angles or to cause strength degradation after some inelasticity.

### **11.5. Summary the applications of seismic fuse system and nonlinear-response history analysis**

The general fuses used in prototype buildings are divided into three groups according to the applications studied previous literature review. The three groups are named as follows: First, Single Row of Links (SRLs), which indicates a set of links in a row, which is based on the EBF, linking beam and linked column applications, etc. Second, Multiple Rows of Links (MRLs), which is based on the panel behavior (e.g. bay bridge application). Third, Perimeter Rows of Links (PRLs) which is based on the implementation of the links in the solid steel plate (e.g. steel shear walls).

The strategically shifting the ductile mechanism from buckling and yielding in tension toward local flexure and shear yielding would enhance the hysteric behavior and energy dissipation. The results from the effect of the link investigation on different prototype buildings and the comparison between the structural system having links with the structure without any links are investigated. It is shown that new configurations and design concepts that convert global shear deformations into local flexural yielding mechanisms would be beneficial for steel structures applications because they improve the energy dissipation capability and reduces the demand on the structural boundary

elements. By controlling, the yielding mechanisms to occur as the flexure and shear across the discrete segments of the steel, the prototype buildings resist the buckling efficiently.

Based on the mechanics, equations, and the results of the parametric studies using FE models, design tools are developed that allow individual tuning aspects of lateral resistance behavioral features such as stiffness, and strength. The possibility of developing mathematical equations to describe the behavior of implementation of links in prototype building is expected.

Next, the effect of implementation of the seismic links in multi-story structures is investigated by analyzing two prototype structures, with butterfly-shaped links and simple conventional beam. The results of the nonlinear response history analysis are summarized for 44 ground motions under MCE and DBE ground motion hazard levels. It is shown that implementation of the butterfly-shaped links in buildings with similar stiffness and strength to conventional system will lead to higher dissipated energy or larger hysteric curves compared to conventional EBF systems. In addition, it is shown that the demand for the lower story boundary elements for conventional system is larger than the corresponding demand for the systems with structural seismic links. The general stiffness and strength of the system with the butterfly-shaped link is close to conventional models; however, the demands on the boundary elements are lower than the corresponding conventional model.

## **11.6. Concluding remarks and recommendation for further studies:**

By synthesizing the results, design and proportioning rules were developed with an emphasis on the ability to separately design for the system properties such as strength, stiffness, and ductility. Design considerations will be explored to determine how these new concepts could be applied in real structures such as buildings and bridges. The practical guidelines leading to efficient performance of seismic fuses is one of the contributions of this research that will be disseminated to the structural engineering community.

The studies conducted in this research investigated the behavior of the yielding links elements. Although yielding links have been used in a limited way in prior research, the computational and analytical studies led to a fundamental knowledge about the mechanics of how a ductile link behave under loading. The results of this project has the potential to improve the seismic

performance of the built environment and reduce the earthquake losses. Further recommendation for future studies are as follows:

- By the general procedures mentioned in this research, it is possible to investigate other structural seismic fuse systems for ductile and brittle limit states (e.g. lateral torsional buckling).
- The effect of axial loading on buckling behavior equation is recommended to be further studied and incorporated in governing differential equations, although it is expected that this effect is limited compared to lateral torsional buckling effect as one of the main brittle limit states.
- The seismic design parameters, such as the R factor, is recommended to be derived. The overstrength factor used for seismic design is elaborated in this research for seismic investigation.
- The effect of steel plate shear walls for the multi-story building is recommended for further investigations, the studies in this work show that these steel plate shear walls with seismic links are able to dissipate a significant amount of energy while reducing the boundary element demand forces.

# REFERENCES

- Asselin R.E., Fahnestock L.A., Abrams D.P., Robertson N., Ozaki-Train R. and Mitsuyuki S. (2012), “Behavior and Design of Fuse-Based Hybrid Masonry Seismic Structural Systems I”. *15 WCEE conference*, Lisbon.
- Aschheim M. and Halterman A. (2002), “Reduced Web Section Beams: Phase One Experimental Findings And Design Implications”. *The Earthquake Engineering Online Archive*, NISEE e-Library.
- El-Bahey S., and Bruneau M. (2012), “Bridge Piers with Structural Fuses and Bi-Steel Columns”, *Journal of Bridge Engineering*, 17 (1).
- Berman J., and Bruneau M. (2003), “Plastic Analysis and Design of Steel Plate Shear Walls”, *Journal of Structural Engineering*, 129 (11).
- Buckle I., Dusicka P., and Itani A. (2005), “Development of built-up shear links as energy dissipaters for the seismic protection of long-span bridges”, *Bridge Structures*, 1 (1), pp. 19-27.
- Cortes G., and Liu J. (2008), “Steel slit panel configurations”, *The 14<sup>th</sup> World Conference on Earthquake Engineering, Beijing, China*.
- Castiglioni C.A., Drei A., Kanyilmaz A., Calado L., Vayas I., Hoffmeister B., Gonçalves R. (2012), “Numerical and Experimental Results of Project FUSES (Seismic Resistant Composite Steel Frames)”, *15 WCEE, Lisbon*.
- Chaofeng Z., Zhisheng Z., and Jinfei S. (2012), “Development of high deformation capacity low yield strength steel shear panel damper”, *Journal of Constructional Steel Research*, 75(2012): 116-130.
- Chan R., Albermani F., and Williams M. (2009), “Evaluation of yielding shear panel device for passive energy dissipation” *Journal of Constructional Steel Research*, 65 (2009) 260–268.
- Cheng C. and Chen C. (2004), “Test and behavior of steel beam and reinforced concrete column connections”. *3rd World Conference on Earthquake Engineering, Vancouver, B.C., Canada*.

- Deng K., Pan P., Sun J., Liu J., and Xue Y. (2014), “Shape optimization design of steel shear panel dampers,” *Journal of Constructional Steel Research*, vol. 99, pp. 187–193.
- Dusika P., M. Itani A., and G. Buckle I. (2004), “Cyclic response of plate steels under large inelastic strains”, *Journal of Constructional Steel Research*, 63 (2), pp. 156-164.
- Dusika P., M. Itani A., and G. Buckle I. (2004), “Finite element investigation of steel built-up shear links subjected to inelastic deformations”. *Earthquake Engineering and Engineering Vibration*, 3 (2), pp. 195-203.
- Dutta A. (2008), “Design of Eccentrically Braced Frames”, Presentation. [http://engineering.sfsu.edu/download/Design\\_of\\_Eccentrically\\_Braced\\_Frames.pdf](http://engineering.sfsu.edu/download/Design_of_Eccentrically_Braced_Frames.pdf)
- Eatherton M. (2010), “large-scale cyclic and hybrid simulation testing and development of a controlled-rocking steel building system with replaceable fuses”, the University of Illinois at Urbana-Champaign, Dissertation.
- Enrique J. and Rueda M. (2002), “On the Evolution of Energy Dissipation devices for seismic design”, *Earthquake Spectra*, 18 (2), pp. 309-346.
- Egorova N, Eatherton M., and Maurya A. (2014) “Experimental study of ring-shaped steel plate shear walls”, *Journal of Constructional Steel Research*, vol. 103, pp. 179-189.
- El-Bahey S., and Bruneau M. (2010), “Structural Fuse Concept for Bridges”, *Proceedings of the 9th U.S. National and 10th Canadian Conference on Earthquake Engineering*. Toronto, Ontario, Canada.
- El-Bahey S., Bruneau M., Fujikura S., and Keller D. (2010), “Structural Fuses and Concrete-Filled Steel Shapes for Seismic- and Multi-Hazard Resistant Design”, *NZSEE Conference*.
- Farzampour A. and Eatherton M. (2019), “Yielding and lateral torsional buckling limit states for butterfly-shaped shear links “, *Engineering Structures*, vol. 180, pp. 442-451.
- Farzampour A. and Eatherton M. (2018a), “Investigating Limit States for Butterfly-Shaped and Straight Shear Links “, *16th European Conference on Earthquake Engineering, 16ECEE, USA*.

Farzampour A. and Eatherton M. (2018b), "Parametric Study on Butterfly-shaped Shear Links with Various Geometries", *11th National Conference on Earthquake Engineering, 11NCEE, Los Angeles, USA*.

Farzampour A., Mansouri I. and Hu J.W. (2018c), "Seismic behavior investigation of the corrugated steel shear walls considering variations of corrugation geometrical characteristics", *International Journal of Steel Structures*, 18 (4), pp. 1297-1305.

Farzampour A., Mansouri I., Lee C.H., Sim. H. and Hu J.W. (2018d), "Analysis and design recommendations for corrugated steel plate shear walls with a reduced beam section", *Thin-Walled Structures*, vol. 132, pp. 658-666.

Farzampour A., Eatherton M., Mansouri I. and Hu J.W. (2018f), "Simultaneous Consideration of Shear and Flexural Stresses for Butterfly-Shaped Dampers Design", *The 3rd International Conference on Material Engineering and Application*, China.

Farzampour A. and Eatherton M. (2017), "Buckling Of Butterfly-Shaped Shear Links", *SSRC Annual Stability Conference, San Antonio, Proc. of Annual Stability Conference Structural Stability Research Council, Best paper, Vinnakota Award, San Antonio, USA*.

Farzampour A., Mansouri I. and Hu J.W. (2017), "Investigation of seismic behavior of corrugated steel shear walls considering variations of corrugation geometrical characteristics", *9th International Symposium on Steel Structures*, Korea.

Farzampour A., Laman J. A. and Mofid M. (2015), "Behavior Prediction of Corrugated Steel Plate Shear Walls With Openings", *Journal of Construction Steel Research*, vol. 144, pp. 258-268.

Farzampour A. and Yekrangnia M. (2014), "On the Behaviour of Corrugated Steel Shear Walls with and without Openings," *Second European Conference on Earthquake Engineering and Seismology*.

Ghabrai K., Chan R., Huang X., and Xie Y. (2010), "Shape optimization of metallic yielding devices for passive mitigation of seismic energy," *Journal of Constructional Steel Research*, vol. 32, pp. 2258–2267.

Hanson R.D., Xia C., and Su Y. (1992), “Design supplemental steel damping devices for buildings”, *Earthquake Engineering*, Tenth Conference.

Harries K., Gong M., Shahrooz B. (2000), “Behavior and Design of Reinforced Concrete, Steel, and Steel-Concrete Coupling Beams”. *Earthquake Spectra*, 16(4), pp. 775-799.

He H., Wang X., and Zhang X. (2016), “Energy-Dissipation Performance of Combined Low Yield Point Steel Plate Damper Based on Topology Optimization and Its Application in Structural Control”, *Advances in Materials Science and Engineering*, vol. 2016

Hitaka T., and Matsui C. (2003), “Experimental Study on Steel Shear Wall with Slits”. *Journal of Structural Engineering*, 129(5).

Hitaka T., and Matsui C. (2006), “Seismic performance of Steel Shear Wall with Slits integrated with multi-story composite moment frame” *5th, International conference on the behavior of steel structures in seismic areas; Stessa 2006, Yokohama, Japan.*

Hanson R.D., Xia C., and F.Su Y. (1992), “Design of supplemental Steel Damping devices for buildings”, *Earthquake Engineering*, Tenth World Conference.

Ji X., Ma., Q, Wang. Y., and Okazaki T. (2014), “Cyclic behavior of steel shear Links used in replaceable coupling beams,” *Tenth U.S. National Conference on Earthquake Engineering*.

Ji X., Wang. Y., Ma Q., and Okazaki T. (2015), “Cyclic behavior of steel shear Links,” *Journal of Structural Engineering*, 143 (2).

Kawai Y., Ono T., Sato A., and Kondo M. (2016) “ Allowable Design Formula for Steel Sheet Shear Walls with Burring Holes”. *Proceedings of the 7th International Conference on Coupled Instabilities in Metal Structures Baltimore, Maryland.*

Katayama T., Ito S., Kamura H., Ueki T., and Okamoto H.(2000), “Experimental Study On Hysteretic Damper With Low Yield Strength Steel Under Dynamic Loading”, *WCEE Conference*.

Kobori T., Y. Miura, Fukuzawa, T. Yamanda, T. Arita, Y. Takenaka, N. Miyagwa, N. Tanaka, and T. Fukumoto (1992), “Development and application of hysteresis steel dampers”, *Earthquake Engineering*, Tenth Conference.

Köken A., and Alpaslan Köroğlu M. (2013), “Use of Steel Slit Dampers in Beam to Column Connections of Steel Frame Structures”, *International Conference Proceedings 2013*, Miskolc, Hungary

Köken A. and Köroğlu M.A. (2015), “Experimental Study on Beam-to-Column Connections of Steel Frame Structures with Steel Slit Dampers”. *Journal of Performance of Constructed Facilities*, 29(2).

Koppal and Eatherton (2013), “Perforated Steel Plate Shear Walls for Tunable Seismic Resistance”, *Structure Congress*.

Lee C., K. Ju Y., Min J., Lho S., and Kim S. (2015), “Non-uniform steel strip dampers subjected to cyclic loadings”, *Engineering Structures*, 99 (2015), pp. 192–204.

Lee C., Kim S., Kim D., Ryu J., and K. Ju Y. (2016), “Numerical and experimental analysis of the combined behavior of shear type friction damper and non-uniform strip damper for multi-level seismic protection”, *Engineering Structures*, 14 (2016), pp. 75–92.

Lee C., Lho S., Kim D., Oh J., and K. Ju Y. (2015), “Hourglass-shaped strip damper subjected to monotonic and cyclic loadings”, *Engineering Structures*, 119 (2016), pp. 122–134.

Lee C., Woo S., K. Ju Y., Lee D., Oh J., Kim S. (2014), “Modified Fatigue Model for Hourglass-Shaped Steel Strip Damper Subjected to Cyclic Loadings”, *Journal of Structural Engineering*, 141 (8).

Lepage A., Ascheim M. and Senescu R. (2004), “Shear-Yielding Steel Outriggers for High-Rise Construction”, *13th World Conference on Earthquake Engineering, Vancouver, B.C., Canada*.

Li H., and Li G. (2007), “Earthquake-Resistant Design Of Rc Frame With “Dual Functions” Metallic Dampers”, *ASME Pressure Vessels and Piping Division Conference. San Antonio, Texa.s*

Li H., and Li G. (2013), “Experimental Study and Application In Steel Structure Of ‘Dual Functions’ Metallic Damper”, *Advanced Steel Construction*, 9(3), pp. 247-258.

Li H., and Li G. (2010), “Advances in Structural Control in Civil Engineering in China”, *Mathematical Problems in Engineering*, Volume 2010.

Li H., and Li G. (2007), "Earthquake-Resistant Design Of Rc Frame With "Dual Functions" Metallic Dampers", *ASME Pressure Vessels and Piping Division Conference*. San Antonio, Texas

Liu Y., and Shimoda M. (2013), "Shape optimization of shear panel damper for improving the deformation ability under cyclic loading", *Struct Multidisc Optim*, 48:427-435.

Lopes A.P., Dusicka P., and W. Berman J. (2012), "Design of the Linked Column Frame structural system", *Taylor & Francis Group, Stessa*.

Lopez W.A., and Sabelli R. (2004), "*Seismic Design of Buckling-Restrained Braced Frames*". Structural Steel Educational Council, Technical information and product service. NEHRP Seismic Design Technical Brief No. 11, NIST GCR 15-917-34.

Luth G., Krawinkler H., McDonald B., Park M. (2008), "USC School of Cinema, An Example of Reparable Performance Based Design", *SEAOC 2008 CONVENTION PROCEEDINGS*.

Liu Y., and Shimoda M. (2013), "Shape optimization of shear panel damper for improving the deformation ability under cyclic loading", *Struct Multidisc Optim*, 48:427-435.

M. Itani, Lanuad C., and Dusika P. (2003), "Analytical evaluation of built-up shear links under large deformations", *Computers & Structures*, 81 (8-11), pp. 681-696.

Ma X., Eric B., Pena A., Krawinkler H., Billington S., Deirelein G., (2011), "Design and behavior of Steel Plate Shear Walls with Opening Dissipation Fuses", *Department of Civil and Environmental Engineering Stanford University*. Report No. 173.

McCloskey D.M. (2006). "Steel Slit Panels for Lateral Resistance of Steel Frame Buildings", *Thesis in Purdue University West Lafayette, Indiana*.

Maleki S. and Bakeri S. (2010), "Pipe damper, Part I: Experimental and analytical study", *Journal of Constructional Steel Research*, 66 (8-9), pp. 1088-1095.

Malakoutian M., W. Berman J., and Dusika P. (2012), "Seismic response evaluation of the linked column frame system", *International Association for Earthquake Engineering*, 42 (6), pp. 795-814.

Nader M., Manzanarez R., and Maroney B. (2000), “Seismic design strategy of the new east bay bridge suspension Span”, *12 WCEE*.

Oh S., Kim Y., Tyo H. (2009), “Seismic performance of steel structures with slit dampers”, *Engineering Structures*, 31 (9), pp. 1997-2008.

P. Boresi A., J. Schmidt R., and M. Sidbottom O. (1992), “Advanced Mechanics of Materials”, John Wiley, Fifth Edition.

R. Phillips A., Eatherton M., and Koutromanos I. (2014), “Demonstrating the Applicability of Ring-Shaped – Steel Plate Shear Walls for Improved Seismic Performance”, *SEAOC 83<sup>rd</sup> Annual Conference Proceedings*.

RHINO, *Prefabricated steel building*,” <http://www.rhinobldg.com/prefabricated-steel-buildings>”.

M. Shahrooz B., E. Remmetter M., and Qu Fei “Seismic design and performance of Composite Coupled Beam”, *Journal of Structural Engineering*, 119 (11).

Shin M., Kim S., Halterman A., and Aschheim M. (2017), “Seismic toughness and failure mechanisms of reduced web-section beams: Phase 1 tests”. *Engineering Structures*. 141 (15), pp. 198–216

Shubhrata Nagpal and S.Sanyal, Nitin Jain (2011), “Mitigation Curves for Determination of Relief Holes to Mitigate Stress Concentration Factor in Thin Plates Loaded Axially for Different Discontinuities”, *International Journal of Engineering and Innovative Technology*, 2 (3).

Soong, T. T. (1990), *Active Structural Control: Theory and Practice*, 2nd edn., John Wiley.

Teruna D., A. Majid T., and Budiono. (2015), “Experimental Study of Hysteretic Steel Damper for Energy Dissipation Capacity”, *Advances in Civil Engineering*. Hindawi Publishing Corporation, 2015.

Tsai K., Chen H., Hong C., and Su Y. (1992), “Design of Steel TADAS Energy absorbers for seismic-resistant structures”, *Earthquake Spectra*, 9 (3), pp. 505-528.

Vian D., and Bruneau M. (2006), “Testing of special LYS Steel Plate Shear Walls”, *4th International Conference on Earthquake Engineering, Taipei, Taiwan*.

Whittaker A., V. Berto V., L. Thompson C. and L. Javier A. (1991), “Seismic testing of steel plate energy dissipation devices”, *Struct Multidisc Optim*, 48:427-435.

W.K. Chan R., and Albermani F. (2008) “Experimental study of steel slit damper for passive energy dissipation”. *Engineering Structures*. 30 (4), pp. 1058–1066.

Xiang N., Li J., and Guan Z. (2017), “Performance test of steel damper and its application in seismic mitigation of bridges”, *NZSEE Conference*.

Xu Y., Li Aiqun., Zhou X., and Sun P. (2011), “Shape Optimization Study of Mild Steel Slit Dampers,” *Trans Tech Publications, Switzerland*.

# APPENDIX

## APPENDIX A: FINITE ELEMENT MODELING PROCEDURES, PROCEDURES, AND RECOMMENDATIONS:

### A.1. Modeling techniques for structural fuses:

In this section, the procedure to set up the computational modeling is established. For this purpose, the mesh should be fine enough to have reasonable accuracy in capturing the behavior. (Figure 227). A study on the mesh size refining would show the appropriate number of elements along the different lengths of the butterfly-shaped links to reach to the desired results. The shell element with four nodes in reduced integration condition is chosen. The reduced integration property for finite element analysis is set to prevent the shear locking effect.

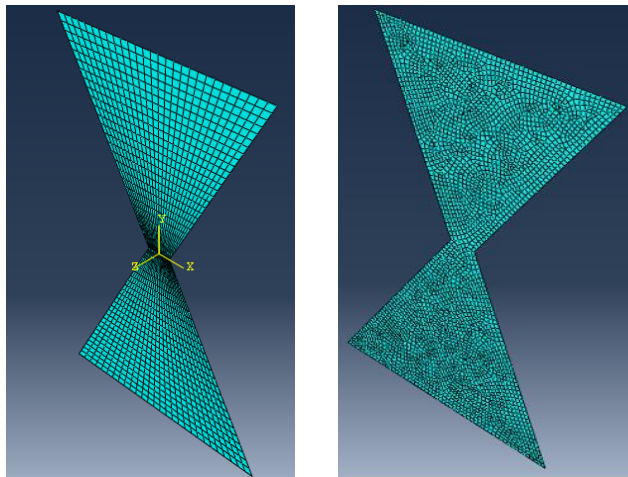


Figure 227. Structural and Free Meshed Butterfly link in ABAQUS

The simulation with the locally refined mesh required considerably less CPU time than the analysis with the very fine mesh. It is common to omit small details like fillet radii from a finite element model to simplify the analysis and to keep the model size reasonable. However, the introduction of any sharp corner (Figure 228) into a model may lead to a stress singularity at that location. This normally has a negligible effect on the overall response of the model, but the predicted stresses close to the singularity will be inaccurate.

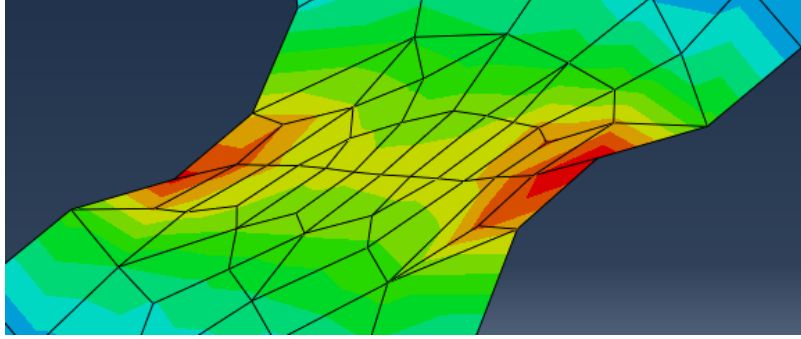


Figure 228. Singular points

The effect of the different fillet radii based on the general geometry of the section has been investigated through literature (Teruna et al. 2015). The problem associated with fillet in all the models is that the curvy fillet makes the problem of needle shape elements (Figure 229). Some needle-shaped elements inevitably would be generated which makes the equivalent plastic strain analysis imprecise.

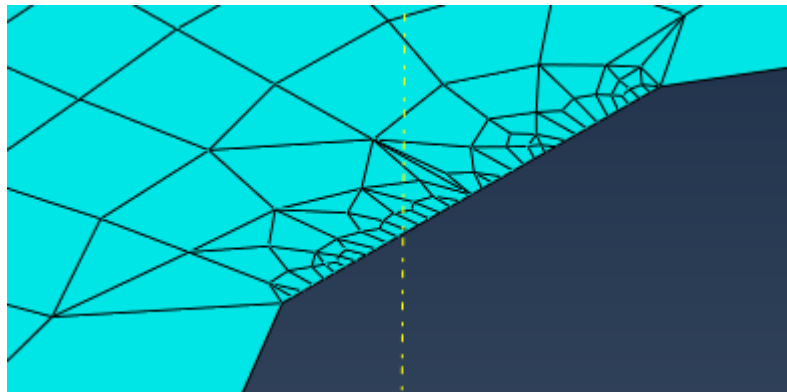


Figure 229. The fillet and the needle shape elements

The best way of generating mesh is through the angle edges and definition of a number of seeds due to making more reasonable consistent elements size at the sharp angles. The result of the mentioned suggestion is indicated in Figure 230. The pushover curve having enough number of elements at boundaries and at the middle would lead to precise results. The Equivalent Plastic Strain (PEEQ) for all of these models have converged as indicated in Table 29.

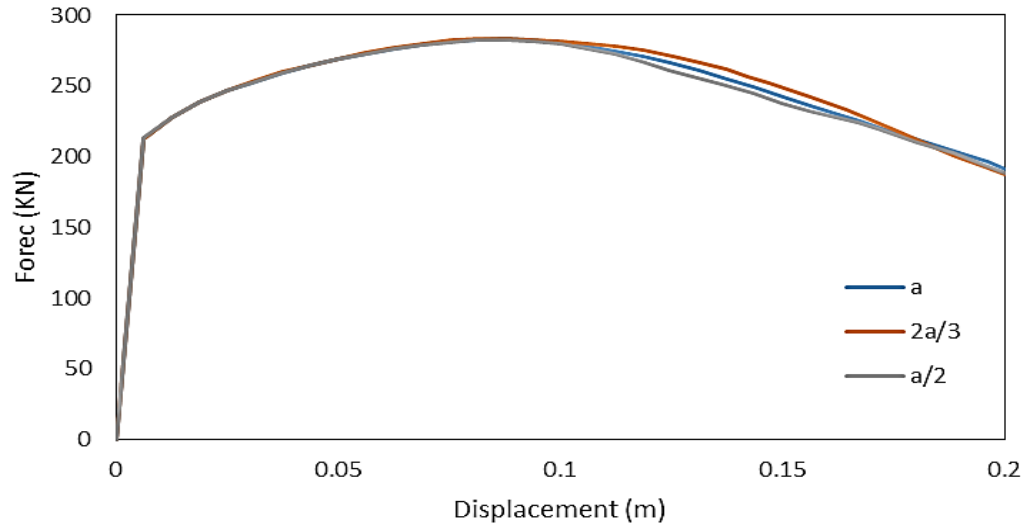


Figure 230. The mesh sensitive analysis and push over curves of different size elements

Table 29. The element size effect on equivalent plastic strain

Element size	Buckling initiation Displacement
a	0.22
2a/3	0.2325
a/3	0.23

For studying the sharp edges effect, sharp edges have removed and appropriate fillet size based on the literature (Teruna et al., 2015) is chosen based on the fillet size chosen in previous studies for straight links. The models are constructed in AutoCAD software first and then imported in ABAQUS. The meshing was chosen with a more regular pattern.

The rectangular plate with an aspect ratio of 4 to 1 and the butterfly link with b/a ratio of 3 are modeled with three different mesh sizes. In all the models the thickness is assumed to be 0.015mm. Table 30 and Table 31 shows the results of the study. Making the models in AutoCAD to be imported in the FE program would not make a significant difference in outputs based on the results. In general, the pushover curves would be converging with coarser mesh sizes. However, the equivalent plastic strain which is associated with some specified elements in the model would be converging with finer meshed models.

Table 30. The convergence for butterfly-shaped links

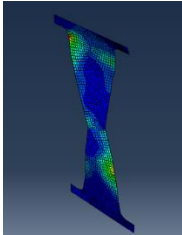
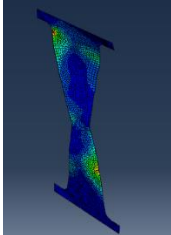
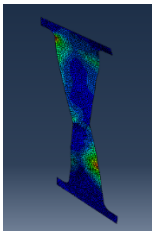
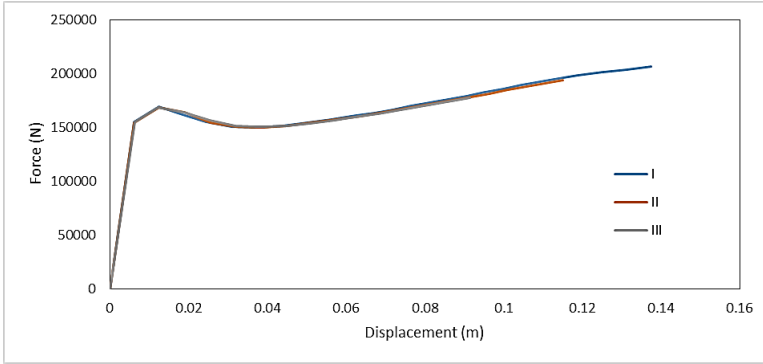
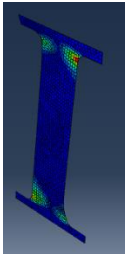
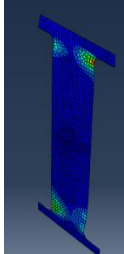
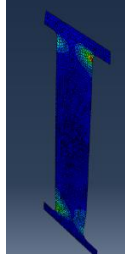
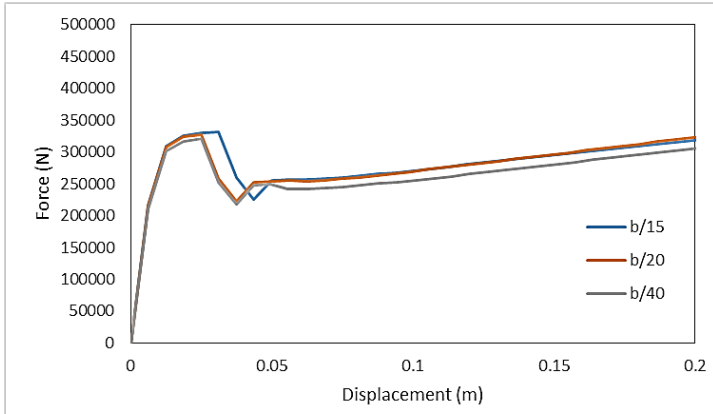
Name	Element size		
	I	II	III
Edge	$h/30$	$h/35$	$h/40$
Up/Down	$b/20$	$b/25$	$b/30$
Middle	$a/8$	$a/15$	$a/20$
			
Equivalent plastic strain	0.121	0.129	0.127
Pushover			

Table 31. The convergence for straight links

	Element size		
Edge Size Middle	b/15	b/20	b/40
The model behavior			
Equivalent plastic strain	0.106	0.117	0.13
Pushover			

## A.2. Meshing strategy:

This part is the summary of the number of models done in ABAQUS for mesh conversancy, basic modeling and verification purposes. The meshing strategy introduces a procedure for having the most accurate results from the FE program.

### A.2.1 Strategy:

-It is recommended that the points with the potential of singularity (sharp edges) should be modeled with the curved transition and with a reasonable radius which should be about the  $[\frac{a}{2} \text{ up to } a]$ , although the results would not be significantly different (more than 10 percent), specifically, in out-puts related to the whole elements (e.g. strength). Having the sharp edges

curved would impose some needle-shape elements to be developed, which would increase the analysis computational time tangibly.

-The fillet radii should be adequate. Small radius would impose needle shape meshed elements also.

-Based on the Mesh Sensitivity Analysis (MSA), for the butterfly-shaped link, it is recommended that the edges should be seeded by at least 30 elements, the upper and lower edges should be meshed by at least 20 elements and the middle part is recommended to be seeded by at least 8 elements noted that Ma et al. (2011) recommend to have at least 6 elements at the middle.

-For straight links, the link is recommended to be meshed at the upper or lower edges by at least 30, and the sides at least with 60.

-If the mesh is generalized by the mentioned strategy, the accuracy of equivalent plastic strain convergence has would be more than 92% compared to highly fined mesh and the pushover curves would have the accuracy of 98% compared to fine mesh. The error function is indicated in Eq. (160).

$$Error = \frac{(PEEQ_{fine} - PEEQ_{coarse})}{PEEQ_{fine}} \quad (160)$$

-Any larger size elements would lead to a difference in the element-type results (equivalent plastic strain) and has some effects on the general results of the system (e.g. pushover results).

-More refining of the mesh than what is recommended here would not have a significant effect on the general response of the structure.

-The general free mesh is also a suitable choice for meshing due to not making any needle shape elements, especially around the edges. The general mesh is conservatively chosen as the minimum value of between the element size at the inclined edge, element size at the side and element size at the middle.

### A.2.2. Notes on Meshing Strategy:

-Getting the equivalent plastic strain converged would be highly sensitive to mesh size because this quantity is sensitive to mesh size variation. Therefore, 8 percentage of error is considered satisfactory.

-If the equivalent plastic strain is converged, the pushover curves are already converged in most of the cases, which are verified based on the MSA study.

-AutoCAD sketches are recommended, because the fillet would be sketched highly precise, as opposed to the ABAQUS filleting toolbox, which is incapable of constructing smooth curves.

-Another way to mesh the butterfly-shaped link is to have the link in three different section as indicated in Figure 231. The meshing strategy for each section is according to Table 32. This meshing strategy would converge fast with satisfactory results.

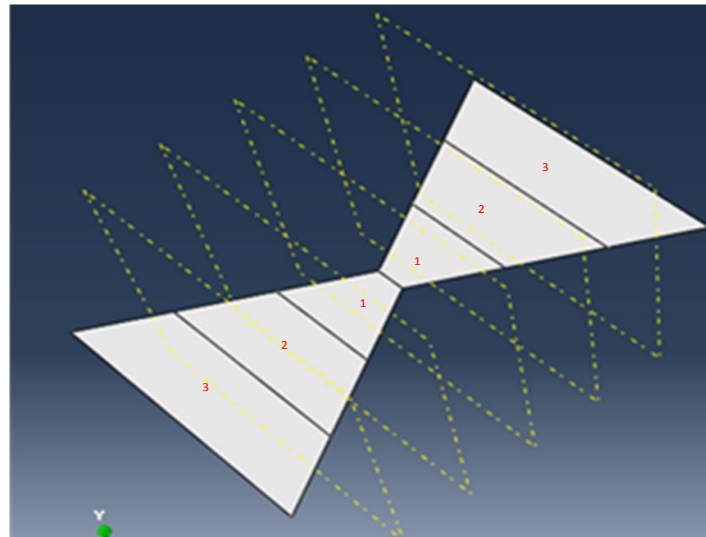


Figure 231. The three-zone meshing strategy

Table 32. The mesh size recommendation

Section No.	The element size (seed)
1	$\frac{[2(\frac{b}{20}) + (\frac{a}{8})]}{3}$

2	$\frac{\left[\left(\frac{b}{20}\right) + \left(\frac{a}{8}\right)\right]}{2}$
3	$\frac{\left[\left(\frac{b}{20}\right) + 2\left(\frac{a}{8}\right)\right]}{3}$

-To fully capture the effect of the boundary the band zone effect is considered in the FE analysis. The band zone is the rectangular shape zone at the bottom and the top of the butterfly-shaped link.

## APPENDIX B: IMPERFECTION STUDY:

As it is noted in any buckling problem, the effect of initial imperfection is undeniable. In this section, two different methods to apply the initial imperfections to the models are investigated. The effect of different values for imperfection study would be represented. The appropriate value for initial imperfection based on the literature would be proposed.

### B.1. Method I:

This method is done by setting up a shape for the specified buckled model and apply force on the edge to have the first buckling mode generated as indicated in Figure 232. Table 33 indicates the models implemented for this study, and the amount of the imperfection load applied to the edges of the butterfly-shaped links.

Table 33. First method imperfection study

L	a/b	b/L	L/t	a	b	t	Pflexure	Pshear	Percentage of the capacity	Imperfection loading (N)	Imperfection loading over the length (N/m)
0.5	0.33	0.2	60	0.033	0.100	0.008	22.110	47.631	0.02	442.200	884.400
0.5	0.33	0.2	60	0.033	0.100	0.008	22.110	47.631	0.1	2211.000	4422.000
0.5	0.33	0.2	60	0.033	0.100	0.008	22.110	47.631	0.2	4422.000	8844.000
0.5	0.33	0.2	60	0.033	0.100	0.008	22.110	47.631	0.3	6633.000	13266.000
0.5	0.33	0.2	60	0.033	0.100	0.008	22.110	47.631	0.6	13266.000	26532.000

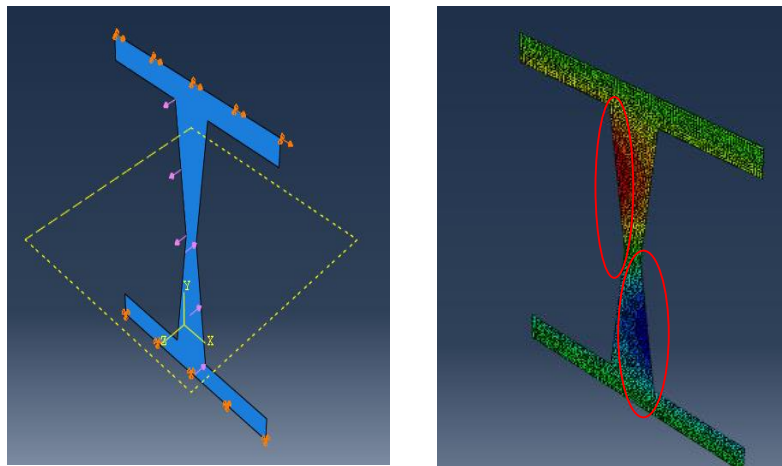


Figure 232. The first method of applying imperfection with edge purple loading

The result indicates that the general out-of-plane displacement would be different based on the loading applied to the edge. It is concluded that the initial imperfection does not have an effect on the pushover behavior of the links if the imperfection loading is within range of less than 30 percent

of capacity. Figure 233 is the summary of the pushover analysis for different cases with different imperfection loadings.

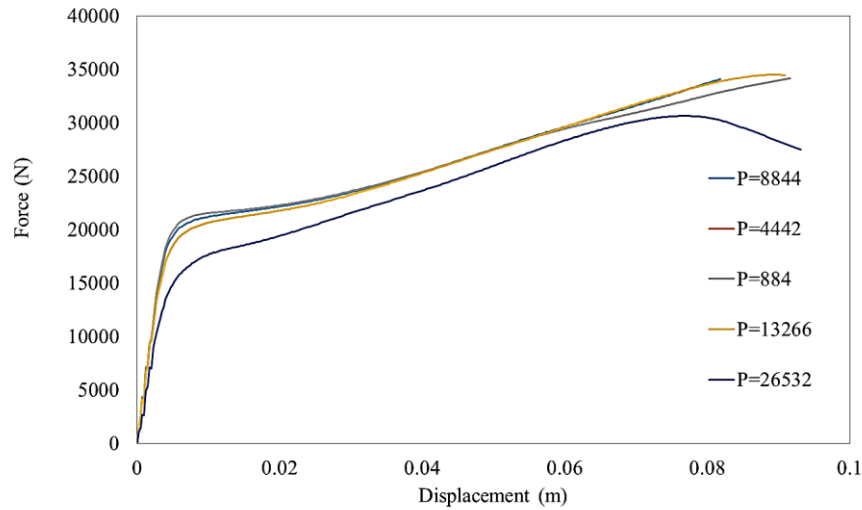


Figure 233. The effect of imperfection on pushover curves

To verify the results, the FE models are checked against the displacement equation that the entire imperfection loading has been just applied. The Eq. (161) is utilized to verify the out of plane displacement with displacement equations. Figure 234 indicates the simplified model for deflection calculation. The results are summarized in Table 34.

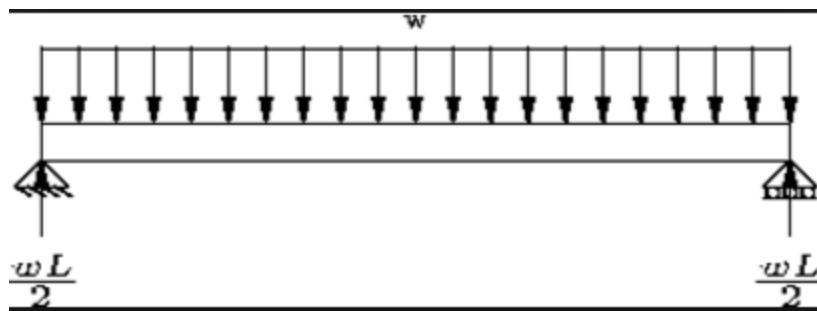


Figure 234. The imperfection loading condition simplified model for deflection estimation

The out of plane displacement is calculated based on the following equation.

$$\delta = \frac{5}{384} \frac{wL^4}{EI} \tag{161}$$

L is equal to 0.25 m, the I is taken with respect to the average size of the section which is the section at the middle of the butterfly-shaped link.

Table 34. The imperfection loading results for method 1

<b>L=0.5, a/b =0.33, b/t=0.2, L/t=60</b>					
P (N)	844	4442	8844	13266	26532
Max(U <sub>3</sub> in m)	1.5e-4	7.4e-4	1.3e-3	2.1e-3	4.0e-3
	L/602	L/500	L/384	L/238	L/131
Eq. (161) Calc.	1.4e-4	8.1e-4	1.63e-3	2.63-3	5.3e-3

P indicates the amount of imperfection loading per unit length applied to the structure, the max (U<sub>3</sub>) indicates the out-of-plane displacement of the model after the end of the analysis. It was decided to use a set value of 2mm for out-of-plane displacement, which indicates that if the out of plane displacement gets equal to 2mm, then the U<sub>1</sub> would be recorded as indicated Figure 235.

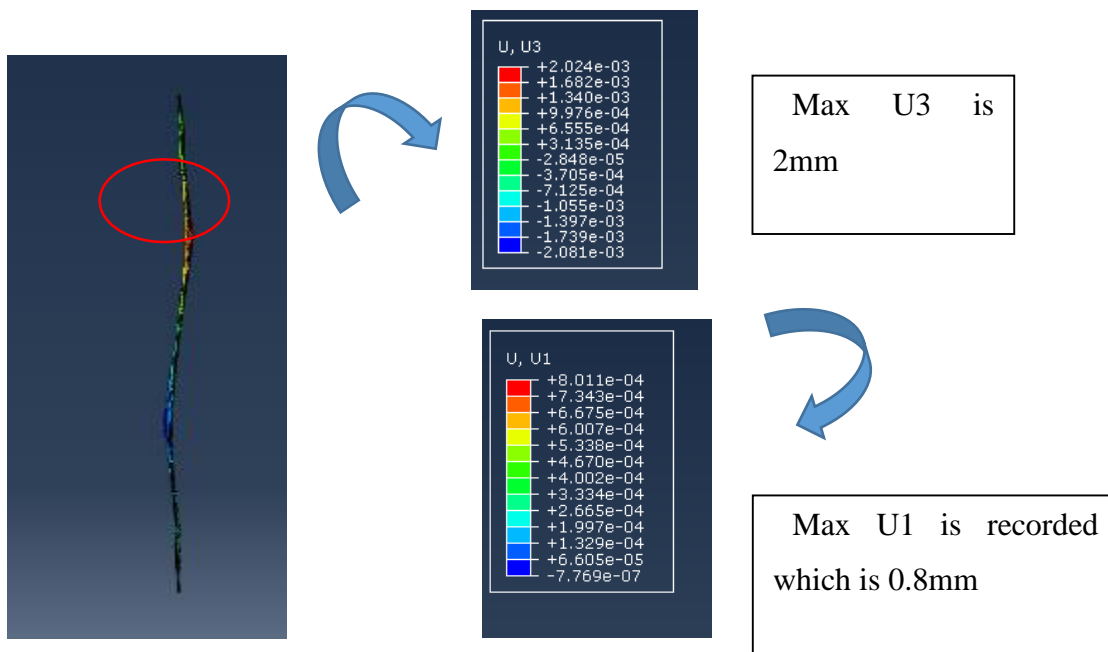


Figure 235. The procedure of recording the angle of shear for buckling investigation

Table 35 summarizes the shear angle for imperfection analysis of the butterfly-shaped links. It also indicates the associated U<sub>1</sub> values for each specified value of U<sub>3</sub>. By increasing the imperfection loads on the edges, the lower displacements (U<sub>1</sub>), would reach to the specified out-of-plane value of 2mm (U<sub>3</sub>). It is concluded that this method has limited accuracy in establishing the initial imperfections.

Table 35. Summary of the method 1 results

Load	U3	U1	shear angle
884	2mm	No buckling	NA
4442	3mm	8mm	0.016
8844	3mm	5.6mm	0.0112
13266	3mm	4mm	0.008
26532	3mm	0.8mm	0.0016

## B.2. Method II:

To investigate the imperfection behavior of the models the same model used in previous chapters with the same properties of  $L=0.5$ - $a/b=0.33$ - $b/L=0.2$ -  $L/t=60$  is considered. In this method, the buckling analysis of the first mode is done to estimate the buckling shape of the first mode for the butterfly-shaped links, as well as the first mode critical loading. The difference of this method with the method I is that in this method we are able to exactly define the amount of out-of-plane displacement based on any buckling mode. To model the fuse, first, a wire attached to the butterfly link with a tie would be defined. Then unit line load would be applied at the wire to induce the buckling loading condition, and subsequently buckling analysis will be conducted (Figure 236).

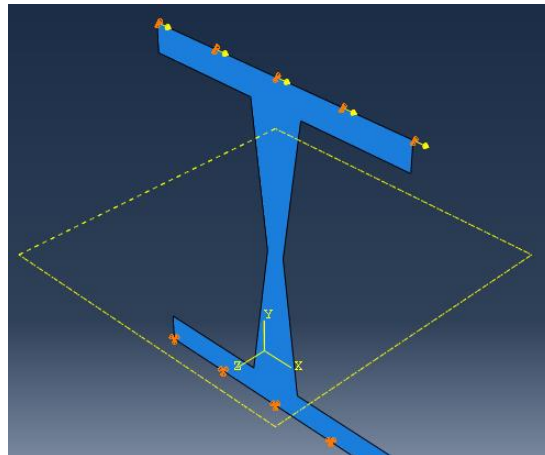


Figure 236. All the loadings and boundary conditions ( no vertical load)

The first four modes are indicated in Figure 237.

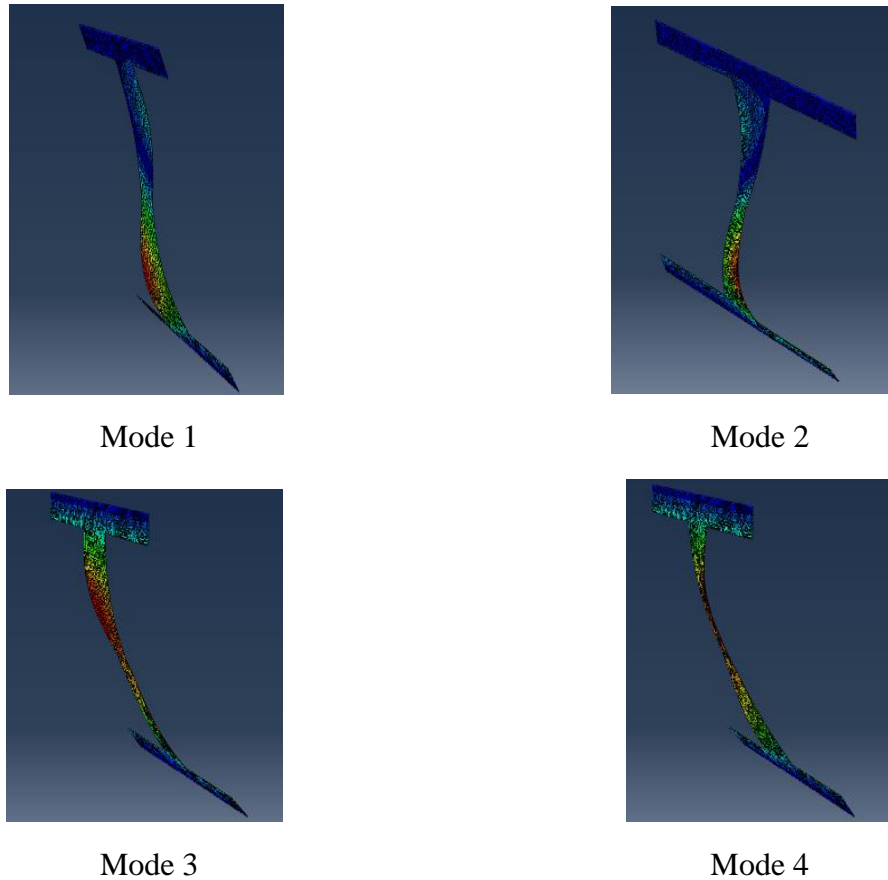


Figure 237. The first four different mode shapes of the butterfly-shaped link

As it is noted, the first and second modes are similar to each other. The third and fourth mode also are similar to each other. The total loading to initiate the buckling is estimated based on the EigenValue analysis of the four modes indicated in Table 36.

Table 36. The Eigen Value analysis

Eigenvalue		
mode	loading per distance (N/M)	Total loading (N)
mode 1	98505	29551.5
mode 2	-98563	-29568.9
mode 3	1.35E+05	40500
mode 4	-1.35E+05	-40500

To investigate the effect of the initial imperfection, the four different models with imperfections of 0, L/500, L/50, L/5 are considered. Figure 238 indicates the effect of the imperfection on the

pushover curves which would result in a large difference in strength and stiffness of the whole system.

As indicated in Figure 238, the initial imperfection, would affect pushover. As the imperfection increases, the initial stiffness barely differs, but the ultimate strength is affected significantly. The degradation is obvious by increasing the imperfection. The ductility is highly affected. In addition, as the imperfection decreases the capacity of the system to resist the load in higher displacement is increased. It is observed that by a significant amount of the imperfection, the pushover of the system would be highly affected. Table 37 summarizes the imperfection results for method II.

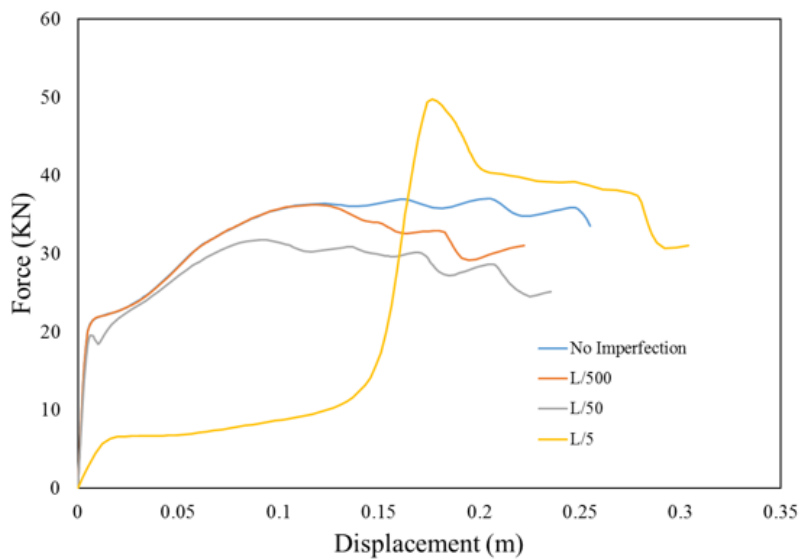


Figure 238. The effect of imperfection on pushover curves

Table 37. The results of imperfection analysis for method II

<b>LOAD</b>	<b>U3(MM)</b>	<b>U1(MM)</b>	<b>SHEAR ANGLE</b>
NO IMP	6	255	0.51
L/500	6	167	0.334
L/50	6	6.4	0.0128
L/5	6	5	0.01

### *B.2.1. The appropriate imperfection value:*

References are investigated to have a rough estimation of imperfection. In all the references there are some thresholds indicating that the imperfection should not exceed a certain amount. In AISC

for the beams, the imperfection of  $L/200$ - $L/360$  is stated. It also indicates that the imperfection threshold for different plates varies based on the thickness, length, and number of waves in general.

In the study by Egorova et al. (2014), the different imperfection displacement is reported, which was in the range of  $L/254$  up to  $L/434$ . It is clearly stated that the imperfection more than  $L/100$  is not desirable cause it affects the stiffness and the strength of the whole system. However, Ma et al. (2011) considered imperfection in sinusoidal shape with a value of  $L/100$ .

It is concluded that from the method I, the large amount of imperfection just changes the pushover curves slightly. However, Method II despite the Method I considers the imperfection precisely based on the buckling modes. Higher modes even take more load to be initiated, which is observed in Method II results. Method II also is able to analyze the system based on any buckling mode desired. It is observed that the imperfection would have signed on the strength of the system (degradation of strength), and just barely affects the initial stiffness of the system. From the literature and FE study, it is concluded that imperfection value of  $L/250$  could be suitable for butterfly-shaped links study. In the next section, the procedure to apply the imperfection in FE software is delineated.

## **APPENDIX C: APPLYING THE IMPERFECTION REGARDING THE METHOD II IN ABAQUS:**

The program ABAQUS is not able to directly incorporate the initial imperfection associated with different modes. So, there should be some secondary steps to incorporate such steps in the ABAQUS. For that, first, we need to do a Buckling Step in which the mode shapes of the system would be indicated. Based on the mode shapes (the one which has a higher effect on the imperfection behavior which is commonly the first one) we are able to set the imperfection for the next step.

Since the ABAQUS does not have a direct module for such investigations, it is needed to have the imperfection coded and add it in the keyword. First, the node displacement should be extracted from the first buckling analysis, and then the Riks method would be applied to extract the pushover curves. The code for buckling analysis module:

*\*Output, field, variable=PRESELECT*

*\*NODE FILE*

*U*

*\*End Step*

Then the buckling analysis file should be taken as an input for the Riks method or any other solver method, which would be the general pushover analysis in which the imperfection is considered. The code for the Rik's module is as follows:

...

*\*IMPERFECTION, FILE=results\_file, STEP=step*

Data lines specifying the mode number and its associated scale factor

...

\*\*

\*\* -----

*\*IMPERFECTION, FILE=Buck-05-033-01-60-wire, STEP=1*

*1, 1e-3*

\*\* -----

\*\*

*\*\* STEP: Step-1*

It is noted that a Riks analysis is subject to the following restrictions:

1- A Rik's step cannot be followed by another step in the same analysis. Subsequent steps must be analyzed by using the restart capability.

2- If a Rik's analysis includes irreversible deformation such as plasticity and a restart using another Rik's step is attempted while the magnitude of the load on the structure is decreasing, ABAQUS/Standard will find the elastic unloading solution. Therefore, a restart should occur at a point in the analysis where the load magnitude is increasing if plasticity is present.

3- For post-buckling problems involving loss of contact, the Riks method will usually not work; inertia or viscous damping forces (such as those provided by dashpots) must be introduced in a dynamic or static analysis to stabilize the solution.

## APPENDIX D: THE DETAILED RESULTS OF PARAMETRIC STUDY:

### D.1. The group of butterfly-shaped link fuses with $L=0.5$ , $a/b=0.1$

#### D.1.1. The butterfly-shaped links with $b/L=0.1$

Table 38, Table 39 and Figure 239 show the behavior of the set of butterfly links with low  $a/b$  ratio of mid-width to end-width, and significant narrow end-width to length. The trend of the pushover curves is pretty much the same. In the normalized curves, it has been observed that this set of butterfly-shaped links have a clear point of buckling with significant out-of-plane displacements happened during pushover analysis regardless of the thickness of the original plate. If the curves are investigated within 10 percent of drift, an obvious change of slope would be observed at the  $P/P_{pred}$  of 1 which indicates that the equations have captured this limit state.

Table 38. The geometrical properties and predicted values for set of models with  $L=0.5$ ,  $a/b=0.1$  and  $b/L=0.1$

$L=0.5$ - $a/b=0.1$ - $b/L=0.1$ Model	a	b	t	L	a/b	b/L	l/t	Pp flexure	Pp Shear	Total Capacity
10	0.005	0.05	0.05	0.5	0.1	0.1	10	13.50	43.30	13.5
20	0.005	0.05	0.025	0.5	0.1	0.1	20	6.75	21.65	6.7
40	0.005	0.05	0.0125	0.5	0.1	0.1	40	3.38	10.83	3.3
60	0.005	0.05	0.00833	0.5	0.1	0.1	60	2.25	7.22	2.2
80	0.005	0.05	0.00625	0.5	0.1	0.1	80	1.69	5.41	1.6
100	0.005	0.05	0.005	0.5	0.1	0.1	100	1.35	4.33	1.3

Table 39. The output results for set of models with  $L=0.5$ ,  $a/b=0.1$  and  $b/L=0.1$

L/t	equivalent plastic strain	Pmax (KN)	Mend (KN.m)	hinge location	Disp Buckling $u_3=5e-3$	Fs/Fpred	deltas/L	deltau/L	Fu/Fpred	Eng index
10	0.074	30.15	7.54	0.22	NA	0.86	0.012	0.09	2.21	1.72
20	0.059	15.04	3.76	0.22	0.509	0.86	0.012	0.08	2.21	1.70
40	0.062	7.56	1.89	0.22	0.48	0.86	0.012	0.09	2.21	1.62
60	0.071	5.03	1.26	0.22	0.1	0.9	0.012	0.08	2.27	1.71
80	0.067	3.76	0.94	0.22	0.05	0.9	0.012	0.08	2.27	1.70
100	0.074	3.00	0.75	0.22	0.04	0.9	0.012	0.08	2.27	1.74

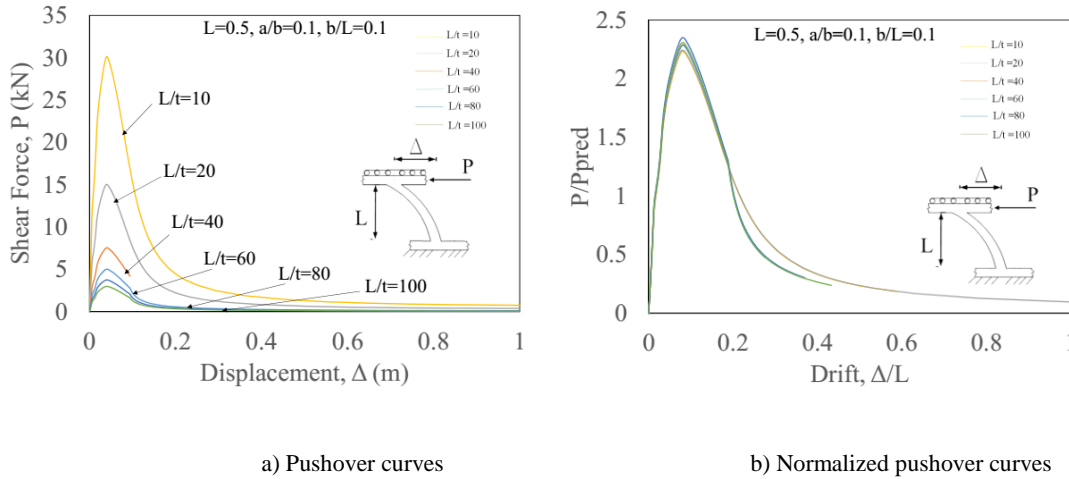


Figure 239. The pushover curves for a set of models with  $L=0.5$ ,  $a/b=0.1$  and  $b/L=0.1$

### D.1.2. The butterfly-shaped links with $b/L=0.2$

Table 40, Table 41 and Figure 240 show the summary of the behavior of a butterfly-shaped links with  $a/b = 0.1$ ,  $b/L=0.2$ , and  $L=0.5$ . As it is represented although the ration of  $a/b$  is small, the pushover results shows tangible better resistance against buckling. It is concluded that the effect of end width on the possibility of the buckling occurrence is significant. Obviously, the buckling capacity, shear and flexural capacity of the links are improved compared to lower end width cases. In this set of butterfly-shaped links, the flexural limit state has happened early in the pushover analysis, following the flexural limit state; the second-order behavior is initiated. The shear limit has been occurred to significantly reduce the load-bearing capacity.

Table 40. The geometrical properties and predicted values for set of models with  $L=0.5$ ,  $a/b=0.1$  and  $b/L=0.2$

L=0.5-a/b=0.1- b/L=0.2 Model	a	b	t	L	a/b	b/L	l/t	Pp flexure	Pp Shear	Total Capacity
10	0.01	0.1	0.05	0.5	0.1	0.2	10	54.00	86.60	54
20	0.01	0.1	0.025	0.5	0.1	0.2	20	27.00	43.30	27
40	0.01	0.1	0.0125	0.5	0.1	0.2	40	13.50	21.65	13.5
60	0.01	0.1	0.00833	0.5	0.1	0.2	60	9.00	14.43	9
80	0.01	0.1	0.00625	0.5	0.1	0.2	80	6.75	10.83	6.7

100	0.01	0.1	0.005	0.5	0.1	0.2	100	5.40	8.66	5.4
-----	------	-----	-------	-----	-----	-----	-----	------	------	-----

Table 41. The output results for set of models with  $L=0.5$ ,  $a/b=0.1$  and  $b/L=0.2$

L/t	equivalent plastic strain	Pmax (KN)	Mend (KN.m)	hinge location	Disp Buckling $u_3=5e-3$	Fs/Fpred	deltas/L	deltau/L	Fu/Fpred	Eng index
10	0.085	237.13	59.28	0.228	0.62	0.96	0.0069	0.75	2.81	1.71
20	0.108	74.90	18.72	0.228	0.5	0.96	0.0069	0.96	2.7	1.72
40	0.106	39.85	9.96	0.228	0.43	0.96	0.0069	0.5	2.45	1.74
60	0.106	28.87	7.22	0.228	0.2	0.94	0.01	0.74	2.42	1.73
80	0.097	19.37	4.84	0.228	0.18	0.94	0.01	0.74	2.07	1.63
100	0.09	16.47	4.12	0.228	0.15	0.94	0.01	0.74	1.97	1.52

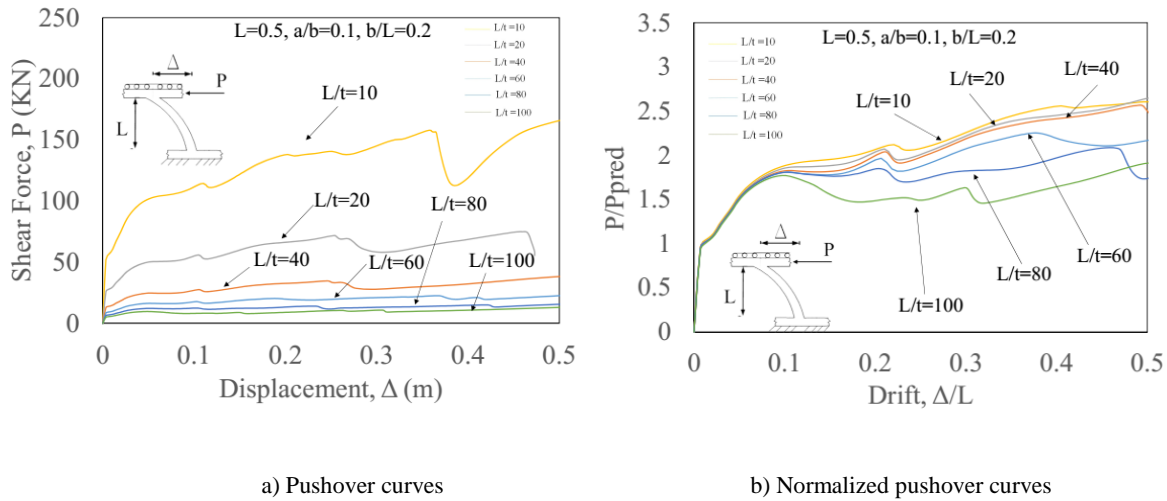


Figure 240. The pushover curves for a set of models with  $L=0.5$ ,  $a/b=0.1$  and  $b/L=0.1$

### D.1.3. The butterfly-shaped links with $b/L=0.3$

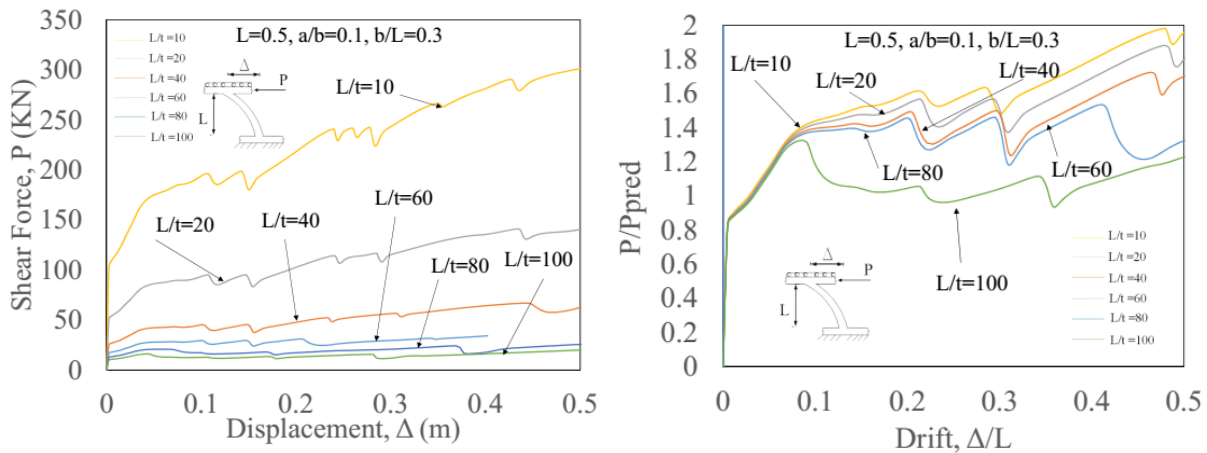
Table 42, Table 43 and Figure 241 indicate the behavior of the butterfly-shaped links with geometrical properties of  $a/b=0.1$ ,  $b/L=0.3$ , and  $L=0.5$ . The overstrength factor for higher width butterfly-shaped links are highly dependent on the geometry. The buckling resistance is improved by increasing the end-width length. In these set of models, the flexural and shear limit state has been initiated together approximately, although the flexural limit state has occurred first. After the occurrence of the limit states, the second order behavior is initiated. Due to enough slenderness, the buckling initiation for these models is prevented significantly for higher thickness plates. From all of the models in this set, for the  $L/t$  equal to 100, the buckling limit state has happened which significantly changed the load-bearing capacity.

Table 42. The geometrical properties and predicted values for set of models with  $L=0.5$ ,  $a/b=0.1$  and  $b/L=0.3$

L=0.5-a/b=0.1-b/L=0.3 Model	a	b	t	L	a/b	b/L	L/t	Pp flexure	Pp Shear	Total Capacity
10	0.015	0.15	0.05	0.5	0.1	0.3	10	121.50	129.90	121.5
20	0.015	0.15	0.025	0.5	0.1	0.3	20	60.75	64.95	60.7
40	0.015	0.15	0.0125	0.5	0.1	0.3	40	30.38	32.48	30.3
60	0.015	0.15	0.0083	0.5	0.1	0.3	60	20.25	21.65	20.2
80	0.015	0.15	0.00625	0.5	0.1	0.3	80	15.19	16.24	15.1
100	0.015	0.15	0.005	0.5	0.1	0.3	100	12.15	12.99	12.1

Table 43. The output results for set of models with  $L=0.5$ ,  $a/b=0.1$  and  $b/L=0.3$

L/t	equivalent plastic strain	Pmax (KN)	Mend (KN.m)	hinge location	Disp Buckling $u_3=5e-3$	Fs/Fpred	deltas/L	deltai/L	Fu/Fpred	Eng index
l/t	0.18	313.36	78.34	0.231	NA	0.88	0.007	0.86	2.34	1.40
10	0.18	147.17	36.79	0.231	0.24	0.84	0.006	0.88	2.31	1.36
20	0.18	82.29	20.57	0.231	0.21	0.9	0.0039	0.89	2.1	1.29
40	0.2	51.03	12.76	0.231	0.2	0.74	0.003	0.98	2.1	1.27
60	0.2	51.03	12.76	0.231	0.17	0.74	0.003	0.98	1.61	1.20
80	0.21	51.03	12.76	0.231	0.15	0.74	0.003	0.98	1.27	1.10



a) Pushover curves

b) Normalized pushover curves

Figure 241. The pushover curves for a set of models with  $L=0.5$ ,  $a/b=0.1$  and  $b/L=0.3$

#### D.1.4. The butterfly-shaped links with $b/L=0.4$

Table 44, Table 45 and Figure 242 indicate the behavior of the butterfly-shaped links with geometrical properties of  $a/b=0.1$ ,  $b/L=0.4$ , and  $L=0.5$ . The inelasticity concentration location would be still the same in the middle since the width still would be significantly narrow in the middle. The degradation in stiffness and strength limit capacity of the butterfly-shaped fuses

happen with smoother trends. In these set of models, the shear limit state is initially occurred, then the second-order behavior has been initiated. Following the second-order, the flexural limit state has occurred. The shear limit state governing over the flexural limit state could be verified with the equations provided in previous chapters. The  $(b-a)/L$  factor is more than 0.28 which indicates that the shear would be governing.

Table 44. The geometrical properties and predicted values for set of models with  $L=0.5$ ,  $a/b=0.1$  and  $b/L=0.4$

L=0.5-a/b=0.1-b/L=0.4 Model	a	b	t	L	a/b	b/L	L/t	Pp flexure	Pp Shear	Total Capacity
10	0.02	0.2	0.05	0.5	0.1	0.4	10	216.00	173.21	173.2
20	0.02	0.2	0.025	0.5	0.1	0.4	20	108.00	86.60	86.6
40	0.02	0.2	0.0125	0.5	0.1	0.4	40	54.00	43.30	43.3
60	0.02	0.2	0.00833	0.5	0.1	0.4	60	36.00	28.87	28.8
80	0.02	0.2	0.00625	0.5	0.1	0.4	80	27.00	21.65	21.6
100	0.02	0.2	0.005	0.5	0.1	0.4	100	21.60	17.32	17.3

Table 45. The output results for set of models with  $L=0.5$ ,  $a/b=0.1$  and  $b/L=0.4$

L/t	equivalent plastic strain	Pmax (KN)	Mend (KN.m)	hinge location	Disp Buckling $u_3=5e-3$	Fs/Fpred	deltas/L	deltai/L	Fu/Fpred	Eng index
10	0.26	444.10	111.03	0.25	0.75	1.1	0.0039	0.1	1.47	1.43
20	0.23	191.96	47.99	0.25	0.33	1.1	0.013	0.11	1.47	1.42
40	0.24	82.38	20.60	0.25	0.36	1.1	0.0045]	0.101	1.47	1.45
60	0.24	49.90	12.47	0.25	0.15	1.1	0.0061	0.1	1.46	1.50
80	0.25	32.29	8.07	0.25	0.1	1.1	0.0061	0.1	1.4	1.21
100	0.24	26.61	6.65	0.25	0.05	1.1	0.0061	0.1	1.15	1.09

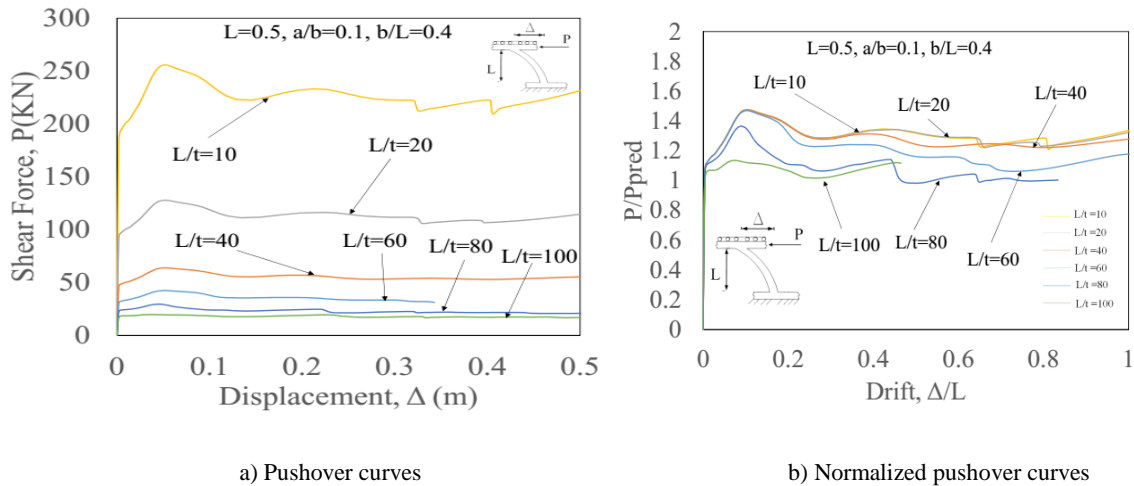


Figure 242. The pushover curves for a set of models with  $L=0.5$ ,  $a/b=0.1$  and  $b/L=0.4$

## D.2. The group of butterfly-shaped link fuses with $L=0.5$ , $a/b=0.33$

### D.2.1 The butterfly-shaped links with $b/L=0.1$

Table 46, Table 47 and Figure 243 indicate the behavior of the butterfly-shaped links with geometrical properties of  $a/b=0.33$ ,  $b/L=0.1$ , and  $L=0.5$ . Due to the lower values of end width, the buckling is observed in all the models with different thicknesses. The hinge location is far from the sharp ends because of the  $a/b$  ratio. The flexural limit state has been occurred in the initial stages of pushover analysis, but increasing the load values, the second order effect takes off, this effect would be taking off with less rate compared to the corresponding  $a/b$  equal to 0.1 the buckling limit state have been occurred in almost all of the thicknesses before having shear limit state governing the behavior. The buckling in all the models has occurred in 20 percent drift approximately. The special geometry of the link imposes to have the tension resistance takes off right after the flexural limit state initiated in the models.

Table 46. The geometrical properties and predicted values for set of models with  $L=0.5$ ,  $a/b=0.33$  and  $b/L=0.1$

L=0.5, a/b=0.33, b/L=0.1 Model	a	b	t	L	a/b	b/L	L/t	Pp flexure	Pp Shear	Total Capacity
10	0.0165	0.05	0.025	0.5	0.33	0.1	10	33.17	142.89	33.1
20	0.0165	0.05	0.025	0.5	0.33	0.1	20	16.58	71.45	16.5
40	0.0165	0.05	0.0125	0.5	0.33	0.1	40	8.29	35.72	8.29
60	0.0165	0.05	0.0083	0.5	0.33	0.1	60	5.53	23.82	5.5
80	0.0165	0.05	0.00625	0.5	0.33	0.1	80	4.15	17.86	4.1
100	0.0165	0.05	0.005	0.5	0.33	0.1	100	3.32	14.29	3.3

Table 47. The output results for set of models with  $L=0.5$ ,  $a/b=0.33$  and  $b/L=0.1$

L/t	equivalent plastic strain	Pmax (KN)	Mend (KN.m)	hinge location	Disp Buckling $u_3=5e-3$	Fs/Fpred	deltas/L	deltatau/L	Fu/Fpred	Eng index
10	0.033	67.55	16.89	0.105	0.261	0.997	0.023	0.16	2.031	1.70
20	0.033	33.77	8.44	0.105	0.261	0.997	0.023	0.16	2.031	1.70
40	0.03	16.83	4.21	0.105	0.25	0.886	0.023	0.16	2.04	1.35
60	0.032	11.20	2.80	0.105	0.24	0.886	0.023	0.16	2.04	1.37
80	0.021	8.37	2.09	0.105	0.2	0.886	0.016	0.16	2.04	1.32
100	0.014	6.71	1.68	0.105	0.18	0.886	0.023	0.16	2.04	1.20

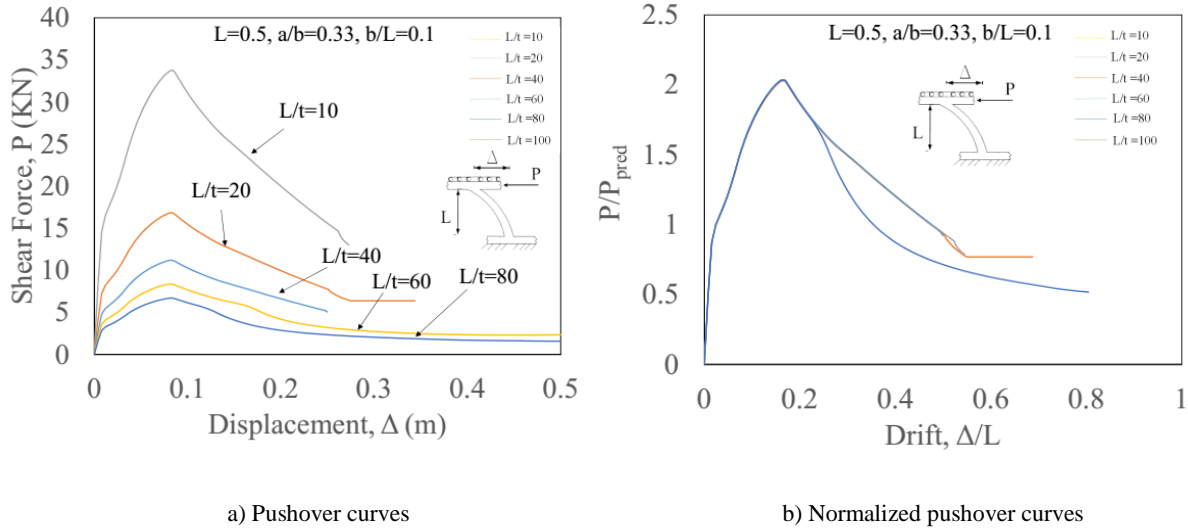


Figure 243. The pushover curves for a set of models with  $L=0.5$ ,  $a/b=0.33$ , and  $b/L=0.1$

### D.2.2. The butterfly-shaped links with $b/L=0.2$

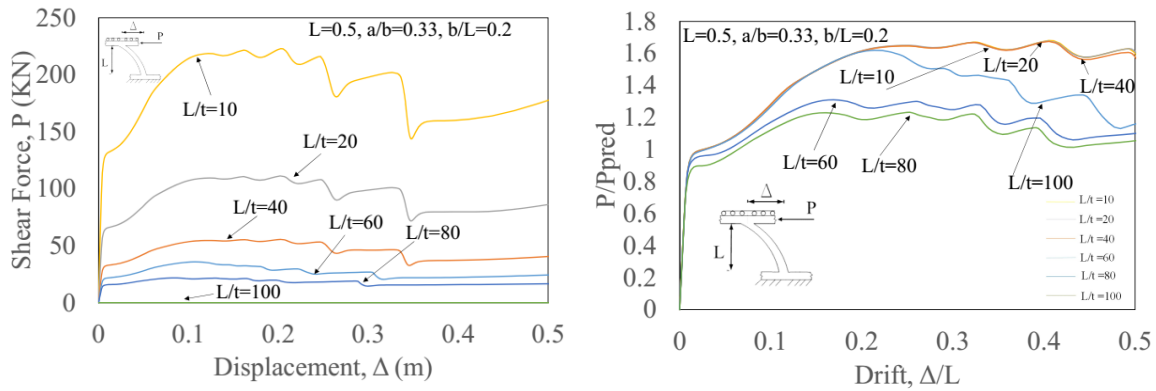
Table 48, Table 49 and Figure 244 indicate the behavior of the butterfly-shaped links with geometrical properties of  $a/b=0.33$ ,  $b/L=0.2$ , and  $L=0.5$ . The geometrical properties and predicted values for a set of models with  $L=0.5$ ,  $a/b=0.33$ , and  $b/L=0.2$  are reported. Having greater values for  $b/L$  represents that the buckling is postponed significantly. The equivalent plastic strain values indicating the accumulated plastic strain in models are less than other geometrical properties; due to the fact, the hinges are located in quarter points far from the sharp edges. In these set of models, the flexural limit state has occurred at the initial stages, but the buckling conditions did not allow the models to experience the complete shear limit state; therefore, the models have experienced the buckling before shear limit state.

Table 48. The geometrical properties and predicted values for set of models with  $L=0.5$ ,  $a/b=0.33$  and  $b/L=0.1$

L=0.5, a/b=0.33, b/L=0.2 Model	a	b	t	L	a/b	b/L	L/t	Pp flexure	Pp Shear	Total Capacity
10	0.033	0.1	0.05	0.5	0.33	0.2	10	132.66	285.79	132.66
20	0.033	0.1	0.025	0.5	0.33	0.2	20	66.33	142.89	66.3
40	0.033	0.1	0.0125	0.5	0.33	0.2	40	33.17	71.45	33.165
60	0.033	0.1	0.0083	0.5	0.33	0.2	60	22.11	47.63	22.11
80	0.033	0.1	0.00625	0.5	0.33	0.2	80	16.58	35.72	16.5825
100	0.033	0.1	0.005	0.5	0.33	0.2	100	13.27	28.58	13.266

Table 49. The output results for set of models with  $L=0.5$ ,  $a/b=0.33$  and  $b/L=0.2$

L/t	equivalent plastic strain	Pmax (KN)	Mend (KN.m)	hinge location	Disp Buckling $u_3=5e-3$	Fs/Fpred	deltas/L	deltai/L	Fu/Fpred	Eng index
10	0.109	222.85	55.71	0.13	0.63	0.97	0.014	0.41	1.167	1.37
20	0.108	111.23	27.81	0.13	0.42	0.97	0.014	0.32	1.16	1.36
40	0.106	55.53	13.88	0.13	0.31	0.97	0.014	0.32	1.16	1.35
60	0.05	35.80	7.52	0.13	0.091	1	0.007	0.21	1.61	1.36
80	0.03	22.24	5.56	0.13	0.071	0.89	0.007	0.21	1.31	1.17
100	0.03	16.34	4.09	0.13	0.065	0.89	0.007	0.21	1.21	1.17



a) Pushover curves

b) Normalized pushover curves

Figure 244. The pushover curves for a set of models with  $L=0.5$ ,  $a/b=0.33$ , and  $b/L=0.2$

### D.2.3. The butterfly-shaped links with $b/L=0.3$

Table 50, Table 51 and Figure 245 indicate the behavior of the butterfly-shaped links with geometrical properties of  $a/b=0.33$ ,  $b/L=0.3$ , and  $L=0.5$ . The behavior of this set of models is similar to the previous one. The buckling is post ponded, and the thinner the plate used for the links, the less ability to dissipate the energy. Hinge location due to the geometry of the link is at the middle part. The flexural limits state would be governing the behavior. In these set of models for the  $L/t$  equal to 10 and  $L/t$  equal to 20, the flexural limit state has occurred and following the flexural limit state the shear limit state have happened by having the second order pushover behavior. In the rest of the models with  $L/t$  more than 40, the buckling has initiated and the shear limit state was not completely occurred.

Table 50. The geometrical properties and predicted values for set of models with  $L=0.5$ ,  $a/b=0.33$  and  $b/L=0.3$

L=0.5-a/b=0.33- b/L=0.3 Model	a	b	t	L	a/b	b/L	L/t	Pp flexure	Pp Shear	Total Capacity
10	0.0495	0.15	0.05	0.5	0.33	0.3	10	298.49	428.68	298.485
20	0.0495	0.15	0.025	0.5	0.33	0.3	20	149.24	214.34	149.2
40	0.0495	0.15	0.0125	0.5	0.33	0.3	40	74.62	107.17	74.6
60	0.0495	0.15	0.0083	0.5	0.33	0.3	60	49.75	71.45	49.7
80	0.0495	0.15	0.00625	0.5	0.33	0.3	80	37.31	53.59	37.3
100	0.0495	0.15	0.005	0.5	0.33	0.3	100	29.85	42.87	29.8

Table 51. The output results for set of models with  $L=0.5$ ,  $a/b=0.33$  and  $b/L=0.3$

L/t	equivalent plastic strain	Pmax (KN)	Mend (KN.m)	hinge location	Disp Buckling $u_3=5e-3$	Fs/Fpred	deltas/L	deltai/L	Fu/Fpred	Eng index
10	0.014	420.67	105.17	0.137	0.69	0.9981	0.0148	0.23	1.39	1.17
20	0.014	209.97	52.49	0.137	0.49	0.9981	0.014	0.23	1.39	1.16
40	0.012	96.48	24.12	0.137	0.43	1	0.01	0.23	1.39	1.15
60	0.01	51.03	12.76	0.137	0.4	0.89	0.027	0.16	1.01	0.91
80	0.01	37.52	9.38	0.137	0.33	0.89	0.027	0.16	1.01	0.90
100	0.01	29.16	7.29	0.137	0.3	0.89	0.011	0.12	0.93	0.81

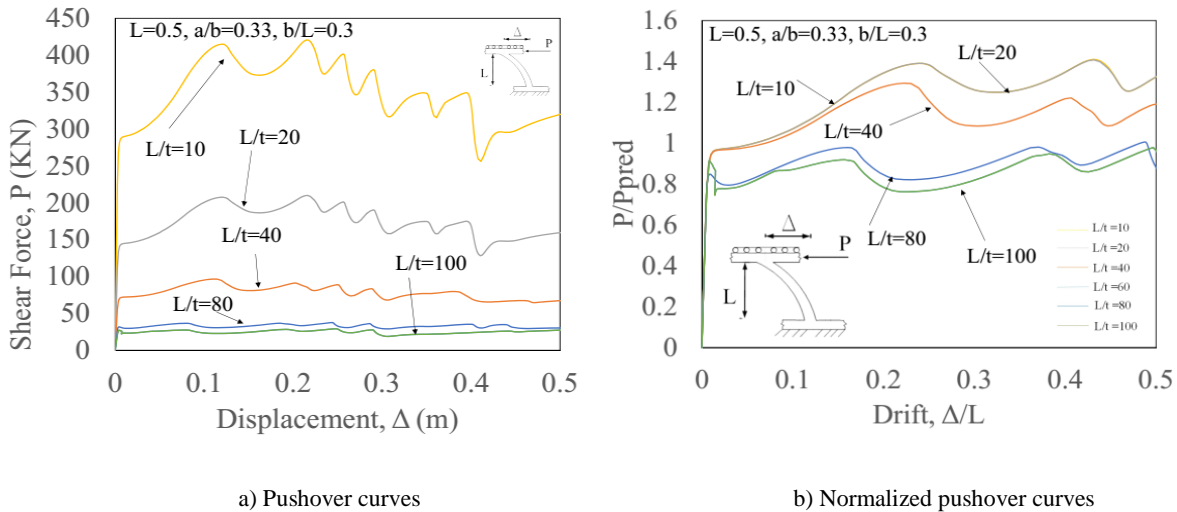


Figure 245. The pushover curves for a set of models with  $L=0.5$ ,  $a/b=0.33$ , and  $b/L=0.3$

#### D.2.4. The butterfly-shaped links with $b/L=0.4$

Table 52, Table 53 and Figure 246 indicate the behavior of the butterfly-shaped links with geometrical properties of  $a/b=0.33$ ,  $b/L=0.4$ , and  $L=0.5$ . The geometrical properties and predicted values for a set of models with  $L=0.5$ ,  $a/b=0.33$ , and  $b/L=0.4$  are reported. The geometrical properties and predicted values for a set of models with  $L=0.5$ ,  $a/b=0.33$ , and  $b/L=0.4$ . According

to normalized curves, it is concluded that the thicker plates such (e.g.  $L/t = 10$ ,  $L/t=20$ ) would follow the pushover trend with catenary action happening after first limits state; however, if the thinner plate is used (e.g.  $L/t=40$ ,  $L/t=80$ ,  $L/t=100$ ) the buckling would take place. In these set of models, the  $L/t$  equal to 10 and  $L/t$  equal to 20 would experience the flexural limit state at the initial stages of pushover analysis. By increasing the displacement controlled loading, the second order behavior takes place until the shear limit stat. The buckling was being initiated for the models with  $L.t$  more than 40 mm, which reduced the ability to reach to shear limit state.

Table 52. The geometrical properties and predicted values for set of models with  $L=0.5$ ,  $a/b=0.33$  and  $b/L=0.4$

$L=0.5-a/b=0.33-b/L=0.4$ Model	a	b	t	L	a/b	b/L	L/t	Pp flexure	Pp Shear	Total Capacity
10	0.066	0.2	0.05	0.5	0.33	0.4	10	530.64	571.58	530.64
20	0.066	0.2	0.025	0.5	0.33	0.4	20	265.32	285.79	265.32
40	0.066	0.2	0.0125	0.5	0.33	0.4	40	132.66	142.89	132.6
60	0.066	0.2	0.0083	0.5	0.33	0.4	60	88.44	95.26	88.44
80	0.066	0.2	0.00625	0.5	0.33	0.4	80	66.33	71.45	66.33
100	0.066	0.2	0.005	0.5	0.33	0.4	100	53.06	57.16	53.064

Table 53. The output results for set of models with  $L=0.5$ ,  $a/b=0.33$  and  $b/L=0.4$

L/t	EQUIVALENT PLASTIC STRAIN	Pmax (KN)	Mend (KN.m)	hinge location	Disp Buckling $u_3=5e-3$	Fs/Fpre d	deltas/L	deltau/L	Fu/Fpre d	Eng index
10	0.014	696.65	174.16	0.144	NO	0.943	0.006	0.32	1.39	1.05
20	0.015	348.41	87.10	0.144	NO	0.943	0.006	0.32	1.391	1.08
40	0.013	131.44	32.86	0.14	0.007	0.89	0.26	0.26	0.99	0.90
60	0.016	81.25	20.31	0.14	0.0041	0.802	0.012	0.23	0.91	0.88
80	0.016	59.40	14.85	0.14	0.0038	0.87	0.012	0.23	0.88	0.82
100	0.016	46.59	11.65	0.14	0.0033	0.67	0.005	0.21	0.83	0.79

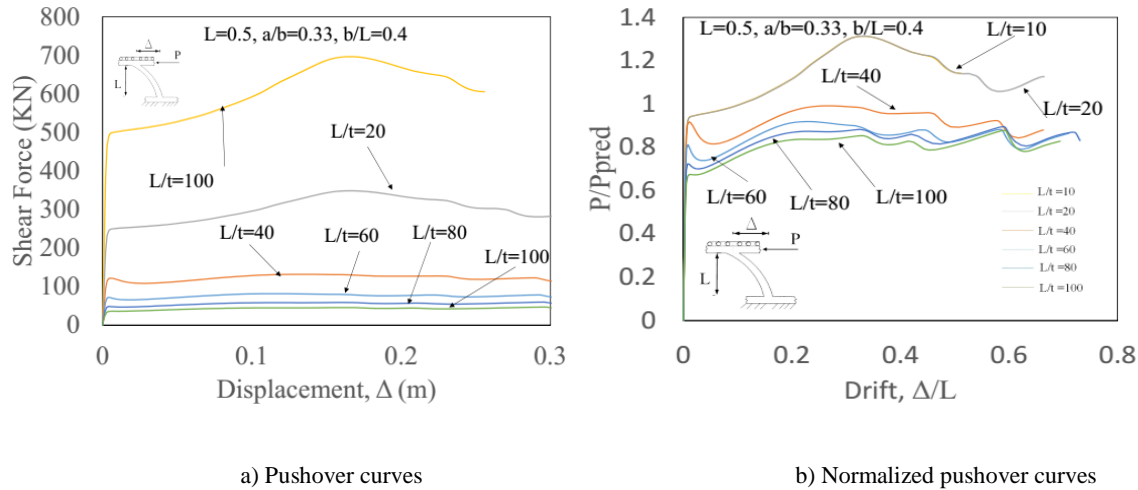


Figure 246. The pushover curves for a set of models with  $L=0.5$ ,  $a/b=0.33$ , and  $b/L=0.4$

### D.3. The group of butterfly-shaped link fuses with $L=0.5$ , $a/b=0.75$

#### D.3.1. The butterfly-shaped links with $b/L=0.1$

Table 54, Table 55, and Figure 247 indicate the behavior of the butterfly-shaped links with geometrical properties of  $a/b=0.75$ ,  $b/L=0.1$ . The buckling obviously happened at the initial stages of pushover loading. The hinge location is at the end of the butterfly-shaped link, indicating that the flexure hinging is the governing limit state. The flexural limit state has happened in all the models at first, then the second-order behavior takes off rapidly, and well before the shear limit state, the buckling was occurred to greatly reduce the load-bearing capacity of the links.

Table 54. The geometrical properties and predicted values for set of models with  $L=0.5$ ,  $a/b=0.75$  and  $b/L=0.1$

$L=0.5$ - $a/b=0.75$ - $b/L=0.1$ Model	a	b	t	L	a/b	b/L	L/t	Pp flexure	Pp Shear	Total Capacity
10	0.0375	0.05	0.05	0.5	0.75	0.1	10	37.50	324.76	37.50
20	0.0375	0.05	0.025	0.5	0.75	0.1	20	18.75	162.38	18.70
40	0.0375	0.05	0.0125	0.5	0.75	0.1	40	9.38	81.19	9.30
60	0.0375	0.05	0.0083	0.5	0.75	0.1	60	6.25	54.13	6.20
80	0.0375	0.05	0.00625	0.5	0.75	0.1	80	4.69	40.59	4.60
100	0.0375	0.05	0.005	0.5	0.75	0.1	100	3.75	32.48	3.70

Table 55. The output results for set of models with  $L=0.5$ ,  $a/b=0.75$  and  $b/L=0.1$

L/t	EQUIVALENT PLASTIC STRAIN	Pmax (KN)	Mend (KN.m)	hinge location	Disp Buckling $u_3=5e-3$	Fs/Fpred	deltas/L	deltai/L	Fu/Fpred	Eng index
10	0.031	156.90	39.23	0.01	NA	1.01	0.016	0.3	4.11	2.24
20	0.033	78.00	19.50	0.01	0.509	1.01	0.016	0.3	4.11	2.17
40	0.03	38.77	9.69	0.01	0.48	1.01	0.016	0.3	4.11	2.22
60	0.032	25.65	6.41	0.01	0.448	1.01	0.016	0.3	4.11	2.21
80	0.028	19.05	4.76	0.01	0.38	1.01	0.016	0.3	4.11	2.17
100	0.028	15.00	3.75	0.01	0.3	1.01	0.016	0.3	4.11	1.60

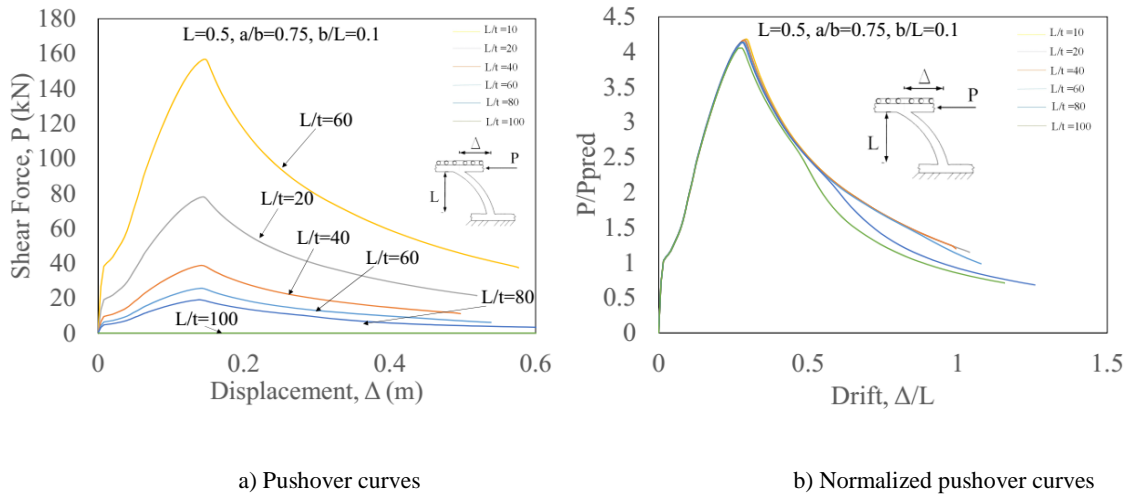


Figure 247. The pushover curves for a set of models with  $L=0.5$ ,  $a/b=0.75$ , and  $b/L=0.1$

### D.3.2. The butterfly-shaped links with $b/L=0.2$

Table 56, Table 57 and Figure 248 indicate the behavior of the butterfly-shaped links with geometrical properties of  $a/b=0.75$ ,  $b/L=0.2$ . The buckling is not fully resisted; however, the hinges are developed at the end width of butterfly-shaped links. The normalized curves show that the two limit states have happened for all the models. In these set of models, flexural yielding has been occurred at first, the second order behavior takes place but not as fast as the previous set of models. The occurrence of buckling kept the models from fully experiencing the shear limit state as the displacement loading increased.

Table 56. The geometrical properties and predicted values for set of models with  $L=0.5$ ,  $a/b=0.75$  and  $b/L=0.2$

$L=0.5$ - $a/b=0.75$ - $b/L=0.2$ Model	a	b	t	L	a/b	b/L	L/t	Pp flexure	Pp Shear	Total Capacity
10	0.075	0.1	0.05	0.5	0.75	0.2	10	150.00	649.52	150.00
20	0.075	0.1	0.025	0.5	0.75	0.2	20	75.00	324.76	75.00
40	0.075	0.1	0.0125	0.5	0.75	0.2	40	37.50	162.38	37.50
60	0.075	0.1	0.0083	0.5	0.75	0.2	60	25.00	108.25	25.00
80	0.075	0.1	0.00625	0.5	0.75	0.2	80	18.75	81.19	18.70
100	0.075	0.1	0.005	0.5	0.75	0.2	100	15.00	64.95	15.00

Table 57. The output results for set of models with  $L=0.5$ ,  $a/b=0.75$  and  $b/L=0.2$

L/t	EQUIVALENT PLASTIC STRAIN	Pmax (KN)	Mend (KN.m)	hinge location	Disp Buckling $u_3=5e-3$	Fs/Fpred	deltas/L	deltau/L	Fu/Fpred	Eng index
10	0.109	461.60	115.40	0.01	0.85	1.01	0.01	0.38	2.69	1.43
20	0.108	237.08	59.27	0.01	0.84	1.01	0.01	0.38	2.69	1.34
40	0.106	118.54	29.63	0.01	0.43	1.01	0.01	0.38	2.69	1.39

60	0.05	74.31	18.50	0.01	0.2	1.01	0.01	0.38	2.69	1.39
80	0.03	49.11	12.28	0.01	0.15	1.01	0.01	0.38	2.69	1.26
10	0.027	37.79	9.45	0.01	0.2	1.01	0.01	0.38	2.69	1.20
0										

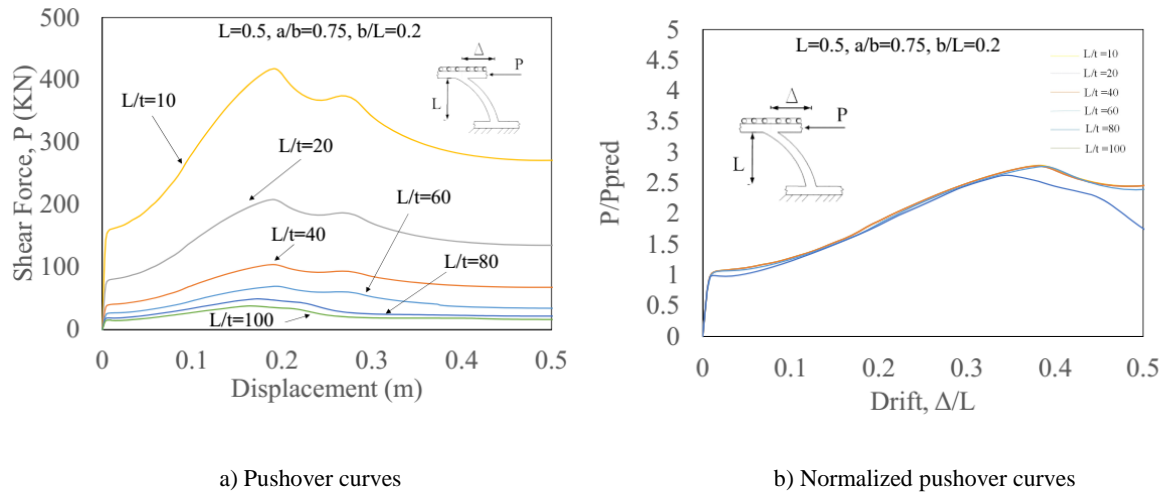


Figure 248. The pushover curves for a set of models with  $L=0.5$ ,  $a/b=0.75$ , and  $b/L=0.2$

### D.3.3. The butterfly-shaped links with $b/L=0.3$

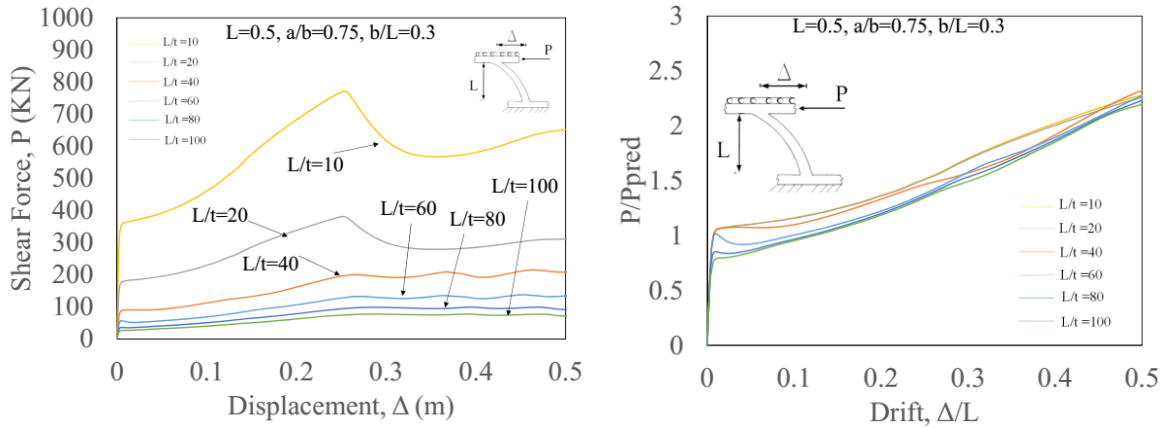
Table 58, Table 59, Figure 249 indicate the behavior of the butterfly-shaped links with geometrical properties of  $a/b=0.75$ ,  $b/L=0.3$ . Compared to previous models, it is concluded that the buckling is being resisted more efficiently, the catenary action clearly has initiated after the initial limit state. For these links, the hinges developed at the end of the length also. For the  $L/t$  equal to 10 the flexural limit state, second-order behavior, and the shear limit state have been occurred without having significant buckling. However, for the rest of the models, the buckling has initiated after second order behavior, which greatly reduced the load bearing capacity and prevented the shear limit state to occur.

Table 58. The geometrical properties and predicted values for set of models with  $L=0.5$ ,  $a/b=0.75$  and  $b/L=0.3$

$L=0.5$ - $a/b=0.75$ - $b/L=0.3$ Model	a	b	t	L	a/b	b/L	L/t	Pp flexure	Pp Shear	Total Capacity
10	0.1125	0.15	0.05	0.5	0.75	0.3	10	337.50	974.28	337.50
20	0.1125	0.15	0.025	0.5	0.75	0.3	20	168.75	487.14	168.70
40	0.1125	0.15	0.0125	0.5	0.75	0.3	40	84.38	243.57	84.30
60	0.1125	0.15	0.0083	0.5	0.75	0.3	60	56.25	162.38	56.20
80	0.1125	0.15	0.00625	0.5	0.75	0.3	80	42.19	121.78	42.10
100	0.1125	0.15	0.005	0.5	0.75	0.3	100	33.75	97.43	33.70

Table 59. The output results for set of models with  $L=0.5$ ,  $a/b=0.75$  and  $b/L=0.3$

L/t	EQUIVALENT PLASTIC STRAIN	Pmax (KN)	Mend (KN.m)	hinge location	Disp Buckling $u_3=5e-3$	Fs/Fpred	deltas/L	deltau/L	Fu/Fpred	Eng index
10	0.014	893.57	223.39	0.01	0.73	1.03	0.0078	0.51	2.27	1.17
20	0.014	381.44	95.36	0.01	0.75	1.03	0.0078	0.51	2.27	1.17
40	0.014	240.14	60.03	0.01	0.24	1.03	0.0078	0.51	2.27	1.19
60	0.01	154.17	38.54	0.01	0.16	1.03	0.0078	0.51	2.27	1.06
80	0.01	99.39	24.85	0.01	0.16	1.03	0.0078	0.51	2.27	1.07
100	0.01	77.78	19.44	0.01	0.01	1.03	0.0078	0.51	2.27	1.04



a) Pushover curves

b) Normalized pushover curves

Figure 249. The pushover curves for a set of models with  $L=0.5$ ,  $a/b=0.75$ , and  $b/L=0.3$

#### D.3.4. The butterfly-shaped links with $b/L=0.4$

Table 58, Table 60, Table 61 and Figure 250 indicate the behavior of the butterfly-shaped links with geometrical properties of  $a/b=0.75$ ,  $b/L=0.4$ . The catenary action has happened after the first limit state happened during the pushover analysis. The  $U_1$  displacement in which the out of plane displacement is reached 0.005, is significantly more than the other corresponding models indicating that the buckling resistance is even more clear. In this set of links, the flexure limit state occurred at first and the second order effect following that. The buckling for these set of butterfly links are prevented so, in general, they reached to the same values calculate for shear limit state.

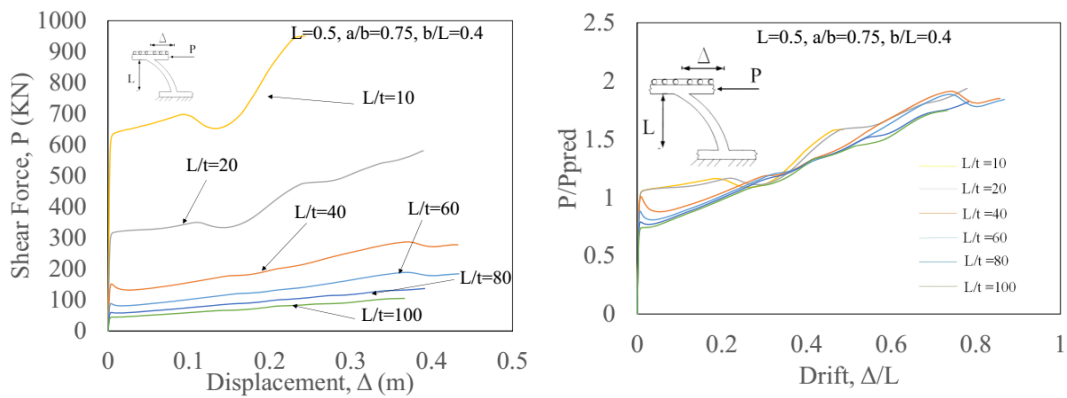
Table 60. The geometrical properties and predicted values for set of models with  $L=0.5$ ,  $a/b=0.75$  and  $b/L=0.4$

L=0.5-a/b=0.75-b/L=0.4 Model	a	b	t	L	a/b	b/L	L/t	Pp flexure	Pp Shear	Total Capacity
10	0.15	0.2	0.05	0.5	0.75	0.4	10	600.00	1299.04	600.00
20	0.15	0.2	0.025	0.5	0.75	0.4	20	300.00	649.52	300.00
40	0.15	0.2	0.0125	0.5	0.75	0.4	40	150.00	324.76	150.00
60	0.15	0.2	0.008	0.5	0.75	0.4	60	100.00	216.51	100.00
80	0.15	0.2	0.00625	0.5	0.75	0.4	80	75.00	162.38	75.00

100	0.15	0.2	0.005	0.5	0.75	0.4	100	60.00	129.90	60.00
-----	------	-----	-------	-----	------	-----	-----	-------	--------	-------

Table 61. The output results for set of models with  $L=0.5$ ,  $a/b=0.75$  and  $b/L=0.4$

L/t	EQUIVALENT PLASTIC STRAIN	Pmax (KN)	Mend (KN.m)	hinge location	Disp Buckling $u_3=5e-3$	Fs/Fpred	deltas/L	deltai/L	Fu/Fpred	Eng index
10	0.014	950.56	237.64	0.01	NA	1.1	0.013	0.48	NA	1.12
20	0.015	580.48	145.12	0.01	0.38	1.1	0.013	0.48	NA	1.16
40	0.013	286.86	71.71	0.01	0.36	1.1	0.013	0.48	NA	1.05
60	0.016	188.45	47.11	0.01	0.25	1.1	0.013	0.48	NA	0.94
80	0.015	136.52	34.13	0.01	0.18	1.1	0.013	0.48	NA	0.94
100	0.012	104.88	26.22	0.01	0.16	1.1	0.013	0.48	NA	0.86



a) Pushover curves

b) Normalized pushover curves

Figure 250. The pushover curves for a set of models with  $L=0.5$ ,  $a/b=0.75$ , and  $b/L=0.4$

## D.4. The group of butterfly-shaped link fuses with $L=0.5$ , $a/b=1$

### D.4.1. The butterfly-shaped links with $b/L=0.1$

Table 62, Table 63, and Figure 251 indicate the behavior of the butterfly-shaped links with geometrical properties of  $a/b=1$ ,  $b/L=0.1$ . The hinges happened at the end of the link, for these links the flexural hinges would always govern the limit state behavior. Since the  $a/b$  is equal to 1, these links are generally behaving as flexural dominated links. The flexural limit state has occurred in the initial stages, the buckling limit state has been occurred after having second-order behavior. These links which are commonly known as straight links, which would generally show the flexural

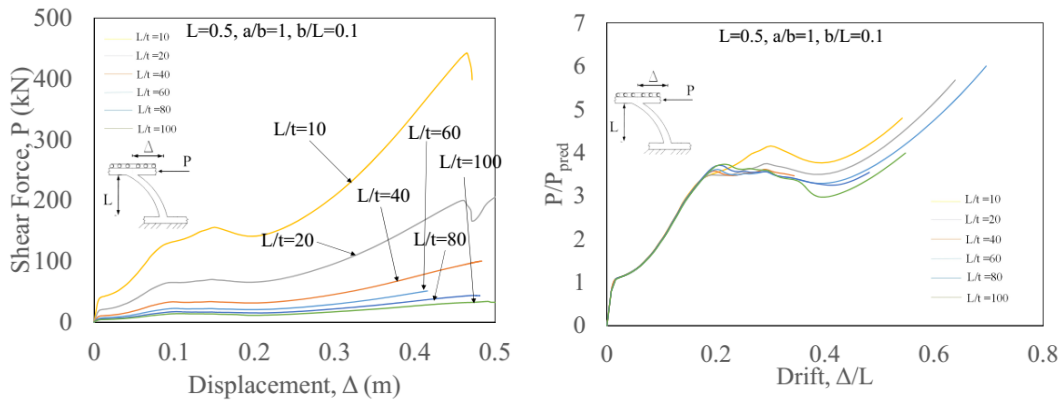
hinging at the end. Chapter 4 indicates the mathematical concepts for justifying the behavior of these links. In addition, Lee et al. (2015) and Ma et al. (2010) observed the same behavior from the experimental models.

Table 62. The geometrical properties and predicted values for set of models with  $L=0.5$ ,  $a/b=1$  and  $b/L=0.1$

L=0.5-a/b=1-b/L=0.1 Model	a	b	t	L	a/b	b/L	L/t	Pp flexure	Pp Shear	Total Capacity
10	0.05	0.05	0.05	0.5	1	0.1	10	37.50	433.01	37.50
20	0.05	0.05	0.025	0.5	1	0.1	20	18.75	216.51	18.70
40	0.05	0.05	0.0125	0.5	1	0.1	40	9.38	108.25	9.30
60	0.05	0.05	0.008333333	0.5	1	0.1	60	6.25	72.17	6.20
80	0.05	0.05	0.00625	0.5	1	0.1	80	4.69	54.13	4.60
100	0.05	0.05	0.005	0.5	1	0.1	100	3.75	43.30	3.70

Table 63. The output results for set of models with  $L=0.5$ ,  $a/b=1$  and  $b/L=0.1$

L/t	EQUIVALENT PLASTIC STRAIN	Pmax (KN)	Mend (KN.m)	hinge location	Disp Buckling $u_3=5e-3$	Fs/Fpred	deltas/L	deltau/L	Fu/Fpred	Eng index
10	0.066	442.62	110.66	0.25	NA	0.92	0.01	0.28	4.1	2.16
20	0.065	254.45	63.61	0.25	NA	0.92	0.01	NA	NA	2.11
40	0.055	100.27	25.07	0.25	NA	0.92	0.01	NA	NA	2.14
60	0.059	51.14	12.79	0.25	0.4	0.91	0.012	NA	NA	2.23
80	0.059	43.69	10.92	0.25	0.4	0.91	0.012	NA	NA	2.22
100	0.059	33.85	8.46	0.25	0.4	0.91	0.012	NA	NA	2.12



a) Pushover curves

b) Normalized pushover curves

Figure 251. The pushover curves for a set of models with  $L=0.5$ ,  $a/b=1$ , and  $b/L=0.1$

### D.4.2. The butterfly-shaped links with $b/L=0.2$

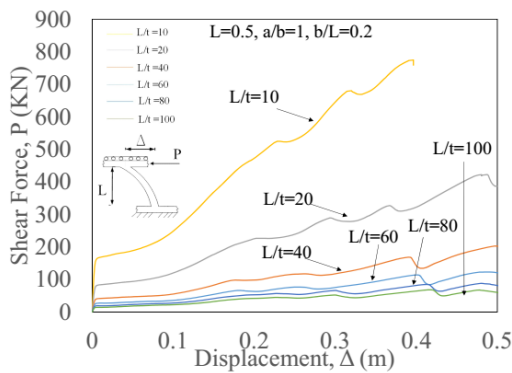
Table 64, Table 65 and Figure 252 indicate the behavior of the butterfly-shaped links with geometrical properties of  $a/b=1$ ,  $b/L=0.2$ . The hinges happened at the end of the link. For these links, the flexural hinges would always govern the limit state behavior. It is noted that the considerable amount of equivalent plastic strain values have happened within this model since the accumulation of plastic strains are concentrated at the end of the links where the shape angles exist. The flexural limit state for these set of butterfly-shaped links occurred first, the second-order took off and the buckling happened for the models with  $L/t$  more than 40. For the models with  $L/t$  less than 40, the buckling was not clearly initiated.

Table 64. The geometrical properties and predicted values for set of models with  $L=0.5$ ,  $a/b=1$  and  $b/L=0.2$

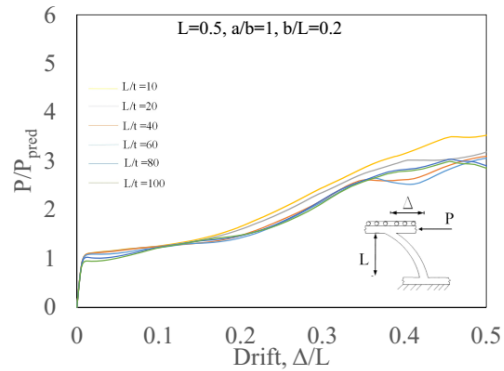
L=0.5-a/b=1-b/L=0.1 Model	a	b	t	L	a/b	b/L	L/t	Pp flexure	Pp Shear	Total Capacity
10	0.1	0.1	0.05	0.5	1	0.2	10	150.00	866.03	150.00
20	0.1	0.1	0.025	0.5	1	0.2	20	75.00	433.01	75.00
40	0.1	0.1	0.0125	0.5	1	0.2	40	37.50	216.51	37.50
60	0.1	0.1	0.0083	0.5	1	0.2	60	25.00	144.34	25.00
80	0.1	0.1	0.00625	0.5	1	0.2	80	18.75	108.25	18.70
100	0.1	0.1	0.005	0.5	1	0.2	100	15.00	86.60	15.00

Table 65. The output results for set of models with  $L=0.5$ ,  $a/b=1$  and  $b/L=0.2$

L/t	EQUIVALENT PLASTIC STRAIN	Pmax (KN)	Mend (KN.m)	hinge location	Disp Buckling $u_3=5e-3$	Fs/Fpred	deltas/L	deltai/L	Fu/Fpred	Eng index
10	0.221	774.60	193.65	0.25	NA	0.96	0.0069	NA	NA	1.35
20	0.23	517.05	129.26	0.25	NA	0.96	0.0069	NA	NA	1.33
40	0.19	218.11	54.53	0.25	0.56	0.96	0.0069	NA	NA	1.29
60	0.16	122.89	30.72	0.25	0.41	0.96	0.0069	NA	NA	1.26
80	0.16	87.83	21.96	0.25	0.34	0.96	0.0069	NA	NA	1.25
100	0.16	68.17	17.04	0.25	0.41	0.96	0.0069	NA	NA	1.19



a) Pushover curves



b) Normalized pushover curves

Figure 252. The pushover curves for a set of models with  $L=0.5$ ,  $a/b=1$ , and  $b/L=0.2$

### D.4.3. The butterfly-shaped links with $b/L=0.3$

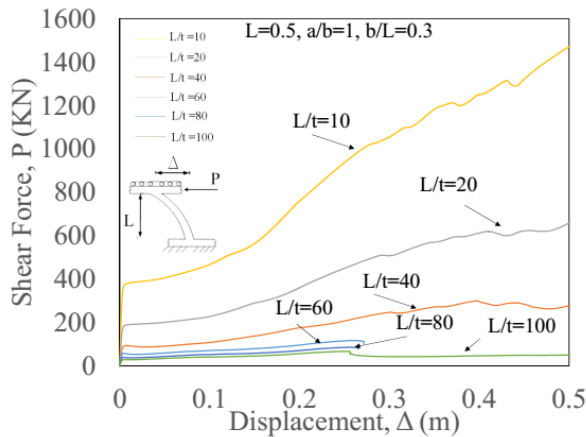
Table 66, Table 67, Figure 253 indicate the behavior of the butterfly-shaped links with geometrical properties of  $a/b=1$ ,  $b/L=0.3$ . The catenary action has been observed clearly in these set of models. It is noted that the large amount of equivalent plastic strain values have happened within this model even compared to previous models with lower  $b/L$  values since the accumulation of plastic strains are concentrated at the end of the links thicker plates where the shape angles exist.

Table 66. The geometrical properties and predicted values for set of models with  $L=0.5$ ,  $a/b=1$  and  $b/L=0.3$

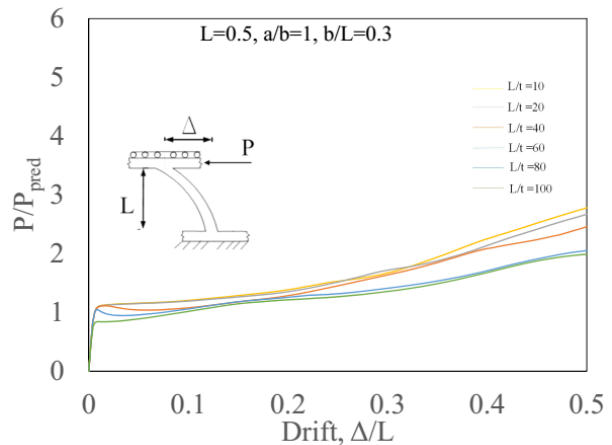
L=0.5-a/b=1-b/L=0.3 Model	a	b	t	L	a/b	b/L	L/t	Pp flexure	Pp Shear	Total Capacity
10	0.15	0.15	0.05	0.5	1	0.3	10	337.50	1299.04	337.50
20	0.15	0.15	0.025	0.5	1	0.3	20	168.75	649.52	168.70
40	0.15	0.15	0.0125	0.5	1	0.3	40	84.38	324.76	84.30
60	0.15	0.15	0.0083	0.5	1	0.3	60	56.25	216.51	56.20
80	0.15	0.15	0.00625	0.5	1	0.3	80	42.19	162.38	42.10
100	0.15	0.15	0.005	0.5	1	0.3	100	33.75	129.90	33.70

Table 67. The output results for set of models with  $L=0.5$ ,  $a/b=1$  and  $b/L=0.3$

L/t	Equivalent plastic strain	Pmax (KN)	Mend (KN.m)	hinge location	Disp Buckling $u_3=5e-3$	Fs/Fpred	deltas/L	deltai/L	Fu/Fpred	Eng index
10	0.23	1488.65	372.16	0.25	0.46	1.08	0.016	NA	NA	1.23
20	0.18	886.87	221.72	0.25	0.24	1.07	0.007	NA	NA	1.22
40	0.18	340.78	85.20	0.25	0.21	1.01	0.007	NA	NA	1.11
60	0.2	116.67	29.17	0.25	0.1	1.01	0.003	0.98	2.1	0.99
80	0.2	85.65	21.41	0.25	0.05	0.91	0.003	0.98	2.1	1.02
100	0.19	66.95	16.74	0.25	0.03	0.88	0.003	0.98	2.1	0.96



a) Pushover curves



b) Normalized pushover curves

Figure 253. The pushover curves for a set of models with  $L=0.5$ ,  $a/b=1$ , and  $b/L=0.3$

#### D.4.4. The butterfly-shaped links with $b/L=0.4$

Table 68, Table 69, and Figure 254 indicate the behavior of the butterfly-shaped links with geometrical properties of  $a/b=1$ ,  $b/L=0.4$ . The equivalent plastic strain values indicate large accumulation of strains at the sharp angles located at the end of the link, which would not be desired for the seismic resistance application despite the appropriate buckling resistance. For these butterfly-shaped links, the flexural limit state occurred at first, the second-order behavior took off and the buckling happened without experiencing the shear limit state.

Table 68. The geometrical properties and predicted values for set of models with  $L=0.5$ ,  $a/b=1$  and  $b/L=0.4$

L=0.5-a/b=1-b/L=0.1 Model	a	b	t	L	a/b	b/L	L/t	Pp flexure	Pp Shear	Total Capacity
10	0.15	0.15	0.05	0.5	1	0.3	10	337.50	1299.04	337.50
20	0.15	0.15	0.025	0.5	1	0.3	20	168.75	649.52	168.70
40	0.15	0.15	0.0125	0.5	1	0.3	40	84.38	324.76	84.30
60	0.15	0.15	0.0083	0.5	1	0.3	60	56.25	216.51	56.20
80	0.15	0.15	0.00625	0.5	1	0.3	80	42.19	162.38	42.10
100	0.15	0.15	0.005	0.5	1	0.3	100	33.75	129.90	33.70

Table 69. The output results for set of models with  $L=0.5$ ,  $a/b=1$  and  $b/L=0.4$

L/t	Equivalent plastic strain	Pmax (KN)	Mend (KN.m)	hinge location	Disp Buckling $u_3=5e-3$	Fs/Fpred	deltas/L	deltatau/L	Fu/Fpred	Eng index
10	0.71	2516.83	629.21	0.25	0.77	1.08	0.005	NA	NA	1.14
20	0.72	1088.17	272.04	0.25	0.61	1.07	0.006	NA	NA	1.18
40	0.72	519.39	129.85	0.25	0.55	1.08	0.0045	NA	NA	0.97
60	0.68	235.12	58.78	0.25	0.5	0.95	0.0061	NA	NA	0.89
80	0.64	228.74	57.18	0.25	0.4	0.88	0.0061	NA	NA	0.90
100	0.68	181.11	45.28	0.25	0.33	0.88	0.0061	NA	NA	0.87

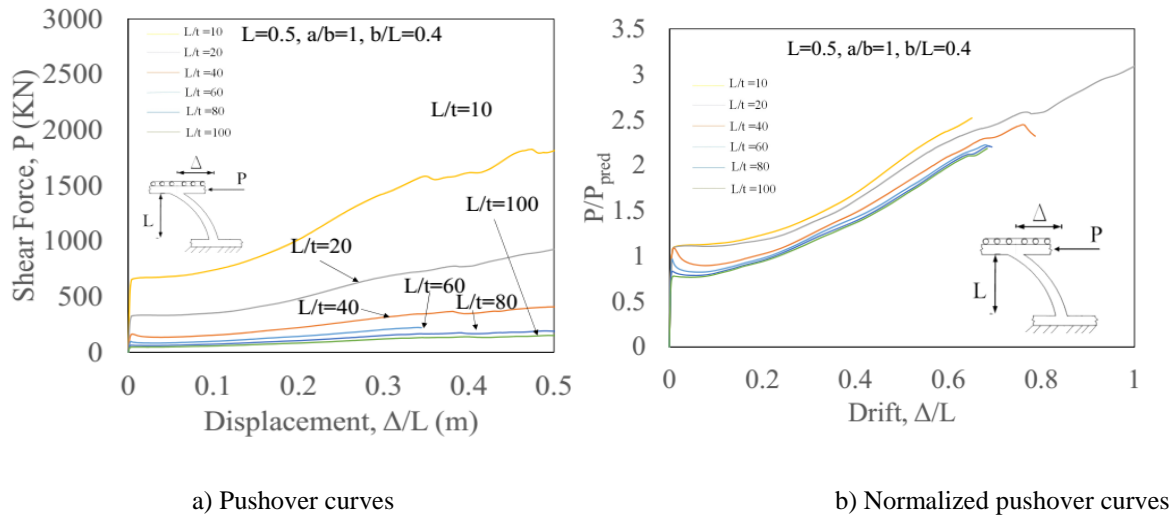


Figure 254. The push over curves for set of models with  $L=0.5$ ,  $a/b=1$  and  $b/L=0.4$

## **APPENDIX E: THE REGRESSION STUDY FOR CRITICAL MOMENT:**

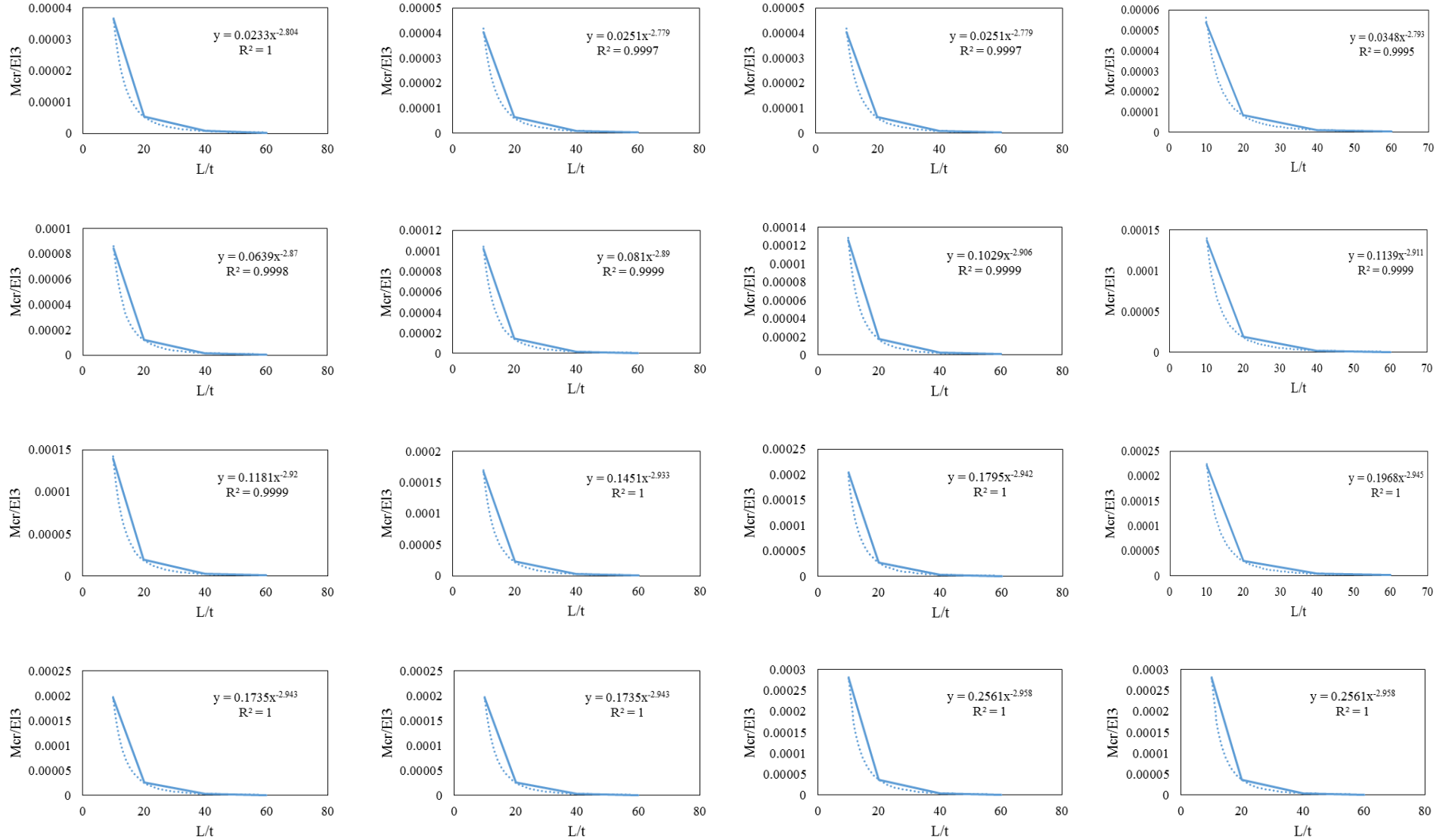


Figure 255. The regression study for conservative lateral torsional moment estimation

## APPENDIX F: THE PARAMETRIC RESULTS:

<i>Model</i>	<i>Pp under flexure</i>	<i>Pp under Shear</i>	<i>Total Capacity</i>	<i>drift</i>	<i>equivalent plastic strain</i>	<i>Pmax (KN)</i>	<i>Mend (KN.m)</i>	<i>hinge location (m)</i>	<i>Disp Buckling</i>	<i>Fy/Fpred</i>	<i>deltay/L</i>	<i>deltau/L</i>	<i>Fu/Fpred</i>	<i>Eng index</i>
<i>0.5-0.1-0.1-10</i>	13.50	43.30	13.5	0.05	0.074	30.15	7.54	0.22	NA	0.86	0.012	0.09	2.21	1.72
<i>0.5-0.1-0.1-20</i>	6.75	21.65	6.7	0.05	0.059	15.04	3.76	0.22	0.509	0.86	0.012	0.08	2.21	1.70
<i>0.5-0.1-0.1-40</i>	3.38	10.83	3.3	0.05	0.062	7.56	1.89	0.22	0.48	0.86	0.012	0.09	2.21	1.62
<i>0.5-0.1-0.1-60</i>	2.25	7.22	2.2	0.05	0.071	5.03	1.26	0.22	0.1	0.9	0.012	0.08	2.27	1.71
<i>0.5-0.1-0.1-80</i>	1.69	5.41	1.6	0.05	0.067	3.76	0.94	0.22	0.05	0.9	0.012	0.08	2.27	1.70
<i>0.5-0.1-0.1-100</i>	1.35	4.33	1.3	0.05	0.074	3.00	0.75	0.22	0.04	0.9	0.012	0.08	2.27	1.74
<i>0.5-0.1-0.2-10</i>	54.00	86.60	54	0.05	0.085	237.13	59.28	0.228	0.62	0.96	0.0069	0.75	2.81	1.71
<i>0.5-0.1-0.2-20</i>	27.00	43.30	27	0.05	0.108	74.90	18.72	0.228	0.5	0.96	0.0069	0.96	2.7	1.72
<i>0.5-0.1-0.2-40</i>	13.50	21.65	13.5	0.05	0.106	39.85	9.96	0.228	0.43	0.96	0.0069	0.5	2.45	1.74
<i>0.5-0.1-0.2-60</i>	9.00	14.43	9	0.05	0.106	28.87	7.22	0.228	0.2	0.94	0.01	0.74	2.42	1.73
<i>0.5-0.1-0.2-80</i>	6.75	10.83	6.7	0.05	0.097	19.37	4.84	0.228	0.18	0.94	0.01	0.74	2.07	1.63
<i>0.5-0.1-0.2-100</i>	5.40	8.66	5.4	0.05	0.09	16.47	4.12	0.228	0.15	0.94	0.01	0.74	1.97	1.52
<i>0.5-0.1-0.3-10</i>	121.50	129.90	121.5	0.05	0.18	313.36	78.34	0.231	NA	0.88	0.007	0.86	2.34	1.40
<i>0.5-0.1-0.3-20</i>	60.75	64.95	60.7	0.05	0.18	147.17	36.79	0.231	0.24	0.84	0.006	0.88	2.31	1.36
<i>0.5-0.1-0.3-40</i>	30.38	32.48	30.3	0.05	0.18	82.29	20.57	0.231	0.21	0.9	0.0039	0.89	2.1	1.29
<i>0.5-0.1-0.3-60</i>	20.25	21.65	20.2	0.05	0.2	51.03	12.76	0.231	0.2	0.74	0.003	0.98	2.1	1.27
<i>0.5-0.1-0.3-80</i>	15.19	16.24	15.1	0.05	0.2	51.03	12.76	0.231	0.17	0.74	0.003	0.98	1.61	1.20
<i>0.5-0.1-0.3-100</i>	12.15	12.99	12.1	0.05	0.21	51.03	12.76	0.231	0.15	0.74	0.003	0.98	1.27	1.10
<i>05-0.1-04-10</i>	216.00	173.21	173.2	0.05	0.26	444.10	111.03	0.25	0.75	1.1	0.0039	0.1	1.47	1.43
<i>05-0.1-04-20</i>	108.00	86.60	86.6	0.05	0.23	191.96	47.99	0.25	0.33	1.1	0.013	0.11	1.47	1.42
<i>05-0.1-04-40</i>	54.00	43.30	43.3	0.05	0.24	82.38	20.60	0.25	0.36	1.1	0.0045]	0.101	1.47	1.45
<i>05-0.1-04-60</i>	36.00	28.87	28.8	0.05	0.24	49.90	12.47	0.25	0.15	1.1	0.0061	0.1	1.46	1.50
<i>05-0.1-04-80</i>	27.00	21.65	21.6	0.05	0.25	32.29	8.07	0.25	0.1	1.1	0.0061	0.1	1.4	1.21
<i>05-0.1-04-100</i>	21.60	17.32	17.3	0.05	0.24	26.61	6.65	0.25	0.05	1.1	0.0061	0.1	1.15	1.09

<i>Model</i>	<i>Pp under flexure</i>	<i>Pp under Shear</i>	<i>Total Capacity</i>	<i>drift</i>	<i>equivalent plastic strain</i>	<i>Pmax (KN)</i>	<i>Mend (KN.m)</i>	<i>hinge loc.</i>	<i>Disp Buckling</i>	<i>Fy/Fpred</i>	<i>deltay/L</i>	<i>deltau/L</i>	<i>Fu/Fpred</i>	<i>Eng index</i>	<i>Fs/Fpred</i>
<i>0.5-0.33-0.1-10</i>	33.17	142.89	33.165	0.05	0.033	67.55	16.89	0.105	0.261	0.997	0.023	0.16	2.031	1.70	0.997
<i>0.5-0.33-0.1-20</i>	16.58	71.45	16.5825	0.05	0.033	33.77	8.44	0.105	0.261	0.997	0.023	0.16	2.031	1.70	0.997
<i>0.5-0.33-0.1-40</i>	8.29	35.72	8.29125	0.05	0.03	16.83	4.21	0.105	0.25	0.886	0.023	0.16	2.04	1.35	0.886
<i>0.5-0.33-0.1-60</i>	5.53	23.82	5.5	0.05	0.032	11.20	2.80	0.105	0.24	0.886	0.023	0.16	2.04	1.37	0.886
<i>0.5-0.33-0.1-80</i>	4.15	17.86	4.1	0.05	0.021	8.37	2.09	0.105	0.2	0.886	0.016	0.16	2.04	1.32	0.886
<i>0.5-0.33-0.1-100</i>	3.32	14.29	3.3	0.05	0.014	6.71	1.68	0.105	0.18	0.886	0.023	0.16	2.04	1.20	0.886
<i>0.5-0.33-0.2-10</i>	132.66	285.79	132.66	0.05	0.109	222.85	55.71	0.13	0.63	0.97	0.014	0.41	1.167	1.37	0.97
<i>0.5-0.33-0.2-20</i>	66.33	142.89	66.3	0.05	0.108	111.23	27.81	0.13	0.42	0.97	0.014	0.32	1.16	1.36	0.97
<i>0.5-0.33-0.2-40</i>	33.17	71.45	33.165	0.05	0.106	55.53	13.88	0.13	0.31	0.97	0.014	0.32	1.16	1.35	0.97
<i>0.5-0.33-0.2-60</i>	22.11	47.63	22.11	0.05	0.05	35.80	7.52	0.13	0.091	1	0.007	0.21	1.61	1.36	0.9
<i>0.5-0.33-0.2-80</i>	16.58	35.72	16.5825	0.05	0.03	22.24	5.56	0.13	0.071	0.89	0.007	0.21	1.31	1.17	0.89
<i>0.5-0.33-0.2-100</i>	13.27	28.58	13.266	0.05	0.03	16.34	4.09	0.13	0.065	0.89	0.007	0.21	1.21	1.17	0.89
<i>0.5-0.33-0.3-10</i>	298.49	428.68	298.485	0.05	0.014	420.67	105.17	0.137	0.69	0.9981	0.0148	0.23	1.39	1.17	0.9981
<i>0.5-0.33-0.3-20</i>	149.24	214.34	149.2	0.05	0.014	209.97	52.49	0.137	0.49	0.9981	0.014	0.23	1.39	1.16	0.9981
<i>0.5-0.33-0.3-40</i>	74.62	107.17	74.6	0.05	0.012	96.48	24.12	0.137	0.43	1	0.01	0.23	1.39	1.15	0.9
<i>0.5-0.33-0.3-60</i>	49.75	71.45	49.7	0.05	0.01	51.03	12.76	0.137	0.4	0.89	0.027	0.16	1.01	0.91	0.89
<i>0.5-0.33-0.3-80</i>	37.31	53.59	37.3	0.05	0.01	37.52	9.38	0.137	0.33	0.89	0.027	0.16	1.01	0.90	0.89
<i>0.5-0.33-0.3-100</i>	29.85	42.87	29.8	0.05	0.01	29.16	7.29	0.137	0.3	0.89	0.011	0.12	0.93	0.81	0.89
<i>0.5-0.33-0.4-10</i>	530.64	571.58	530.64	0.05	0.014	696.65	174.16	0.144	NO	0.943	0.006	0.32	1.39	1.05	0.943
<i>0.5-0.33-0.4-20</i>	265.32	285.79	265.32	0.05	0.015	348.41	87.10	0.144	NO	0.943	0.006	0.32	1.391	1.08	0.943
<i>0.5-0.33-0.4-40</i>	132.66	142.89	132.6	0.05	0.013	131.44	32.86	0.14	0.007	0.89	0.26	0.26	0.99	0.90	0.89
<i>0.5-0.33-0.4-60</i>	88.44	95.26	88.44	0.05	0.016	81.25	20.31	0.14	0.0041	0.802	0.012	0.23	0.91	0.88	0.802
<i>0.5-0.33-0.4-80</i>	66.33	71.45	66.33	0.05	0.016	59.40	14.85	0.14	0.0038	0.87	0.012	0.23	0.88	0.82	0.87
<i>0.5-0.33-0.4-100</i>	53.06	57.16	53.064	0.05	0.016	46.59	11.65	0.14	0.0033	0.67	0.005	0.21	0.83	0.79	0.67

<i>Model</i>	<i>Pp under flexure</i>	<i>Pp under Shear</i>	<i>Total Capacity</i>	<i>drift</i>	<i>equivalent plastic strain</i>	<i>Pmax (KN)</i>	<i>Mend (KN.m)</i>	<i>hinge loc.</i>	<i>Disp Buckling</i>	<i>Fy/Fpred</i>	<i>deltay/L</i>	<i>deltau/L</i>	<i>Fu/Fpred</i>	<i>Eng index</i>	<i>Fs/Fpred</i>
<i>0.5-0.75-0.1-10</i>	37.50	324.76	37.50	0.05	0.031	156.90	39.23	0.01	NA	1.01	0.016	0.3	4.11	2.24	1.01
<i>0.5-0.75-0.1-20</i>	18.75	162.38	18.70	0.05	0.033	78.00	19.50	0.01	0.509	1.01	0.016	0.3	4.11	2.17	1.01
<i>0.5-0.75-0.1-40</i>	9.38	81.19	9.30	0.05	0.03	38.77	9.69	0.01	0.48	1.01	0.016	0.3	4.11	2.22	1.01
<i>0.5-0.75-0.1-60</i>	6.25	54.13	6.20	0.05	0.032	25.65	6.41	0.01	0.448	1.01	0.016	0.3	4.11	2.21	1.01
<i>0.5-0.75-0.1-80</i>	4.69	40.59	4.60	0.05	0.028	19.05	4.76	0.01	0.38	1.01	0.016	0.3	4.11	2.17	1.01
<i>0.5-0.75-0.1-100</i>	3.75	32.48	3.70	0.05	0.028	15.00	3.75	0.01	0.3	1.01	0.016	0.3	4.11	1.60	1.01
<i>0.5-0.75-0.2-10</i>	150.00	649.52	150.00	0.05	0.109	461.60	115.40	0.01	0.85	1.01	0.01	0.38	2.69	1.43	1.01
<i>0.5-0.75-0.2-20</i>	75.00	324.76	75.00	0.05	0.108	237.08	59.27	0.01	0.84	1.01	0.01	0.38	2.69	1.34	1.01
<i>0.5-0.75-0.2-40</i>	37.50	162.38	37.50	0.05	0.106	118.54	29.63	0.01	0.43	1.01	0.01	0.38	2.69	1.39	1.01
<i>0.5-0.75-0.2-60</i>	25.00	108.25	25.00	0.05	0.05	74.31	18.50	0.01	0.2	1.01	0.01	0.38	2.69	1.39	1.01
<i>0.5-0.75-0.2-80</i>	18.75	81.19	18.70	0.05	0.03	49.11	12.28	0.01	0.15	1.01	0.01	0.38	2.69	1.26	1.01
<i>0.5-0.75-0.2-100</i>	15.00	64.95	15.00	0.05	0.027	37.79	9.45	0.01	0.2	1.01	0.01	0.38	2.69	1.20	1.01
<i>0.5-0.75-0.3-10</i>	337.50	974.28	337.50	0.05	0.014	893.57	223.39	0.01	0.73	1.03	0.0078	0.51	2.27	1.17	1.03
<i>0.5-0.75-0.3-20</i>	168.75	487.14	168.70	0.05	0.014	381.44	95.36	0.01	0.75	1.03	0.0078	0.51	2.27	1.17	1.03
<i>0.5-0.75-0.3-40</i>	84.38	243.57	84.30	0.05	0.014	240.14	60.03	0.01	0.24	1.03	0.0078	0.51	2.27	1.19	1.03
<i>0.5-0.75-0.3-60</i>	56.25	162.38	56.20	0.05	0.01	154.17	38.54	0.01	0.16	1.03	0.0078	0.51	2.27	1.06	1.03
<i>0.5-0.75-0.3-80</i>	42.19	121.78	42.10	0.05	0.01	99.39	24.85	0.01	0.16	1.03	0.0078	0.51	2.27	1.07	1.03
<i>0.5-0.75-0.3-100</i>	33.75	97.43	33.70	0.05	0.01	77.78	19.44	0.01	0.01	1.03	0.0078	0.51	2.27	1.04	1.03
<i>0.5-0.75-0.4-10</i>	600.00	1299.04	600.00	0.05	0.014	950.56	237.64	0.01	NA	1.1	0.013	0.48	NA	1.12	1.1
<i>0.5-0.75-0.4-20</i>	300.00	649.52	300.00	0.05	0.015	580.48	145.12	0.01	0.38	1.1	0.013	0.48	NA	1.16	1.1
<i>0.5-0.75-0.4-40</i>	150.00	324.76	150.00	0.05	0.013	286.86	71.71	0.01	0.36	1.1	0.013	0.48	NA	1.05	1.1
<i>0.5-0.75-0.4-60</i>	100.00	216.51	100.00	0.05	0.016	188.45	47.11	0.01	0.25	1.1	0.013	0.48	NA	0.94	1.1
<i>0.5-0.75-0.4-80</i>	75.00	162.38	75.00	0.05	0.015	136.52	34.13	0.01	0.18	1.1	0.013	0.48	NA	0.94	1.1
<i>0.5-0.75-0.4-100</i>	60.00	129.90	60.00	0.05	0.012	104.88	26.22	0.01	0.16	1.1	0.013	0.48	NA	0.86	1.1

<i>Model</i>	<i>Pp</i> <i>under</i> <i>flexure</i>	<i>Pp</i> <i>under</i> <i>Shear</i>	<i>Total</i> <i>Capacity</i>	<i>drift</i>	<i>equivalent</i> <i>plastic</i> <i>strain</i>	<i>Pmax</i> <i>(KN)</i>	<i>Mend</i> <i>(KN.m)</i>	<i>hinge</i> <i>location</i> <i>m</i>	<i>Disp</i> <i>Buckling</i>	<i>Fy/Fpred</i>	<i>deltay/L</i>	<i>deltau/L</i>	<i>Fu/Fpred</i>	<i>Eng</i> <i>index</i>	<i>Fs/Fpred</i>
<i>0.5-1-0.1-10</i>	37.50	433.01	37.50	0.05	0.066	442.62	110.66	0.25	NA	0.92	0.01	0.28	4.1	2.16	0.92
<i>0.5-1-0.1-20</i>	18.75	216.51	18.70	0.05	0.065	254.45	63.61	0.25	NA	0.92	0.01	NA	NA	2.11	0.92
<i>0.5-1-0.1-40</i>	9.38	108.25	9.30	0.05	0.055	100.27	25.07	0.25	NA	0.92	0.01	NA	NA	2.14	0.92
<i>0.5-1-0.1-60</i>	6.25	72.17	6.20	0.05	0.059	51.14	12.79	0.25	0.4	0.91	0.012	NA	NA	2.23	0.91
<i>0.5-1-0.1-80</i>	4.69	54.13	4.60	0.05	0.059	43.69	10.92	0.25	0.4	0.91	0.012	NA	NA	2.22	0.91
<i>0.5-1-0.1-100</i>	3.75	43.30	3.70	0.05	0.059	33.85	8.46	0.25	0.4	0.91	0.012	NA	NA	2.12	0.91
<i>0.5-1-0.2-10</i>	150.00	866.03	150.00	0.05	0.221	774.60	193.65	0.25	NA	0.96	0.0069	NA	NA	1.35	0.96
<i>0.5-1-0.2-20</i>	75.00	433.01	75.00	0.05	0.23	517.05	129.26	0.25	NA	0.96	0.0069	NA	NA	1.33	0.96
<i>0.5-1-0.2-40</i>	37.50	216.51	37.50	0.05	0.19	218.11	54.53	0.25	0.56	0.96	0.0069	NA	NA	1.29	0.96
<i>0.5-1-0.2-60</i>	25.00	144.34	25.00	0.05	0.16	122.89	30.72	0.25	0.41	0.96	0.0069	NA	NA	1.26	0.96
<i>0.5-1-0.2-80</i>	18.75	108.25	18.70	0.05	0.16	87.83	21.96	0.25	0.34	0.96	0.0069	NA	NA	1.25	0.96
<i>0.5-1-0.2-100</i>	15.00	86.60	15.00	0.05	0.16	68.17	17.04	0.25	0.41	0.96	0.0069	NA	NA	1.19	0.96
<i>0.5-1-0.3-10</i>	337.50	1299.04	337.50	0.05	0.23	1488.65	372.16	0.25	0.46	1.08	0.016	NA	NA	1.23	1.08
<i>0.5-1-0.3-20</i>	168.75	649.52	168.70	0.05	0.18	886.87	221.72	0.25	0.24	1.07	0.007	NA	NA	1.22	1.07
<i>0.5-1-0.3-40</i>	84.38	324.76	84.30	0.05	0.18	340.78	85.20	0.25	0.21	1.01	0.007	NA	NA	1.11	1.01
<i>0.5-0.1-0.3-60</i>	56.25	216.51	56.20	0.05	0.2	116.67	29.17	0.25	0.1	1.01	0.003	0.98	2.1	0.99	1.01
<i>0.5-0.1-0.3-80</i>	42.19	162.38	42.10	0.05	0.2	85.65	21.41	0.25	0.05	0.91	0.003	0.98	2.1	1.02	0.91
<i>0.5-0.1-0.3-100</i>	33.75	129.90	33.70	0.05	0.19	66.95	16.74	0.25	0.03	0.88	0.003	0.98	2.1	0.96	0.88
<i>0.5-1-0.4-10</i>	600.00	1732.05	600.00	0.05	0.71	2516.83	629.21	0.25	0.77	1.08	0.005	NA	NA	1.14	1.08
<i>0.5-1-0.4-20</i>	300.00	866.03	300.00	0.05	0.72	1088.17	272.04	0.25	0.61	1.07	0.006	NA	NA	1.18	1.07
<i>0.5-1-0.4-40</i>	150.00	433.01	150.00	0.05	0.72	519.39	129.85	0.25	0.55	1.08	0.0045	NA	NA	0.97	1.08
<i>0.5-1-0.4-60</i>	100.00	288.68	100.00	0.05	0.68	235.12	58.78	0.25	0.5	0.95	0.0061	NA	NA	0.89	0.95
<i>0.5-1-0.4-80</i>	75.00	216.51	75.00	0.05	0.64	228.74	57.18	0.25	0.4	0.88	0.0061	NA	NA	0.90	0.88
<i>0.5-1-0.4-100</i>	60.00	173.21	60.00	0.05	0.68	181.11	45.28	0.25	0.33	0.88	0.0061	NA	NA	0.87	0.88